Scuola Internazionale Superiore di Studi Avanzati
International School for Advanced Studies

thesis submitted for the degree of
Doctor Philosophiæ

Formation and Evolution of Massive Early-Type Galaxies at high redshift

Candidate:
Lulu Fan

Supervisors:
Prof. Luigi Danese
Prof. Alessandro Bressan
Dr. Andrea Lapi

To Ailing,Xinghe and my parents

ABSTRACT

In this thesis I present the results obtained during my PhD studies at SISSA in the field of galaxy formation, with focus on the problem of formation of Early Type Galaxies (ETGs) at high redshift. The interest to this issue has been increasing with time, since in the last decade observational evidence brought the idea that the formation and evolution of quasars is strictly related to that of ETGs. In order to tackle the galaxy formation most of the efforts has been put in developing semi-analytical and numerical codes based on the assumption that the hierarchy of galaxy Dark Matter halos traces the history also of baryons (stars and gas) through continuous merging. On the other hand, the group in SISSA and in Padua Observatory put forward the concept that the galaxy and quasar phenomenology at high redshift is related chiefly to physical processes (such as cooling, collapse, star formation, accretion onto the central Black Hole seed and feedback) occurring in the gas associated to the phase of fast collapse/merging of the central 30-40% of the mass of DM halos, while the later phase of slow accretion is little affecting the evolution of stars and quasars.

My main contributions to the line of research in SISSA have been *i)* the analysis of the relationship between star formation and dust in the primeval galaxies at $z \sim 2$; *ii)* the exploration of the effects of large gas outflows triggered by stellar and quasar feedback on the structure of newly formed ETGs. I also have been collaborating in the analysis of the very exciting results obtained with the HERSCHEL-ATLAS survey.

Main results are as follows:*i)* We construct a sample of spectroscopically confirmed

z_{850}-band-selected galaxies at redshift $z \sim 2$ from the GOODS-MUSIC sample, with a well sampled SED from the rest frame UV to near IR ,which can allow us to have the analysis of their physical parameters by means of the usual spectral population synthesis technique. We have combined a local (U)LIRGs sample with a sample of normal galaxies and we have re-calibrated a relation between $L_{8\mu m}$ and L_{IR}. We find that the usual spectral population synthesis technique with a fixed extinction law cannot reproduce the observed IR luminosity for the whole sample. We have outlined a new method that adds IR luminosity to the global SEDs and uses a generalized Calzetti law with variable R_V. With this new method we could determine in a unprecedent robust way the physical parameters ,namely SFR, attenuation and age. We confirm that low luminosity galaxies harbor, on average significantly older stellar populations and are also less massive than the brighter ones. Thus we confirm that the observed downsizing effect is consistent with a picture where less massive galaxies actually form first, but their star formation lasts longer, consistent with the anti-hierarchical galaxy formation scenario. *ii)*We show that the observed compact size (kpc or even sub-kpc) of high redshift ETGs is expected by theoretical predictions based on the largely accepted assumption that most of the stars have been formed during dissipative collapse of cold gas.The available observational data strongly suggests that most of the size evolution occurs at $z \geq 1$, while at $z < 1$ sizes increase by no more than 40%. Moreover, a large fraction of high-z passively evolving galaxies have projected stellar mass within their effective radii a factor of 2 larger than those of local ETGs with the same stellar mass, within the same physical radius. It is also shown that the size distribution of high redshift ETG progenitors is broader than the corresponding distribution for local ETGs. While a significant fraction of massive high redshift ETGs already exhibit sizes as large as those of their local counterparts with the same mass, for a bunch of ETGs the size has to increase by a factor of 4-6 to match the local half mass radius. All the above results are easily accounted for if most of the size evolution is due to a puffing up driven by the rapid expulsion of large amounts of mass. The contribution of dry minor merger to the size evolution can be up to a factor of 2 which is constrained by the mass function evolution.

BASED ON

1. **Lulu Fan**; Andrea Lapi; Alessandro Bressan ;Mario Nonino; Gianfranco De Zotti;and Luigi Danese, Dust attenuation, star formation rate and stellar mass in redshift $z \sim 2$ galaxies, in prep. , 2011

2. A. Lapi;J. González-Nuevo;**L. Fan**;A. Bressan;G. De Zotti;L. Danese;M.Negrello, +32 coauthers, Herschel-ATLAS Galaxy Counts and High Redshift Luminosity Functions: The Formation of Massive Early Type Galaxies, ApJ accepted, 2011

3. **Fan, L.**; Lapi, A.; Bressan, A.; Bernardi, M.; De Zotti, G.; Danese, L.. Cosmic Evolution of Size and Velocity Dispersion for Early-type Galaxies ApJ 718 1460 (2010)

4. **Fan, LuLu**; Wang, HuiYuan; Wang, Tinggui; Wang, Junxian; Dong, Xiaobo; Zhang, Kai; Cheng, Fuzhen. The Correlation Between X-ray and UV Properties of BAL QSOs ApJ 690 1006(2009)

5. **Fan, L.**; Lapi, A.; De Zotti, G.; Danese, L. The Dramatic Size Evolution of Elliptical Galaxies and the Quasar Feedback. ApJ 689 L101(2008)

6. González-Nuevo, J.; de Zotti, G.; Andreani, P.; Barton, E. J.; Bertoldi, F.; Birkinshaw, M.; Bonavera, L.; Buttiglione, S.; Cooke, J.; Cooray, A.; Danese, G.; Dunne, L.; Eales, S.; **Fan, L.**; +43 coauthors. A&A 518L(2010)

7. Eales, S.; Dunne, L.; Clements, D.; Cooray, A.; de Zotti, G.; Dye, S.; Ivison, R.; Jarvis, M.; Lagache, G.; Maddox, S.; +89 coauthers. The Herschel ATLAS. Publications of the Astronomical Society of the Pacific, 122:499-515, (2010)

8. Dong, Xiaobo; Wang, Tinggui; Yuan, Weimin; Shan, Hongguang; Zhou, Hongyan; **Fan, Lulu**; Dou, Liming; Wang, Huiyuan; Wang, Junxian; Lu, Honglin. SDSS J160531.84+174826.1: A Dwarf Disk Galaxy with an Intermediate-Mass Black Hole. ApJ 657 700(2007)

9. Shu, X. W.; Wang, J. X.; Jiang, P.; **Fan, L. L.**; Wang, T. G. Investigating the Nuclear Obscuration in Two Types of Seyfert 2 Galaxies. ApJ 657 167 (2007)

CONTENTS

Chapter 1

INTRODUCTION

Galaxy formation is one of the major issues in modern Physical Cosmology. The quite large amount of high quality data collected from ground and space in the last three decades has impressively moved forward the frontier of our understanding of galaxy formation process even at quite high redshift. We have presently the capability of detecting galaxies up to redshift $z \sim 10$, corresponding to a time ~ 400 million years since the Big Bang (see e.g. Oesch et al. 2011[243]). Their stellar populations are now as old as the Universe itself.

The formation of galaxies is an important step in the more general process of the development of structures from primordial tiny perturbations of density field. Nowadays, most of the galaxy phenomenology is explained by assuming that galaxies are characterized by two components, the Dark Matter (DM) and the baryons, the former being largely dominating the gravitating mass (the halo mass). The nature of DM, in particular the possibility that DM is Cold (CDM) or Warm (WDM), is still debated, though observations of the large scale structure favors the former possibility. However, warm, or self-interacting, or coupled DM can not yet be excluded, especially on galaxy scales. On top of that, the relation between luminosity distance and redshift for type Ia Supernovae detected in galaxies at substantial redshift and the power spectrum of Cosmic Microwave Background (CMB) anisotropy require an additional component in the Universe, the so called Dark Energy (DE), which is characterized by a negative pressure and which is presently accelerating the cosmic expansion. In the following, we will

study galaxy formation in the framework of the largely accepted Cosmological Concordance Model. Throughout the Thesis we adopt a standard, flat ΛCDM cosmology (see Komatsu et al. 2011) with matter density parameter $\Omega_M = 0.27$ and Hubble constant $H_0 = 70$ km s^{-1} Mpc^{-1}. We also adopt a Bardeen et al. (1986) cold dark matter power spectrum with primordial index $n_s = 1$ and cosmic mass variance $\sigma_8 = 0.81$.

In the context of galaxy formation, the formation of massive Early-Type Galaxies (ETGs) deserves a specific attention. These galaxies are spheroidal systems, which predominantly consist of old stars with mass-weighted ages of $\geq 8 - 9$ Gyr (Thomas et al. 2005a[325], see Renzini 2006[274] for a review) and so must have formed most of their stars at redshift $z \geq 1 - 1.5$. High spatial resolution photometric and spectroscopic observations of local massive ETGs have shown that they generally harbor a central Super-Massive Black Hole (SMBH) (e.g., Kormendy & Richstone 1995[181]; Richstone et al. 1998[276]; Magorrian et al. 1998[204]; Kormendy & Gebhardt 2001[180]) with either mass proportional to the mass in stars (Magorrian et al. 1998[204]; McLure & Dunlop 2002[224]; Marconi & Hunt 2003[214]) or to velocity dispersion of the stellar spheroidal component (i.e., the $M_\bullet - \sigma$ relation; Ferrarese & Merritt 2000[114]; Gebhardt et al. 2000[122]; Tremaine et al. 2002[332]). These dormant/inactive BHs have been interpreted as the remnants of the past quasar activity (Silk & Rees 1998). As matter of fact, Salucci et al. (1999) have shown that mass function of the local SMBHs is consistent with the mass function of the mass accreted during the past quasar/AGN phase, under quite general hypotheses (see also Marconi et al 2004; Shankar et al. 2004). This conclusion is now widely accepted . The general correlation between stellar and central SMBH mass prompted out the idea of co-evolution of stars and SMBH in ETGs (Granato et al 2001, 2004; Di Matteo et al. 2005; Croton et al. 2006; Hopkins et al. 2008; Somerville et al. 2008). At first, SMBHs have been found to be ubiquitous in the centers of spheroidal galaxies (e.g., Kormendy & Richstone 1995[181]; Richstone et al. 1998[276]; Kormendy & Gebhardt 2001[180]), and the masses of these black holes are correlated with either the mass (Magorrian et al. 1998[204]; McLure & Dunlop 2002[224]; Marconi & Hunt 2003[214]) or velocity dispersion (i.e., the $M_\bullet - \sigma$ relation; Ferrarese & Merritt 2000[114]; Gebhardt et al. 2000[122]; Tremaine et al. 2002[332]) of spheroids, demonstrating a direct link between the origin of spheroidal galaxies and SMBHs. Also, the QSOs feedback has been proposed to quench the star formation to explain the sparse luminous galaxies compared to the space density of dark matter halos with corresponding mass. Silk &

Rees(1998)[306] proposed that the central black holes and their host galaxies should be taken as a whole into the model of galaxy formation and evolution.

This adds interest to the ETGs, not only as good probes of galaxy assembly, star formation and metal enrichment in the early Universe, but also because they are directly connected with the formation and evolution of the quasars.

Historically, there were two main scenarios for the formation of ETGs: the so-called Monolithic Collapse model (Eggen, Lynden-Bell & Sandage 1962[106], Larson 1974[191], Arimoto & Yoshii 1987[7], Bressan, Chiosi & Fagotto 1994[45]), and the Hierarchical Merging model (e.g., Toomre 1977[329]; White & Rees 1978[360], Benson 2010[20]). In the former scenario elliptical galaxies form on a short time scale through collapse and virialization from idealized 'uncollapsed' initial conditions whose prior evolution is not considered. If the star-formation time scale is short compared to the free-fall time scale the collapse is effectively dissipationless. If the two time scales are comparable, then radiative energy losses are important and one speaks of dissipational collapse. The main characteristic of this scenario is that the stars form simultaneously with the assembly of the final galaxy. In the latter scenario, an elliptical forms when two or more pre-existing and fully formed galaxies merge together. The main differences with respect to the monolithic collapse scenario is that formation of the stars occurs before, and effectively independently of, the assembly of the final galaxy.

1. The monolithic collapse scenario:

This scenario was initially suggested by Eggen, Lynden-bell & Sandage (1962)[106] with the evidence from the orbits of dwarf stars in the Galaxy. ETGs form in a single burst of intense star formation at high redshift, which is coincident with their collapse to equilibrium and is followed by passive evolution of their stellar populations to the present day (Partridge & Peebles, 1967[252]; Larson, 1975[192]). This scenario was inspired by the fact that ETGs appear to be a remarkably homogeneous class of objects with uniformly old stellar populations. The $N-$body simulations incorporating cooling processes, star formation, SNae feedback and chemical evolution well reproduced basic properties of ETGs (Chiosi & Carraro 2002[66]). The general picture of monolithic formation successfully interprets the fundamental plane (Djorgovski & Davis 1987[96]; van Dokkum & Stanford 2003[346]), the mass-to-light ratio versus central velocity dispersion(Burstein et al. 1997[52]), color-magnitude relation (Bower, Lucey & Ellis 1992[40];Kodama et al. 1998[178]) and gross chemical evolution properties (Gibson & Matteucci 1997[128]) of

both dwarf and giant ellipticals. Recent analysis of a sample of over 2000 galaxies from the Sloan Deep Sky Survey (SDSS) has reconstructed the concentration halo parameter c and has derived scaling relations between stellar mass and the velocity dispersion, which are consistent with the numerical simulations and sufficient to recover the tilt of the fundamental plane (Lintott, Ferreras & Lahav 2006[196]).

However, theoretical difficulties with the monolithic collapse scenario arise because its initial conditions are not well motivated and are difficult to reconcile with the cold dark matter paradigm. The basic problems are the following:
i) why was there no significant star formation before the onset of collapse?
ii) why did all star formation cease immediately after collapse?
iii) why the brightest UV selected galaxies at high redshift are relatively rare, when compared to the present number density of massive ETGs?
iv) how do we relate the formation of ellipticals to that of other galaxies and other kinds of structures in order to understand why ellipticals are predominantly the most massive galaxies and are preferentially found in clusters?

2. The merger scenario:

The pioneer computational work of galactic interaction was first carried out by Toomre & Toomre(1972)[330]. They suggested the possibility of close galaxy encounters in the local Universe. Toomre (1977) argued that in these encounters discs are destroyed and the resulting star distribution is similar to the distribution of ETGs.

The growth of more massive halos by inclusion of smaller ones has been studied first by Press and Schechter (1974), who associated the halos to the gaussian random density field of DM in the primordial Universe. This study prompted the concept of halo merging, which has been subsequently developed the introduction of the merger tree as the sequence of merging events that statistically describes the formation of the halos (Lacey & Cole 1994). The hierarchy of the halo formation has then been extended to galaxy formation (see e.g. Cole et al. 2000). The baryons are supposed to trace the formation of dark matter halos. Under this scenario, the small gas-rich spirals form primely at high redshift. Then these spirals turn into the massive ellipticals by merging at lower redshift (White & Rees 1978[360]; White & Frenk 1991[359]).

According to the mass ratio $M_1/M_2(M_1 \geq M_2)$, mergers are often separated into major (with $M_1/M_2 > 1/3$ and minor $M_1/M_2 \leq 1/3$. Numerical simulations (e.g. Bournaud et al. 2005[35]) show that major mergers are able to destroy any disks in the ingoing

galaxies and leave a spheroidal remnant, while minor mergers tend to leave disks in place (although somewhat thickened).

Mergers can also be divided into 'wet'(gas-rich, and therefore dissipational) and 'dry' (gas-poor, dissipationless).The remnants of major mergers of purely stellar disk systems, while spheroidal, do not look like elliptical galaxies.As shown by Hernquist et al. (1993)[147] their phase space densities are too low in the central regions compared to observed ellipticals. This implies that mergers between reasonably gas rich galaxies are required. The presence of gas allows for dissipation and the formation of higher phase-space density cores. Robertson et al. (2006)[280] find that similar gas fractions and the subsequent dissipation are required to produce the observed tilt in the fundamental plane of elliptical galaxies.

On the other hand, wet mergers have difficulty in producing remnants that are slow rotating and boxy galaxies, as the majority of luminous ellipticals are. In particular, the presence of a dissipative component causes the production of a steep central cusp which is not only inconsistent with the shallow cusps seen in massive ellipticals, but also destabilizes the box orbits responsible for the boxiness of the isophotes (Gerhard & Binney, 1985[125]; Merritt & Fridman, 1996[226]). It has therefore been suggested that massive ellipticals are the remnants of dry mergers of elliptical progenitors. This is supported by numerical simulations, which seem to indicate that the remnants of dry mergers between elliptical progenitors of roughly equal mass are typically slow rotating, boxy ellipticals (e.g. Khochfar & Burkert, 2005[172]; Naab et al., 2006[235]; Cox et al., 2006[81]) that lie on the fundamental plane (Nipoti et al., 2003[241]; Boylan-Kolchin et al., 2006[42]; Robertson et al., 2006[280]). Hence, massive ellipticals apparently form via dissipationless ('dry) mergers (spheroidal-spheroidal mergers), while less massive counterparts seem to require dissipational ('wet') mergers (gas-rich disk-disk mergers).

However, several bodies of evidence are difficult to reconcile with this scenario. ETGs are characterized by old and homogeneous stellar populations. Correlations tight enough to allow little room for random processes such as a sequence of mergers (apart from small mass additions through minor mergers at late epochs, see Kaviraj et al. 2008[168]), and sensitivity to the environment (color-luminosity; fundamental plane relations; dynamical mass-luminosity) have been known for a long time and have been recently confirmed with very large samples, and shown to persist up to substantial redshifts (Renzini 2006[274]; Clemens et al. 2009[71]; Thomas et al. 2010[326]; Rogers et al. 2010;[282] Peebles &

Nusser 2010[253], and references therein). More recently, a remarkably tight luminosity-size correlation has been reported (Nair et al. 2010[236]). In addition, as mentioned above, ETGs were found to host SMBHs whose mass is rather tightly proportional to the bulge and also roughly proportional the halo mass of the host galaxy (see Magorrian et al. 1998[204]; also Ferrarese & Ford 2005[113] for a review). All that indicates that the formation and evolution of ETGs is almost independent of environment, and driven mainly by self-regulation processes and intrinsic galaxy properties such as mass.

There are rather tight, albeit not inescapable, observational constraints on the star formation timescale in the most massive ETGs. An upper limit comes from the observed α-enhancement or, more properly, iron under-abundance compared to α elements. Depending on the slope of the assumed initial mass function (IMF), the observed α/Fe element ratios requires star formation timescales $< 10^9$ yr (e.g. Matteucci 1994[219]; Thomas 1999[323]). But in merger-driven galaxy formation models star formation in ellipticals typically does not truncate after 1 Gyr (Thomas & Kauffmann 1999[324]; however, see Arrigoni et al. 2010[8], Khochfar & Silk 2011[173]). If a standard IMF is assumed a lower limit comes from (sub-)mm counts, implying that several percent of massive galaxies are forming stars at rates of thousands $M_\odot\ yr^{-1}$ peaking at $z \sim 2-3$ (see Chapman et al. 2003, 2005[61][62]). This requires that this star-formation rate (SFR) is sustained for ≥ 0.5 Gyr, much longer than the timescale of a merger-induced starburst, which is of order of the dynamical time (~ 0.1 Gyr). Integral-field near-IR spectroscopy of galaxies with less extreme SFRs (of few $10^2 M_\odot\ yr^{-1}$) at $z \sim 2$, that appear to be very productive star formers in the universe (Dekel et al. 2009[92]), has shown that in many cases they have ordered, rotating velocity fields with no kinematic evidence for ongoing merging (Genzel et al. 2006[123]; Förster-Schreiber et al. 2009[117]). Still, they harbor several star forming clumps: a complex morphology is not necessarily a symptom of merging. These galaxies show tight SFR-mass correlations, with small dispersions (Daddi et al. 2007[87]; Pannella et al. 2009[249]; Dunne et al. 2009[99]; Rodighiero et al. 2010[281]; Maraston et al. 2010[212]). This is not easily reconciled with a scenario in which star formation proceeds through a series of short starbursts interleaved by long periods of reduced activity and these galaxies have been caught in a special, starburst moment of their existence. The data are more easily accounted for if the high SFRs are sustained for some $1-2$ Gyr, much longer that a dynamical time typical of starbursts. A comparison of the stellar mass functions at $z \sim 1.5$ with the

local one shows that little additional growth can have occurred for $z \leq 1.5$ through minor mergers (Mancone et al. 2010[209]; Fan et al. 2010[108]; Kaviraj et al. 2009[169]).

While the merging hypothesis follows the hierarchy expected for the DM halo, it fails, at least in the versions so far implemented, in reproducing at the same time the short timescale for the formation of most of the stars in ETGs as implied by the observed α enhancement, and the high star formation rates required by the recent sub millimeter counts of the Herschel-ATLAS and Herschel-HERMES surveys (Lapi et al. 2011; see below Chapter 3). At a quite basic level there is evidence that the most massive local ETGs exhibit older stellar populations and that the luminosity/mass function of galaxies at substantial redshift ($z \gtrsim 1$) evolves much less at the bright/massive end than at the faint end (the so called downsizing). This means that the assembly of stars in ETGs is reversed respect to the bottom top hierarchy of DM halos.

In conclusion, it is apparent that one ideally should insert galaxy formation into the hierarchical frame of DM halo formation, but preserving the astrophysically nice aspects of the monolithic hypothesis. More specifically, the formation of galaxy halos has to follow the hierarchical path indicated by analytical and numerical analysis of primordial DM perturbations, while the baryon component of primeval ETGs has to form stars as a consequence of a quick cooling, in order to reproduce the results obtained by implementing the monolithic collapse scenario. In addition, the growth of the SMBH at the galaxy center must be strictly related to the star formation activity.

In order to solve these problems, Granato et al. (2001, 2004)[137][136] elaborated a physical model for the early co-evolution of massive spheroidal galaxies and active nuclei in their centers. In the model, the formation rate of galaxy halos is dictated by the evolution of mass halo mass function, specifically in the form suggested by Sheth & Tormen(2002)[305]. The diffuse gas within the galaxy halo potential well falls into the star formation region at a rate ruled by the cooling and dynamic timescales. The gas evolution is also controlled by feedback from SNae and from the luminosity liberated by the gas accretion onto the growing central BH. More specifically in the very central region of the galaxy the radiation drag damps down the angular momentum of cold gas, which inflows into a gas reservoir around the central black hole. The reservoir gas fuels the growth of black hole according to viscous accretion subject to the Eddington limit; the growth of the central BH lasts as long as the power radiated by the nuclear accretion is large enough to expel the available cold gas and to quench the star formation. A scheme

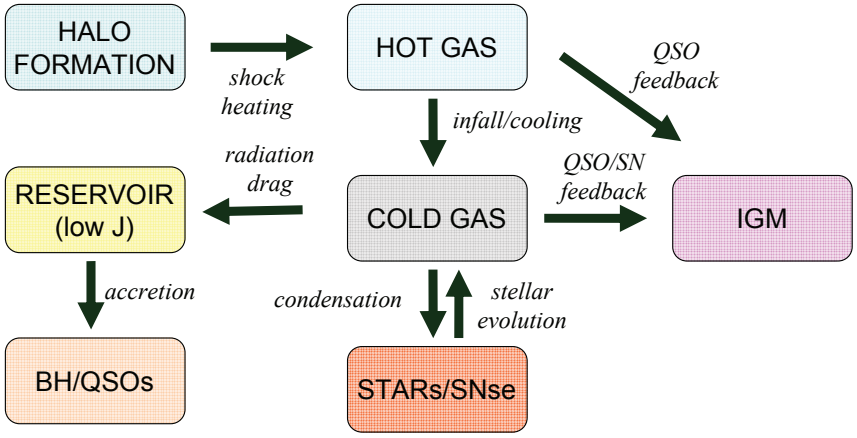

Figure 1.1: Scheme of the baryonic components included in the model (boxes) and of the corresponding mass transfer processes (arrows).

description can be found in Figure 1.1. In Appendix A, we present the basic equations of the physical processes included in the model, their analytic approximations.

In the model the star formation rate associated to a galaxy halo in essence depends on the dynamical and cooling timescales of the baryons and on the effect of the SNae feedback, while the final mass in star depends also on the time required by the seed central BH to reach the luminosity large enough to expel the cold gas. Quite interestingly at redshift of interest (z$\gtrsim$1.2-1.5) for massive ETGs ($M_h \gtrsim 10^{12}$ $M_\odot$) the predicted star formation rates range between a few hundreds to a few thousands solar mass per year, in nice agreement with those detected in the sub-mm surveys . Also the time scale for the onset of the final quenching quasar activity is such that most of the stars ($\gtrsim$80%) are formed within less than 1 Gyr, as required in order to avoid large iron enrichment by type I*a* SNae. As a consequence only a fraction ($\lesssim$ 30%) of the total baryons associated with the galaxy halo is involved in star formation, the rest of the gas remaining in the outer region of the galaxy halo. The timescale for chemical enrichment of the cold star forming gas is quite short, allowing formation of significant dust amount quite soon after the star formation onset; as a consequence most of the star formation occurs in a dusty

phase. The ensuing evolution for high redshift massive galaxies, the progenitors of present day ETGs, passes through 4 phases(see also Figure 1.2):
1) a very short UV bright phase with dust-free star formation,
2) a submillimeter bright phase with intense dust-enshrouded star formation,
3) a optically luminous quasar phase, when large quasar driven winds are produced and star formation and nuclear activity ends up;
4) a phase of almost passively evolution towards the local ETGs, allowing limited stellar increase contributed by (dry) minor merger.

This thesis is aimed to analyze two relevant issues in galaxy formation at high redshift, namely the star formation and the dust attenuation in high redshift galaxies and the effect of large gas outflows driven by stellar and quasar feedback on the structural properties of ETGs. We will contrast the merging driven models and the Granato model; in the former case all the time scale of fueling of star formation and nuclear activity is directly related to the general time scale of mergers (major), while in the latter case the relevant time scales are more directly related to the time scales of cooling and heating of the gas in the central regions of the galaxy halo.

This thesis will be organized following the evolutionary line predicted by our reference model. In Chapter 2, we focus on the high redshift UV-selected galaxies. We reproduce the LFs of LBGs at different redshifts, complementing the model with a simple, physically plausible recipe for the evolution of dust attenuation in metal-poor galaxies. We show that the observed weaker evolution of the LBG LF, compared to that of the halo mass function, is due to the short UV-bright lifetimes of massive objects that strongly mitigate the effect of the fast increase in the massive halo density with decreasing redshift. Using a z_{850}-band selected sample, we confirm the quick dust production in high redshift galaxies. However, we mention that the dust extinction can be more complicated than expected by Calzetti law (Calzetti 2000[54]). In Chapter 3, we compute the luminosity functions (LFs) at rest-frame wavelengths of 100 and 250 μm at $z \geq 1$, for bright sub-mm galaxies , by exploiting the H-ATLAS SDP survey data. We find the computed 100 and 250 μm LFs and the observed number counts at wavelengths ranging from $250\mu m$ to ≈ 1 mm are all in good agreement with G04 model predictions. An efficient method to select submillimeter bright , strongly lensed galaxies (SLGs) is proposed based on the model. Using H-ATLAS SDP data, five SLGs are confirmed (Negrello et al. 2010[239]). Chapter 4 contains a short review of the predictions of G04 model on the LF of observed high redshift optical

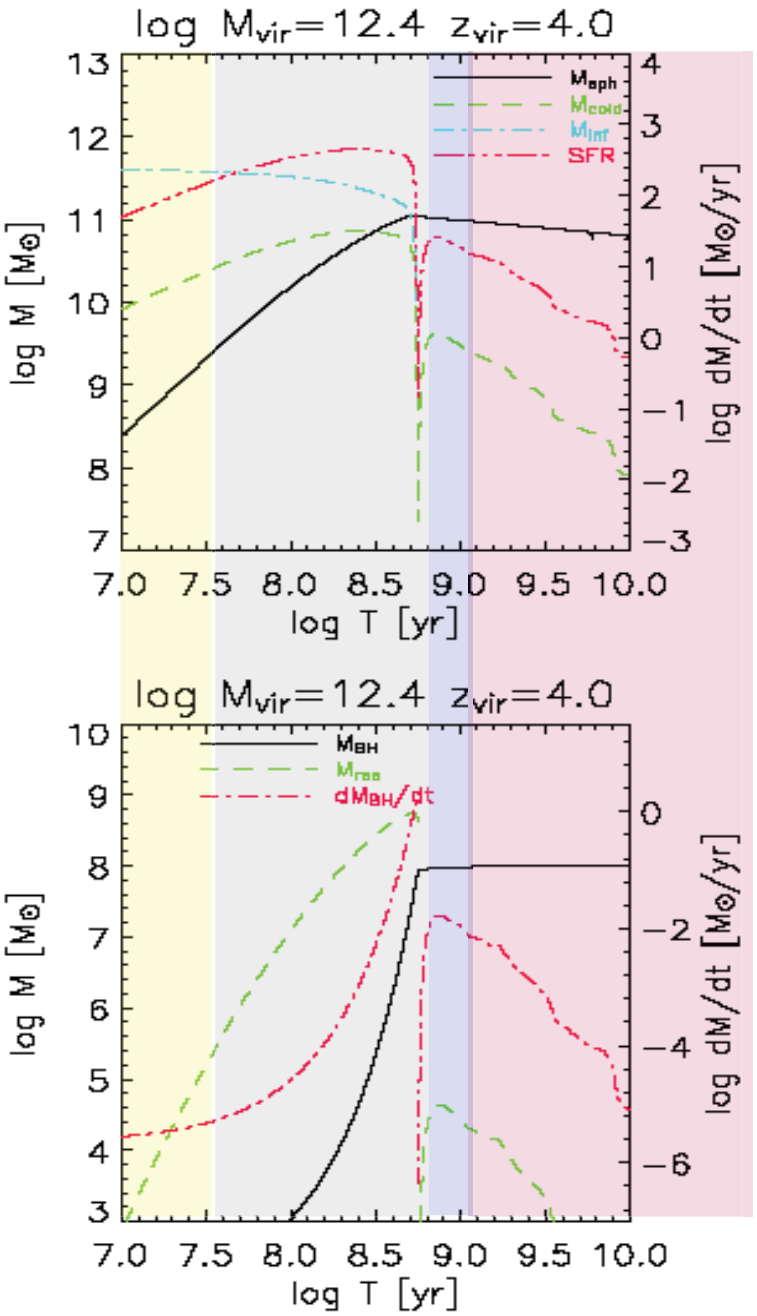

Figure 1.2: Evolution with galactic age of the stellar, reservoir, BH masses (left axis scale) and of the SFR (right axis scale) in G04 model (Granato et al. 2004[136]) for galaxy halo with mass $10^{12.4}$ $M_{\odot}$ formed at $z \sim 4.0$. The different evolutionary phases are marked by different colors: UV bight phase:yellow; Submm bright phase: light blue; QSOs phase: blue and passively evolved phase: pink.

and hard X-ray QSOs, and it has been inserted in the thesis for sake of completeness and clarity. In Chapter 5, we present the observed size evolution of massive, passively evolved galaxies at high redshift and its indication on the galaxy formation and evolution. In the last Chapter, the content of the thesis is summarized.

Chapter 2

UV-SELECTED STAR FORMING GALAXIES

The rest-frame UV band is the spectral window that can be more easily accessed by large ground telescopes or by the Hubble Space Telescope to study directly the high redshift star forming galaxies. Very recently, with the advent of the Spitzer Space Telescope, this window has been extended to optical and even near infrared wavelengths in the rest frame.

From the observational point of view, The Lyman break dropout technique (Steidel & Hamilton 1993[315]) is one of the most efficient methods to select high redshift star forming galaxies, first applied to select $z \approx 3$ galaxies (Steidel et al. 1996[314]; Lowenthal et al. 1997[199]) and subsequently extended to redshifts of up to $\sim$ 10 (Steidel et al. 1999, 2003[312][313]; Dickinson et al. 2004[94]; Giavalisco et al. 2004[127]; Ouchi et al. 2004[246]; Bunker et al. 2004[51]; Vanzella et al. 2005, 2006[349][350]; Bouwens & Illingworth 2006[36], Oesch et al. 2011[243], Bouwens et al. 2010, 2011[38][37]).

In the recent years, systematic studies of high redshift galaxies have been conducted thank to the completion of deep multi-wavelength photometric surveys and corresponding spectroscopic follow-up, such as The Great Observatories Origins Deep Survey (GOODS, Dickinson et al. 2003 [93]) and The Cosmic Evolution Survey (COSMOS; Scoville et al. 2007[296]). They provide the best opportunity to explore the nature of their stellar populations and of the properties of their interstellar medium. From the theoretical point of view, it's important to reproduce these properties under a consistent galaxy formation and evolution scenario.

In this Chapter, I will analyze the observed properties of high redshift star forming

galaxies and compare them with the predictions of the G04 model.

2.1 UV Luminosity Function of LBGs

In the following I will first summarize the results of the study by Mao et al. (2007)[211] which is one of the more comprehensive attempts to interpret the observations of high-redshift LBGs in the framework of a galaxy formation model.

Dust attenuation plays an important role to explain the observed LBGs LFs and their evolution.

The dust attenuation is expected to be proportional both to some power of star-forming gas mass (or equivalently of the SFR) that reflects the dust column density, and to some power of the metallicity that reflects the fraction of metals locked into dust grains (see also Jonsson et al. 2006[164]).

A simple, average relation between UV attenuation, SFR, and Z is proposed

$$A_{1350} \approx 0.35 \left(\frac{\dot{M}_\star}{M_\odot \ \mathrm{yr}^{-1}}\right)^{0.45} \left(\frac{Z}{Z_\odot}\right)^{0.8}, \tag{2.1}$$

The dust attenuation at other wavelengths can be computed using the wavelength dependence of the Calzetti law [54]. For example, the attenuation at other typical UV wavelengths is $A_{1216} = 1.1A_{1350}$, $A_{1600} = 0.9A_{1350}$, $A_{1700} = 0.87A_{1350}$. Equation 2.1 is the key relation that allows one to convert the theoretical models into observational predictions, in the UV pass-bands.

In fact, the absolute magnitude at $\lambda \approx 1350$ Å, including attenuation, can be written as

$$M_{1350} = 51.\,59 - 2.\,5 \ \log \frac{\bar{L}_{1350}}{\mathrm{erg\ s^{-1}\ Hz^{-1}}} - 2.\,5 \ \log \frac{\dot{M}_\star}{M_\odot \ \mathrm{yr}^{-1}} + A_{1350}\ , \tag{2.2}$$

where $\bar{L}_{1350} \approx 1.\,2{\times}10^{28}$ erg s^{-1} Hz^{-1} is the monochromatic luminosity for $\dot{M}_\star = 1 M_\odot$ yr^{-1} adopting the Romano IMF (Romano et al. 2005[283]).

Using the model described in Appendix A, which provides the star formation $\dot{M}_\star(t)$ and metal enrichment $Z(t)$ history for any halo mass M_H and virialization redshift z_{vir}, we can compute the evolution of the the attenuation in LBGs and thus compare their observational properties with the galaxy formation models.

The evolution with galactic age of the attenuation for LBGs with different halo masses

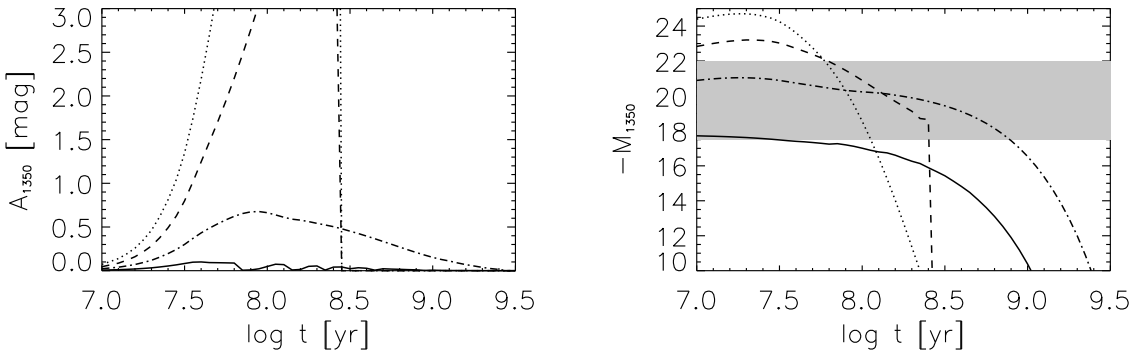

Figure 2.1: Attenuation (left panel) and attenuated magnitude (right panel) at 1350 Å as a function of galactic age, computed using Equation (2.1) and the quantities $\dot{M}_\star(t)$ and $Z(t)$ provided by G04 model(see Appendix A. The shaded area shows the range probed by the observed LFs. Lines are for halo masses $M_H = 10^{10}\ M_\odot$ (*solid* line), $10^{11}\ M_\odot$ (*dot-dashed* line), $10^{12}\ M_\odot$ (*dashed* line), and $10^{13}\ M_\odot$ (*dotted* line), virialized at $z = 6$

is shown in Figure 2.1 (left panel). The attenuation is predicted to be small for LBGs hosted by low-mass halos, while it quickly increases with time for higher masses, so that more massive galaxies are UV-bright for shorter times. The more massive LBGs spend approximately 90% of their burst time in an interstellar medium optically thick to their UV emission. The right panel of Figure 2.1 shows the predicted evolution of UV luminosity with galactic age, including the attenuation given by Equation. (2.1), at $z = 6$ for several halo masses.

The rest-frame UV LF of LBGs can be estimated coupling the UV luminosity and halo mass derived from the G04 model with the halo formation rate. The rest-frame UV LF at a cosmic time t is then

$$\Phi(M_{1350},\ t) = \int \mathrm{d}M_H\ \frac{\mathrm{d}^2\ N_{\mathrm{ST}}}{\mathrm{d}M_H\ \mathrm{d}t}\ \frac{\mathrm{d}}{\mathrm{d}M_{1350}}\ \tau[M_{1350}|M_H,\ t]\ , \tag{2.3}$$

where $\tau[M_{1350}|M_H,\ t]$ is the time lapse spent at magnitude brighter than M_{1350}. After the consideration of dust attenuation of Equation 2.1, we obtain the luminosity function of Lyman break galaxies shown as Figure 2.2. The model predictions are well consistent with the observational results. Especially, the recent results by Bouwens et al. (2011)[37] and Oeschi et al. (2011)[243] confirm the model prediction of $z \sim 10$ LBGs LFs.

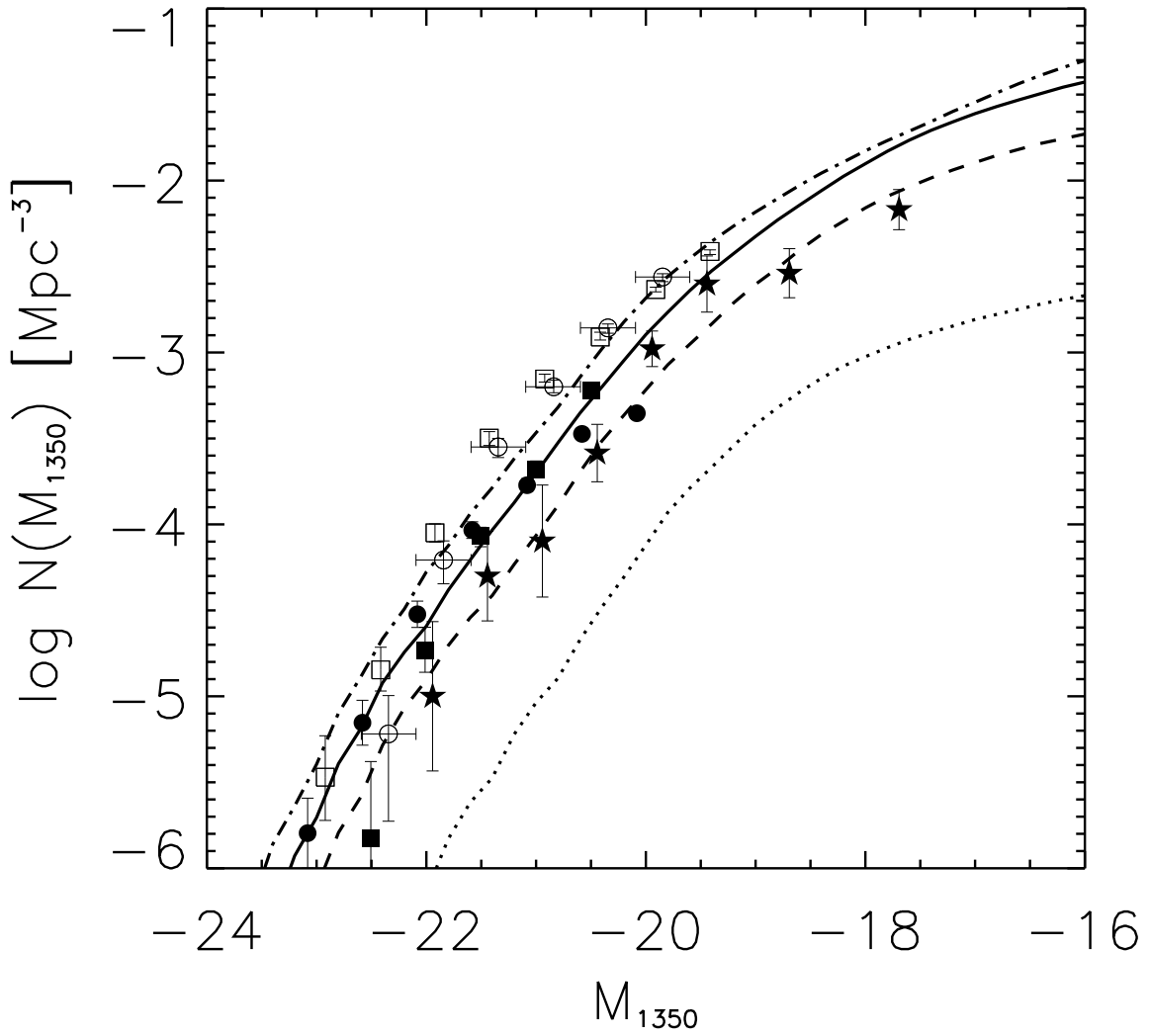

Figure 2.2: Model luminosity functions of LBGs at 1350 Å for $z = 3$ (*dot-dashed* line), $z = 5$ (*solid* line), $z = 7$ (*dashed* line), and $z = 10$ (*dotted* line), based on the attenuation given by Equation (2.1). Data at $z \approx 3 - 4$ are from Steidel et al. (2001; *empty circles*) and Yoshida et al. (2006; *empty squares*); at $z \approx 4 - 5$ are from Iwata et al. (2007; *filled circles*) and Yoshida et al. (2006; *filled squares*); at $z \approx 5 - 7$ from Bouwens et al. (2005; *stars*). The Steidel data have been converted from 1700 Å to 1350 Å setting $M_{1350} \approx M_{1700} + 0.2$, as suggested by Bouwens et al. (2005) on the basis of the composite spectrum of $z \approx 3$ LBGs.

2.2 Star Formation and Dust Attenuation in High Redshift Galaxies

In previous section, we have shown that the strong dependence of dust attenuation on halo mass has clearly a key role in shaping the UV LF and determining its evolution. The

G04 model combined with Equation 2.1 predicts a much faster increase with galactic age of attenuation in more massive galaxies, endowed with higher SFRs. These objects have therefore shorter lifetimes in the LBG phase. The short UV-bright lifetimes of massive objects strongly mitigate the effect of the fast increase of the massive halo density with decreasing redshift, thus accounting for the weaker evolution of the LBG LF, compared to that of the halo mass function.

In this section, we will select a high redshift sample ($z > 1.4$) to exploit the relation between star formation and dust attenuation. The sample is z_{850}-band selected from the GOODS-MUSIC catalogue(Grazian et al. 2006[138]). Using z_{850}-band selection compared to the Lyman break selection, we can not only select the dust free star forming galaxies, but also can select those galaxies with heavily dust obscured star formation, thus allowing a better sampling of the early evolution of the spheroids. In order to find the dust attenuation in high redshift galaxies and its effect on determining the stellar populations, such as age and stellar mass, we employ a new stellar population synthesis (SPS) technique to explore the stellar properties from the rest-frame UV to NIR multiwavelength photometric data.We use the updated simple stellar population(SSP) considering the nebular emission and only assume the constant star formation and constant E(B-V) for all SSPs(See more details in Appendix B).The constant star formation and E(B-V) are a good approximation of G04 model prediction(See Figure 1.2).

2.2.1 A high redshift sample from GOODS-MUSIC catalogue

The data we use are taken directly from GOODS-MUSIC(GOODS MUlticolour Southern Infrared Catalog) sample (Grazian et al. 2006[138], Santini et al. 2010[288]). Photometry is available in 12 bands, namely U-band form the 2.2ESO(U_{35} and U_{38}) and VLT-VIMOS (U_{VIMOS}), the $F435W$ (B-band), $F606W$ (V-band), $F775W$ (i-band), and $F850LP$ (z-band) ACS images, the JHK_S VLT data, and the 3.6, 4.5, 5.8 and 8.0 μm bands from Spitzer IRAC instrument. In the following we will use U_{VIMOS} instead of U_{35} and U_{38} because the former is much deeper than the other two. The largest fraction of the sample is 90% complete at $z_{850} = 26$ (AB magnitude). A spectroscopic redshift to more than 1000 sources is obtained after cross-correlation the data with all the available spectroscopic catalogs.

The last release of the catalogue (Version 2) presents several important improvements:

(1)The IRAC photometry are improved using new IRAC PSFs and background subtraction for the 3. 6, 4. 5, 5. 8 and 8. 0 μm bands; IRAC photometry is essential to extend the wavelength baseline into the rest frame near infrared.

(2)New spectroscopic redshifts available after the Version 1 release were added. Thanks to the release of new spectroscopic data in the GOODS-South Field (FORS2: Vanzella et al. 2006, 2008[350][348]; VIMOS: Popesso et al. 2008[263]), the new version contains a much larger spectroscopic sample than that presented in Grazain et al. (2006)[138]. The quality of all spectroscopic redshifts is marked with a $quality\_flag$ flag which is divided into four classes: very good, good, uncertain and very uncertain, represented by 0, 1, 2 and 3, respectively.

(3)The 24μm photometry by the MIPS instrument are added. The information of 24μm photometry can be very important to explore the stellar properties of the $z \sim 2$ galaxies, which can be used as an independent indicator of infrared luminosity and therefore the star formation rate.Usage of 24μm inferred infrared luminosity as a prior can help to break the age-attenuation degeneracy.

Photometry For our analysis we used the z_{850}-selected catalog which has a typical z_{850}-band ($\lambda \sim$8750Å) magnitude limit, z_{850}=26. 0, for most of the catalog and extending down to z_{850}=26. 18 in limited areas. The galaxies are selected from the z_{850}-selected catalog with the flag $selgal = 1$.

We further selected only the galaxies with at least one of JHK_S bands, one of four IRAC bands and seven bands detected totally, in order to explore the stellar properties using stellar population synthesis modeling.

Redshifts

We used both spectroscopic and photometric redshifts. First of all we checked the quality of spectroscopic redshifts marked with $quality\_flag = 2$ or 3 using SED fitting. We thus rejected those spectroscopic redshifts that were clearly in contrast with the observed SED. We then computed photometric redshifts for the full sample with EAZY (Brammer et al. 2008[44]). The comparison with 1675 spectroscopic redshifts with $quality\_flag = 0$ or 1 shows that the quality of the photometric redshifts is fairly good, with an accuracy of $\langle |z_{phot} - z_{spec}|/(1 + z_{spec}\rangle = 0.07$ (See Figure. 2.3).

The z-band selected sample In the present study only the galaxies with $1.4 < z < 5.5$ were selected in which redshift range the bulk of stars in the spheroids has been formed.

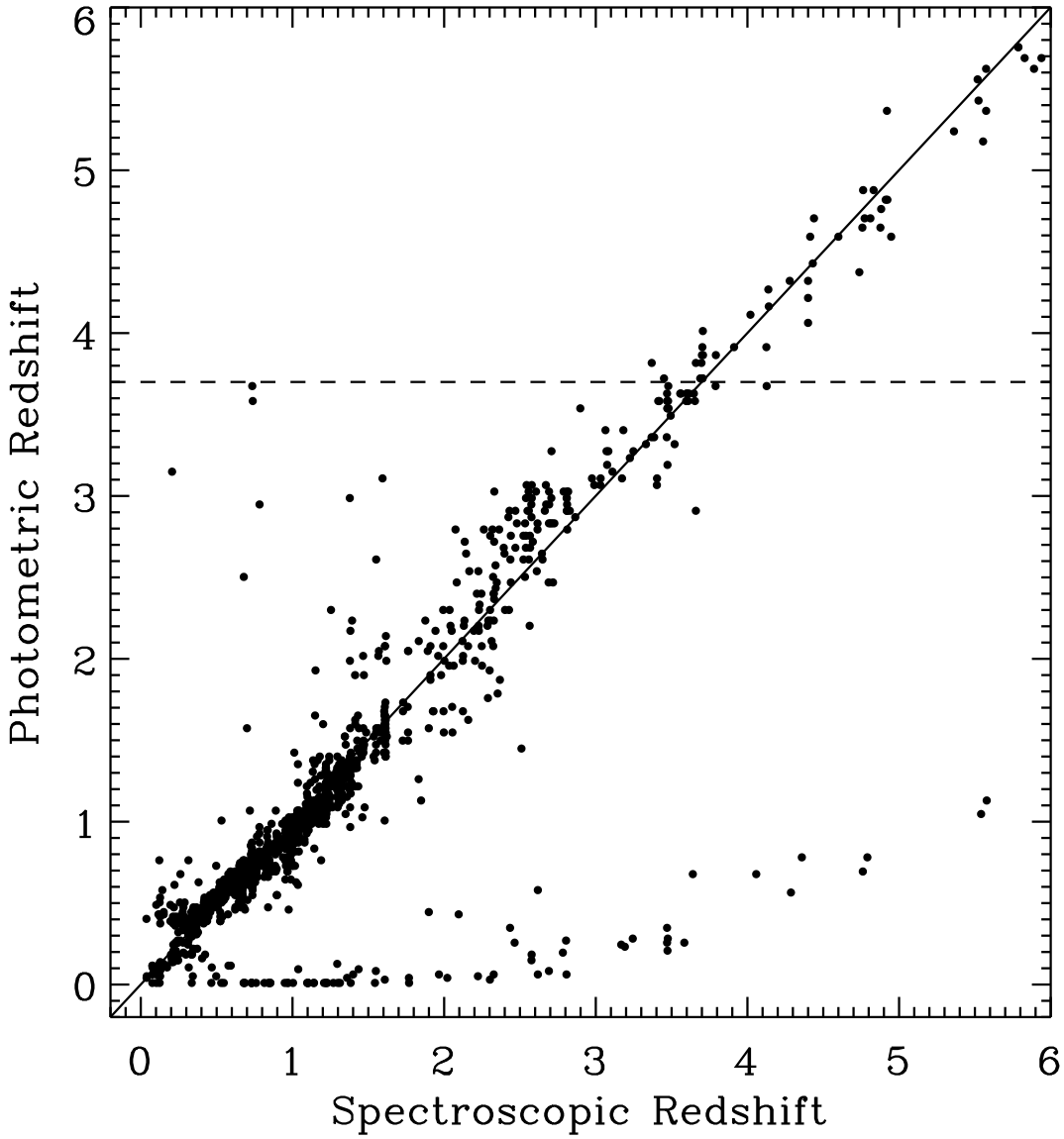

Figure 2.3: Spectroscopic redshift vs. photometric redshift given by EAZY(Brammer et al. 2008)[44].

We also divided the full z-band selected galaxies sample into four redshift bins: $1.4 \leq z < 2.5$, $2.5 \leq z < 3.7$, $3.7 \leq z < 4.5$ and $4.5 \leq z < 5.5$, with the mean value $z \sim 1.9$, 3.0, 4.0 and 5.0, respectively.

In total we got a spectroscopic sample of 407 z_{850}-band selected galaxies with the redshift range $1.4 \leq z < 5.5$: 238 at z~ 1.9, 127 at z~ 3.0, 24 at z~ 4.0 and 18 at z~ 5.0, respectively.

This sample was complemented by objects with only photometric redshifts in the following way. We first applied the synthesis technique (see Appendix B) using photometric redshifts, to the above spectroscopic sample. For this sample we find that the accuracy

of $\langle|z_{phot} - z_{spec}|/(1 + z_{spec}\rangle = 0.12$. In some cases, the photometric redshift estimate fails catastrophically, with $|z_{spec} - z_{phot}| > 1$. This happens especially for the galaxies with spectroscopic redshift $z_{spec} \sim 2 - 3$ and the problem arises because in this redshift range there is a strong degeneracy between the SED parameters and the redshift. A particular example is that of the relatively featureless blue SEDs that can be fit equally well either at $z \sim 0$ or at $z \sim 2-3$. As a result of this degeneracy there is a large scatter in the values of the physical parameters, such as the stellar mass, star formation rate and attenuation based on photometric redshift estimation.

However, we noticed that this degeneracy disappears above $z \sim 3.7$. Indeed we could obtain a much higher accuracy, $\langle|z_{phot} - z_{spec}|/(1 + z_{spec}\rangle = 0.03$, considering only high redshift objects, i. e. $3.7 \leq z_{phot} < 5.5$. In this redshift domain the possibility of catastrophic failures is significantly reduced because of the presence of the Lyman break feature. For these galaxies we find a much smaller scatter in E(B-V) and SFR between spectroscopic and spectro-photometric samples, e.g. $\langle|E(B-V)_{phot} - E(B-V)_{spec}|\rangle \sim 0.05 \pm 0.05$ and $\langle|SFR_{phot} - SFR_{spec}|/SFR_{spec}\rangle = 0.43 \pm 0.47$, respectively. Indeed the plots of $E(B-V)_{spec}$ vs. SFR_{spec} overlap those of $E(B-V)_{phot}$ vs. SFR_{phot}.

Based on these considerations and since our primary goal was to increase the number of objects to a statistically significant level, we complemented the spectroscopic sample with the photometric sample, in the redshift range of $3.7 \leq z_{phot} < 5.5$. This sample contains additional 169 galaxies at $z_{phot} \sim 4$ and 52 at $z_{phot} \sim 5$, respectively.

2.2.2 Dependence of Dust attenuation on Star Formation Rate

We have applied the population synthesis technique described in Appendix B, to derive star formation rate, attenuation, ages and masses of this large sample of high redshift galaxies.

In previous studies of local galaxies it has been found that there is a correlation, though loose, between SFR and the amount of dust attenuation (Wang & Heckman 1996[357]; Heckman et al. 1998[146]; Calzetti 2001[53]; Sullivan et al. 2001[318]; Buat et al. 2002[48]; Calzetti et al. 2007[55]). This correlation still hold even in high-z galaxies (Meurer et al. 1999; Adelberger & Steidel 2000[1]; Vijh, Witt & Gordon 2003[356]; Ouchi et al. 2004[246]; Shapley et al. 2001, 2005[300][301]).

The results of our population synthesis confirm that the more powerful star forming

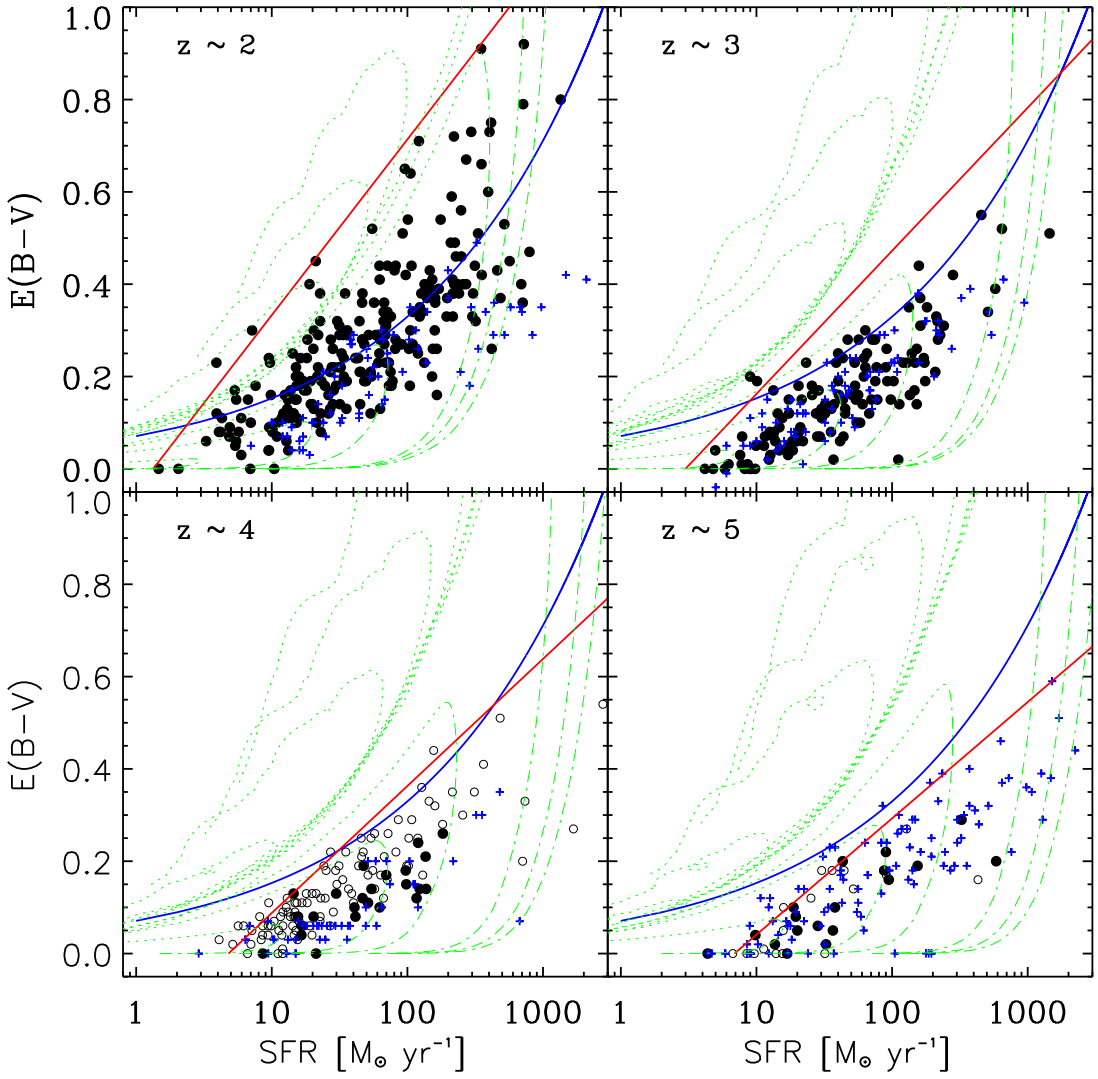

Figure 2.4: Dependence of dust attenuation on the star formation rate at four redshift bins ($z \sim 2$, 3, 4 and 5). The filled circles on all panels show the galaxies with spectroscopic redshift. And the open circles on two bottom panels ($z \sim 4$ and $z \sim 5$) show those galaxies with only photometric galaxies. The crosses on every panel show the results of Lyman Break Galaxies at corresponding redshift range using the similar SED fitting method($z \sim 2$: Shapley et al. (2005)[301]; $z \sim 3$: Shapley et al. (2001)[300]; $z \sim 4$: Pentericci et al. (2007)[255]; $z \sim 5$: Yabe et al. (2009))[362]. The red solid lines show our selection effect at different redshift range, assuming magnitude limit $z_{850} = 26.0$ and using a 100Myr-old population with the constant star formation rate as the template. The blue solid line shows the power-law fitting result ($E(B-V) = 0.07SFR^{0.33}$) of our $z \sim 2$ sample. The green dotted and dot-dashed lines represent the model predictions(See more details on text).

galaxies are more heavily obscured. In Figure 2.4, we plot the best-fit SFR and the color excess E(B-V) parameters obtained for our z-selected sample, at z$\sim$2, 3, 4 and 5, respectively. The filled circles indicate galaxies with spectroscopic redshift, while the open circles on two bottom panels ($z \sim 4$ and $z \sim 5$), mark those galaxies with only photometric redshifts. In every redshift bin ($z \sim 2$, 3, 4 and 5), there is a clear tendency for the reddening to increase with the SFR The color excess E(B-V) is expected to be proportional to some power of SFR (Mao et al. 2007[211]; Calzetti et al. 2007[55]). In the case of the lowest redshift bin we obtain the following relation $E(B-V) = (0.07 \pm 0.06 SFR^{(0.33 \pm 0.17)}$. This curve is shown in blue color in the upper left panel and is also reported, for comparison, in all the other panels of Figure 2.4.

Also plotted in the figure is the expected E(B-V) threshold locus (red line) above which, a galaxy with a 100 Myr constant star formation, would remain undetected because it fall below the detection limit of the survey, here assumed $z_{850} = 26.0$

In the same figure we have plotted with blue crosses the results obtained for several LBGs samples, found in literature. We have considered the following samples. $z \sim 2$ Shapley et al. (2005)[301]; $z \sim 3$ Shapley et al. (2001)[300]; $z \sim 4$ Pentericci et al. (2007)[255]; $z \sim 5$ Yabe et al. (2009)[362].

From Figure 2.4 it is evident that, at any SFR, we are able to detect objects with higher attenuation. This is more evident in the $z \sim 2$ sample where all the LBGs galaxies fall below our best fitting relation. At higher redshifts the differences become less significant mainly because the detection limit of our survey selects progressively less extinguished galaxies.

The difference between our result and that of Shapley et al. (2005)[301] at $z \sim 2$ arises from two aspects.

The first one is that the magnitude limits of the two samples are different. In our sample, the magnitude limit is at $z_{850} \approx 26.0$ while, in Shapley et al. (2005)[301], the limit is at $R \approx 25.0$

The second reason is that the sample selection criteria are different. We have constructed our sample according to the z_{850}-band images, which allow us to detect more heavily obscured galaxies at $z \sim 2$. In contrast, Shapley et al. (2005) selected their sample by means of the Lyman-break technique which is not sensitive to the galaxies with E(B-V) greater than 0.45.

In any case, Figure 2.4 illustrates that the observed relation between the attenuation

and the star formation rate, is a complex combination of the intrinsic properties of the galaxies and the criteria used to build up the sample.

In order to disentangle these effects we have plotted in Figure 2.4 the predictions of the G04 model. The dust attenuation is expected to be proportional both to some power of star-forming gas mass (or equivalently of the SFR) that reflects the dust column density and to some power of the metallicity that reflects the fraction of metals locked into dust grains. Mao et al. (2007) have shown that it is possible to describe the luminosity-reddening relation found by Shapley et al. (2001) for $z \approx 3$ LBGs with equation 2.1.

In Figure 2.4, we over-plot G04 model expectations with green dotted and dash-dotted lines. With the simple law we adopted in Equation 2.1, G04 model can reproduce the observed dust attenuation and SFR relation at all redshift bins($z \sim 2,\ 3,\ 4$ and 5).

As anticipated, the observed dust attenuation and SFR relation arises from two basic aspects. One is the sample selection criteria which makes us not be able to observe those old passive-evolved galaxies with low SFR and moderate dust attenuation. The other one is the fact that the more massive galaxies will have more intense star-forming and faster metal enrichment, which makes the galaxies with high SFR and low dust attenuation rare.

2.2.3 The relation between $8\mu m$ luminosity and the infrared luminosity

As seen in the previous sections, the SED fitting procedure allows one to reconstruct the contribution of the different stellar populations to the integrated light and, in particular, the current star formation rate and the mass in stars already present in the galaxy. However it is well known that the results obtained in this way may be affected by several uncertainties that are connected with some basic assumptions of the procedure, in particular the amount and the wavelength dependence of the attenuation and, to a less extent, the kind of star formation law and the metallicity.

The amount of the attenuation is a result of the fitting procedure, but in practice it depends on the wavelength dependence of the attenuation law adopted and on the degeneracy between galaxy age, chemical composition and attenuation. For example, both an increase of the metallicity and an increase of dust attenuation mimic an increase of age.

In the previous analysis we have assumed a "Calzetti" attenuation law, which looks

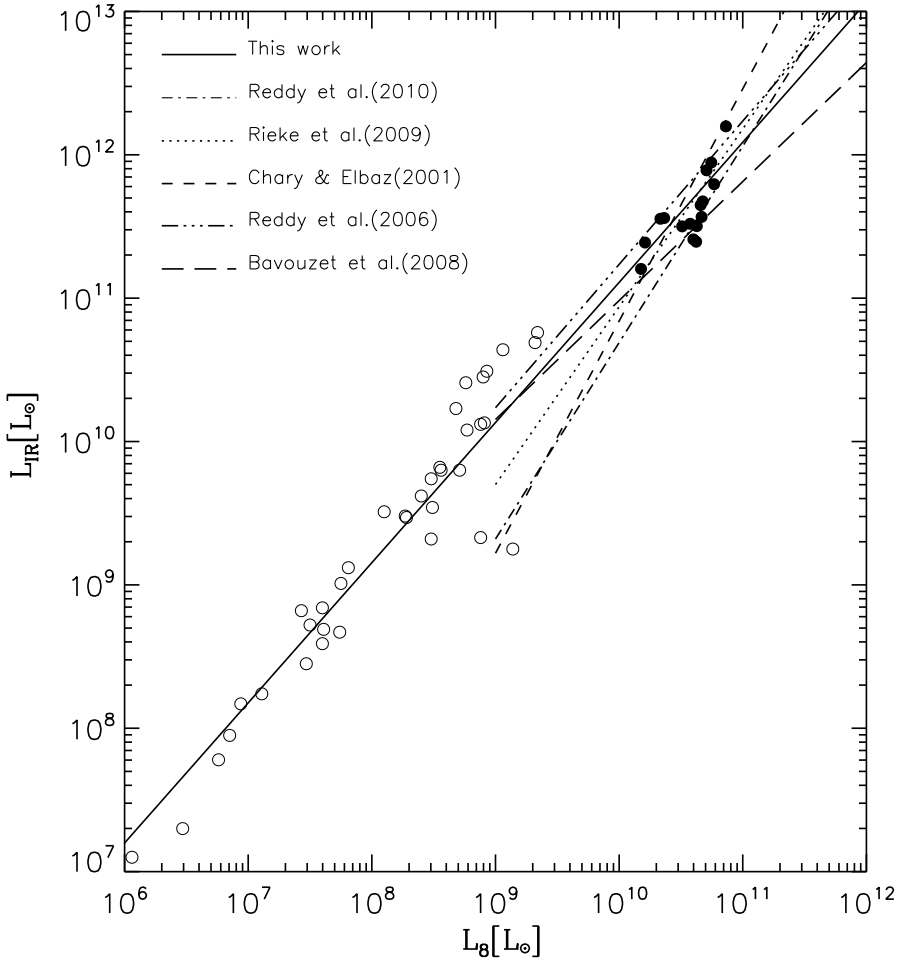

Figure 2.5: Relation between L_8 and L_{IR} of a local sample. The open circles represent galaxies selected from SINGS sample(Dale et al. 2007[89]). The filled circles are local (U)LIRGs selected from Vega et al. (2008)[351]. Other published calibrations between L_8 and L_{IR} are also plotted.

appropriate for luminous star-bursts. For less luminous galaxies an attenuation law similar to that of the SMC could be more suitable. Moreover, as discussed by Calzetti (2000)[54] and by Silva et al (1998)[308] the attenuation of the young stellar populations could be larger than that of older stars. In the previous analysis we did not take into account this effect, even if our code was originally devised to account for an age dependent attenuation. An age independent attenuation was preferred in order to keep the number of independent free parameters to a minimum value.

For young populations the effect of metallicity is less severe than that of the attenuation. We checked that varying the chemical composition from solar to 1/3 solar, did not change significantly the results.

The attenuation instead, affecting especially the ultraviolet spectral region, may introduce a significant bias toward older ages. In our case, the degeneracy between attenuation and age is at least partly controlled by the large spectral coverage we have, from Far UV to rest-frame K-band.

On top of that we remind that any fitting procedure like the one we used, will tend to underestimate the star formation rate if a significant fraction of the emitted light remain obscured even at the rest frame wavelengths corresponding to our reddest bands.

Since the energy absorbed by dust at UV and optical wavelengths is thermally re-radiated in the MIR/FIR beyond 3-4 μm, the only safe way to obtain the bolometric luminosity would be by complementing UV-optical data with the total infrared luminosity. In particular, as long as the intrinsic emission is dominated by massive stars, as in young star forming objects, the bolometric luminosity and hence the current star formation rate, are simply provided by the sum of the observed UV and far infrared luminosities.

Thus, since the far infrared luminosity cannot be easily obtained, especially for high redshift objects, there have been in the past many attempts to obtain estimates of the bolometric luminosity directly from the UV spectral properties themselves, e. g. trying to estimate the UV attenuation from the UV slope. One of such attempts is the so called IRX-β relation of local starburst galaxies, i. e. the relation between their UV spectral slope β_{UV}, defined as $f(\lambda) \propto \lambda^{\beta_{UV}}$ within the wavelength range 1250Å $-$ 2600Å, and the ratio between their infrared and UV luminosity, L_{IR}/L_{UV}, all quantities evaluated in the rest frame (Meurer et al. 1999[227], Calzetti et al 2000[54]).

More recently, with the advent of space IR telescopes, it has been possible to derive a more direct estimate of the total infrared luminosity, that involves its relation with the emission in the mid infrared. Rieke et al 2009[278] have found that, in local star forming galaxies, the total infrared luminosity correlates fairly well with the luminosity at 8 μm, $L_8=\lambda L_\lambda$(at 8μm), over a wide range of luminosity, $10^8 \lesssim L^8 \lesssim 10^{11}$ $L_\odot$. Similar results were obtained by Chary end Elbaz (2001)[65] and Calzetti et al (2007)[55].

Reddy et al. (2010)[270] have recently confirmed that this correlation holds also in high (z$\sim$2) redshift galaxies. To this purpose they have shown that there is a good correlation between the dust-corrected H_α luminosity and the $L_{8\mu m}$ luminosity. Since the intrinsic H_α luminosity is directly proportional to the star formation rate as the IR luminosity is, then Reddy et al (2010)[270] proposed a relation between L_{IR} and L_8 (cfr. their

Equation 3), derived for galaxies with luminosity in the range $10^{10} \lesssim L^8 \lesssim 10^{11}$ $L_\odot$.

The $L_{IR} - L_8$ relation is particularly important because the latter can be obtained by SPITZER IRAC and MIPS observations for a large number of local and high redshift galaxies, respectively.

Indeed a strong implementation of the second version of the GOODS-MUSIC catalogue is constituted by the 24μm MIPS flux measurement. In our sample, 135 objects have been detected at 24μm and, since their redshift is $\sim$2, their $8\mu m$ rest-frame luminosity can be derived from the observed $24\mu m$ flux, after a suitable k-correction. Using e. g. the Reddy et al relation, we could derive the total infrared luminosity from the $8\mu m$ rest-frame luminosity, and thus obtain the star formation rate and dust attenuation in a way independent from the SED modeling procedure.

Before applying this method, and in particular the Reddy et al (2010)[270] relation, we have to consider that, in strongly star forming galaxies, a significant fraction of the SFR may be completely hidden at optical wavelengths so that, even after dust attenuation correction the H_α luminosity could sample only a fraction of the total FIR luminosity (Poggianti, Bressan, & Franceschini 2001[262], Valdes et al. 2005[339]).

To avoid this eventual bias with the intrinsic luminosity of the source, we have revisited the relation between L_{IR} and L_8 making use of two well studied local samples of galaxies that, all together, span about five order of magnitudes in infrared luminosity.

We have combined a well studied local (U)LIRGs sample (Vega et al. 2008[351]) with that of a nearby galaxies sample from the Spitzer Infrared Nearby Galaxies Survey(SINGS) (Dale et al. 2007[89]). The local (U)LIRGs sample contains objects with infrared luminosity between $10^{11} \lesssim L^8 \lesssim 2 \times 10^{12}$ $L_\odot$. It has been drawn from the original sample of compact ULIRGs (Condon et al. 1991[74]) and it is characterized by a well sampled SED from the NIR to the radio wavelengths. The corresponding SEDs have been thoroughly analyzed by Vega et al. (2008)[351] with GRASIL synthesis code (Silva et al. 1998[308]). Vega et al. were able to derive the environmental parameters of these galaxies among which the current SFR, the dust obscuration and the fractional contribution of the total FIR luminosity possibly coming from the AGN. They also provide the best fit model SED from which we have derived both L_{IR} and the rest frame L_8. For the SINGS sample, we computed the 8μm rest frame luminosity directly from the Spitzer IRAC 8μm band while the IR luminosity was obtained by fitting the Spitzer MIPS 24, 70 and 160μm fluxes and the SCUBA 450 and 850μm fluxes, when available, with two

modified black body spectra. In both cases we have minimized the possible effect of the non stellar contribution by a central black hole excluding from the local (U)LIRGs sample those galaxies with an estimated AGN contribution to the 1-1000μm luminosity larger than 10 percent and discarding, from the SINGS sample, those galaxies which are identified as Seyferts or LINERs. The resulting sample consists of 54 galaxies with infrared luminosity ranging from 10^7 to a few $10^12 L_\odot$ of which 16 galaxies belong to the local (U)LIRGs sample and 37 belong to the SINGs sample, respectively.

The relation obtained between L_8 and L_{IR} is plotted in Figure 2.5, where filled circles represent the (U)LIRGs sample and the open circles the SINGS sample, respectively. The best fit between L_8 and L_{IR}, represented by the solid line, is a nearly linear relation:

$$log[L_{IR}/L_\odot] = (0.98 \pm 0.03) \times log[L_{8\mu m}/L_\odot] + 1.\ 33 \pm 0.25\ , \tag{2.4}$$

In the same figure we compare our relation with few other published relations found in the recent literature. Notice the very good agreement with the recent relation derived by Reddy et al. (2010)[270], though the latter tend to slightly overestimate the FIR luminosity in the domain of ULIRGs. On the other hand all other relations plotted in the figure, but the one by Bavouzet et al (2008)[17], though reproducing the (U)LIRGS data tend to severely underestimate the FIR luminosity of less active galaxies. The relation by Bavouzet et al (2008)[17] match our data only at intermediate luminosities.

The empirical relation plotted in Figure 2.5(Equation 2.4) indicates that in star forming galaxies, the luminosity at 8μm is an almost fixed fraction of the total infrared luminosity, independently of the galaxy type. Said in more physical grounds, it tells us that an almost constant fraction of the luminosity, $\sim$5%, is reprocessed by *hot dust*.

This is quite surprising given the large variety of galaxy environments where dust reprocessing is operating. Suffice here to recall that while in normal spirals the attenuation of massive stars drops significantly after a few Myr, as deduced for example from the observed location of the bluest side of the main sequence in the HR diagrams, in ULIRGs they may remain embedded in the parental clouds for the entire age of the starburst. There are many examples of the so called "molecular cloud dominated" SEDs in the (U)LIRGs sample (see Vega et al. 2008[351] and Vega et al. 2005[352] for a detailed discussion). Thus while in (U)LIRGs dust reprocessing mainly happens within dense molecular clouds for almost the whole duration of the burst, in less active galax-

ies dust reprocessing after a few Myr is mainly due to a more diffuse dust component (the "cirrus"). These two very different environments where dust reprocessing operates bears on the MIR spectral shape. The MIR emission from dense molecular clouds is due to hot dust in the very inner regions of the clouds while that of the diffuse component is characterized by the presence of prominent polycyclic aromatic hydrocarbon (PAH) complexes, with one of such complexes being centered at 7. $7\mu m$.

At high infrared luminosity, the $8\mu m$ emission originates from the hot dust in the inner regions of the dense molecular clouds while at low infrared luminosity the $8\mu m$ emission originates from the excitation of PAHs in the diffuse dust component. Thus even if two different mechanisms are at work, the 8μm rest frame luminosity, L_8, remain a very good proxy for L_{IR}, both at low and high luminosity.

2.2.4 The SED-inferred infrared luminosity

We will now use Eq. 2.4 to obtain the infrared luminosity of the galaxies detected at 24μm ($z < 3.\ 0$). This *observed* infrared luminosity will thus be compared with the SED-inferred infrared luminosity.

Galaxies detected at 24μm have typical redshift z$\sim$2 and their rest frame spectra span the wavelength range from UV at around 1000Å to $\sim 8\mu$m. Therefore we expect that the galaxy SEDs at shorter wavelengths are significantly affected by dust absorption, while at $\sim 8\mu$m they are dominated by the radiation from thermal dust.

Dust absorption and re-radiation in galaxies is a quite complex process. A detailed description would require to exploit dust composition, including chemical composition and grain size, dust and star distribution in the galaxy under scrutiny and the solution of the radiative transfer equation (see e. g. Mathis 1990[218]; Dwek 1997[100]; Silva et al 1998[308]; Draine 2003[97]). Although dust and stars are mixed in galaxies (in various configuration) , it is possible to describe the light attenuation in terms of "effective extinction", i.e. the extinction that would absorb the total light of the galaxy by a dusty screen giving the same amount of attenuation as the dust actually present within the galaxy. By introducing this attenuation term (which has an attenuation curve different from the actual extinction curve of dust in the galaxy) , it is possible to describe the dust attenuation with the simple relation:

$$L_{obs} = L_S(\lambda)10^{-0.4A_\lambda} \tag{2.5}$$

where $L_S(\lambda)$ is the intrinsic stellar specific luminosity and the attenuation $A_\lambda = k_\lambda E(B-V)$ is the product of the attenuation curve k_λ and of the color excess E(B-V).

The luminosity absorbed by dust is then

$$L_{abs} = \int_0^\infty L_S(\lambda)[1 - 10^{-0.4A(\lambda)}]d\lambda; \tag{2.6}$$

Since most of this energy is in fact re-radiated in the wavelength range 20-200 μm we have, from energy conservation, that the infrared luminosity is

$$L_{IR} \backsimeq L_{abs} \tag{2.7}$$

The SED fitting technique allow us to derive separately the quantities $L_S(\lambda)$ and $A(\lambda)$ so that, at the end of the procedure we can easily compute L_{abs}, and thus obtain the SED-inferred infrared luminosity, L_{IR}.

We can now compare the SED inferred infrared luminosity to that estimated by means of equation 2.4, for the 135 objects of our sample that have been detected at $24\mu m$. Since we are dealing with galaxies at redshift $\sim$2, their $8\mu m$ rest-frame luminosity can be derived from the observed $24\mu m$ flux, k-corrected using the average mid-IR spectral shape of local starburst galaxies, as estimated by Reddy et al. (2006)[272]. We will refer to this quantity as the *observed* L_8.

We plot in figure 2.6 the relation between the *observed* L_8 luminosity and the SED L_{IR}, derived from the best fit parameters and the corresponding attenuation, as described in Appendix B. In Figure 2.6 we split our sample according to the total infrared luminosity, namely $L_{IR} > 10^{12} L_\odot$ (solid red) for ULIRGs, $L_{IR} \leq 10^{12} L_\odot \geq 10^{11}$ (solid blue) for LIRGs and $L_{IR} \leq 10^{11} L_\odot$ (solid green) for LOW-L galaxies. This criterium translates into bins in L_8 luminosity.

Superimposed to our data are the same relations plotted in Figure 2.5.

Though the points distribute around relation 2.4, the scatter is **much** larger than that of Figure 2.5 and there is a clear trend of underproducing L_{abs} at increasing *observed* L_8. At the brightest luminosities, about half of the galaxies are a factor of $\gtrsim 5$ below L_{abs} suggested by relation 2.4. On one side the large L_8 and bolometric luminosity of these objects are witnessing large SFR and, on the other hand, the high ratio between the FIR luminosity (deduced from L_8) and the observed UV luminosity indicate strong UV attenuation ($A_{1600} \gtrsim 3$, see below). In those objects the emerging UV radiation may

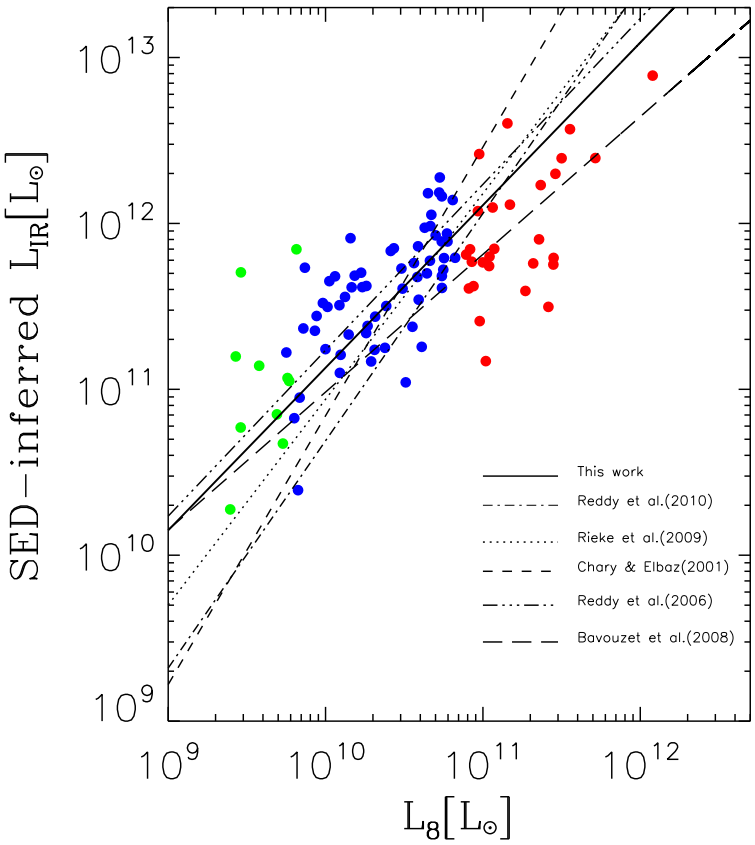

Figure 2.6: Comparison of the SED-inferred infrared luminosity and the $8\mu m$ *observed* luminosity $L_{8\mu m}$. The former is computed from the best fit model assuming constant SFR and a Calzetti attenuation law. Data points are colored following their bolometric luminosity, $L_{bol} > 10^{12} L_{\odot}$ (red) for ULIRGs, $10^{12} L_{\odot} \geq L_{bol} \geq 10^{11} L_{\odot}$ (blue) for LIRGs and $L_{bol} < 10^{11} L_{\odot}$ (green) for low luminosity (LOW-L) galaxies. Overplotted calibrations are the same of Figure 2.5. There is a spread of $\sim$ two order of magnitudes in the derived SFR over the entire range of $8\mu m$ luminosity.

not even directly mirror the global attenuation of star formation process, because it may originate in regions that are occasionally located in a less dust enshrouded ambient, or in a few regions where young stars emerge from the dusty ambient in a relatively shorter time scale (Silva et al 1998[308]; Panuzzo et al 2003[250]). Local examples of strongly extinguished star forming regions are the ULIRGs, for which the average attenuation in the NIR may reach several tens of magnitudes (Vega et al. 2008[351]). When the attenuation is so high, a few regions relatively transparent to UV radiation can largely affect the estimate of the absorbed luminosity from observed SED, lowering the predicted absorbed luminosity. This effect shifts the estimated absorbed luminosity below the value expected by extrapolating the relationship holding for galaxies with lower average attenuation. In such galaxies the bulk of IR luminosity and the bulk of UV luminosity

could originate from different regions, as found in nearby starburst galaxies (Goldader et al 2002[131]).

At the fainter edge the galaxies distribute according to relation 2.4 indicating that, to a first approximation, the Calzetti law is appropriate for normal star-forming galaxies out to $z \sim 2$. However the scatter remain too large in comparison with that of Figure 2.5. In this case we cannot invoke the same mechanism of before, i. e. that a significant fraction of the SF may remain hidden at UV wavelengths, because this effect should become less problematic as the bolometric luminosity decreases. In fact, in some objects the predicted SFR is even larger than that expected from the corresponding L_8, in some cases by even an order of magnitude. Thus other possibilities have to be considered such as the validity of the Calzetti law or the method of fitting the data.

2.2.5 The observed IRX-β relation in z$\sim$2 galaxies

The comparison of the observed infrared luminosity with that derived from the SED fitting indicates that though at a first glance the fits look reasonable, the models fail to reproduce the correct bolometric luminosity and hence the correct star formation rate and attenuation. It is remarkable that in some cases the fitting technique predicts a far infrared luminosity which is larger than the observed one.

This is a critical point because it indicates that even the shape of the adopted attenuation law may be wrong. Indeed in some cases, the observed shape of the UV/optical continuum seems to require a total attenuation larger than that allowed by the observed infrared luminosity. Say in other words, we have hints that also the form of the real attenuation curve may be different from the adopted one.

To better highlight this point we have used the observed IR luminosity and the continuum UV flux, to check the IRX-β relation of our sample. For a sample of local starburst galaxies, Meurer et al. (1999)[227] in fact have pointed out a tight correlation between the IR-to-UV luminosity ratio L_{IR}/L_{UV} and the rest-frame UV slope β_{UV}, which is known as IRX-β relation. For all the galaxies detected at 24μm we have calculated the slope β_{UV} by performing a linear fit to all available photometric data with rest-frame central wavelengths falling in the range 1250Å $-$ 2600Å. For instance, U_{VIMOS}, *F435W* (B-band), *F606W* (V-band), and *F775W* (i-band), if available, were used for the galaxies at z$\sim$2. We have used L_{1600}=λ(1600)L$_\lambda$(1600) as an approximation of the observed

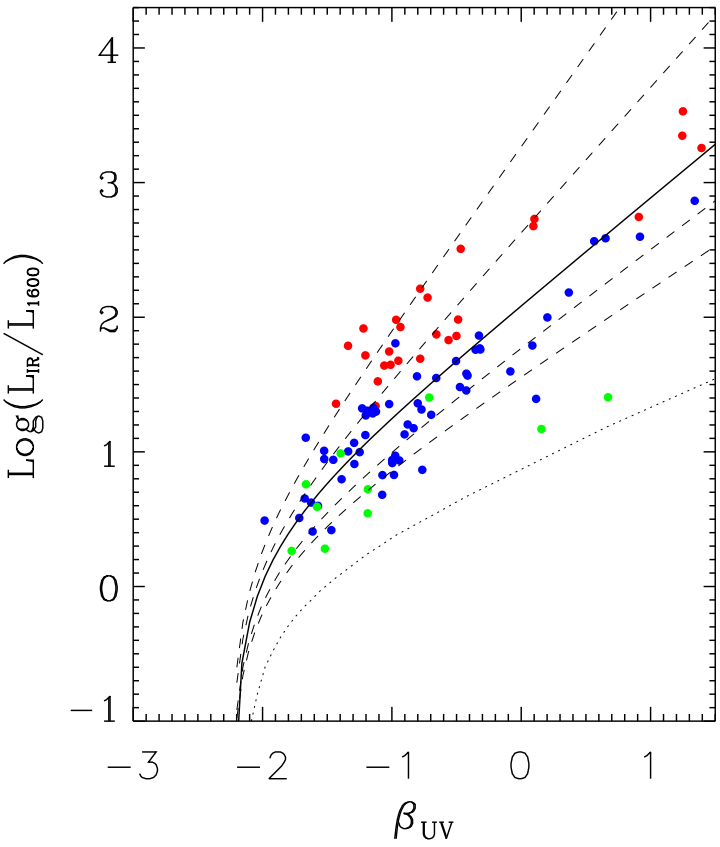

Figure 2.7: The rest-frame IRX $-\beta_{UV}$ relation of the z selected galaxies. Data points are splitted by their bolometric luminosities($L_{bol} > 10^{12}L_{\odot}$:red; $L_{bol} \leq 10^{12}L_{\odot} \geq 10^{11}$:blue; $L_{bol} \leq 10^{11}L_{\odot}$: green). The solid line shows the local Meurer relation while the dotted line the corresponding relation obtained adopting the SMC extinction law (e. g. Bouchet et al. 1985[34]). The dashed lines have been obtained by changing the parameter R_V, which measure the total (A_V) to selective E(B-V) extinction, in the Calzetti law. R_V ranges from 1. 5 (bottom dashed curve) to =10.

L_{UV}. It is worth noticing that the far infrared luminosity, the UV luminosity and the slope so obtained are all model independent.

The resulting IRX-β relation of our $z \sim 2$ sample is shown in Figure 2.7. We find that the normal star-forming galaxies at $z \sim 2$(blue points) follow the local Meurer relation. It's consistent with the results of Reddy et al. (2006, 2010)[272][270], whose samples are also at $z \sim 2$. For the typical star-forming galaxies, the holding of IRX-β can be understood most simply as a sequence in the overall dust content of the galaxies(Charlot & Fall, 2000[64]). However, the Meurer relation seems to be the lower envelope for the bolometrically luminous galaxies with $L_{bol} > 10^{12}L_{\odot}$. Systematically larger IRX ratios are also found in the local ULIRGs (Goldader et al. 2002[131]), $z \sim 2$ ULIRGs (Reddy

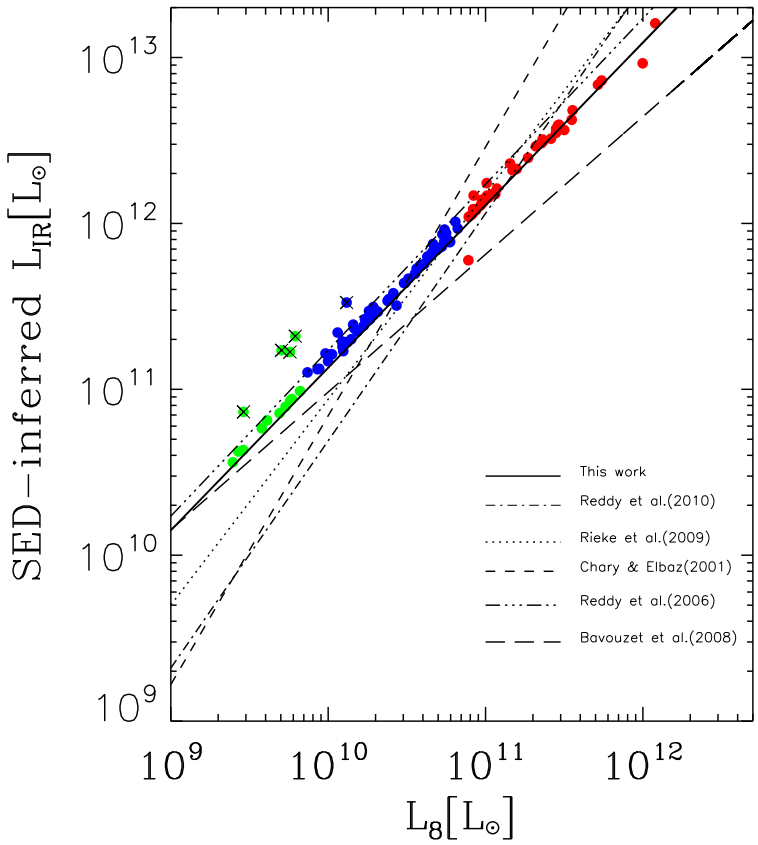

Figure 2.8: Same as Figure 2.6 for best fit models constrained by the *observed* infrared luminosity. To stress the quality of the fitting procedure and only in this figure, a 5% error in the L_{IR} has been assumed, instead of the true error.

et al. 2010[270]) and radio-selected SMGs (Chapman et al. 2005[62]). This bias is generally attributed to the fact that significant amounts of star formation are completely obscured in the UV and the observed UV photons come from the older stellar population, which formed before the starbursts and have escaped from the molecular clouds (Reddy et al. 2006[272]; Papovich et al. 2006[251]; Chapman et al. 2005[62]).

In the same figure we have plotted the result obtained by using different attenuation curves. The dashed lines have been obtained by changing the parameter R_V, which measures the total (A_V) to selective A_B-A_V extinction, in the Calzetti law. The values range from R_V=1. 5, for bottom dashed curve, to R_V=10, for the top curve. The dotted line represents the relation obtained adopting the SMC curve (Bouchet et al. 1985[34]).

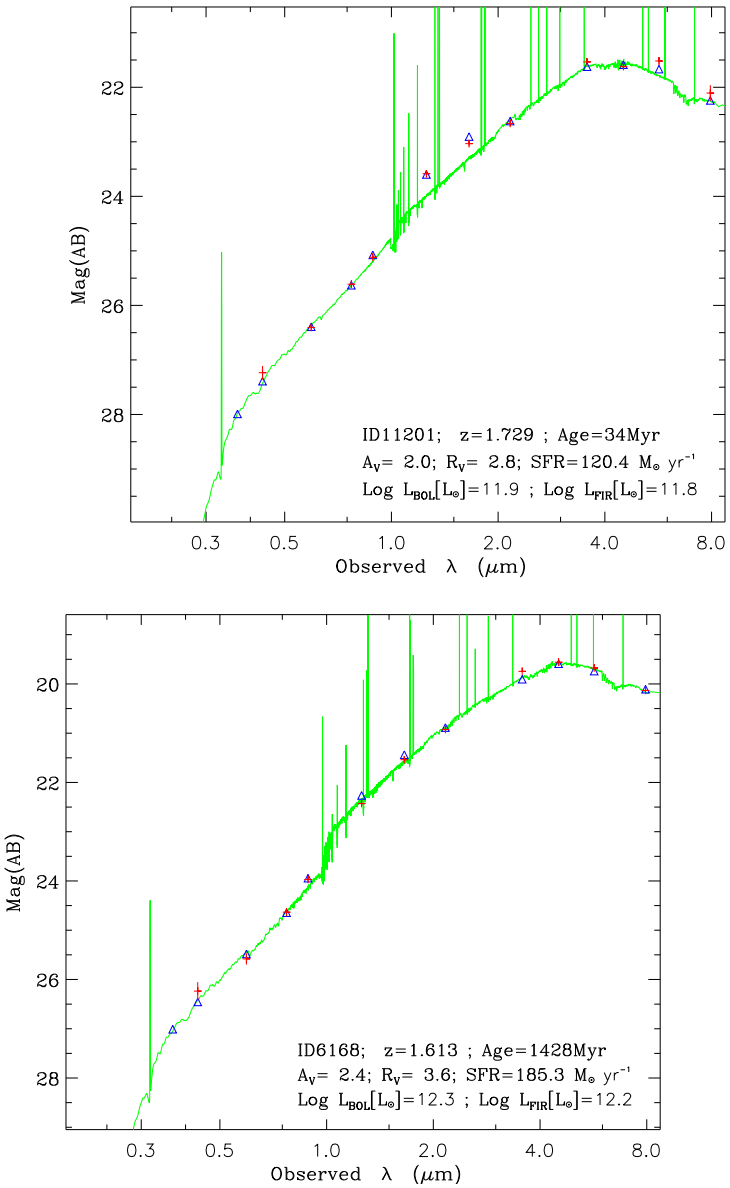

Figure 2.9: Best SED fitting models assuming the far infrared prior and a variable R_V ratio in the attenuation curve. The fit is forced to reproduce the observed L_{IR} luminosity.

2.2.6 L_{IR} AS A PRIOR FOR SED FITTING

It is evident from the previous discussion that the SED modeling technique suffers from two main limitations. One is the presence of totally obscured star formation and the other is the intriguing interplay between other factors like, age, metallicity and dust/star geometry. The first effect is easily accounted for if we know the FIR luminosity as shown by many relevant studies of the subject. The second effect is more difficult to deal with, if not practically impossible when the galaxy is modeled as a single zone like in our simple procedure. On the other hand the observational constraints are too low to

use more sophisticated models.

In order to complain with the former point we have included the infrared luminosity L_{IR} as a further constraint in our fitting procedure. For the latter point the best thing we could do is to follow the *observational* evidence that in the IRX-β diagram galaxies are consistent with different *attenuation* laws.

The code has been modified to allow the calculation of the absorbed luminosity and to let the model to treat this value as a constrain of the minimization (e. g. Mayya et al 2004[220]). The observed infrared luminosity has been normalized to the luminosity in a selected reference band with the ratio $L_{IR}/(\lambda_e \times L_{\lambda_e})$. The relation between intrinsic (rest frame) and observed quantities is simply

$$\lambda_e \times L_{\lambda_e} = 4\pi D_l^2 \lambda_o \times f_{\lambda_o} \tag{2.8}$$

where λ_e=λ_o/(1+z) and f_{λ_o} are the observed fluxes and L_{λ_e} is the specific model luminosity computed in the de-redshifted normalization band.

Thus the observed ratio is

$$IR_O = \frac{L_{IR}}{4\pi D_l^2 \lambda_o \times f_{\lambda_o}} \tag{2.9}$$

while the corresponding model prediction is

$$IR_M = \frac{L_{abs}}{\lambda_e \times L_{\lambda_e}} \tag{2.10}$$

At the same time we have treated the R_V ratio of the attenuation law as a free parameter in the fitting procedure. The reddening curve $k(\lambda)$ is the Calzetti-like form (Calzetti et al. 2000[54]):

$$\begin{aligned} k(\lambda) &= 2.659\ (-1.857 + 1.040/\lambda) + R_V \qquad 0.63\ \mu m \leq \lambda \leq 2.20\ \mu m \\ &= 2.659\ (-2.156 + 1.509/\lambda - 0.198/\lambda^2 + 0.011/\lambda^3) + R_V \\ & \qquad 0.12\ \mu m \leq \lambda < 0.63\ \mu m. \end{aligned} \tag{2.11}$$

R_V was let to vary within the range 1.5≤R_V≤10 as shown in Figure 2.7.

By exploiting the L_8-L_{IR} together with the simultaneous fit of all other photometric band, we are able to constrain in a fairly robust way the stellar population parameters characterizing our z∼2 z_{850} selected galaxies.

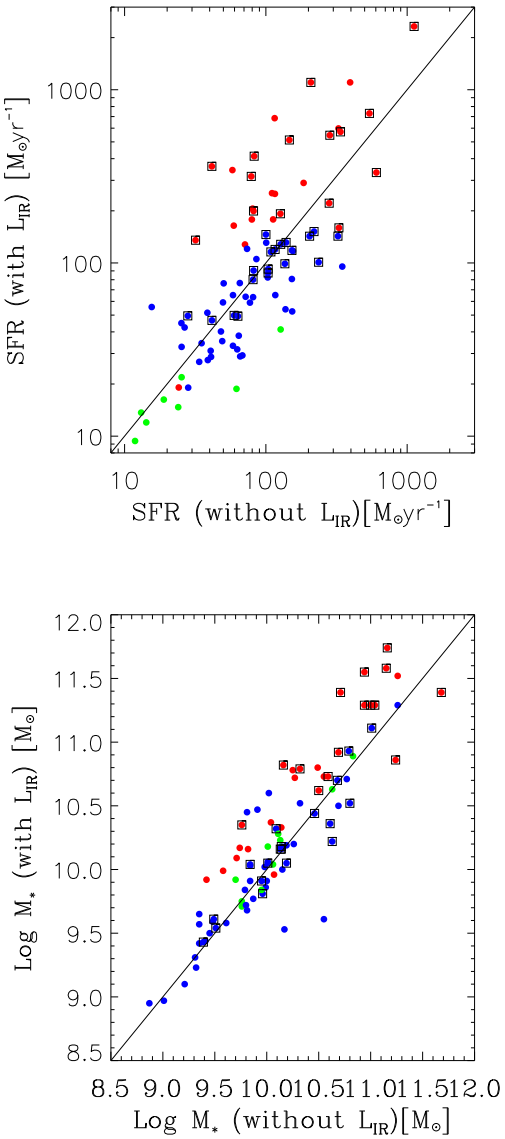

Figure 2.10: Left panel: comparison between the star formation rates derived with and without imposing the L_{IR} prior. Right panel: comparison of the masses derived with and without the far infrared prior. Data with error on the 24μm flux $\leq$ 15% have been surrounded by boxes.

- The SFR. The far infrared luminosity is a prior that provides the unbiased level of the SFR. For a given IMF, the error on the SFR is mainly observational, though there is some dependence on the for of the adopted law and on the metallicity of the stellar populations, as already discussed by Shapley et al. (2005)[301]. Determining the correct shape of the SFR will require by far additional information, such as spectral emission and absorption lines and thermal and non-thermal radio continuum emission. These effects probe the different contribution of the stellar populations of different ages and can be used, in principle, to disentangle the correct form of the

SFR (e. g. Bressan et al. 2002[47], Vega et al. 2008[352]).

- The attenuation. With the SFR essentially determined by the far infrared luminosity, the observed UV continuum mainly fixes the level of attenuation. This is also a quite robust result because the far infrared luminosity is mainly produced by the absorbtion of the UV light.

- The Age and the mass. The observed SED from the UV to the near infrared is the result of the combination of the form of the attenuation and the age of the galaxy. There can be some level of degeneracy between age, metallicity and shape of attenuation, but the number of constraint is also quite high.

A check of the whole fitting procedure is shown in Figure 2.8. In constructing this figure we deliberately assigned an error of 5% to the infrared luminosity, this figure is only meant to show the ability of the procedure to recover the input far infrared luminosity. It is also worth noticing that, using only the L_{IR} prior but adopting a fixed attenuation law, did not produce a significant improvement in the results. Indeed in several cases, imposing the FIR luminosity resulted in a very poor fit of the global SED.

The SED fit is in general very good. There are however still a few galaxies for which the predicted value of the FIR is different than the observed one. These are mainly low luminosity galaxies, where, the reddening deduced from the UV-NIR SED would require a higher global attenuation producing a far infrared luminosity twice as larger than the observed one. An inspection of Figure 2.7 shows that these galaxies lie near the region covered by the SMC law, with a high UV slope, β, and a correspondingly low IRX ratio. For these few galaxies we have repeated the whole procedure with the SMC attenuation law, and then their FIR is very well reproduced.

It is interesting to note the presence of objects for which the standard SED fitting technique overestimates the far infrared flux by even a significant factor. In these objects the reddening deduced from the UV-NIR SED, if interpreted by means of the usual Calzetti law would require a higher global attenuation producing a far infrared luminosity twice as larger than the observed one.

The comparison of the SFR derived from the best fit models obtained with and without the far infrared prior is shown in the left panel of Figure 2.10. The dispersion increases at increasing star formation and for the $\mathrm{L}_I R$ brightest objects the SFR can be underestimated by even an order of magnitude. At intermediate and low luminosities the SFR is on the

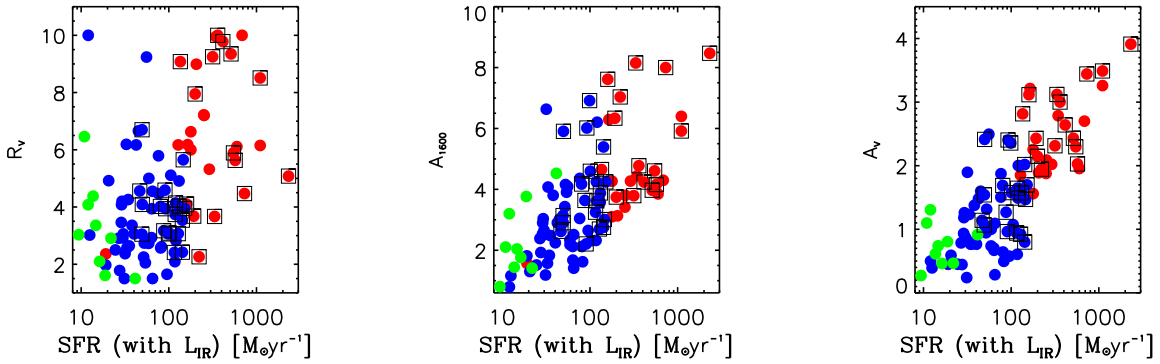

Figure 2.11: Dependence of the selective to global attenuation (R_V), UV (A_{1600}, middle panel) and visual (A_V, right panel) attenuation, on the star formation rate.

average slightly underestimated.

The right panel of the same Figure shows the comparison of the masses. Here the mass is the integral of the SFR over the age of the galaxy and it does not take into account the mass returned into the interstellar medium due to stellar wind and SN explosion. The different sub-samples are colored as in Figure 2.6 and data with error on the 24μm flux $\leq$15% have been surrounded by boxes. We see from this panel that the fitting technique commonly adopted (that without the L_{IR} prior) underestimates the total mass by an average factor of about 50%. Individual values may be offset by even a factor of 4.

2.2.7 Physical properties of z_{850}-selected galaxies at z$\sim$ 2

We start the discussion by considering one of the basic assumptions in our fitting technique, the R_V ratio in the attenuation law, that we treat as a free parameter.

The run of the R_V ratios as a function of the star formation rate is shown in the left panel in Figure 2.11. There is a broad tendency of R_V to increase with the strength of the SFR but the scatter, at a given value of the SFR, is quite large. The value of R_V for the Calzetti law is $R_V \sim 4$. At increasing R_V the attenuation law becomes progressively flatter, i. e. more neutral. In particular, while for a typical Calzetti law the ratio of the attenuation in the K and V band is $A_K/A_V \sim 0.1$, for R_V=10 $A_K/A_V \sim 0.6$. This mens that the attenuation in the K band is not more negligible with respect to that in the visual band, as usually found. Several ultra luminous sources are well fitted by $R_V > 4$ or by an attenuation law which is more neutral than the typical Calzetti law. Indeed it is well known that in local ULIRGs the molecular clouds associated with the star

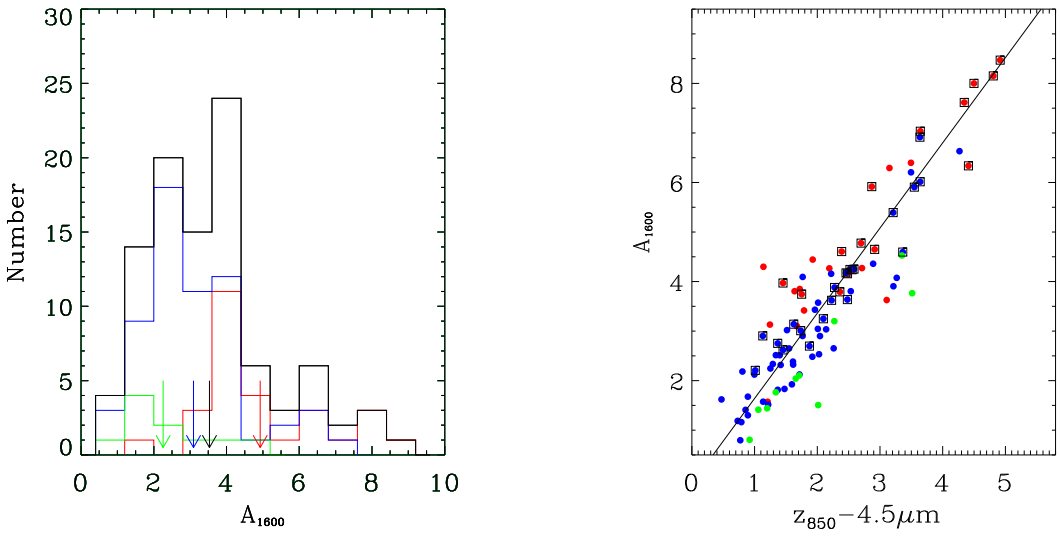

Figure 2.12: Left panel: distribution of the UV attenuation ($\sim$ 1600Å). Arrows indicate the average value of global sample (black, A_{1600} $\sim$3. 3 mag) and of the sub-samples. Right panel: The relation between dust attenuation at 1600Å and the colour $z_{850} - 4.5\mu m$.

forming regions may be optically thick even at the mid infrared wavelengths (Vega et al. 2008[351]). Thus, in order to reproduce the *observed* far infrared luminosity together with the observed UV slope, a flatter attenuation law is required, otherwise the spectral shape would be too steep. We remind here that our parametrization is only meant to be a good description of the attenuation resulting from the combination of different processes such as age dependent extinction, geometrical effects, including eventual holes along the line of sight, and even real differences in the dust mixture.

In the middle and right panels of Figure 2.11 we show the relation between A_{UV} and A_V with the star formation rate. In both cases the attenuation grows with the SFR as found by other authors. It is interesting to note that the dispersion decreases significantly when we move from the ultraviolet band to the visual band.

The distribution of the UV attenuation is shown in the left panel of Figure 2.12. The average attenuation in the UV is $\simeq$ 3. 3 mag and the maximum value is $\simeq$ 9 mag.

We have also searched for other possible indicators of dust attenuation, trying to exploit on one side the wide baseline coverage of the data and, on the other, the fact that we have been able to derive quite accurate estimates of the bolometric luminosity. These indicators could be possibly used whenever any rest frame data beyond NIR is lacking.

For our sample we found a tight correlation between the UV attenuation and the $z_{850} - 4.5\mu$m colour, as shown in Figure 2.12. The colored symbols are the same

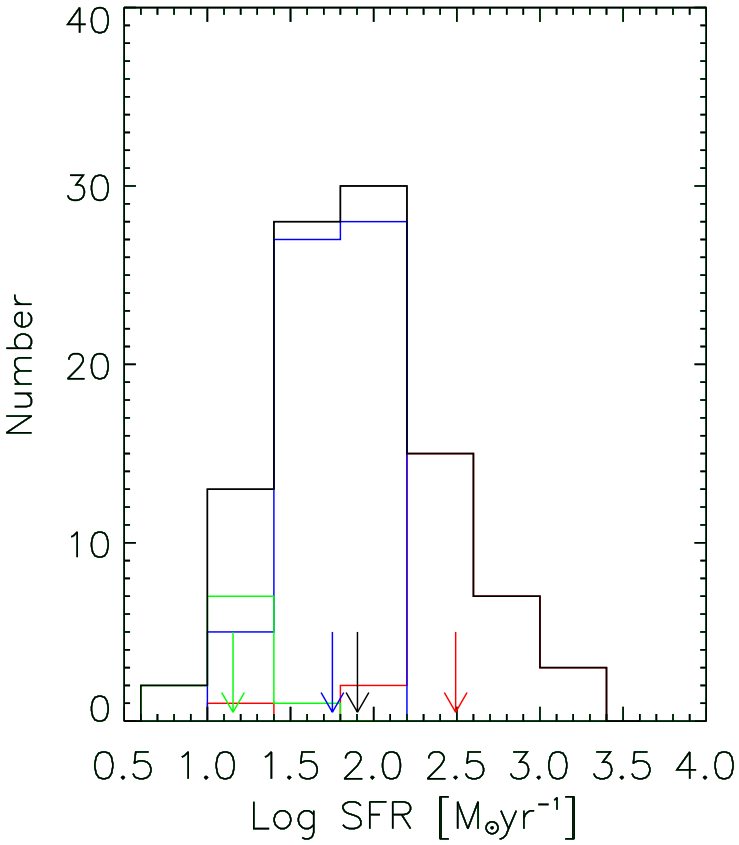

Figure 2.13: Distribution of the star formation rates in our z selected galaxy sample. Arrows mark the average value of the full sample (black, SFR=80$M_\odot$/yr) and of the sub-samples selected as in Figure 2.6.

as in the left panel of Figure 2.7. Using the expectation-maximization(EM) algorithm which is implemented in the ASURV statistical software package(Isobe et al. 1986), we perform linear regression on our whole sample, including $24\mu m$ detected and undetected sources. Our best fit is (solid line):

$$A_{1600} = (-0.65 \pm 0.16) + (1.\ 59 \pm 0.07)(z_{850} - 4.\ 5\mu m) \tag{2.12}$$

It is worth noticing that, in contrast with the UV slope, the $z_{850} - 4.\ 5\mu m$ colour is relatively insensitive to the form of the attenuation law.

In the absence of any prior on the star formation rate we may use equation 2.12 to obtain the UV attenuation and, after correcting for attenuation the UV luminosity, we can use a suitable calibration to obtain the star formation rate.

The distribution of the star formation rates in our galaxy sample is shown Figure

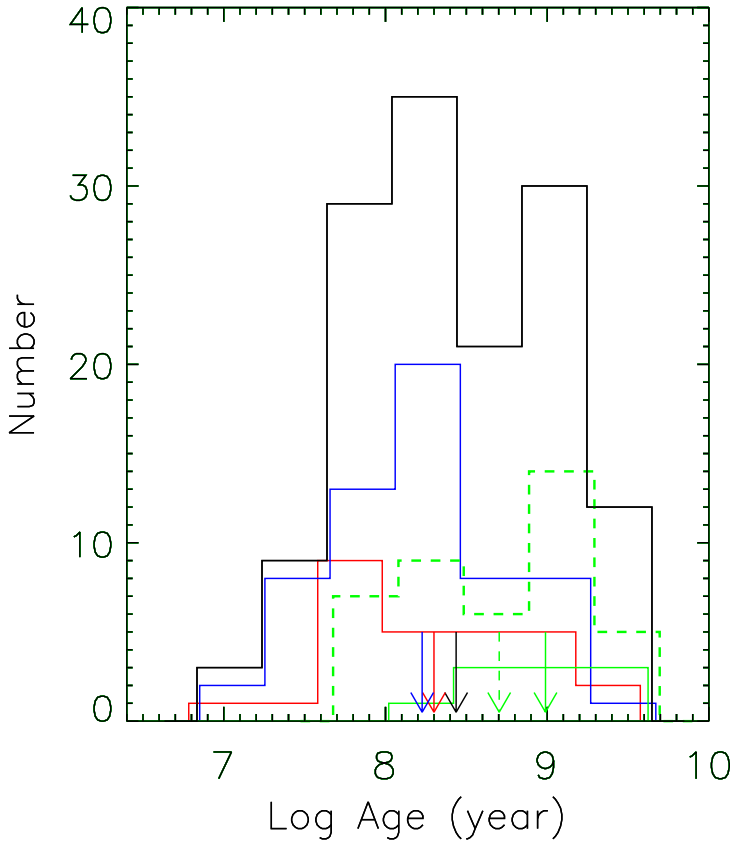

Figure 2.14: Age distribution of our sample galaxies. The arrows indicate the average values of global sample (Age=270 Myr) and of the subsamples, color coded as in Figure 2.6. The thick shaded histogram represents the age distribution of 24μm undetected galaxies as discussed in the text.

2.13. The primary selection in the z band allows us to detect galaxies with a wide range of star formation rates, from a few $M_\odot$/yr to $\geq 10^3$ $M_\odot$/yr. However the further selection at 24μm, imposes a threshold at about 10 $M_\odot$/yr. Since the depth of the 24μm observations is not the same in the different fields, the exact value of this threshold is somewhat variable. This will be discussed in a following section.

The average value of the final sample is SFR$\sim$80$M_\odot$/yr (black arrow in the Figure). Average values of the sub-samples selected following the total far infrared luminosity, are also shown.

In Figure 2.14 we plot the age distribution of the sub-samples selected according to the total infrared luminosity, namely $L_{IR} > 10^{12} L_\odot$ (solid red) for ULIRGs, $L_{IR} \leq 10^{12} L_\odot \geq 10^{11}$ (solid blue) for LIRGs and $L_{IR} \leq 10^{11} L_\odot$ (solid green) for LOW-L galaxies.

Figure 2.14 shows that the lower limit to the ages of ULIRGs and LIRGs are not

significantly different and, perhaps more important, they are quite young. In both classes, very young objects can be detected with ages of only a few 10 Myr. This implies that a significant amount of dust must already be formed in such a short time.

The distribution of ULIRGs is significantly flatter than that of LIRGs but, in both cases objects as old as about 2 Gyr have been found. The average age of their distribution is $\sim$ 180 Myr (red and blue arrows in the figure)

In contrast the distribution of the less luminous galaxies (solid green line) is skewed toward significantly older ages, with an average age of $\sim$ 1 Gyr. From figure 2.14 we notice that these objects have the lowest star formation rates as detected from the combined SED analysis. Thus one possibility is that low star formation rates can be maintained for a longer time as if the star formation efficiency were lower. For instance, in the case of the downsizing scenario, low mass objects looks younger because their lower star formation rate lasted for a longer time and not because they *formed* later. So one possibility is that we could have selected the brightest tail of the lower mass galaxies that, because of the downsizing effect, have formed at earlier epochs.

Another possibility is that this effect arises because of our selection criteria. The sample is originally selected in the z band. With the further addition of the the 24μm criterion we exclude objects with SFR $\leq$20 $M_\odot$/yr and we put in the low luminosity class objects with SFR around the above threshold (see figure 2.13). But in order to be selected in the z band, an object with a low SFR must be relatively old so that its mass is at least comparable with that of higher star forming objects. This could favor the selection of older objects i. e. objects with larger t=M_{tot}/SFR.

To better clarify this point we may consider the mass distribution, shown in Figure 2.15. The masses range from M$\sim 10^9 M_\odot$ to M$\sim 4\times 10^{11} M_\odot$. Ultra luminous galaxies have a quite flat mass distribution up to the higher values and an average mass of M$=1.2 \times 10^{11} M_\odot$. In contrast LIRGs and LOW luminous galaxies show a well defined peak around M$\sim 10^{10} M_\odot$ and a very similar average value M$\sim 2\times 10^{10} M_\odot$.

Since LOW-L galaxies can be as massive as the more luminous LIRGs sources, it is likely that the above result arise from our selection criteria. However their number is really small and, to draw more robust conclusions it will be desirable to extend the above analysis to the full z selected sample. We remind that with the 24μm threshold we have cut about half of our original z selected sample, and the majority of the excluded object are of course low star forming objects.

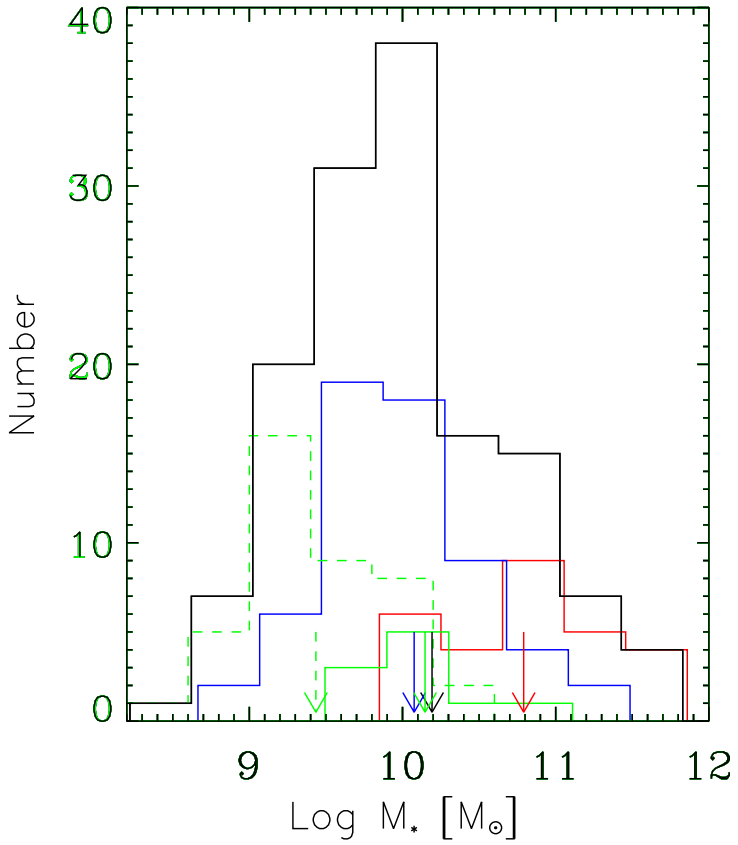

Figure 2.15: Distribution of the masses in our z selected galaxy sample. Arrows mark the average value of the full sample (black, M=1.6×$10^{10}$$M_{\odot}$) and of the sub-samples color coded as in Figure 2.6. The dashed histogram represents the mass distribution of 24μm undetected galaxies as discussed in the text.

The 24μm luminosity was used as a prior in our fitting procedure to provide more reliable values of the physical parameters of the galaxies, especially when the obscuration is high. However we notice from Figure 2.10, that for the low luminosity sample the prior knowledge of the infrared luminosity is not so important as for the high luminosity galaxies. In the former domain, the star formation rates obtained *without* assuming the L_{IR} prior are actually even slightly overestimated. The reason behind this effect is that the R_V adopted in the standard fitting procedure, that of the Calzetti law, is larger than that characteristic of low star forming objects. Indeed the median value of R_V for objects with SFR $\leq$30 $M_{\odot}$/yr is $R_V \sim 2.5$. When repeated with such value of R_V the fits without L_{IR} prior reproduce fairly well those with the L_{IR} prior.

Thus we may use the standard procedure for the analysis of the sub-sample of galaxies undetected at 24 μm, provided that we adopt a Calzetti law with a lower value of

$R_V \sim 2.5$.

We notice that the fits of the SEDs of these galaxies are not as good as those of the sample detected at 24μm. These galaxies are intrinsically less luminous and the photometric uncertainties are on average larger, being typically between 0.2 mag and 0.5 mag in half of the bands. In several objects the derived SFR is higher than the average threshold imposed by the 24μm criterion, but the object was not detected at 24μm either because of lower exposure depth or because the SED inferred SFR was significantly affected by the photometric errors. We thus excluded from this sample those object with a derived SFR $\geq$30 $M_\odot$/yr for which, according to figure 2.10, the knowledge of the L_{IR} prior is needed.

In total we have 41 objects with $L_{BOL} \leq 10^{11}$. Their age and mass distribution are shown as dashed green histograms in Figures 2.13 and 2.15, respectively.

We now see more clearly that low luminosity objects have older age and lower masses than the rest of the sample. This is expected from a downsizing scenario induced by an anti-hierarchical mass assembly process, i. e. lower mass galaxies on average formed first but their star formation lasted for a longer period due to their inability of getting rid of the gaseous component. The 24μm detected LOW-L galaxies constitute the higher mass tail of the former sample due to the combination of different selection effects.

In Table 2.1 we list a summary of the median properties of our sample, where we have now included also the latter sample of 24μm un-detected LOW-L galaxies.

Table 2.1: Median properties of different sub-samples

	N	SFR $M_\odot$/yr	$M_\star$ 10^{10} $M_\odot$	Age Myr
24μm detected				
ULIRG ($L_{bol} > 10^{12} L_\odot$)	28	316	6.2	177
LIRG ($10^{12} L_\odot \geq L_{bol} \geq 10^{11} L_\odot$)	60	63	1.0	149
Low-L ($L_{bol} < 10^{11} L_\odot$)	10	14	1.5	1386
24μm un-detected				
Low-L ($L_{bol} < 10^{11} L_\odot$)	41	6.6	0.3	627
Total	139	60.3	1.5	187

2.2.8 Mass to light ratios.

In Figure 2.16 we plot the stellar mass vs absolute H band magnitude. In the left panel the plot is done using the observed luminosity and the stellar mass derived from the SED fitting in a 'classical' way (without L_{IR} as a prior) while, in the right panel we

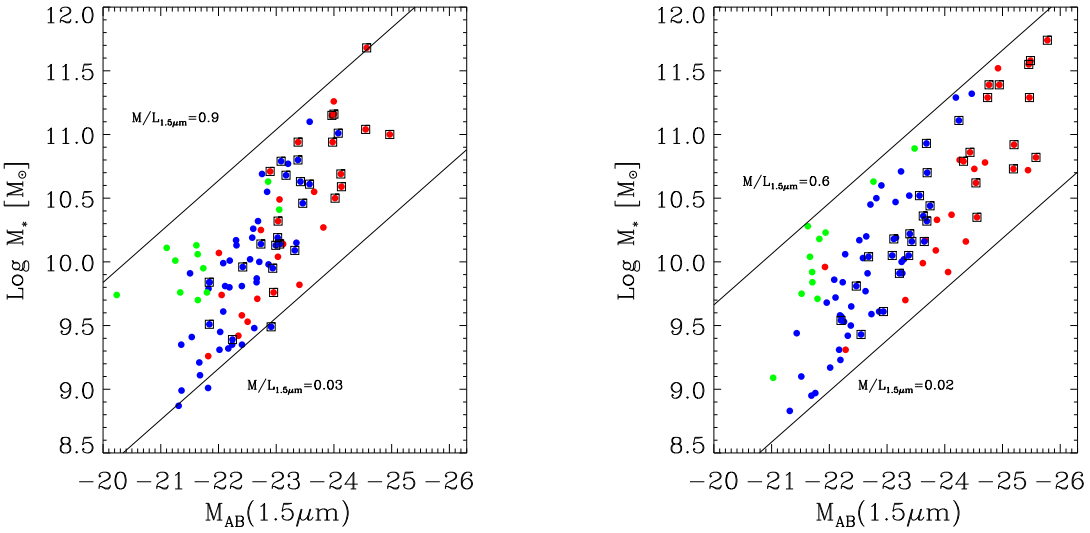

Figure 2.16: Stellar mass vs absolute H band magnitude. Left panel: using the observed luminosity from the SED fitting in a 'classical' way (without L_{IR} as a prior); right panel: intrinsic i. e. after the luminosity is corrected for attenuation as derived from the best fit model (with L_{IR} as a prior).

used the intrinsic luminosity, corrected for attenuation as derived from the best fit model (with L_{IR} as a prior) .

First, we check that the SSP we use can reproduce the observed M/L ratio of the oldest population.We compute for the SSP with the age of 12 Gyr the M/L_K equals to 1.61, which is very close to the value of the local galaxies.

With the 'classical' SED fitting method, the obtained mass to light ratio span a factor of $\geq$ 30 from 0.03 to 0.9, with the higher value close to the local old metal rich systems (see Shapley et al 2005). However, the lowest value of the H band mass to light ratio is only half of that in Shapley et al (2005).This difference may come from the choice of our different SSPs. The SSPs we adopt include the nebular emission (not only line emissions, but also continua). The consideration of nebular emission will have more important effect on the young population than on the old one. When using the SED fitting with L_{IR} as a prior (the H band luminosity corrected for attenuation) the range is lower of $\geq$ 30 from 0.02 to 0.6, and in particular, objects do not reach the high values of local old galaxies (Figure 2.16 right panel). Compared to the left panel of Figure 2.16, the higher value of the mass to light ratio is lower.Using the SED fitting with L_{IR} as a prior instead of the 'classical' method, the stellar mass will increase by a factor of 2 on average.However, the H band luminosity will increase more due to the correction for dust attenuation.As a result, the range of mass-to-light ratio is shorten. In our SED fitting

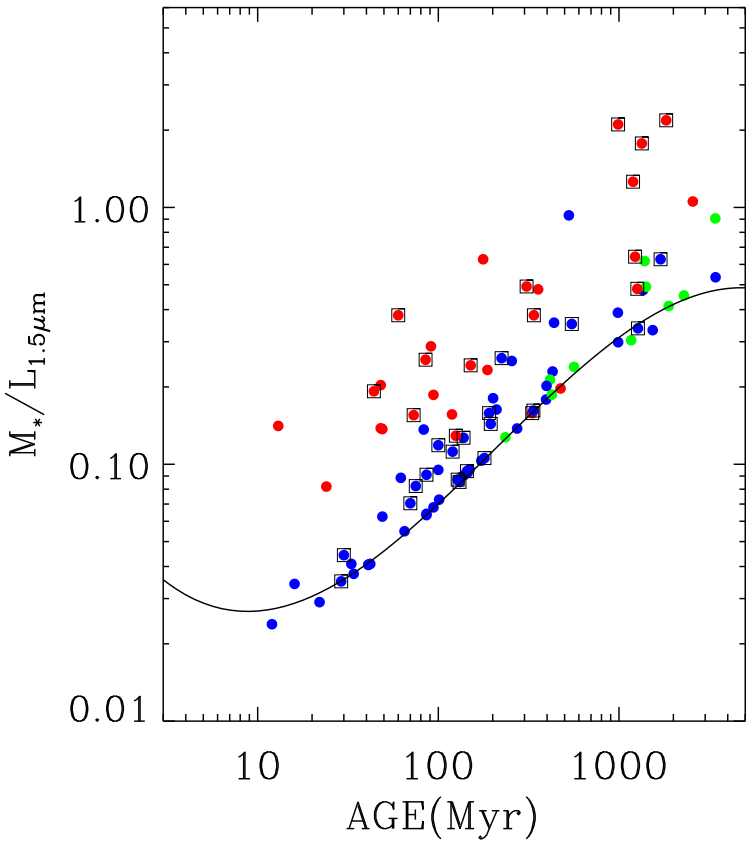

Figure 2.17: Observed mass to light ratio in the rest-frame H band vs age of the galaxy. The solid line represents the locus of the un-attenuated models, i. e. the observed spread at a given age is only due to attenuation, as expected in G04 models.

model with L_{IR} as a prior the former result is caused by attenuation which is large even in the rest frame NIR bands.

Finally, in Figure 2.17 we plot the observed mass to light ratio versus the age of the galaxy. In this figure the data points correspond to the observed luminosity (without correction for dust attenuation) while the solid line represents the locus of the un-attenuated models. The observed spread at a given age is only due to attenuation, as expected in our SED fitting model with L_{IR} as a prior.

2.3 Summary

In this Chapter, we focus our attention on the high redshift UV bright star forming galaxies — the early evolutionary phase of ETGs.

At first, we review the main results in Mao et al.(2007) that the rest-frame UV LF of LBGs can be reproduced by coupling the UV luminosity and halo mass derived from the G04 model with the halo formation rate.

And then, we construct a sample of 298 spectroscopically confirmed z_{850}-band-selected galaxies at redshift $z \sim 2$ from the GOODS-MUSIC sample, with a well sampled SED from the UV to IRAC. This allows the analysis of their physical parameters by means of the usual spectral population synthesis technique. For this purpose we have built the SEDs of a set of simple stellar populations that include also the nebular emission and we have applied our minimization technique adopting a minimum number of free parameters, namely constant SFR from a starting age and age independent attenuation.

The z_{850} selection includes objects with a wide range of SFR, between a few $M_\odot$/yr to 1000 $M_\odot$/yr and with different strengths of attenuation.

Since about half of the sample (135 objects) has been detected at MIPS 24μm with SPITZER and since it has been claimed that the rest frame 8μm luminosity is a quite good proxy of the star formation rate (Reddy et al. 2010) we could check, for the first time for an intermediate redshift sample, the accuracy of the SED fits.

Given the wide range of SFR encompassed by our sample we have derived a new relation between the rest frame 8μm luminosity and the total infrared luminosity, which is normally used as a robust indicator of the star formation rate.

For this purpose we have combined a local (U)LIRGs sample with a sample of normal galaxies and we have re-calibrated a relation between $L_{8\mu m}$ and L_{IR}.

Our first result is thus that

- *We have obtained a new calibration between $L_{8\mu m}$ and L_{IR} which encompasses a range of SFR from a few $M_\odot$/yr to 1000 $M_\odot$/yr (cf. eq. 2.4).*

We have then compared the *observed* 8μm luminosity with that obtained from combining the SED inferred far infrared luminosity (the absorbed light) with our $L_{8\mu m}$ versus L_{IR} relation. This allows, for the first time, a robust check of the star formation rates of high redshift galaxies inferred from SED fits. We find that

- *the standard SED fitting technique is not accurate enough to provide reliable SFR and, correspondingly, attenuation, age and masses of the galaxies.*

There is a large scatter in the predicted vs expected far infrared luminosity (that can reach even a factor of ~ 50).

The discrepancy increases at increasing star formation and, for the L_{IR} brightest objects, the standard technique underestimates the SFR by even an order of magnitude.

Surprisingly, the discrepancy is not limited to the most obscured galaxies, as expected, but it is present also in the low luminosity sample and, in some cases, the predicted SFR from SED is even larger than that inferred from the observed 24μm luminosity.

Without L_{IR} prior the total mass is on average underestimated by an average factor of about 50%. Individual values may be offset by even a factor of 4.

Combining the observed infrared luminosity with the observed UV spectral slope we have also constructed the rest frame IRX-β diagram for this redshift z$\sim$ 2 sample. This diagram is similar to other ones existing in literature and shows a large spread around the average relation of Meurer et al. (1999)[227]. This spread can be well reproduced by changing the ratio R_V between the neutral and the selective attenuation, in the Calzetti law.

We interpreted this fact as a real difference between an attenuation law and an attenuation law, the latter being the result of the combination of many effects, such as an age dependent attenuation, different geometries between dust and stars and possible differences between grain compositions and sizes.

We have thus reanalyzed the 24μm detected sub-sample exploiting these new characterizing features: the knowledge of the total FIR luminosity and the possibility of varying the attenuation law to cope with the previous observational evidence.

Moreover, instead of adopting usual conversions from the L_{IR} to the SFR (e.g. Kennicutt, Panuzzo et al 2003), that hold only in particular conditions (e.g. fixed duration of star formation episode, assumed geometry etc...) we have used the *observed* far infrared luminosity as a constraint in the minimization technique.

As a further result, we have outlined a new method that should be used when the knowledge of the far infrared luminosity can be added to the global SED. The most noticeable difference between the methodology used in the present with respect to previous works rest on

- the use of the far infrared constraint, here derived from the observed 24μm;
- the use of a generalized Calzetti law with variable R_V.

With this new method we could determine in a unprecedent robust way the physical parameters that characterize our galaxies, namely SFR, attenuation and age. These are summarized in the following.

- *Attenuation.*

  There is a general trend of increasing attenuation with SFR, or, equivalently, the un-obscured absolute UV magnitude, but the correlation is not tight. The ratio R_V shows a large scatter at all values of the SFR indicating a variety of concomitant effects that may bear on the combined attenuation low. This was already suggested by our IRX-β diagram but the run of the scatter with the star formation rate is more indicative that these processes appear at any scale.

  The relation between the attenuation and the SFR become tighter toward larger wavelengths. This is consistent with the fact that, in general at shorter wavelengths images show more knotty structures that overall combine to give a different attenuation curve.

  Especially high values of R_V were generally required to fit the SEDs of ULIRGs. In this case the attenuation curve is very flat and the attenuation remains relatively significant even in the NIR. Indeed from the analysis of local ULIRGs, it was expected that a fraction of the star formation could be significantly attenuated even at these long wavelengths.

  For the low luminosity galaxies ($L_{IR}<10^{11}L_\odot$) the knowledge of the L_{IR} prior is not as important as for those with high luminosity. This threshold corresponds to a star formation rate of about $20M_\odot$/yr. However if we use a pure Calzetti low for these galaxies, the standard procedure slightly overestimates the SFR. A more suitable attenuation law is that with $R_V \sim 2.5$. One possible is that in these galaxies the absorption is not isotropic and that a larger fraction of the UV light escapes , not being reprocessed by dust, this results into a SED-inferred SFR(dust-corrected) higher than that inferred from the FIR.

  There is a fair relation of the UV attenuation and the $z_{850}-4.5\mu m$ colour. This could eventually be used to obtain the absolute UV magnitude in absence of a infrared

luminosity prior, but its effective usefulness has not been studied in detail.

- *SFR, ages and masses*

  Our z selected sample includes objects with a wide range of SFR, between a few $M_\odot$/yr to 1000 $M_\odot$/yr. The average SFR of the sample is about 80 $M_\odot$/yr. In this respect the sample complements other samples selected by means of drop-out technique etc....

  The mass distribution ranges from M$\sim 10^9 M_\odot$ to M$\sim 4\times 10^{11} M_\odot$.

  If we take into account the sample of low luminosity 24μm un-detected source there is a strong evidence that the average mass increases at increasing star formation. ULIRGs show a flat mass distribution with a minimum mass of $\sim 1.2\times 10^{10} M_\odot$.

  The age distribution of our sample ranges from a few tens of Myr to more than 1 Gyr. For the first time we can obtain accurate ages of severely obscured high redshift objects with very high star formation rates.

  Low luminosity star forming galaxies detected at 24μm show on average a significantly more prolonged star formation with respect to more luminous star forming objects, though their mass is not significantly different. However the 24μm detection threshold is too heavy for this sub-sample and must be released in order to produce a statistically significant number of objects. By releasing this constraint and using the attenuation law with R_V=2.5 in the standard procedure, we could increase the sub-sample to 41 galaxies. As explained above, for low luminosity objects this method does not affect the accuracy of the results.

  With this increased sample we confirm that low luminosity galaxies harbor, on average significantly older stellar populations and are also less massive than the brighter ones. Those selected at 24μm constitute actually the brightest tail of the Low-L sub-sample. Thus we confirm that the observed downsizing effect is consistent with a picture where less massive galaxies actually form first, but their star formation lasts longer, consistent with the anti-hierarchical galaxy formation scenario.

- *Mass to light ratios*

  We find that care must be taken when dealing with M/L ratios because, while it is customarily assumed that attenuation is scarce at NIR wavelengths, one of the results of our investigation is that this is not the case for luminous high redshift

objects.

After imposing the LIR constraint we find that, in order to fit the whole SED, we need a flatter attenuation curve implying that the attenuation is not negligible at NIR wavelengths. Correspondingly, the NIR M/L ratios obtained after a proper attenuation correction, never reach those of nearby galaxies, as claimed by other authors and remain about a factor of three lower.

The dispersion of the M/L ratios looks independent from the corrected absolute magnitude, without the apparent trend of increasing M/L at increasing luminosity. The latter trend is instead clearly evident if one neglects the effects of attenuation. But, when attenuation is properly taken into account, the M/L ratios align on a single path with decreasing value at decreasing age.

In this respect the objects with the higher M/L ratio are the low luminosity sources, because they are also the oldest galaxies.

Chapter 3

SUBMILLIMETER GALAXIES

Submillimeter galaxies (SMGs) are among the most bolometrically luminous galaxies in the distant Universe with $L_{bol} \geq 10^{12} L_{\odot}$ and the peak of their redshift distribution around 2. Their bolometric output is dominated by intense star formation, with typical star formation rates $\sim 100-1000 M_{\odot} yr^{-1}$. Adopting a typical lifetime of SMGs $\Delta t_{sf} \sim 0.5$ Gyr, it will naturally produce a massive galaxies with $M_{\star} \sim 10^{11} M_{\odot}$. On the other hand, the observation shows that the local massive ETGs are characterized by old and homogeneous stellar populations, with mass-weighted ages of $\geq 8-9$ Gyr corresponding to formation redshifts $z \geq 1-1.5$. The observed α-enhancement in local massive ETGs requires the bulk of stars should form in a relatively short timescale ($\leq 10^9$ yr). All that suggests that the high redshift SMGs represent the progenitors of the local massive ETGs.

From the view of G04 model, we also expect the SMGs phase indeed appears during the massive ETGs formation and evolution. The intense star formation is accompanied by rapid dust production (see Chapter 2). The galaxies in massive halos ($\sim 10^{13} M_{\odot}$ will evolve from a short dust-free phase (UV-bright galaxies) to a dust-enshrouded star-forming galaxies phase (SMGs). However, the different galaxy formation and evolution models will predict very different properties for SMGs. The observed properties of SMGs, such as the redshift distribution, the number counts and the luminosity functions, will put important constrains on the models.

In this Chapter, we explore the observed luminosity functions, the number counts and

the redshift distribution of high redshift $z > 1$ SMGs, and the indications on the formation history of massive ETGs, by exploiting the Herschel Astrophysical Terahertz Large Area Survey (H- ATLAS, Eales et al. 2010[103]) Science Demonstration Phase (SDP) survey data. We also show an effective method to select submillimeter-bright, Strongly Lensed Galaxies (SLGs), under the G04 model prediction.

3.1 LFs of high-z SMGs

3.1.1 LFs at 100 and 200μm

We select our sample from H-ATLAS SDP data by the following criteria: i) $S_{250\mu m} \geq 35$ mJy; ii) no optical identification with reliability $R > 0.8$ (Smith et al. 2011a); iii) detection at $\geq 3\sigma$ at $350\mu m$;iv) photometric redshift ≥ 1. The resulting sample is made of 3039 sources. The photometric redshift estimates and K correction are both basee on the SED of SMM J2135-01012 (see more details in Appendix).

We have computed the LFs at rest-frame wavelengths of 100 and 250 μm in 4 redshift intervals ($1.\,2 \leq z < 1.\,6$, $1.\,6 \leq z < 2$, $2 \leq z < 2.\,4$, $2.\,4 \leq z < 4$), exploiting the classical Schmidt's (1968)[292] 1/Vmax estimator. The Vmax was computed, for each galaxy, taking into account the redshift boundaries of the bin and the maximum accessible redshifts implied by the 250 and 350 μm flux density limits. In the case of our preferred SED (SMM J2135-01012) the numbers of sources in these redshift bins are 900, 891, 821, and 502, respectively.

The error on z introduces both a statistical and a systematic effect. The latter is related to the Eddington bias, that can be quantified with a Bayesian approach. The probability that the true redshift of a source is z when its estimated value is z_e reads

$$p(z|z_e) \approx P(z_e|z)n(z) \tag{3.1}$$

where $P(z_e|z)$ is the probability that the estimated redshift of a source is z_e when its true value is z and $n(z)$ is the true redshift distribution. We take $P(z_e|z)$ to be a Gaussian with mean z and dispersion equal to the rms difference between spectroscopic and photometric redshifts for the galaxies described in Appendix and $n(z_e)$ as a proxy for $n(z)$. The

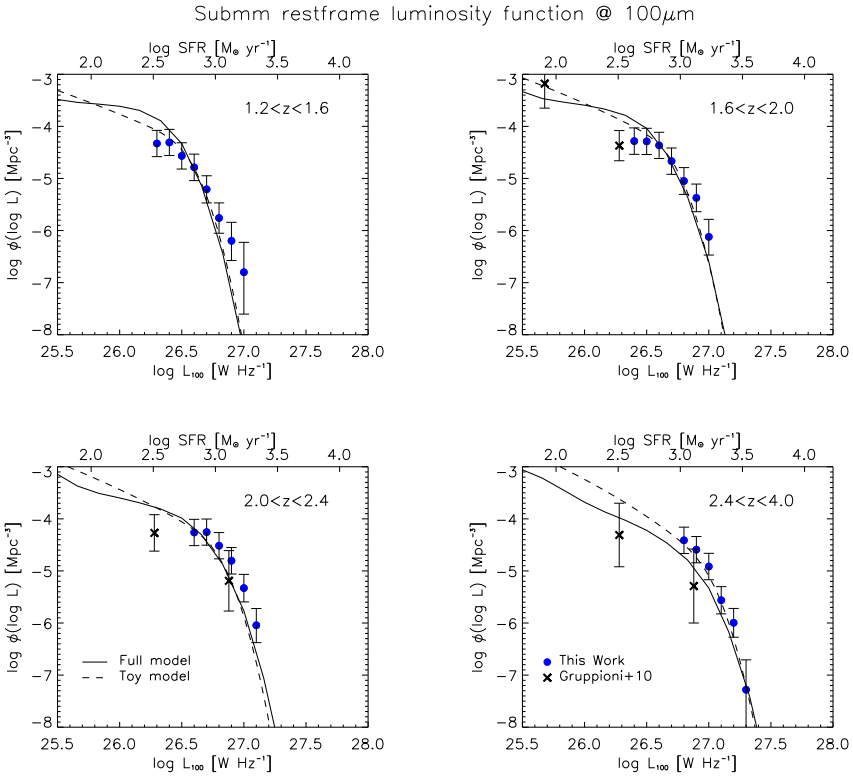

Figure 3.1: Luminosity functions at 100 μm in four redshift intervals compared with models described in the text. The flattening of the LFs at the lowest luminosities may be, at least in part, due to the overestimate of the accessible volume yielded by the 1/Vmax estimator for objects near to the flux limit (Page & Carrera 2000[248]). The 90μm LFs (crosses) estimated by Gruppioni et al. (2010)[139] using PACS data are also shown for comparison.

maximum likelihood estimate of z is the value for which $p(z|z_e)$ peaks. All the luminosity functions presented in this thesis are corrected for this bias. We caution, however, that this correction does not entirely account for the Eddington bias due to the errors on estimated luminosities. The effect is expected to be smaller than that of the error on z, which is the main source of the error on luminosity. We also have to take into account the incompleteness of the SDP catalog. This can be done using the flux density dependent correction factors given in Table 2 of Rigby et al. (2011)[279].

We stress that we exclude the strongly gravitational lensed objects when estimating the LFs. The methods to select the strongly gravitational lensed SMGs are discussed in Section 3.3(see Negrello et al. 2010[239]; González-Nuevo et al. 2011, in prep.).

In Figure 3.1, 3.2, we plot our estimated LFs at 100μm and 250μm. Our LF estimates are compared with those by Gruppioni et al. (2010)[139] and Eales et al. (2010b)[104], respectively. The latter authors adopted a grey body SED with $T = 26K$ and a dust

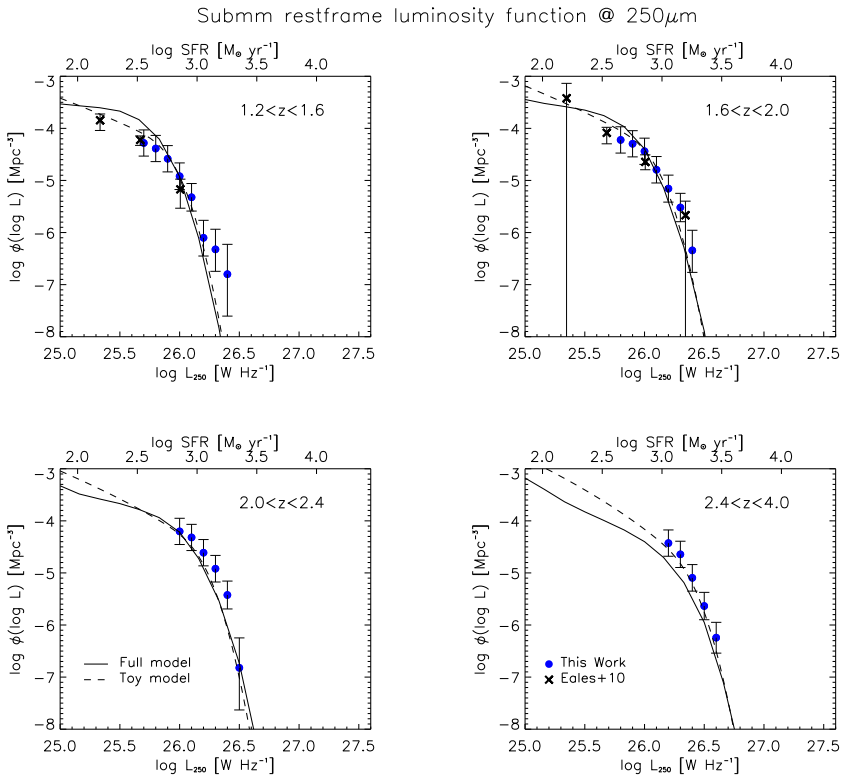

Figure 3.2: Luminosity functions at 250 μm in four redshift intervals based on our reference sample, compared with the predictions of the models discussed in the text and with the estimates by Eales et al. (2010b)[104], after applying the K-corrections based on the SMM J2135-0102 SED, for common redshift ranges.

emissivity index $\beta = 1.5$. The assumed dust temperature is possibly more appropriate for relatively low SFR/far-IR luminosity galaxies while typical dust temperatures of SPIRE-detected $z \approx 2$ galaxies are somewhat higher (Chapman et al. 2010[63]; Amblard et al. 2010[4]). The different choice for the SED has a substantial impact on the K-correction and therefore on the estimated rest-frame luminosity. For example, for a galaxy at $z \approx 1.5$ and a given observed 250 μm flux density, the Eales et al. SED yields a rest-frame 250 μm luminosity a factor ≈ 1.5 higher than that obtained using either the SMM J2135-0102 or the Arp220 SED. Once we replace their K-correction with ours, the LF estimates by Eales et al. (2010b)[104] are found to be in good agreement with ours (see Figure 3.2). The two estimates are to some extent complementary: the deeper samples used by Eales et al. have allowed them to reach lower luminosities, while the larger H-ATLAS SDP area has allowed us to reach higher luminosities at high redshifts.

Gruppioni et al. (2010)[139] exploited the deep PACS data at 100 and 160 μm in the GOODSN field ($\sim 150 arcmin^2$), obtained as part of the PACS Evolutionary Probe

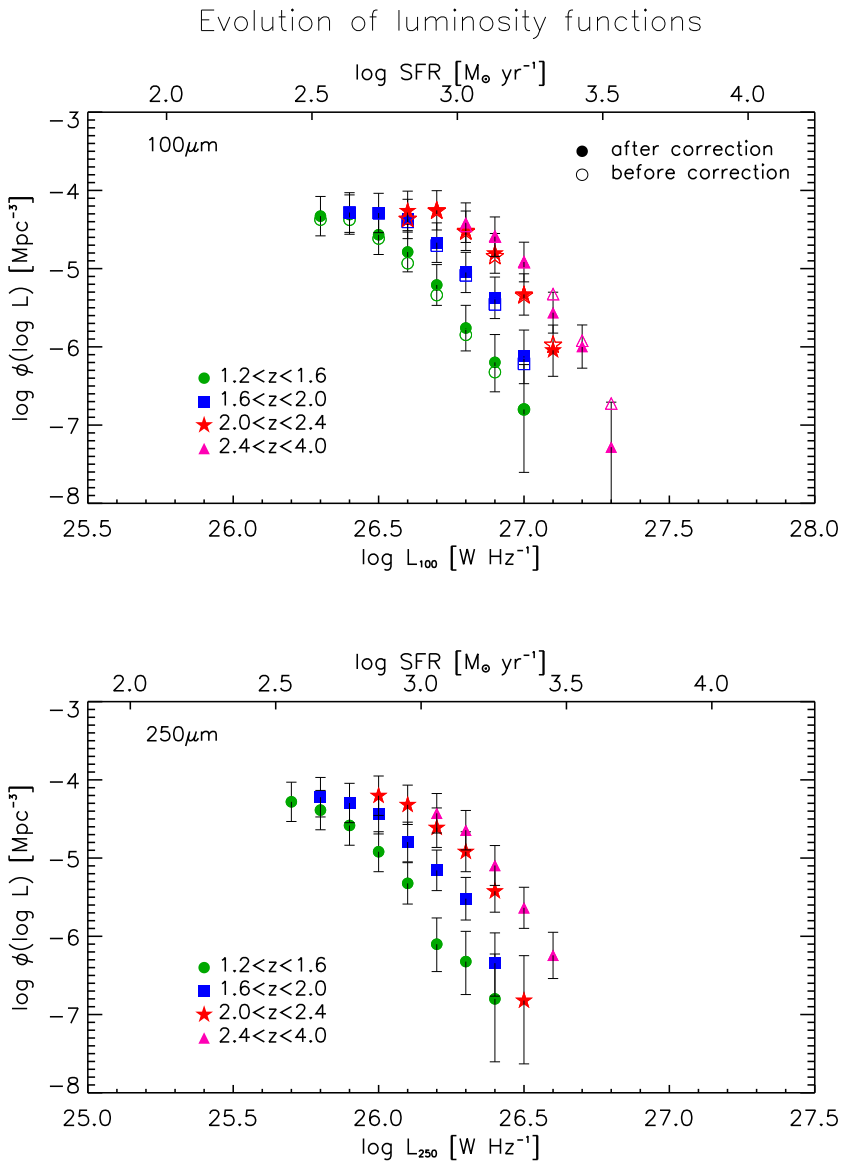

Figure 3.3: Synoptic view of the 100 μm and 250 μm LFs for our reference sample in four redshift intervals. In the 100 μm panel, open and filled symbols show our estimates before and after the correction for the Eddington bias, respectively

(PEP) survey, to estimate the 60 and 90 μm rest-frame LFs up to $z \sim 3$. They have used all the available data to derive the SEDs of their sources. About 31% of Eales et al. sources have spectroscopic redshifts and almost all the others have photometric redshifts typically based on nine optical and near-IR bands. Gruppioni et al. (2010)[139] have spectroscopic redshifts for $\sim$ 70% of their sources; for the remaining $\sim$ 30% they have obtained photometric redshifts from multiwavelength data. The agreement between our LFs and theirs is an additional confirmation that photometric redshifts derived from

sub-mm photometry are good enough for the present purpose.

In Figure 3.3, we plot the Synoptic view of the 100 μm and 250 μm LFs for our reference sample in four redshift intervals. The LFs exhibit an exponential fall off at high luminosity and a flattening at low luminosity. It should be noted that the flattening at the low luminosity may be due to the overestimate of the accessible volume yielded by the 1/Vmax estimator for objects near the flux limit, pointed out by Page & Carrera (2000[248]; see also Eales et al. 2009[102]). The LFs show a substantial luminosity evolution at least up to $z \approx 2.5$, while a weaker evolution at higher z is indicated(see Figure 3.3). The 250 μm luminosity corresponding to $log(\phi/Mpc^{-3}) = -5$ is $log(L_{250}/WHz^{-1}) = 26.02, 26.16, 26.32,$ and 26.38 for $z \approx 1.4, 1.8, 2.2, 3.2,$ respectively. At 100 μm the corresponding luminosities are $log(L_{100}/WHz^{-1}) = 26.65, 26.78, 26.94,$ and 27.01. These results are consistent with those based on PEP survey data (Gruppioni et al. 2010[139]).

The upper scale in Figure 3.1, 3.2 and 3.3 displays the SFR corresponding to the 100 or 250 μm luminosity. Using the SMM J2135-0102 calibration, we have

$$\frac{L_{100\mu m}}{W\ Hz^{-1}} = 5.9 \times 10^{23} \frac{SFR}{M_\odot\ yr^{-1}} \tag{3.2}$$

while for $L_{250\mu m}$ the coefficient is 1.4×10^{23}. Since for galaxies with intense star formation the rest-frame dust emission peaks in the range $\lambda \approx 90-100\mu m$, the 100 μm luminosity is a good estimator of the SFR. For galaxies in the redshift range considered here ($1 \leq z \leq 4$) one of the SPIRE wavelengths is always sampling directly the rest-frame SED in the range $100 \leq \lambda \leq 125\mu m$, implying that K-corrections (and the related uncertainties) are minimal.

3.1.2 Clues on star-formation in massive halos

We now discuss how the LFs of high redshift star forming galaxies at sub-mm wavelengths concur with their clustering properties in probing the process of star formation in SMGs.

At first, we employ a simple model (hereafter referred to as the 'toy model') in order to explore the main processes of star formation, relying on the following assumptions:

1. We adopt that the host halo masses M_H can range from 3×10^{12} to $3 \times 10^{13} M_\odot$, which is suggested by strong clustering of SMGs (Cooray et al. 2010[76]; Maddox et

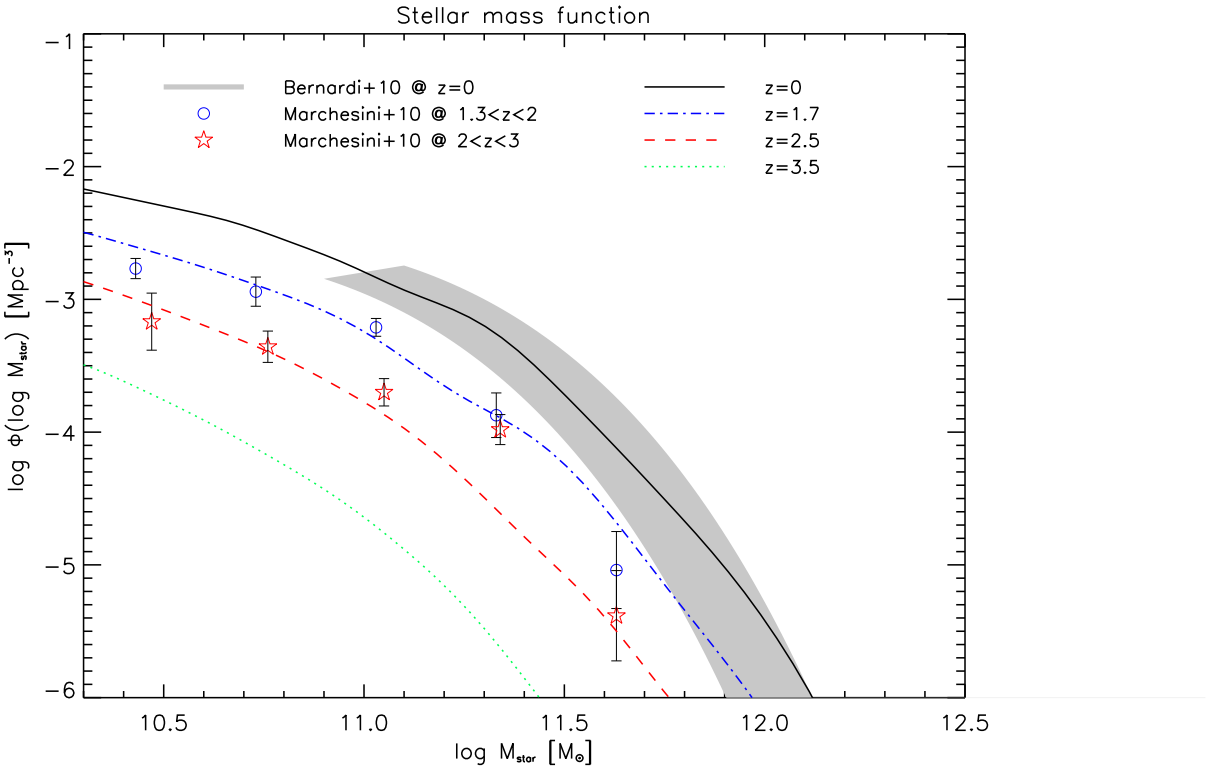

Figure 3.4: Stellar mass functions of ETGs at different redshift predicted by the toy model compared with observational determinations.

al. 2010[203]). Note this mass range is consistent with that of the QSOs host halo.

2. Most of the star formation occurs soon after the fast collapse phase of the halo, as identified by Zhao et al. (2003)[364].

3. At the redshifts ($z > 1$) and for the halo masses ($M_H \geq 3 \times 10^{12} M_\odot$), a good approximation to the halo formation rate is provided by the positive term of the derivative with respect to the cosmic time of the cosmological mass function (e. g. , Haehnelt & Rees 1993[142]; Sasaki 1994[289]); for the latter we adopt the Sheth & Tormen (1999, 2002)[304][305] expression.

4. The SFR is proportional to the halo mass, i. e. , $SFR \propto M_H$, with a small scatter.

5. The lifetime of SMGs Δt_{sf} is roughly constant and shorter than the expansion timescale at the source redshift.

With these assumptions, the simple model can fit the observed LFs very well, adopting

$$\Delta t_{sf} \approx 7 \times 10^8 yr \tag{3.3}$$

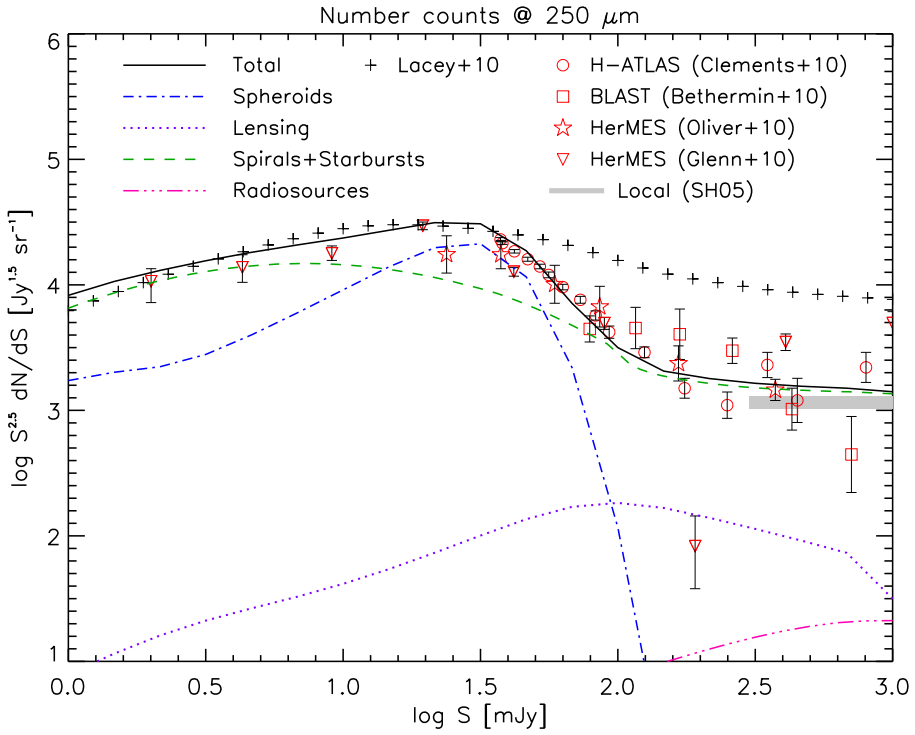

Figure 3.5: Comparison of the observed Euclidean normalized counts at 250 μm(Clements et al. 2010; Oliver et al. 2010; Glenn et al. 2010; Bethermin et al. 2010) with the predictions of our full model (solid line) and of the semi-analytic model by Lacey et al. (2010; crosses). The different lines show the contributions to the counts of the various populations included in our full model: unlensed (blue dot-dashed line) and strongly lensed (purple dotted line) proto-spheroidal galaxies (host halo masses are within the range 2. $5 \times 10^{11} M_{\odot} \leq M_H \leq 3 \times 10^{13} M_{\odot}$), normal late-type plus starburst galaxies (green dashed line), radio sources (magenta triple-dot-dashed line). The radio source counts are from the De Zotti et al. (2005)[91] model. The grey shaded area shows the counts of local galaxies estimated by Serjeant & Harrison (2005)[297]

and

$$SFR = 35 \left(\frac{M_H}{10^{12} M_{\odot}} \right) \left(\frac{1+z}{2.\ 5} \right)^{2.\ 1} M_{\odot}\ yr^{-1} \tag{3.4}$$

with a rather small ($\pm 35\%$) scatter.

In Figure 3.1, 3.2, we also plot the predicted LFs by G04 model, adopting the SED of SMM J2135-0102. We label the resulting LFs as 'Full model'. We stress that the LFs from the Full model are not fits to the data, but have been computed with the same parameters used by Lapi et al. (2006; see their Table 1).

A rough estimate of the mass in stars at the end of the main star-formation episode, for given halo mass and redshift, can be obtained multiplying the appropriate SFR by its lifetime Δt_{sf}, and correcting for the fraction of stellar mass returned to the interstellar medium. For a Chabrier IMF(Chabrier 2003[60]) the latter amounts to $\sim 30\%$ after 0.1 Gyr from a burst of star formation, and increases to $\sim 40\%$ after 1 Gyr and to 50% after

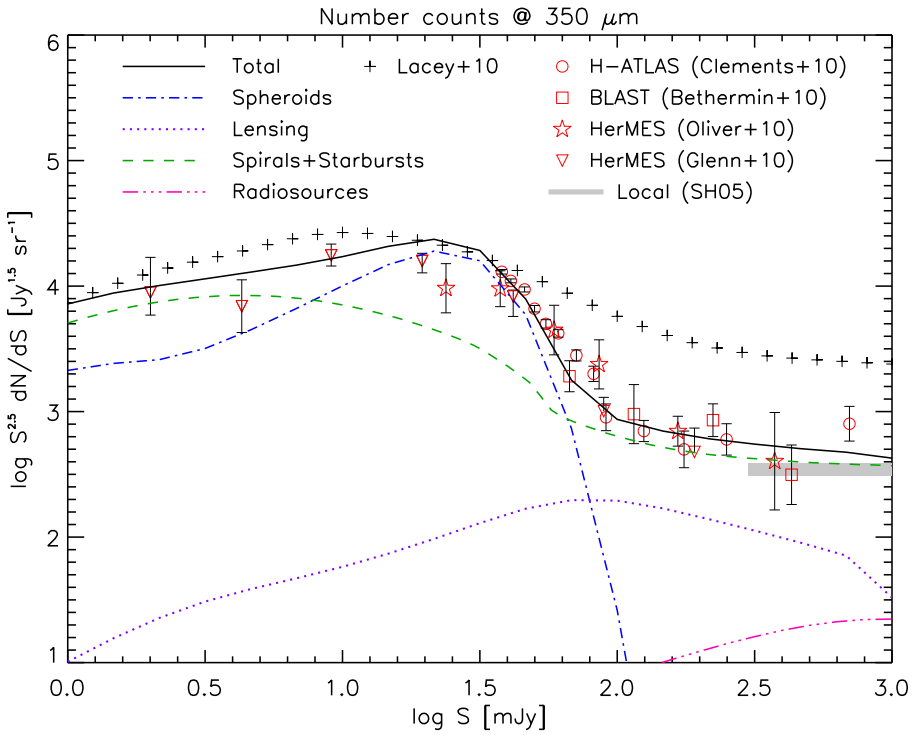

Figure 3.6: $350\mu m$ number counts. The lines are the same as in Figure 3.5.

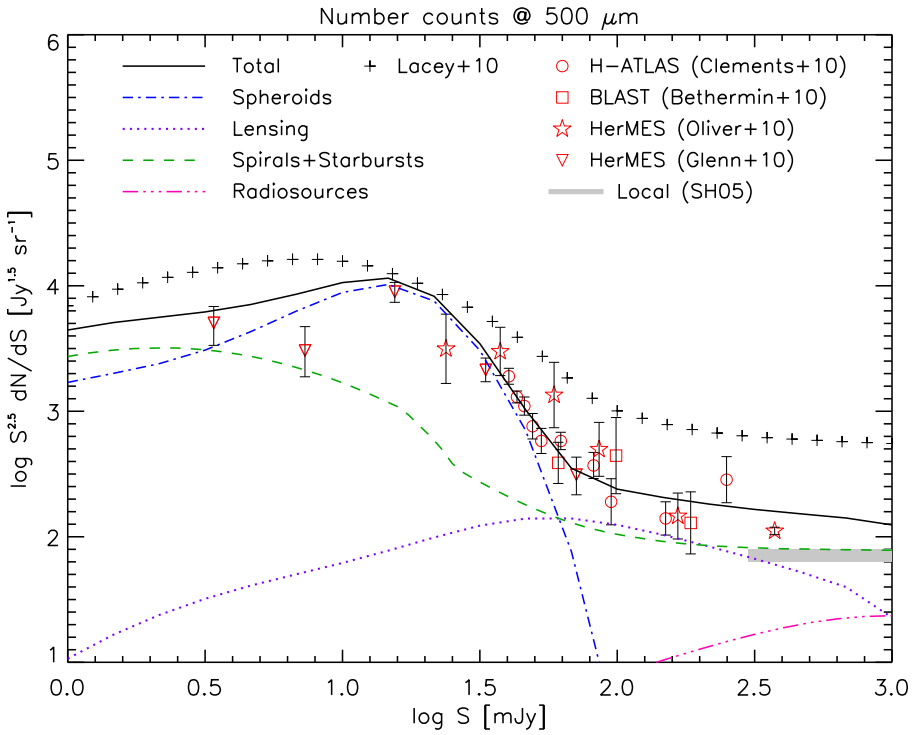

Figure 3.7: $500\mu m$ number counts. The lines are the same as in Figure 3.5.

several Gyrs. Combining with the halo mass function at that redshift we get an estimate of the stellar mass function of ETGs. A comparison with observational determinations at different redshifts is shown in Figure 3.4. The good agreement suggests that the toy model captures the basic aspects of the star formation in high redshift SMGs.

A comparison of our LFs with the UV ones at $z \approx 2-3$ (Sawicki & Thompson 2005[290]; Reddy & Steidel 2009[271]) for galaxies with SFR $\geq 100 M_{\odot}\ yr^{-1}$ shows that the UV space densities are a factor ~ 100 lower, implying that the UV bright, dust-free phase is much shorter than the far-IR bright phase. The far steeper slope of the UV LF, compared with the sub-mm ones, for SFR $\sim 100 M_{\odot}\ yr^{-1}$ implies that, for the corresponding range of galaxy masses, the UV-bright phase is shorter for larger SFRs, which is discussed in Chapter 2. The same can be used to estimate the QSOs lifetime. Peng et al. (2006)[254] shows that the $M_{\bullet}/M_{\star}$ ratio of the optical luminous QSOs at $z > 1.7$ is at least 4 times larger than the local ratio, which is $M_{\bullet}/M_{\star} \sim 2 \times 10^{-3}$ (see also Coppin et al. 2008[78]). The stellar mass function translates immediately into a black hole mass function which, in turn, can be translated into a bolometric luminosity function assuming that the black holes, immediately before being switched off, emit at the Eddington limit for a time t_{vis}. We get:

$$\frac{L_{B,\ QSO}}{L_{\odot}} \approx 2 \frac{M_{\star}}{M_{\odot}} \tag{3.5}$$

At $z \sim 2$, the comoving density of SMGs is $\sim 2.7 \times 10^{-5}$ per Mpc^3 with $M_{\star} \geq 2 \times 10^{11} M_{\odot}$. The comoving density of QSOs brighter than the corresponding luminosity of $L_{B,\ QSO} \approx 4 \times 10^{12} L_{\odot}$ is about 2×10^{-6} per Mpc^3 (Croom et al. 2004[84]). This implies that the optical visibility time of the QSOs is about a factor of 10 shorter than the duration of the sub-mm bright phase, in agreement with independent estimates (Shankar et al. 2004[299]; Marconi et al. 2004[215]; Lapi et al. 2006[190]).

3.2 Submillimeter counts

Figures 3.5, 3.6 and 3.7 compare the predictions of the G04 model with the observed counts at three Herschel SPIRE bands(250μm, 350μm and 500μm). In these figures the contributions to the counts of proto-spheroidal galaxies have been complemented with

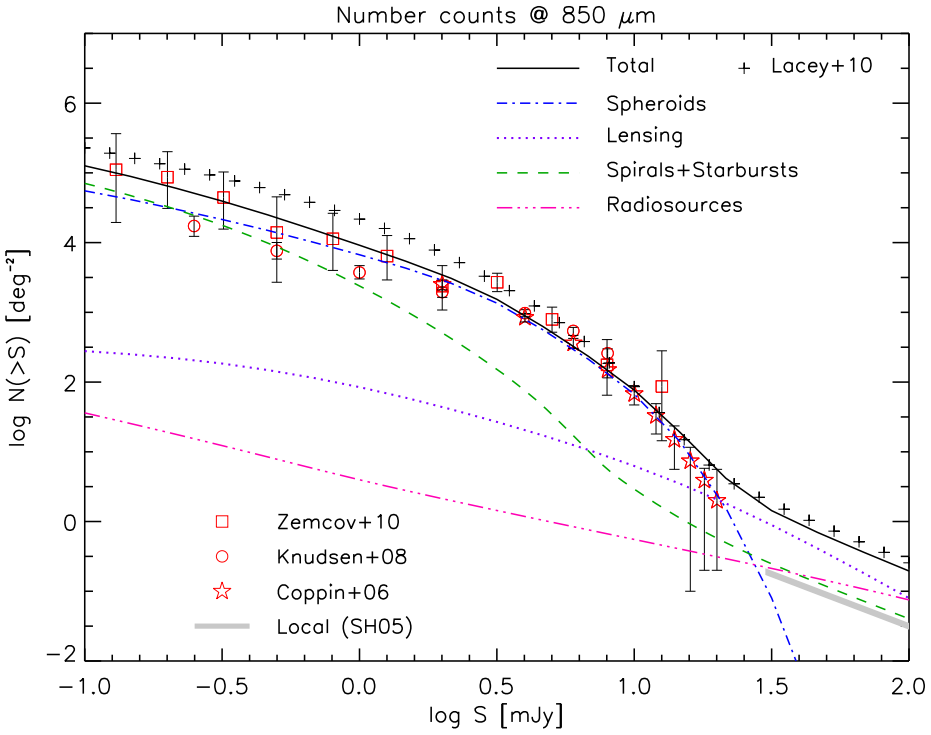

Figure 3.8: Comparison of the observed integral counts at 850 μm(Zemcov et al. 2010[363]; Knudsen et al. 2008[175]; Coppin et al. 2006[77]) with the predictions of our full model (solid line) and of the semi-analytic model by Lacey et al. (2010; crosses). The lines are the same as in Figure 3.5.

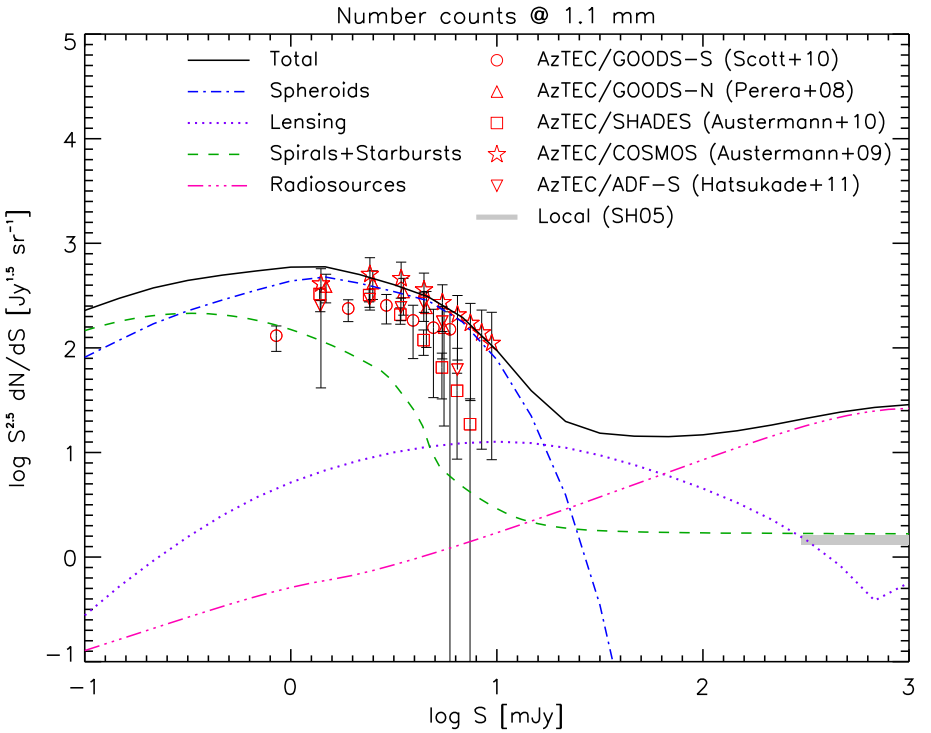

Figure 3.9: Comparison of the observed number counts at 1. 1 mm (Scott et al. 2010[295]; Perera et al. 2008[256]; Austermann et al. 2009, 2010[10][11]) with the predictions of our full model (solid line). The lines are the same as in Figure 3.5.

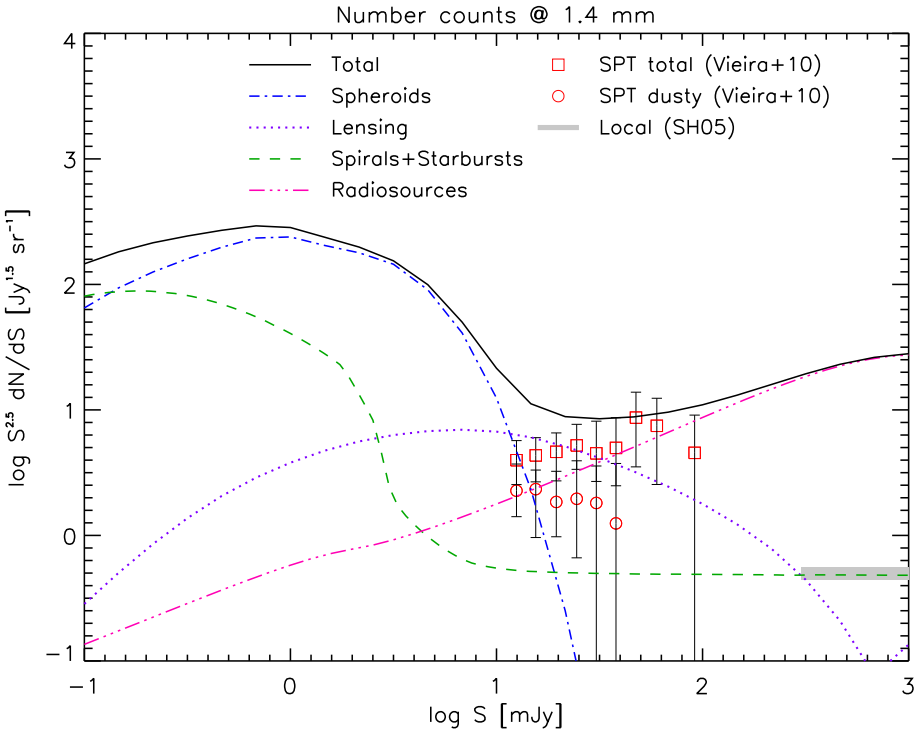

Figure 3.10: Comparison of the observed number counts at 1. 4 mm (Vieira et al. 2010[354]) with the predictions of our full model (solid line). The lines are the same as in Figure 3.5.

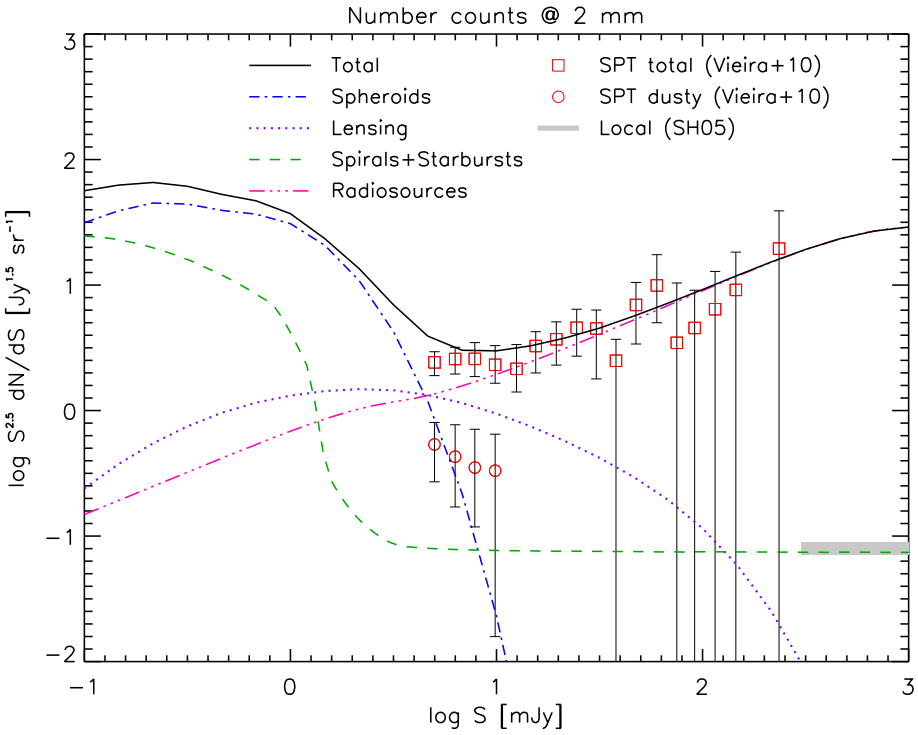

Figure 3.11: Comparison of the observed number counts at 2 mm (Vieira et al. 2010[354]) with the predictions of our full model (solid line). The lines are the same as in Figure 3.5.

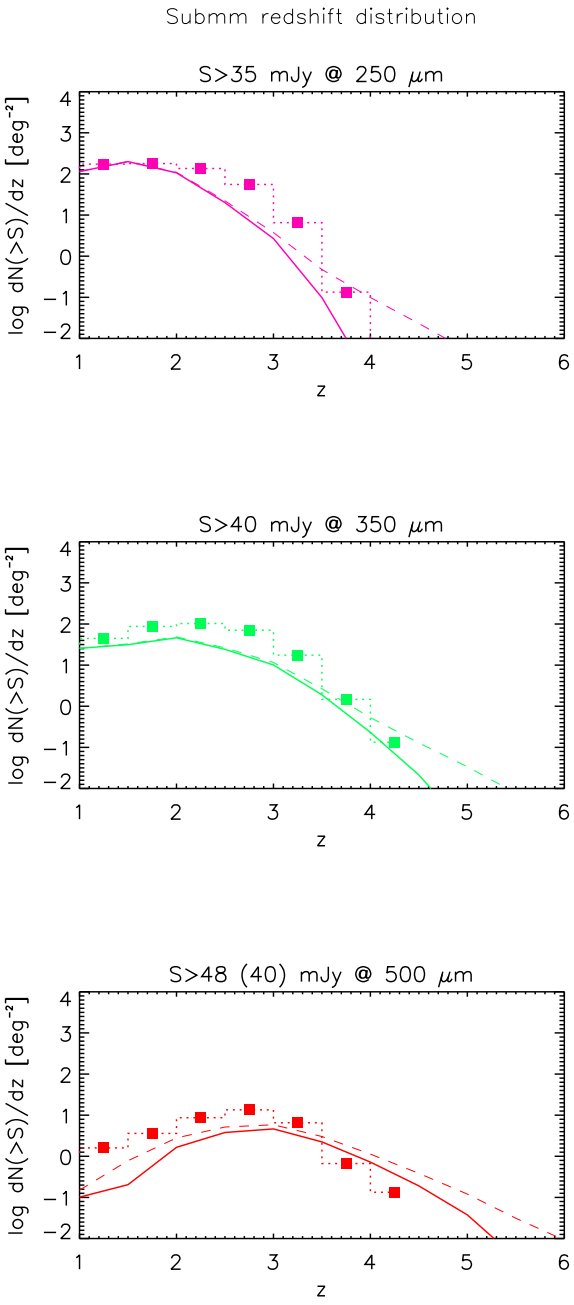

Figure 3.12: Comparison between the estimated redshift distributions (histograms) of proto-spheroidal galaxies at 250 μm ($S_{250\mu m} \geq 35mJy$), 350μm ($S_{350\mu m} \geq 40mJy$), and 500 μm ($S_{500\mu m} \geq 48mJy$), and the predictions of our full model, using the same parameters as in Lapi et al. (2006)[190]; solid lines refer to unlensed, while dashed lines also include the contribution of lensed, proto-spheroids. Because of the flux boosting due to confusion, the catalogued 500 μm flux densities have to be scaled down by the factors given by Clements et al. (2010)[72]. For example, the 500 μm flux density limit of 48 mJy for catalogued sources corresponds to a boosting corrected flux limit of 40 mJy.

phenomenological models for the evolution of normal late-type and starburst galaxies computed by Negrello et al. (2007)[240]. As for massive proto-spheroidal galaxies, the main difference with the counts in the latter paper comes from having replaced the Arp220 SED yielded by GRASIL with that of SMM J2135-0102. The contribution from lensed proto-spheroidal galaxies has been estimated using the amplification distribution of Perrotta et al. (2003)[259] and Negrello et al. (2007)[240].

The G04 model predicts that massive proto-spheroidal galaxies dominate the (sub-)mm counts over a limited flux density range (about a decade). At 250 μm the Euclidean normalized differential counts of these objects peak at $\sim$30 mJy, i. e. roughly at the detection limit of the H-ATLAS survey, and sink down rapidly at fainter fluxes where the contribution of starburst galaxies takes over and accounts for the results of the P(D) analysis by Glenn et al. (2010)[129]. Since the proto-spheroidal galaxies are mostly at $z \geq 1.5$ while late-type galaxies are mostly at $z \leq 1$, the model implies that the redshift distribution drifts towards lower redshifts as we go fainter.

The model accurately fits the source counts from 250 μm to 850 μm (Figures 3.5-3.8). The observed counts at 1. 1 mm (Figure 3.9) span the peak of the Euclidean normalized counts, while those at 1. 4 and 2 mm (Figures 3.10 and 3.11) only cover the brightest tail of the counts, dominated by strongly lensed sources (apart from radio sources). The model somewhat overestimates the counts of strongly lensed galaxies at 1. 4 and 2 mm, and the most recent counts at 1.1 mm.

The flux density range over which massive proto-spheroidal galaxies dominate the counts increases somewhat with increasing wavelength, reflecting the increase of the redshift range through which the strongly negative K-correction makes the flux corresponding to a given luminosity essentially independent of distance. The broadening of the peak in the Euclidean normalized counts of proto-spheroidal galaxies is not very large, however, because massive halos become increasingly rare at high z. At all wavelengths the bright counts of proto-spheroidal galaxies drop down very steeply, reflecting the exponential decline of the halo mass function. This rapid fall-off, borne out by the data, can hardly be accounted for by phenomenological models that evolve the LF of local populations of dusty galaxies backwards in time: spheroidal galaxies are essentially in passive evolution since $z \approx 1.5$ and are therefore not represented in local LFs at far-IR to mm wavelengths.

The physical model by Lacey et al. (2010)[186] works pretty well at 850 μm but does

not correctly predict the rapid fall-off of the counts above 30 mJy at 250 μm, 350 μm and 500 μm. The decline of the counts is most easily understood if the duration of the most active star-formation phase in massive halos is relatively short, as also required by the observed α-enhancement. However, in merger-driven evolutionary models, such as the one by Lacey et al. (2010)[186], the star formation does not truncate after $\sim 0.1Gyr$. At 850 μm consistency with the data can be recovered if sub-mm bright galaxies contain large amounts of cold dust, but this leads to 250 μm, 350 μm and 500 μm counts less steep than observed.

In Figure 3.12 compares the redshift distributions of $z > 1$ H-ATLAS SDP sources detected at $S > 35$, 40, 48 mJy at 250, 350 and 500 μm, respectively, with those predicted by the model. The effective flux correction factors tabulated by Clements et al. (2010)[72] have been applied for this comparison. Since the redshift distributions are a key ingredient for the successful prediction of the abundance of strongly lensed galaxies and of their redshift range (Negrello et al. 2010[239]), they cannot be badly wrong. Thus, the agreement between our estimates and model predictions is a confirmation of the global consistency of our results. The shift in the redshift distribution of sub-mm bright galaxies to higher redshifts with increasing selection wavelength happens because the strongly negative K-correction extends to larger and larger redshifts and the lensing probability increases with z.

3.3 Submillimeter-Bright, Strongly Lensed Galaxies

The first submillimeter-Bright, Strongly Lensed Galaxy was discovered by Blain(1997)[30], which is suffered moderate gravitational lensing magnification, by about a factor of 2-3, experienced throughout the inner few square arcminutes of rich foreground cluster of galaxies at a moderate redshift in the range $z \simeq 0.2 - 0.4$. As pointed out by Blain (1996)[29] and then investigated by several authors (Perrotta et al. 2002[258]; Negrello et al. 2007[240]; Paciga et al. 2009[247]), the submm band is extraordinarily well suited for generating large samples of strongly lensed galaxies at high redshift. One key advantage of observing background galaxies that are gravitationally lensed by foreground mass concentrations in the submm band is that the negative K-correction acts to brighten the distant background lensed galaxy as compared with the lens. The other is the very steep slope of submm counts

and its rapid change at $>$ 10 mJy flux density levels (see Figure 3.5-3.8. The significant changes in the count slope are particularly unusual, and not found in any other waveband. As a result, the magnification bias can be large, increasing the number of detectable bright galaxies.

The observed submm counts can be contributed by several parts, including the unlensed proto-spheroidal galaxies which can be estimated by G04 model, lensed proto-spheroidal galaxies (Perrotta et al. 2002, 2003[258][259]), low redshift spirals and starburst galaxies (Negrello et al. 2007[240]) and radio sources (De Zotti et al. 2005[91]). In Figure 3.7, one can see that the lensed galaxies will dominate at the large flux tail($S_{500\mu m} > 100mJy$). Other important contributors to the bright tail of the submillimeter counts are low-redshift spiral and starburst galaxies and higher redshift radio-bright Active Galactic Nuclei (AGNs) which are easily identified, and therefore removed, in relatively shallow optical and radio surveys. This presents an effective method to select a clean sample of strongly lensed submm galaxies, which is proposed firstly by Perrotta et al. 2002[258] and then investigated by Negrello et al. (2007)[240]. Using this selection criteria ($S_{500\mu m} > 100mJy$), Negrello et al. (2010)[239] selected 11 sources from the Herschel ATLAS SDP catalogue. Ancillary data in the field revealed that six of these objects are contaminants, four are spiral galaxies with spectroscopic redshift in the range of 0.01 to 0.05, one is a previously known radio-bright AGN and one is an extended galactic star forming region. After removing these six objects, there are left five objects as the lensed candidates, identified as ID9, ID11, ID17, ID81 and ID130. Spectroscopic redshifts from CO lines (Frayer et al. 2011[118], upu et al. 2011[200], Neri et al. in prep.)show that all of these candidates are high redshift galaxies ($z_{spec}^{(CO)} \geq 1.5$). Especially, the Submillimeter Array (SMA) images at $880\mu m$ of two candidates ID81 and ID130 reveal extended submillimeter emission with multiple peaks (ID81:four main peaks; ID130:two main peaks). These multiple peaks are consistent with the expected lensed morphology. Even more, all of five candidates have a close counterpart in SDSS or UKIDSS (or both). A likelihood ratio analysis (Smith et al. 2010[310]) showed that the probability of a random association between these bright SMGs and the optical/NIR counterparts is less than a few percent. Therefore, the optical and submillimeter emissions must be physically related either because of the effects of gravitational lensing which boosting the flux of the background source and indirectly affecting the likelihood ratio calculations, or because they are identical objects. The optical spectroscopic redshifts of these

optical/NIR counterparts show they are low redshift objects with $0.2 \leq z_{spec}^{(opt)} \leq 1.0$, compared to the CO line redshifts of lensed candidates. Also, the SED of these optical/NIR objects shows they are dominated by passively-evolved stellar population with massive stellar mass ($\sim 10^{11} M_{\star}$). The high-resolution optical images with the Keck telescope confirm that they all have the morphological type of elliptical galaxies. All of these evidences confirm that the optical/NIR counterparts are the foreground galaxies, acting as the lensing.

We notice that the simply selection criteria ($S_{500\mu m} > 100mJy$) will select those extreme objects with large gravitational amplification by a factor of ~ 10 and large SFRs ($> 500 M_{\odot}\ yr^{-1}$). Those lensed galaxies with more representative SFRs $\sim 100 M_{\odot}\ yr^{-1}$ and moderate gravitational amplification by a factor of $2-5$ will be missed. However, the rapidly increasing counts of unlensed galaxies towards fainter submm fluxes will make harder to identify the 'normal' lensed galaxies (with representative SFRs and moderate gravitational amplification).

Now a luminosity selection method to select the sample of the strongly lensed galaxies has been developing by González-Nuevo et al. (2011, in prep.) 25 candidates in the SDP or a density of ~ 1.67 candidates per square degrees.

3.4 SUMMARY

In this Chapter, mainly based on the work by Lapi et al. (2011), we show the results using the H-ATLAS SDP survey data to investigate the 100 μm and 250 μm LFs of bright SMGs at $z > 1$. Redshifts have been estimated using the SED of SMM J2135-0102 as the template. The rms uncertainties on redshift estimates have been assessed comparing our redshift estimates with spectroscopic redshift measurements for 39 H-ATLAS galaxies at $z > 0.5$ as well as by means of simulations. Both methods yield rms values of $\Delta z/(1+z) \approx 0.2$ or smaller. The uncertainties due to the spread of redshift estimates are added in quadrature to Poisson errors to compute the global uncertainties on the LFs. Our LF estimates are in close agreement (in the common redshift and luminosity range, after applying the same $K-corrections$) with those at 250 μm by Eales et al. (2010b)[104], as well with those at 90 μm by Gruppioni et al. (2010)[139]. We find a significant luminosity evolution at least up to $z \approx 2.5$, while a weaker evolution at higher

z is indicated. We show that the evolution of the LF reflects that of the halo formation rate if the star-formation rate obeys a simple relationship with halo mass and redshift and the lifetime of the main star-formation phase is $\Delta t_{sf} \sim 7 \times 10^8$yr, consistent with the constraint coming from the α-enhancement observed in the most massive ETGs. G04 model is able to reproduce not only the 100 μm and 250μm LFs at different redshifts $z > 1$ but also the counts at wavelengths ranging from 250 μm to $\approx$ 1 mm. We also show , under the guide of the model, an simple , but effective, method has been developed to select the high redshift, strongly-lensed SMGs, which has been proven to be at work (Negrello et al. 2010[239], González-Nuevo et al. in prep.)

Chapter 4

QSOS LUMINOSITY FUNCTIONS AND QSOS FEEDBACK

Supermassive black holes have been found to be ubiquitous in the centers of spheroidal galaxies (e. g. , Kormendy & Richstone 1995[181]; Richstone et al. 1998[276]; Kormendy & Gebhardt 2001[180]), and the masses of these black holes are correlated with either the mass (Magorrian et al. 1998[204]; McLure & Dunlop 2002[224]; Marconi & Hunt 2003[214]) or velocity dispersion (i. e. , the $M_\bullet - \sigma$ relation; Ferrarese & Merritt 2000[114]; Gebhardt et al. 2000[122]; Tremaine et al. 2002[332]) of spheroids, demonstrating a direct link between the origin of spheroidal galaxies and supermassive black holes.

In the G04 model, described in detail in Appendix A, the BH growth is expected to be accompanied by intense star formation. This naturally produces the expected Sanders evolutionary sequence (Sanders et al. 1988[287]), in which the dust-enshroud star formation phase , observationally UltraLuminous Infrared Galaxies(ULIRGs) or Submillimeter galaxies (SMGs), is followed by the QSOs phase. Recent observations give the same indication.A significant fraction of SMGs have been found existing AGN activities according to the deep X-ray observations(Alexander et al. 2005[2],See also Georgantopoulos et al. 2010 and Laird et al. 2010).

In this chapter, we will show that the G04 model can reproduce the observed redshift-dependent luminosity functions of QSOs , based on the work by Lapi et al.(2006)[190]. And also the importance of QSOs feedback will be discussed.

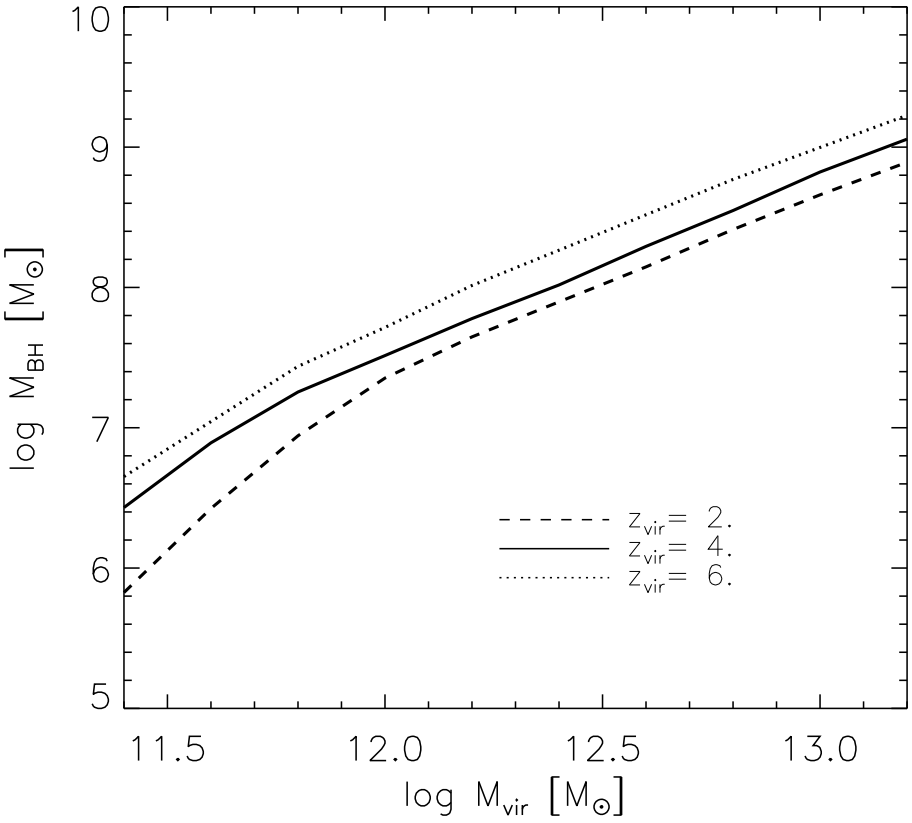

Figure 4.1: BH mass at the accretion peak as a function of the host galaxy virial mass predicted by the G04 model.

4.1 QSOs Luminosity Functions

If the QSOs lifetime is far smaller than the Hubble time, the QSOs luminosity function can be written as (Mahmood, Devriendt & Silk 2005[205]):

$$\phi_{QSO} = \frac{dn(z,\ )}{dL} = \frac{d^2 N_{st}}{dM_{halo} dt} \frac{dM_{halo}}{dM_\bullet} \frac{dM_\bullet}{dL} \tau_{QSO} \tag{4.1}$$

The formation rate of DM halos has been defined by the Equation A.1.

The relation between the halo mass $M_{\rm vir}$ and the BH mass $M_\bullet$ can be obtained by solving the equations presented in Appendix A. In Fig. 4.1, we plot the expected $M_{\rm vir}-M_\bullet$ relation by the G04 model, which can be well approximated by

$$M_\bullet \approx 8 \times 10^6 \ \frac{(M_{\rm vir}/2.\ 2 \times 10^{11}\ \ M_\odot)^{3.\ 97}}{1 + (M_{\rm vir}/2.\ 2 \times 10^{11}\ \ M_\odot)^{2.\ 7}} \ \left(\frac{1+z_{\rm vir}}{7}\right)\ M_\odot \quad . \tag{4.2}$$

This relation is very similar to the result of Shankar et al. (2006)[298] by comparing the

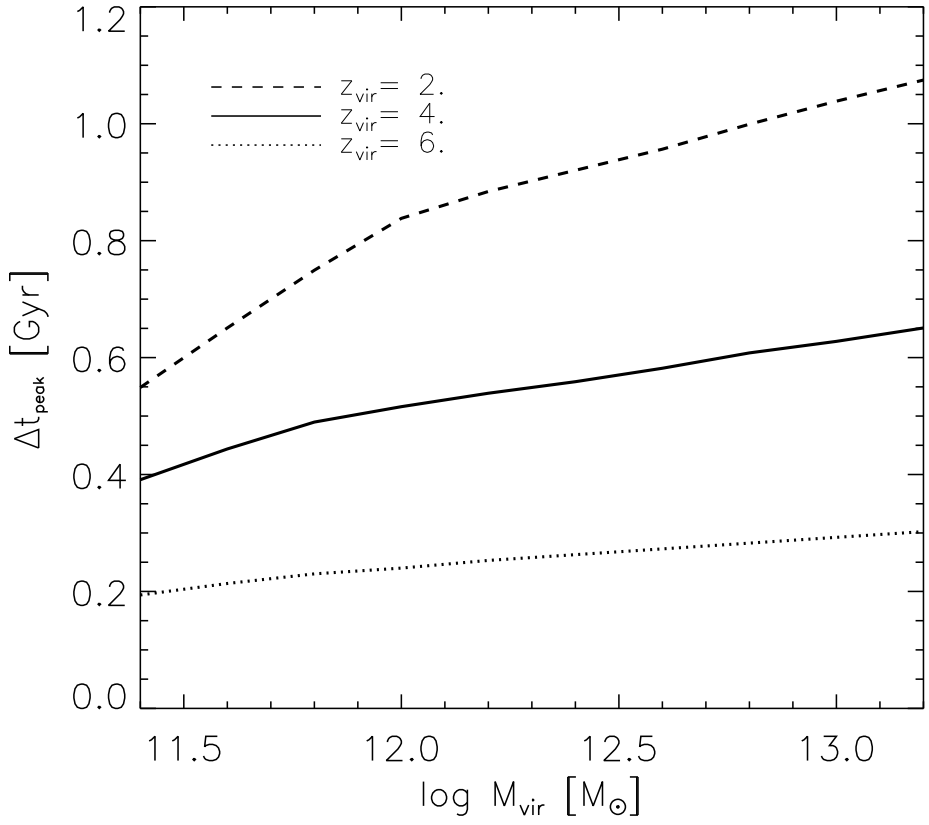

Figure 4.2: Time lag between the host galaxy virialization and the peak in the BH accretion rate, as a function of the host virial mass.

local BH mass function with the galaxy halo mass function.

We also expect the scatter around the average $M_{\rm vir} - M_\bullet$ relation. It's assumed that $M_{\rm vir} - M_\bullet$ relation holds on the average number with a Gaussian dispersion $\Delta M_\bullet$. The halo formation rates can be converted into the BH formation rates through the convolution

$$\frac{{\rm d}^2\ N_{\rm BH}}{{\rm d}t_{\rm vir}\ {\rm d}M_\bullet} = \int {\rm d}\log M'_\bullet \left|\frac{{\rm d}M_{\rm vir}}{{\rm d}M_\bullet}\right|_{M'_\bullet} \frac{{\rm d}^2\ N_{\rm ST}}{{\rm d}t_{\rm vir}\ {\rm d}M_{\rm vir}}\Big|_{M_{\rm vir}(M'_\bullet)} \frac{e^{-(\log M'_\bullet - \log M_\bullet)^2/2\ (\Delta \log M_\bullet)^2}}{\sqrt{2\pi\ (\Delta \log M_\bullet)^2}} \ . \tag{4.3}$$

The QSO LFs can now be computed. Up to its peak, the BH bolometric light curve can be well approximated by the simple exponential form

$$L(t) = \frac{\lambda\ M_\bullet\ c^2}{t_{\rm Edd}}\ e^{(t-t_{\rm vir}-\Delta t_{\rm peak})/\tau_{\rm ef}}\ \theta_H\Big(t_{\rm vir} + \Delta t_{\rm peak} - \Delta t_{\rm vis} \le t \le t_{\rm vir} + \Delta t_{\rm peak}\Big) \ . \tag{4.4}$$

Here $t_{\rm Edd} \approx 4 \times 10^8$ yr is the Eddington timescale, and $\tau_{\rm ef} \approx \eta\ t_{\rm Edd}/(1-\eta)\ \lambda$ is the e-folding time in terms of the BH mass-energy conversion efficiency η and of the Eddington ratio λ. Δt_{peak} is time lag between the host galaxy virialization and the peak in the

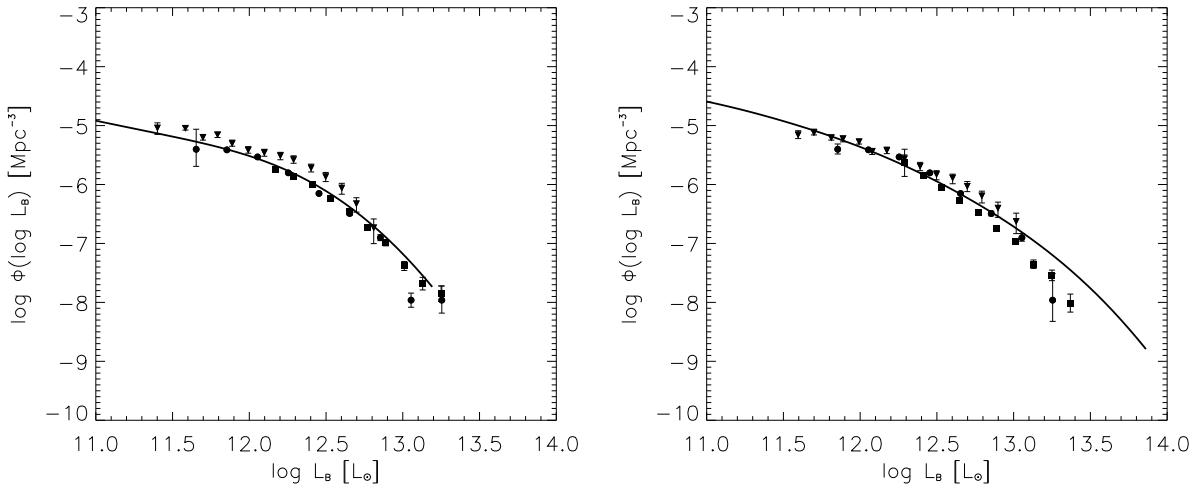

Figure 4.3: Left:QSO LF in the optical B-band at $z = 1.\ 5$, for $\lambda = 0.8$ and $\Delta t_{vis} = 10^8$ yr. Right:QSO LF in the optical B-band at $z = 2$, for $\lambda = 1$ and $\Delta t_{vis} = 10^8$ yr. The data are from Croom et al. (2004; circles), Richards et al. (2005; triangles), and Richards et al. (2006; squares).

BH accretion rate, which can be obtained by solving the system of equations reported in Chapter 1. In Figure 4.2, we plot the model predicted Δt_{peak} as a function of the host virial mass. $\Delta t_{\rm vis}$ is the QSO lifetime, dependent on dust and gas absorption, is taken as a parameter. The Heaviside function θ_H is defined by $\theta_H(x) = 1$, if x is true; $\theta_H(x) = 0$, otherwise. . θ_H specifies that the QSO shines unobscured only during the time interval $\Delta t_{\rm vis}$ before the peak of its light curve.

The QSO LF at a time t and luminosity L is computed by summing up the contributions of all the sources which virialize at epochs $t_{\rm vir} \leq t$ and shine at the time t with luminosity L. One has

$$\Phi(L,\ t) = \int_{t-\Delta t_{\rm peak}}^{t-\Delta t_{\rm peak}+\Delta t_{\rm vis}} {\rm d}t_{\rm vir} \int {\rm d}M_\bullet \ \frac{{\rm d}^2\ N_{\rm BH}}{{\rm d}t_{\rm vir}\ {\rm d}M_\bullet}\ \delta_D\left(L - \frac{\lambda\ M_\bullet\ c^2}{t_{\rm Edd}}\ e^{(t-t_{\rm vir}-\Delta t_{\rm peak})/\tau_{\rm ef}}\right), \tag{4.5}$$

where δ_D indicates the Dirac delta function. The time delay $\Delta t_{\rm peak}$ provided by G04 model ranges from 0.2 Gyr at redshift $z \geq 5$ to 1 Gyr at redshifts $z \leq 2$(see Fig. 4.2).

In addition, it is convenient to compute the black hole mass function from the black hole formation rates:

$$\Psi(\log M_\bullet,\ t) = \int_0^t {\rm d}t_{\rm vir}\ \ \frac{{\rm d}^2\ N_{\rm BH}}{{\rm d}t_{\rm vir}\ {\rm d}\log M_\bullet}\ . \tag{4.6}$$

Before computing the optical and X-ray QSOs LFs, we still need make clear several issues. One is the reasonable range of QSOs lifetime. There are several methods to constrain

the range of QSOs lifetime. A minimum value of 10^5 yr is needed to explain the proximity effect in the Lyman alpha forest(Bajtlik, Duncan & Ostrike 1988[12]), while this effect in high redshift QSOs implies a lifetime of $\sim 10^7$ yr (Haiman & Cen 2002[143]). The estimation of clustering gives the range of 10^6 to 10^8 yr (Martini & Weinberg 2001[217]; Haiman & Hui 2001[144]). From the simulation(Hopkins et al. 2005a), the luminosity-dependent QSOs lifetime for fitting QSOs luminosity function is presented as $t_{vis} = 10^9(L_{QSO}/10^9 L_\odot)^\alpha$ yr, where α is a function of the peak of luminosity(Hopkins et al. 2005a, b[154][157]).

We also need the appropriate bolometric corrections , which are needed to convert the bolometric QSOs LFs computed with Equation 4.5 to the optical and X-ray bands. In general, the proper bolometric correction can be obtained from the multiwavelength composite spectrum(e. g. Elvis et al. 1994; Ueda et al. 2003[337]; Vignali, Brandt & Schneider 2003[355]; McLure & Dunlop 2004[225]; Barger et al. 2005[14]; Richards et al. 2006[275]) The relations from bolometric luminosity L_{bol} to B-band luminosity L_B and X-ray luminosity L_X are $L_{bol} = k_B \nu_B L_B$ and $L_{bol} = k_X L_X$. The widely used values are given as $k_B = 11.\ 8$ and $k_X = 35$ for broad-line AGN. More deliberative values are proposed for optical AGNs as $L_{bol} = 9.\ 74\lambda L_\lambda(4400\text{Å})$ at $z < 0.5$, $L_{bol} = 4.\ 62\lambda L_\lambda(1350\text{Å})$ at $1.\ 5 < z < 3.\ 5$ and $L_{bol} = 4.\ 65\lambda L_\lambda(1450\text{Å})$ at $z > 3.\ 5$ (Vestergaard 2004[353]). For non broad line AGNs, the proper value of bolometric correction in X-ray band is about 85(Barger et al. 2005[14]). Shankar et al. (2004)[299] proposed that the bolometric correction in X-rays is a function of X-ray luminosity:

$$k_X = 17(\frac{L_X}{10^{43} ergs\ s^{-1}})^{0.43} \tag{4.7}$$

The mass range of QSOs host haloes need be constrained. We set the minimum and maximum halo masses as $M_{vir}^{min} \geq 2\times10^{11} M_\odot$ and $M_{vir}^{max} \leq 2\times10^{13} M_\odot$. In fact, $M_{vir} \leq\sim 10^{12} M_\odot$ has the tiny contribution to the final QSOs LFs in our computation. The QSOs host halo masses range $10^{12} \sim 10^{13} M_\odot$ also are suggested by QSOs clustering (Porciani, Magliocchetti & Norberg 2004[264]; Croom et al. 2005[83]), weak lensing observations e. g. , Kochanek & White 2001[177];Kleinheinrich et al. 2004[174]) and kinematical measurements (e. g. , Kronawitter et al. 2000[183]; Gerhard et al. 2001[124]). The same limit is also indicated by the theoretical analysis of Cirasuolo et al. (2005)[70] on the velocity dispersion function of early-type galaxies.

We set λ as a parameter in our computation. A slightly rising λ toward high z is

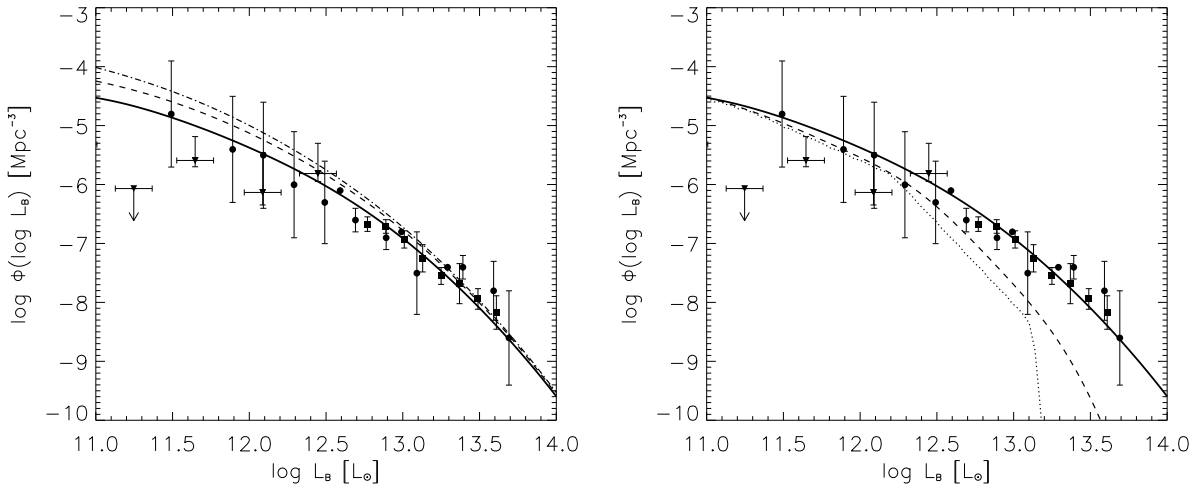

Figure 4.4: Left: predicted QSO LF in the optical B-band at redshift 3 for $\lambda = 1.\ 7$ and different values of the visibility time: $\Delta t_{\rm vis} \approx 5 \times 10^7$ yr (best fit, solid line), $\Delta t_{\rm vis} \approx 10^8$ yr (dashed) and $\Delta t_{\rm vis} \approx 3 \times 10^8$ yr (dot-dashed). Right: effect of the scatter around the mean $\log M_\bullet - \log M_{\rm vir}$ relation. The solid curve is the same as in the left panel and corresponds to a scatter of 0.3 dex. The dashed curve is for a scatter of 0.15 dex and the dotted one for zero scatter. In both panels data are from Pei (1995, *circles*), Hunt et al. (2004, *triangles*), and Richards et al. (2006, *squares*).

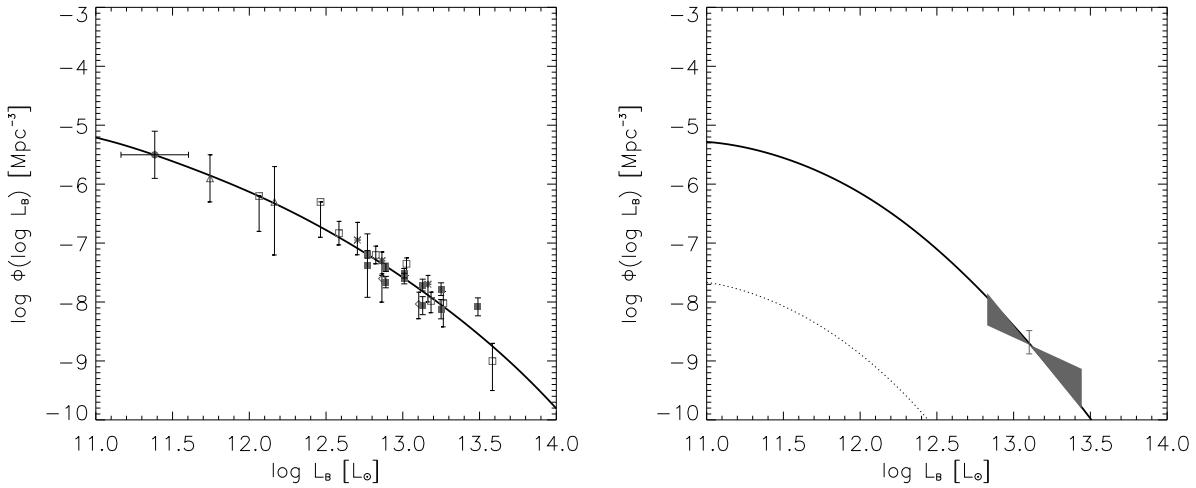

Figure 4.5: Left:QSO LF in the optical B-band at $z = 5$, for $\lambda = 3$ and $\Delta t_{vis} \approx 5 \times 10^7$ yr(solid line), Data points are from Kennefick et al. (1995, open squares); Fan et al. (2001, diamonds and asterisks); Wolf et al. (2003, triangles); Cristiani et al. (2004, circles); Richards et al. (2006, filled squares). Rihgt:QSO LF in the optical B-band at $z = 6$ (solid line) and $z = 8$ (dotted line) for $\lambda = 4$ and $\Delta t_{vis} \approx 5 \times 10^7$ yr(solid line), Data points are from Fan et al. (2004).

needed, and specifically $\lambda = 4$ for $z \geq 6$, $\lambda = 3$ for $5 \leq z \leq 6$, $\lambda = 1.\ 7$ for $3 \leq z \leq 5$, $\lambda = 1$ for $2 \leq z \leq 3$, and $\lambda = 0.8$ for $1.\ 5 \leq z \leq 2$. The empirical formula $\lambda(z) \approx -1.\ 15 + 0.75\ (1 + z)$ works as well in the redshift range $1.\ 5 \leq z \leq 6$. The main motivation for resorting to super-Eddington accretion at high z is to account for the observed space density of very luminous QSOs at $z \geq 5$ (an acceptable fit to lower redshift

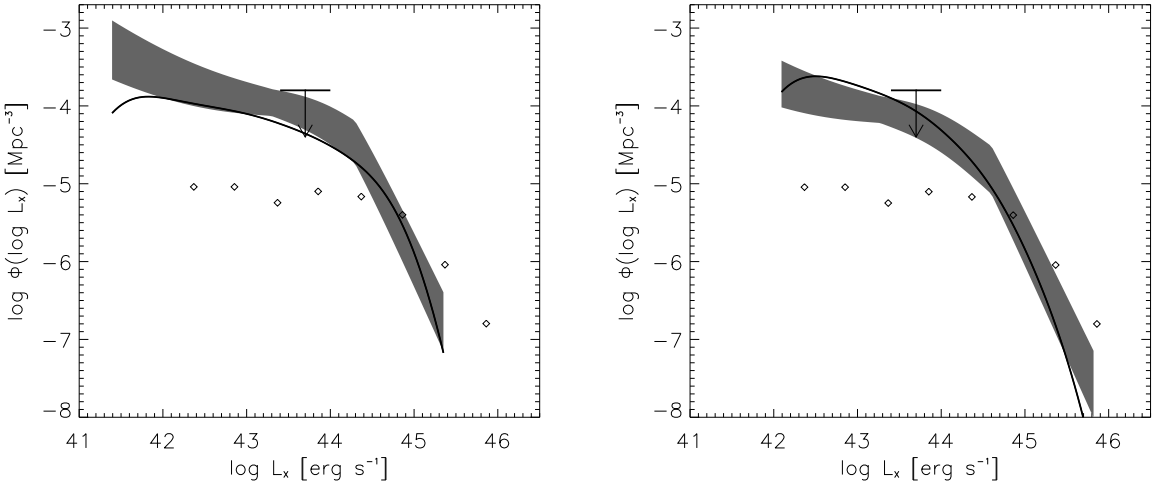

Figure 4.6: Left:QSO LF in the hard X-ray band (2-10 keV) at $z = 1.\,5$ for $\lambda = 0.8$ and $\Delta t_{\rm vis} \approx 3 \times 10^8$ yr. Right:The QSO LF in the hard X-ray band (2-10 keVs) at redshift 2 where $\lambda = 1$, with the visibility time set to $\Delta t_{\rm vis} \approx 3 \times 10^8$ yr; data are from Ueda et al. (2003, *shaded area*), from Barger et al. (2005, *diamonds*), and from La Franca et al. (2005, *arrow*).

data can be obtained keeping $\lambda \approx 1$). Since, as indicated by Equation 4.5, QSOs seen at the cosmic time t are associated to halos virializing at the earlier time $t_{\rm vir} \leq t - \Delta t_{\rm peak}$, and the density of such halos drops with increasing $\Delta t_{\rm peak}$ at high z, to have a sufficient number of massive enough BHs at $z \geq 5$ we need them to grow faster than implied by Eddington-limited accretion. The super-Eddington accretion rates provide the necessary shortening of $\Delta t_{\rm peak}$ and also give high enough luminosities without resorting to too large BH masses. The redshift dependence of λ may thus be seen as a way to parameterize aspects of the physics of the accretion/emission process not properly taken into account by our simple model.

In Figure. 4.3, 4.4, 4.5 and 4.6, we compare G04 model results with of the observations of the B-band QSOs luminosity function at $z \sim 1.\,5,\ 2,\ 3,\ 5,\ 6$ and the hard X-ray QSOs luminosity function at $z \sim 1.\,5,\ 2$(see also Lapi et al. 2006[190]). In Figure 4.5 right panel, we predict that the QSOs luminosity function dramatically drop off at redshift above 6, due to much lower abundances of massive halos. The flattening of the LFs at the low end is due to the flatter slope of the formation rate of less massive halos and to the weak dependence of the peak time, $\Delta t_{\rm peak}$, on the halo mass. A dispersion of 0.3 dex associated to the $M_\bullet - M_{vir}$ relation and the choice of QSOs lifetime t_{vis} are important to reproduce the observed LFs. Figure 4.4 shows the effects with different QSOs lifetime and different scatter. The cutoff of halo mass would yield a drastic drop so that introducing a Gaussian scatter is required for a global fit. Since hard X-ray emission from the growing

black holes is more easily detected,the X-ray luminosity functions in the Figure 4.6 need a visible time about 3×10^8 yr, which is slightly larger than that of optical LFs.

4.2 QSOs FEEDBACK

The theoretical evidence for the importance of AGN feedback has continued to mount. Tabor & Binney (1993)[320] and Binney & Tabor (1995)[28] employed AGN feedback to prevent catastrophic radiative cooling of the Xray emitting gas that surrounds elliptical galaxies. If unopposed, radiative cooling would lead to the deposition of large quantities of cold gas in the central galaxy, and thus cause the galaxy to grow rapidly. Since this appears not to be the case, it was assumed that there must be a heat source that balances the cooling. In a different approach to a similar problem, semi-analytic models of galaxy formation and evolution (e. g. Benson et al. 2003[21]; Croton et al. 2006[85]; Bower et al. 2006[39]) also demonstrated that AGN feedback was necessary to reproduce the observed galaxy luminosity function at large masses, and balance the large radiative cooling rates in clusters of galaxies. In the absence of AGN feedback, the models produced too many massive galaxies.

The question is how something very small (BH) can determine the growth of something very large (galaxy). This is possible because the gravitational potential energy acquired by an object approaching a black hole is a million times larger than the energy of an object orbiting in the potential of a typical galaxy. As a black hole grows to 0.2% of the bulge mass through accreting matter, it releases nearly 100 times the gravitational binding energy of its host galaxy.

The total energy output released during the QSOs lifetime is:

$$E = \bar{\varepsilon} M_{\bullet} c^2 \tag{4.8}$$

where $\bar{\varepsilon} = \bar{\varepsilon_r} + \bar{\varepsilon_m}$ is an efficiency factor, and we use $\bar{\varepsilon_r}$ and $\bar{\varepsilon_m}$ to denote the mean radiative and mechanical efficiencies, respectively. For an early-type galaxy with the mass $M_\star$ and velocity dispersion σ, the gravitational binding energy is roughly $W \sim -M_\star \sigma^2$. The ratio

between total energy output from an AGN to the binding energy of its host galaxy follows

$$\frac{E}{|W|} = \frac{\bar{\varepsilon} M_\bullet}{M_\star} (\frac{c}{\sigma})^2 \tag{4.9}$$

The observational result gives $M_\bullet / M_\star \sim 2 \times 10^{-3}$. Thus, for a massive galaxy with $\sigma \sim 300 kms^{-1}$ the ratio $E/|W|$ is about $2000\bar{\varepsilon}$, indicating that the AGN energy can easily surpass the total binding energy of the host galaxy. Therefore there is no question that an AGN could drastically affect its host galaxy. Whether and how it does so, however, is an open question that depends on how much of the energy released actually interacts with the matter in the galaxy. If the matter consists of gas, perhaps with embedded dust, the radiative output of the black hole can both heat the gas, and drive it via radiation pressure (so-called *Radiative Feedback*). The radiative form of feedback is most effective when the black hole is accreting close to its Eddington limit. Alternatively, if significant AGN power emerges in winds or jets, mechanical heating and pressure provide the link (so-called *Mechanical Feedback*). The mechanical form associated with jets, on the other hand, operates at rates below the Eddington limit.

The momentum-driven feedback and Compton heating are expected to be most important ways of radiative feedback. The former becomes efficient when the the radiation pressure can overcome the gravitational force of the host halo. The gas can flow out from the center in the form of a momentum-driven wind (e. g. Murray et al. , 2005[232]). If all the momentum of the radiation is transferred into the gas, the total energy extracted is roughly a fraction of v/c of the total radiation energy of the AGN, where v is the velocity of the accelerated gas. Thus, the energy feedback generated by radiation pressure is more efficient if the radiation pressure accelerates a smaller amount of gas to a higher velocity. In broad-line QSOs, where the gas outflow velocity can be as high as $\sim 0.2c$, acceleration by radiation pressure is an efficient energy injection mechanism (Sturm et al. 2011, Feruglio et al. 2010, Fischer et al. 2010, Rupke & Veilleux 2011). In Chapter 1, we quantify QSOs feedback assuming this kind of momentum-driven wind dominates. The latter, Compton heating, happens when the Compton scattering between an electron and a photon transfers energy from the photon to the electron and thereby heating the gas, which is ionized and has a temperature lower than the effective (Compton) temperature of the radiation field.

Evidence for mechanical feedback can be seen in a number of elliptical galaxies at the

centers of clusters, which contain X-ray cavities filled with relativistic gas. These X-ray cavities, often loosely referred to as 'bubbles', are believed to be inflated by the jet launched from the central SMBH, and the power involved can be substantial. The typical kinetic power estimated for the central galaxy of a cluster is about $10^{45}\ erg\ s^{-1}$, more than enough to offset the radiative cooling of the intracluster gas.

4.3 Summary

In this Chapter, we briefly review that the QSOs LFs can be well reproduced by the G04 model based on the work of Lapi et al.(2006). In this model, the growth rate of BHs is proportional to the SFR, and the latter is more effectively slowed down by SN feedback in smaller halos, resulting in a relatively more efficient growth of more massive BHs, especially at higher redshifts. Both star formation and BH growth in massive halos are stopped by the feedback from the active nucleus as soon as it becomes powerful enough to sweep out the residual interstellar medium. The BH accretion occurs in host galaxies with very intense star formation, and is heavily dust obscured for the majority of its duration; however, most of the final BH mass is gained during the last 1 - 2 e-folding times in unobscured conditions. The observed epoch-dependent B-band LFs are accurately reproduced for the optical (B-band) visibility time of order of the e-folding time, indicating that only when the AGN is approaching its maximum luminosity it can clear up the surrounding region. The redshift dependence of the space density of optically bright QSOs is controlled by two competing factors. On one side, according to the hierarchical clustering paradigm, the formation rate of very massive halos hosting them is increasing rapidly with decreasing redshift. On the other side, the BH to host halo mass ratio decreases with decreasing redshift, so that at low redshifts relatively more massive hosts are required for a given BH mass. But the galactic halo mass function sinks down exponentially for large halo masses, and is actually cut off at $M_H \approx 2 \times 10^{13} M_\odot$.

Chapter 5

SIZE EVOLUTION OF MASSIVE ETGS

Sizes of Early-Type galaxies (ETGs) in the local universe are found to well correlate with the stellar masses (effective radius $R_e \propto M_\star^{0.55}$, Shen et al. 2003[302], Hyde & Bernardi 2009[158]). However, when moving towards high redshift, ETGs are found to deviate far from the local $R_e - M_\star$ relation. By recent observations(Ferguson et al. 2004[111]; Trujillo et al. 2004, 2006, 2007[336][335][334]; Longhetti et al. 2007[198]; Toft et al. 2007[328]; Zirm et al. 2007[365]; van der Wel et al. 2008[343]; van Dokkum et al. 2008[344]; Cimatti et al. 2008[67]; Buitrago et al. 2008[49]; Damjanov et al. 2009[90]), most of the massive (stellar mass $M_\star \geq 3 \times 10^{10}$ $M_\odot$), passively evolving, galaxies at $z \geq 1$ observed with high enough angular resolution exhibit characteristic sizes of their stellar distributions much more compact than local ETGs of analogous stellar mass. If these observations are indeed true, there are two important questions involving the formation and evolution of massive ETGs arisen :1) How did the small size of massive ETGs form at high redshift? 2) How did the compact, massive ETGs evolve to 'catch up' the local relation? In this Chapter, the recent progress on answering these two questions are reviewed. In Section 5.1, two possible formation mechanisms for smaller size at higher redshift are introduced. In Section 5.2, we show the observed size evolution from z 2. In Section 5.3, several possible mechanisms for explaining observed size evolution are reviewed. In Section 5.4, several observational tests have been checked for constraining the contributions to observed size evolution by different mechanisms.

5.1 Expected sizes of high redshift galaxies

There are two possible mechanisms to form small size of high redshift galaxies. One is according to the fast, dissipative collapse of baryons. The other one is according to gas-rich(wet) disks merger. These two mechanisms will be introduced as follows.

5.1.1 Dissipative collapse of the baryons

The effective radius R_e is defined as the half-mass radius , or the half-luminosity radius if the light traces the mass. Observations show that the brightness profiles of nearly all ETGs with remarkable precision over large dynamic ranges can be fitted by the Sérsic function:

$$I(r) = I(0)\ e^{-b_n\ (r/R_e)^{1/n}}\ , \tag{5.1}$$

(Caon et al. 1993[56] ;Kormendy et al. 2009[179]). Here $I(0)$ is the central surface brightness, and n is the Sérsic's index. The constant b_n can be determined from the condition that the luminosity inside R_e is half the total luminosity $L(R_e) = L_T/2$ (see Prugniel & Simien 1997[269]). The classical de Vaucouleurs profile corresponds to $n = 4$.

The stellar component gravitationally dominates in the inner regions of galaxies, while the DM with its extended halo dominates in the outer regions. To a halo with mass $M_{\rm H}$ we can associate an initial baryon mass $M_{\rm b,\ i} = f_b\ M_{\rm H}$, where $f_b \approx 0.2$ is the cosmic baryon to DM mass ratio. Weak lensing observations (Mandelbaum et al. 2006[210]), extended X-ray emission around ETGs (e. g. , O'Sullivan & Ponman 2004[245]) and the comparison of the statistics of the halo mass function with the galaxy luminosity function (Vale & Ostriker 2004[340]; Shankar et al. 2006[299]; Guo & White 2009[141]; Moster et al. 2010[229]) point to a present-day ratio $m = M_{\rm H}/M_\star \approx 20 - 40$ between the total halo mass to the total mass in stars for red massive galaxies. This result quantifies the inefficiency of the star formation process even in large galaxies, since $M_\star/M_{\rm b,\ i} = 1/(m\ f_b)$. For $M_{\rm H} \geq 3 \times 10^{11}\ M_\odot$, corresponding to $M_\star \geq 10^{10}\ M_\odot$, the dependence on halo mass and formation redshift of ratio m between the halo mass and the surviving stellar mass (i. e. the present day stellar mass fraction) can be approximated as $m \approx 25\ (M_{\rm H}/10^{12}\ M_\odot)^{0.1}\ [(1 + z_{\rm form})/4]^{-0.25}$. At lower masses m increases rapidly with decreasing $M_\star$.

As for the inner regions, we consider the ETG progenitor $1255-0$ at $z \approx 2.2$, for which van Dokkum et al. (2009)[345] and Kriek et al. (2009)[182] find $M_\star \approx 2\times10^{11}\ M_\odot$ within the half-light radius $R_e \approx 0.8$ kpc; local ETGs with the same mass have an average size $R_e \approx 7$ kpc (see Shen et al. 2003[302]; Hyde & Bernardi 2009[158]). If $m \approx 30$, we can associate to $1255-0$ a halo mass $M_{\rm H} \approx 6\times10^{12}\ M_\odot$. Assuming a NFW profile with concentration $c = 4$, it is easy to see that inside the gravitational radius $R_g \approx 3\ R_e \approx 3$ kpc, the DM fraction amounts to $f_{\rm DM} \approx 0.1$. We notice that the DM contribution to the mass within the half-light radius R_e of local ETGs is $f_{\rm DM} \leq 30\%$ (e. g. , Borriello et al. 2003[32]; Tortora et al. 2009[331], Cappellari et al. 2006[57]), and has a small effect on the stellar velocity dispersion. This supports the notion that the dissipationless DM cannot parallel the dissipative collapse of baryons, so that its gravitational effects within R_e can be neglected also during the compact phase of galaxy evolution.

After the dissipative collapse of baryons inside a host DM halo, the gravitational radius of the baryonic component, stars plus gas with mass $M_\star$ and $M_{\rm gas}$ respectively, reads

$$R_g = \frac{G\ M_\star\,(1+f_{\rm gas})}{\sigma_\star^2} \tag{5.2}$$

where $f_{\rm gas} = M_{\rm gas}/M_\star$ is the gas to star mass ratio within the gravitational radius. If light traces mass, the projected half stellar mass radius R_e is related to the gravitational radius R_g by $R_e = S_s(n)\ R_g$, and the density-weighted, 3−dimensional velocity dispersion $\sigma_\star$ is related to the observed line-of-sight *central* velocity dispersion σ_0 by $\sigma_\star = [3\ S_K(n)]^{1/2}\ \sigma_0$. Note that σ_0 is usually measured within a physical size of about $\frac{1}{8}\ R_e$ (e. g. , Jørgensen et al. 1993[165]). At virial equilibrium, the mass is given by:

$$M_\star = S_D(n)\frac{1}{G}\ R_e\ \sigma_0^2 \tag{5.3}$$

where $S_D(n) = 3\ S_K(n)/S_s(n)$. Prugniel & Simien (1997)[269] have tabulated the coefficients S_D, S_K, and $S_s(n)$ for values of the Sérsic index n ranging from 1 to 10; in particular, $S_s(4) \approx 0.34$, $S_K(4) \approx 0.52$, and $S_D(4) = 4.591$. We note that the central gas mass includes the cold component as estimated in the Appendix (see Equation [A.8] and below for analytic approximations).

If before collapse the baryons had the same velocity dispersion $\sigma_{\rm b,\ i}$ as the DM $\sigma_{\rm DM}$, and taking into account that $\sigma_{\rm DM}$ is approximately equal to the halo rotational velocity $V_{\rm H}$ (see Appendix), the 3-D stellar velocity dispersion $\sigma_\star$ at the end of the collapse can be

written as (Fan et al. 2008)[109]:

$$\sigma_\star = f_\sigma \ \sigma_{\rm b,\ i} = f_\sigma \ \sigma_{\rm DM} \approx f_\sigma \ V_{\rm H} \ . \tag{5.4}$$

Recalling that $R_e = S_s(n) \ R_g$, with R_g given by Equation (5.2), and that $V_{\rm H}^2 = G \ M_{\rm H}/R_{\rm H}$ we then obtain R_e in terms of the halo radius $R_{\rm H}$ and mass $M_{\rm H}$:

$$\begin{aligned} R_e &\approx \frac{S_s(n)}{f_\sigma^2} \ \frac{(M_\star + M_{\rm gas})}{M_{\rm H}} \ R_{\rm H} \approx \\ &\approx 0.9 \ \frac{S_s(n)}{0.34} \ \frac{25}{m} \ \left(\frac{1.\ 5}{f_\sigma}\right)^2 \ \left(\frac{M_{\rm H}}{10^{12} \ M_\odot}\right)^{1/3} \ \left(\frac{4}{1+z_{\rm form}}\right) \quad {\rm kpc}, \end{aligned} \tag{5.5}$$

where $z_{\rm form}$ is the redshift when the collapse begins, and we have set $f_{\rm gas} = 1$. This equation shows that the baryon collapse naturally leads to kpc or sub-kpc effective radii and to stellar velocity dispersions higher than halo rotational velocities ($f_\sigma > 1$). Both these properties differ from those observed for local massive galaxies, implying that other ingredients have come into play.

The explicit redshift dependence of R_e in Equation (5.5) comes from the halo radius, which scales as $(1+z_{\rm form})^{-1}$. In addition, the ratio m, which measures the star formation inefficiency and is determined by the physics of baryons, scales as $(1+z_{\rm form})^{-0.25}$ (see Appendix). As a result the effective radius scales like $R_e \propto (1+z_{\rm form})^{-0.75}$. The values of m and of f_σ depend on how and when the star formation and gas heating processes can halt the collapse. The latter must proceed at least until the mass inside the R_e is dominated by stars, as observed in local ETGs.

5.1.2 Gas-rich(wet) Mergers

In the merger scenario, the size of the remnant depends on those of the progenitors as well as on the amount of dissipation and star formation during the merger. In the case of a merger between two galaxies with no gas(a 'dissipationless' or 'dry' merger), it's particularly easy to predict the size of the remnant from the sizes and masses of the progenitors. It's well established in numerical simulations that the effect of any merger of dissipationless components is to enlarge their size by a factor, while roughly, conserving profile shape(Boylan-Kolchin et al. 2005[41], 2006;Hopkins et al. 2008a[155]). In detail, consider two virialized, gas-poor galaxies with stellar mass M_1 and $M_2 = fM_1 (f \leq 1)$ and effective radii R_1 and R_2, which merger to form a galaxy with stellar mass M and

effective radius R. In the simplest case, we only consider the merger with a parabolic orbit and ignore the effects of the stellar mass ejected from the merger remnant due to the violent potential fluctuations and the energy transferred from the stars to the dark matter. Once the merger remnant has established virial equilibrium, the total energy of its stars is given by

$$E = -\eta \frac{G(M_1 + M_2)^2}{2R} \tag{5.6}$$

where η is a form factor. Energy conservation allows us to write

$$\eta \frac{(M_1 + M_2)^2}{R} = \eta_1 \frac{M_1^2}{R_1} + \eta_2 \frac{M_2^2}{R_2} \tag{5.7}$$

In addition, we assume homology, so that $\eta = \eta_1 = \eta_2$.

$$R = R_1 \frac{(1+f)^2}{(1 + f^2 \frac{R_1}{R_2})} \tag{5.8}$$

An equal mass merger will result in $R = 2R_1$. We note here we assume a parabolic orbit and ignore the energy transferred from stars to the dark matter. However, Boylan-Kolchin et al. (2005)[41] have shown that realistic orbits will be elliptic-like and lead to $R = 1.\ 4R_1$.

When taking gas into account, the situation will be much more complicated because the amount of dissipation and star formation during the merger will occur, which processes depend strongly on the gas content of the progenitors and on the details of the merger. Ciotti et al. (2007)[68] have modeled each elliptical galaxy as a non-rotating, isotropic, and spherically symmetric virialized system, characterized by a stellar mass $M_\star$, a gas mass $M_g = \alpha M_\star$(We ignore the tiny contribution by SMBH). If profile shape is roughly preserved, then we expect

$$R = R_1 \frac{(1+f_t)^2}{(A_1 + A_2 f_t^2 \frac{R_1}{R_2})} \tag{5.9}$$

Here $f_t = (M_{\star 1} + M_{g1})/(M_{\star 2} + M_{g2})$ is the ratio of total baryons of two progenitors. $A_1 = 1 + \frac{\epsilon \alpha_1}{1+\alpha_1}$, where ϵ is the fraction of total gas mass in two progenitors converted into stars and $M_{g1} = \alpha M_{\star 1}$. And A_2 has a similar expression as A_1. For the dry merger, $A_1 = A_2 = 1$, $\alpha_1 = \alpha_2 = 0$, and equation 5.9 will reduce to equation 5.8. For an extreme case of wet merger ($\epsilon = 1$ and $\alpha_1 = \alpha_2 = 1$), the equal mass merger will result in $R = \frac{4}{3} R_1$. Even in this case, the remnant size is still larger than those of its progenitors. More realistically, the profile could be changed. Subsequent spheroid-spheroid mergers continue to

scatter stars out to larger radii, building an extended envelope and changing the profile. However, the form factor η is just weakly influenced by the profile shape. A raising of the best-fit Sérsic index by Δn 2 will decrease the size by a factor of upper to 1. 2.

Covington et al. (2008)[79] has given the impulse approximation to estimate the energy loss in the gaseous component, followed by collapse in a self-gravitating starburst. For typical conditions, this reduces to the simple approximation (Hopkins et al. 2008b[153], 2009[156])

$$R = \frac{R_{dry}}{1 + (f_{gas}/f_0)} \tag{5.10}$$

where $f_0 \approx 0.25-0.30$ and R_{dry} is the radius expected for a dry merger remnant which can be computed with equation 5.8. For most major mergers, gas in the disks at the time of the merger will rapidly lose energy, and star formation is very efficient, f_{gas} reflects the gas fractions of the progenitor disks immediately before the merger. The equation 5.10 could not be true in extremely gas-rich mergers($f_{gas} > 0.5$), where torques are inefficient at driving dissipation, and ellipticals may not be formed from even major mergers (Hopkins et al. 2008b[153]). With the limit of $f_{gas} \leq 50\%$, and in case of the equal mass merger, the remnant size will be expected to be $\frac{2}{3}$ to 1 times of the progenitor size dependent on the gas fraction in the progenitor disks.

5.2 Observed size evolution

In this section we present the recent observational results on the cosmic size evolution of ETGs.

A recent analysis by Maier et al. (2009)[206] of a sample including about 1100 galaxies with Sérsic index $n \geq 2.5$, *spectroscopic* redshifts in the range $0.5 \leq z \leq 0.9$ and stellar masses in the range $3 \times 10^{10}\ M_\odot \leq M_\star \leq 3 \times 10^{11}\ M_\odot$ shows that the size evolution for galaxies at $z \sim 0.7$ is within a factor $f_r(0.7) = R_e(0)/R_e(0.7) \leq 1.25$. For galaxies at $0.7 \leq z \leq 0.9$ the size evolution is limited to a factor $f_r(0.9) \leq 1.4$. Small size evolution ($f_r \leq 1.3$) for redshifts $z \leq 0.8$ was previously reported by McIntosh et al. (2005)[222] for a sample of 728 red galaxies with Sérsic index $n \geq 2.5$ and stellar masses in the range $3 \times 10^9\ M_\odot \leq h^2\ M_\star \leq 3 \times 10^{11}\ M_\odot$; in this case, however, the majority of redshifts were photometric. At lower redshift, $z \approx 0.25$, the Brightest Cluster Galaxies (BCGs)

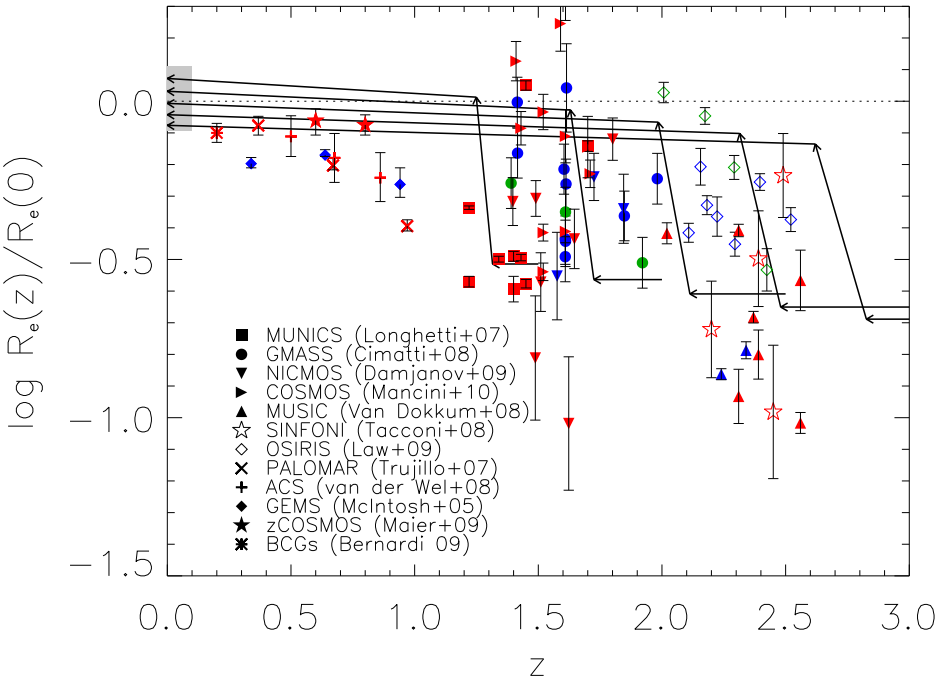

Figure 5.1: Evolution of the effective radius with redshift. The data points show: average sizes of $z \leq 1$ passively evolving galaxies, divided by the local sizes of galaxies of equal stellar mass, in the samples by Trujillo et al. (2007)[334], McIntosh et al. (2005)[222], van der Wel et al. (2008)[343], Maier et al. (2009)[206] and Bernardi (2009)[22], with the associated errors; individual data and error bars for passively evolving galaxies with spectroscopic redshifts $z \geq 1$ by Longhetti et al. (2007)[198], Cimatti et al. (2008)[67], Damjanov et al. (2009)[90], Mancini et al. (2010)[208], and van Dokkum et al. (2008)[344]; data and error bars for individual star forming galaxies with spectroscopic redshifts $z \geq 2$ by Tacconi et al. (2008)[322] and Law et al. (2009)[194]. The color of the data points refers to the stellar mass of the galaxy: red is for $M_\star \geq 10^{11}\ M_\odot$, blue for $3 \times 10^{10}\ M_\odot \leq M_\star \leq 10^{11}\ M_\odot$, and green for $M_\star \leq 3 \times 10^{10}\ M_\odot$. The shaded area reflects the distribution of local SDSS galaxies (Hyde & Bernardi 2009)[158]. Thick solid lines with arrows illustrate typical evolutionary tracks of massive galaxies according to G04 model (with $f_\sigma = 1.\ 5$).

exhibit slow evolution $f_r \leq 1.\ 3$ (Bernardi 2009)[22].

A size evolution somewhat more pronounced (around 40%) than found by Maier et al. (2009)[206] has been claimed by Trujillo et al. (2007)[334] for massive galaxies $M_\star \geq 10^{11}\ M_\odot$ at redshift $z \approx 0.65$. However, restricting the analysis to galaxies with *spectroscopic redshifts* in the range $0.5 \leq z \leq 0.8$ (91 galaxies with $n \geq 2.\ 5$ and mean stellar mass of $1.\ 8 \times 10^{11}\ M_\odot$) we find a mean effective radius of 4. 94 kpc. The mean local effective radius for galaxies with this stellar mass is around 6 kpc, implying an increase by a factor $f_r(0.65) \approx 1.\ 2$. On the other hand, the mean effective radius decreases to 3. 8 kpc for galaxies with the same mean mass but with average redshift $z \approx 0.9$; in this case the size evolution amounts to a factor $f_r(0.9) \approx 1.\ 6$. Similar results are found by Ferreras et al. (2009)[115] for a sample of 195 red galaxies selected in the

redshift range $0.4 \leq z \leq 1.\,2$. They are, on average, more compact than local galaxies with Sérsic index $n \geq 2.\,5$ by a factor of only $f_r \approx 1.\,4$.

A stronger evolution of R_e at fixed stellar mass was reported by van der Wel et al. (2008)[343] for a composite sample of 50 morphologically selected ETGs in the redshift range $0.8 \leq z \leq 1.\,2$. Since we are interested on the evolution at $z \leq 1$ we have confined ourselves to the 20 galaxies in a massive clusters at $z \approx 0.83$. For these we find, on average, $f_r(0.83) \approx 1.\,6$, but with a substantial mass dependence: the most massive galaxies (dynamical mass within R_e of $M_{\rm dyn} \geq 3 \times 10^{11}\ M_\odot$) fall quite close to the local mass vs. R_e relation, while the lower mass galaxies tend to exhibit large size evolution.

All the results mentioned above are shown in Figure 5.1, where we also present a compilation of the data at redshift $z \geq 1$. We note that, while the data points at $z \leq 1$ are averages over large samples, at higher redshift data points refer to individual galaxies.

Assuming that the average evolution of R_e can be described by a power law of the form $R_e \propto (1+z)^\alpha$, Buitrago et al. (2008)[49] find $\alpha = 1.\,48$, while van der Wel et al. (2008)[343] obtain a lower value $\alpha = 1.\,20$. The latter authors also suggest a weaker evolution, corresponding to $\alpha = 0.96$, for $z \leq 1$. However, even this milder evolution is faster than indicated by the most recent data summarized above, and especially by the most extensive and spectroscopically complete study of Maier et al. (2009)[206].

A relevant feature of the data for massive galaxies at high redshift is the quite large spread of the size, as it is apparent from Figure. 5.1 and 5.2. Specifically, for masses larger than $10^{11}\ M_\odot$ the scatter in size of high redshift ETGs amounts to $\sigma_{log(R_e)} \approx 0.41$, significantly wider than in local samples, for which we have typically $\sigma_{log(R_e)} \approx 0.14$ (cfr. Shen et al. 2003[302]; Hyde & Bernardi 2009[158]). In more detail, several high redshift galaxies exhibit the same size as their local counterparts (see e. g. Mancini et al. 2010[208]; Onodera et al. 2010[244]), while about half ETGs exhibit $f_r \geq 3-4$, with several of them having $f_r \geq 8-10$. It is worth noticing that Maier et al. (2009)[206] find for the size distribution at fixed mass of their sample of ETGs at redshift ≈ 0.7 a statistical dispersion $\sigma_{log(R_e)} \approx 0.16$ very close to the local one.

Provided that the presently available data constitute a representative sample of the size of high redshift ETGs, both the average increase of the size and the narrowing of its distribution are to be accounted for. Only large samples of high-z ETGs will allow

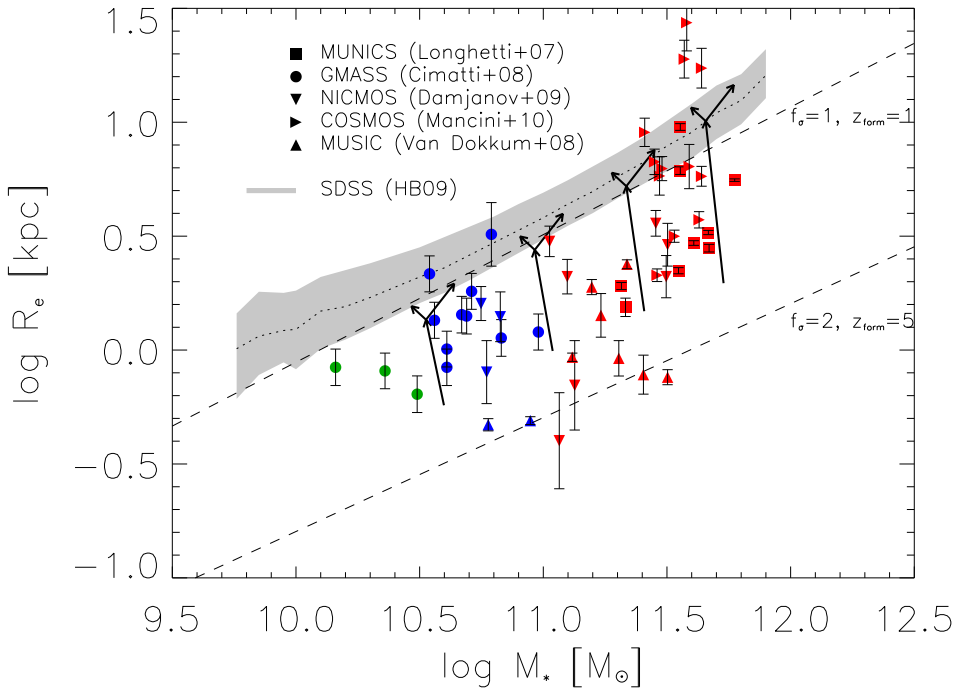

Figure 5.2: Correlation between effective radius and stellar mass. The observations of passively evolving galaxies with spectroscopic redshifts $z \geq 1$ by Longhetti et al. (2007)[198], Cimatti et al. (2008)[67], Damjanov et al. (2009)[90], Mancini et al. (2010)[208], and van Dokkum et al. (2008)[344] are compared with the local correlation (Hyde & Bernardi 2009[158]; the dotted line illustrates the average and the shaded area represents the variance). Color code refers to the stellar mass, as in previous Figure. The dashed lines illustrates the outcomes of Equation (5) for extreme values of the relevant parameters f_σ and $z_{\rm form}$ (see text). Thick lines with arrows illustrate typical evolutionary tracks of massive galaxies according to G04 model (with $f_\sigma = 1.\,5$ and $z_{\rm form} = 3$), featuring first the abrupt size growth due to quasar feedback (almost vertical arrows), and then the possible slow size increase due to mass loss (arrows pointing left) or mass additions by minor mergers (right pointing arrows.).

us to assess the interesting issue of their size distribution. We also note that the paucity of data at $z \geq 1$ prevents the investigation of the possible mass dependence, a crucial aspect for any interpretation of the phenomenon.

So far we have discussed the evolution by comparing high redshift size determinations with the average size of local ETGs. A bias may arise because high-z samples of passively evolving galaxies pick up objects that formed at higher redshifts and therefore have smaller sizes. The majority of local ETGs probably formed at $1.\,5 \leq z_{\rm form} \leq 2.\,5$, but ETG progenitors already in passive evolution at $z \approx 2-2.\,5$ formed about 1 Gyr earlier, i. e. , at $z_{\rm form} \geq 3.\,5$. The latter are expected to have, on average, a factor $\approx 1.\,5 - 2$ smaller size than local ETGs (see Equation 5.5 below). This may explain why Valentinuzzi et al. (2010)[341] find that a substantial fraction (around 22%) of ETGs in local galaxy

clusters (overdense regions were the galaxies typically formed earlier than in the field) are more compact than the local average. In fact, their cluster galaxies are on average 1. 5 Gyr older than local ETGs with 'normal' size. It is worth mentioning that several massive blue galaxies have recently been found to exhibit compact sizes (Trujillo et al. 2009)[333].

Massive starforming galaxies at high-z are heavily obscured by dust and therefore their structure cannot be investigated by means of optical or near-IR observations; however, one can resort to interferometric observations at millimeter and submillimeter wavelengths. In particular CO molecular emission has been spatially resolved for a sample of submillimeter bright galaxies at $z \approx 2$ by Bouché et al. (2007)[33] and Tacconi et al. (2008, 2010)[322][321] with the IRAM Plateau de Bure millimeter interferometer. The results obtained for the galaxies with spectroscopic redshift are shown in Figure 5.1. For these objects the dynamical mass is a good proxy for the mass in stars and gas.

In Figure 5.1 we also plotted the data of Law et al. (2009) on a sample of Lyman break galaxies at redshifts $2 \leq z \leq 3$ and with kinematics dominated by random motions at least in the central $2-3$ kpc. In this case, R_e refers to the $H\alpha$ or [OIII] emissions, which are sensitive to dust extinction. The light distribution is expected to be irregular and knotty, as in fact it is observed. Since the dust distribution inside starforming galaxies follows the star and gas distributions, which peak in the central regions, we expect that the observed light profile is broadened with respect to the true star and gas distribution for rest-frame wavelengths shorter than a few microns (see Joung et al. 2009[166]). Therefore the estimated half-light radii of $H\alpha$ or [OIII] emissions should be considered as upper limits. Nevertheless, Figure 5.1 suggests that large starburst galaxies and high-z passively evolving galaxies, their close descendants, exhibit the same trend of smaller size with respect to the local ETGs.

In Figure 5.2 we compare the observed distribution of local and high-z galaxies in the R_e vs. $M_\star$ plane with expectations from Equation (5.5). A robust upper limit to the high-z correlation (upper dashed line in Figure 5.2) is obtained setting $f_\sigma = 1$ (baryon collapse with no increase of the stellar velocity dispersion) and $z_{\rm form} = 1$, corresponding to a look-back time of about $7-8$ Gyr, a lower limit to the mass-weighted age of local massive ETGs (Gallazzi et al. 2006[121]; Valentinuzzi et al. 2010[341]). The corresponding line falls just at the lower boundary of the distribution of local ETGs, but at the upper boundary of the distribution of high-z passively evolving massive galaxies. The median

size of the latter is a factor around 4 lower than that of local galaxies with the same stellar mass. This argument is not in contrast with the existence, recently reported by Valentinuzzi et al. (2010)[341], of local compact ETGs, which can represent the evolution of the oldest, most compact progenitors.

The lower bound to the high-z correlation is less well defined; in Figure 5.2 the lower dashed line corresponds to $z_{\rm form} \sim 5$ and to $f_\sigma = 2$. In Equation (5.5), we have adopted as our reference values $f_\sigma = 1.\,5$ and $z_{\rm form} = 3$.

5.3 Physical mechanisms for size evolution

Both theory and observations suggest that at least 60% of ETGs evolve in size by at least a factor of $2-4$. One possibility is that the expansion is driven by the expulsion of a substantial fraction of the initial baryons, still in gaseous form, by quasar activity (Fan et al. 2008, 2010[109][108]) and/or by an expulsion of gas associated to stellar evolution (e. g. , Damjanov et al. 2009[90]), which differ in the expulsion timescale, which is shorter than the dynamical time if it is triggered by quasar activity and longer in the case of ejection associated to stellar evolution (with 'standard' IMFs).

Alternatively, the increase in size could be due to minor mergers on parabolic orbits that add stars in the outer parts of the galaxies along the cosmic time from $z \approx 1-2$ to the present epoch (see Maller et al. 2006[207]; Naab et al. 2009[233]; Hopkins et al. 2009b[152]; van der Wel et al. 2009[342]).

There are also other possible mechanisms, such as (1) equal mass dry mergers, (2) a gradient in the M/L ratio (lower in the bluer central regions) which can make the half-light radius in the optical smaller than the half-mass radius (Tacconi et al. 2008)[322], (3) observational effects which are arisen from possible biases in fitting or missed light from surface brightness dimming, or the effects of different definitions of effective radii(Mancini et al. 2010[208];Hopkins et al. 2010[151]).

5.3.1 Gas expulsion

In the case of gas expulsion the final size depends on the timescale of the ejection itself. If the ejection occurs on a timescale shorter than the dynamical timescale of

the system $\tau_{\rm ej} < \tau_{\rm dyn}$, immediately after the ejection the size and velocity dispersion are unchanged but the total energy is larger because the mass has decreased. The system then expands and evolves towards a new equilibrium configuration. In the case of homologous expansion the final size R_f is related to the initial one R_i by (Biermann & Shapiro 1979[27]; Hills 1980[149]):

$$\frac{R_i}{R_f} = 1 - \frac{M_{\rm ej}}{M_f} \tag{5.11}$$

where $M_{\rm ej}$ is the ejected mass and M_f is the final mass.

This simple result has been confirmed by numerical simulations of star clusters (e. g. , Geyer & Burkert 2001[126]; Boily & Kroupa 2003[31]). In particular, the simulations by Goodwin & Bastian (2006)[132] and by Baumgardt & Kroupa (2007)[16] show that the expansion of the half-mass radius occurs in about 20 dynamical times and the new final equilibrium is attained within 40 dynamical times. We note that the case of galaxies differs from that of the star clusters owing to the presence of the DM halo. In ETGs the DM halo exerts its gravitational influence outside the central region dominated by stars and prevents the galaxy disruption when $M_{\rm ej}$ approaches or exceeds M_f; the DM potential can also influence the time taken by the stars to reach the new equilibrium.

When the mass loss occurs on a timescale longer than the dynamical time the system expands through the adiabatic invariants of the stellar orbits and one gets

$$\frac{R_f}{R_i} = 1 + \frac{M_{\rm ej}}{M_f} \ . \tag{5.12}$$

Comparison of the two above equations show that the fast expulsion is more effective in increasing the size.

The dynamical time of the stellar component is

$$\tau_{\rm dyn} = \pi \left(\frac{R_e^3}{2\ G\ M_\star}\right)^{1/2} \approx 3 \times 10^6 \left(\frac{R_e}{1\ {\rm kpc}}\right)^{3/2} \left(\frac{10^{11}\ M_\odot}{M_\star}\right)^{1/2} {\rm yr}, \tag{5.13}$$

about $30 - 50$ times shorter than the typical dynamical timescale in local massive ETGs and not much longer than the dynamical timescale usually associated to star clusters. In the case of mass loss due to stellar feedback (Hills 1980; Richstone & Potter 1982)[277] $\tau_{\rm ej} \gg \tau_{\rm dyn}$ for any reasonable choice of the IMF. For instance, if a Chabrier (2003)[60] or Kroupa (2001)[184] IMF is adopted, after an initial burst about half of the mass of

formed stars returns to the gaseous phase over a timescale of 1 Gyr. If this gas is removed from galaxies, the size may grow by a factor of about 2. The higher the proportion of massive stars, the larger the effect on the size, and the shorter the timescale for the size expansion (see Damjanov et al. 2009[90]).

In the case of quasar winds the typical timescale for gas ejection can be estimated as

$$\tau_{\rm ej} = \frac{M_{\rm gas}}{\dot{M}_{\rm wind}} \approx 5 \times 10^6 \left(\frac{m}{25}\right)^{2/3} \left(\frac{M_\star}{10^{11}\ M_\odot}\right)^{5/3} \times \times \left(\frac{M_\bullet}{2 \times 10^8\ M_\odot}\right)^{-3/2} \left(\frac{1+z}{4}\right)\ {\rm yr}, \quad (5.14)$$

where $\dot{M}_{\rm wind}$ is given by Equation A.27, and we have assumed $M_{\rm gas} \approx M_\star$. An alternative definition of $\tau_{\rm ej}$ is

$$\tau_{ej} = \frac{R_e}{V_e} \approx 10^6 \left(\frac{R_e}{1\ {\rm kpc}}\right)^{1/2} \left(\frac{M_\star}{10^{11}\ M_\odot}\right)^{-1/2}\ {\rm yr}\ , \quad (5.15)$$

where $V_e^2 = 2\ G\ M_\star/R_e$ is the escape velocity from the radius R_e. With both definitions the ejection timescale is of the order of the dynamical timescale.

5.3.2 Minor mergers

In the case of minor mergers on parabolic orbits the initial potential energy of the accreting mass is neglected in the computation. Following Naab et al. (2009)[233] we assume that random motions are dominant in high-z ETG precursors and set $\eta = M_a/M_i$ and $\epsilon = \sigma_a^2/\sigma_i^2$, the i and a indices referring to initial and accreted material. The mass after merging is therefore $M_f = M_i\ (1+\eta)$. If $r \propto M_\star^\alpha$, the virial theorem gives $\epsilon = \eta^{1-\alpha}$. Local ETGs have $\alpha \approx 0.56$ (Shen et al. 2003[302]) or even larger in the case of BCGs (Hyde & Bernardi 2009 [158]); in addition, a value $\alpha \approx 0.5$ is implied by the Faber-Jackson relationship.

From the virial theorem and the energy conservation equation it is easily found that the fractional variations of the gravitational radius and of the velocity dispersion between

the configurations before (i) and after (f) merging are:

$$\frac{R_{g,\,f}}{R_{g,\,i}} = \frac{(1+\eta)^2}{(1+\eta^{2-\alpha})} \,, \qquad \frac{\sigma_f^2}{\sigma_i^2} = \frac{(1+\eta^{2-\alpha})}{(1+\eta)} \,. \tag{5.16}$$

Boylan-Kolchin et al. (2008)[43] showed that minor mergers can be effective only if $\eta \geq 0.1$, lower mass ratios requiring too long timescales.

Recent numerical simulations by Naab et al. (2009)[233] agree with these results. Their simulated galaxy, with a mass in stars $M_\star \approx 8 \times 10^{10}$ $M_\odot$ and half-mass radius $R_e \approx 1$ kpc at $z \approx 2$, by $z = 0$ has doubled its stellar mass through minor mergers, reaching $M_\star \approx 1.\,5 \times 10^{11}$ $M_\odot$, while the half-mass radius has increased by a factor 2. 7. The simulations also suggest that most of the increase, a factor of about 1. 8, occurs at $z \leq 1$, i. e, on a cosmological timescale. This is accompanied by a moderate decrease, $\leq 20\%$, of the central velocity dispersion between $z \approx 3$ and $z \approx 0$ and by a decrease of the central density of stellar distribution with time, due to dynamical friction, despite of the total mass increase. However, these simulations yield a present-day half-mass radius a factor of 2 smaller than expected on the basis of the $M_\star$ vs. R_e relationship of Shen et al. (2003[302]; see also Figure 5.2).

We notice that the size evolution in the merging case occurs on timescale which is comparable with the present Hubble time with size scaling $\propto (1+z)^\beta$; in the simulations of Naab et al. (2009)[233] $\beta \approx 1$ holds, and similarly in the findings of van Dokkum et al. (2010)[347] $\beta \approx 1.\,27$.

5.3.3 Other mechanisms

Besides two main competitive mechanisms, there are also four possible mechanisms, (1) equal mass dry mergers, (2) a gradient in the M/L ratio , (3) observational effects(Hopkins et al. 2010[151]).

- **Equal mass dry mergers** Equal mass dry mergers can increase the galaxy size in a way almost directly proportional to the mass increase (see Equation 5.8) and they were also considered (e. g. , Boylan-Kolchin et al. 2006[42]; Naab et al. 2007[234]) but the required space densities of progenitors were found to be incompatible with the

present-day galaxy mass function (Bezanson et al. 2009[26]; Toft et al. 2009[327]) as well as with the dearth of compact, massive galaxies in the local universe (Trujillo et al. 2009[333]).

- **Mass-to-light ratio gradients** Local massive ETGs have weak colour gradients (McDermid et al. 2006[221]; Sánchez-Blázquez et al. 2007[285], and references therein). However, the same is not necessarily true for high-z ETGs which are relatively young; these can have blue cores at their centers with young stars. The change of colour gradients from high-z to local ETGs can, in principle, yield the evolution in the size at fixed wavelength, while conserving the stellar mass. However, the size evolution can not be obtained up to a factor of 2 using the evolution of mass-to-light ratio gradients from $z = 2$. And the fitted Sérsic indices are expected to increase at high-z, which are in conflict with the observations(van der Wel et al. 2008[343];van Dokkum et al. 2008[344]).

- **Observational effects** The large effective radii of massive, low-redshift ETGs are driven by material in low surface density envelopes at large radii. This is difficult to recover at high redshifts. Moreover, galaxy surface brightness profiles are not perfect Sérsic (1968) profiles, so the best-fitting Sérsic profile and corresponding R_e will depend on the dynamic range observed (see e. g. Boylan-Kolchin, Ma & Quataert 2005[41]; Hopkins et al. 2009[156]). Together, these effects can, in principle, lead to a smaller fitted R_e from sampling only the central regions. At lower redshifts, where surface brightness limits are less severe, more such material would be recovered, leading to apparent size. mass and profile shape evolution (R_e changes at fixed $M_\star$), without central surface density or velocity dispersion evolution. However, attempts to calibrate such effects typically find they lead to bias in high-z sizes up to a factor of 2 (Boylan-Kolchin et al. 2005[41]; Hopkins et al. 2009[156]) or smaller (van der Wel et al. 2008[343]).

5.4 Observational tests

The observational data and the theoretical arguments summarized in the previous sections allow us to test and constrain the different models for size evolution. Since a

size increase by minor dry mergers implies an increase in mass, we start by discussing limits on the latter.

5.4.1 The mass evolution of ETGs

Spectral properties of local ETGs with stellar masses $M_\star \geq 3 \times 10^{10}\ M_\odot$ indicate that their light-weighted age exceeds $8 - 9$ Gyr, independently of the environment (see Renzini 2006[274] for a review and Gallazzi et al. 2006[121] for an extensive statistical study). Since light-weighted ages are lower limits to mass-weighted ages (e. g. , Valentinuzzi et al. 2010[341]), it is generally agreed that most of the stars of massive ETGs formed at $z_{\rm form} \geq 1.\ 5 - 2$. An upper limit $\leq 25\%$ to the fraction of stars formed in ETGs in the last ≈ 8 Gyr, and as a consequence to the fraction of gas accreted at intermediate redshift $z \leq 1$, has been derived from studies of narrow band indices of local field ETGs (e. g. , Annibali et al. 2007[6]). Moreover, all massive galaxies that formed and gathered the bulk of their stars at $z \geq 1$ are presently ETGs or massive bulges of Sa galaxies, since there are no late-type, disc-dominated galaxies endowed with so large masses of old stellar populations.

Thus by comparing the stellar mass function of local ETGs to the mass function of all galaxies at $z \leq 1.\ 5$, we can derive information on the mass evolution.

Bernardi et al. (2010)[25] studied in detail about 2000 morphologically-classified local galaxies extracted from the SDSS sample (see Fukugita et al. 2007[119]). They showed that the concentration index C_r can be used to discriminate among galaxy types. The criterion $C_r > 2.86$ includes almost all ellipticals, about 80% of S0 galaxies and 40% of Sa galaxies, likely those with a larger disk component of younger and bluer stars. Correspondingly, while the fraction of E and S0 massive galaxies ($M_{\rm dyn} \geq 10^{11}\ M_\odot$) older than 8 Gyr is quite large, the fraction of massive and old Sa galaxies is less than 50% (cf. Figure 23 of Bernardi et al. 2010[25]).

Therefore, in order to consistently compare the high redshift mass function with the local one, in Figure 5.3 we report the cumulative mass function for the full Bernardi et al. (2010)[25] sample with concentration index $C_r > 2.86$. We also plot the mass function by Cole et al. (2001[73]; similar results were obtained by Bell et al. 2003[19]), that has been computed with criteria that tend to exclude late type galaxies. These local mass functions are compared with estimates by Pozzetti et al. (2007)[265] and Marchesini et

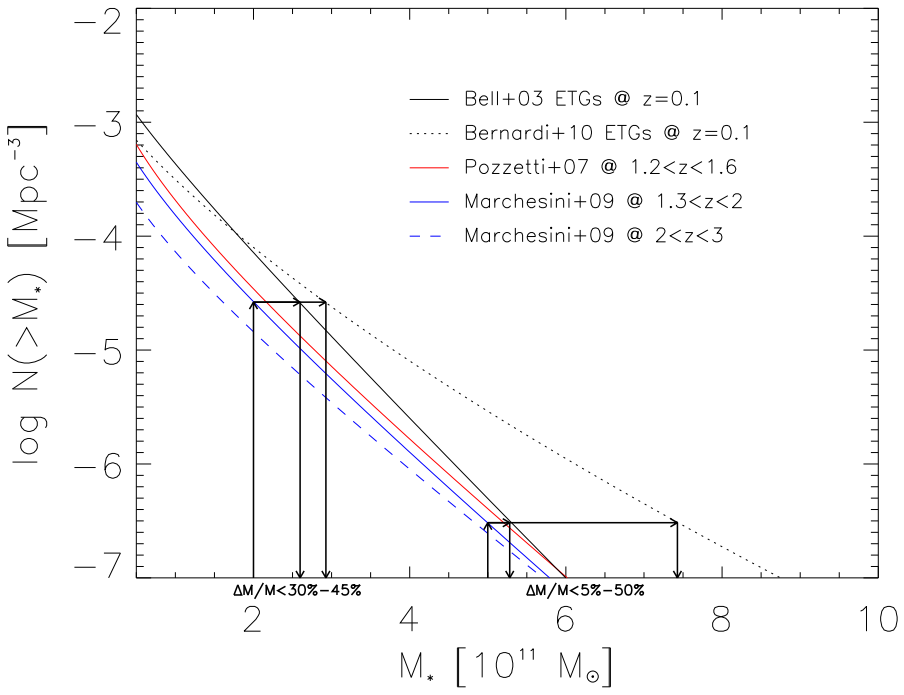

Figure 5.3: Cumulative stellar mass function. The different lines illustrate Schechter fits to the average stellar mass function at different redshifts as estimated by Bell et al. (2003)[19], Bernardi et al. (2009)[22], Pozzetti et al. (2007)[265], and Marchesini et al. (2009)[213]. All estimates have been scaled to Chabrier's (2003) IMF. Thick solid lines with arrows highlight the mass evolution from $z \approx 1.5$ to the present allowed by the observed mass functions, starting from $M_\star \approx 2$ and $5 \times 10^{11}\ M_\odot$.

al. (2009)[213], which refer to redshift $z \approx 1.4$ and $z \approx 1.6$, respectively. All mass functions have been rescaled to Chabrier IMF.

When comparing the local to the high redshift ETG mass function, the first issue is how to make a complete census of high redshift ETG progenitors. Williams et al. (2009)[361] found that in a deep sample (magnitudes $K_{\rm AB} < 22.4$) the most luminous objects at $z \sim 1-2$ are divided roughly equally between starforming and quiescent galaxies. A significant fraction of galaxies at $z \geq 1.5$, forming stars at rates of hundreds to thousands solar masses per year as revealed by far-IR or submillimeter surveys, are easily missed even by deep $K-$band surveys because of their strong dust obscuration (e. g. , Dye et al. 2008[101]). An extreme example is GN10, a galaxy at $z \approx 4$ that exhibits a star formation rate around 1000 $M_\odot$ yr^{-1}, a stellar mass around 10^{11} $M_\odot$ and a dust extinction $A_V \sim 5-7.5$ mag (see Daddi et al. 2009[86]; Wang et al. 2009[358]); this went undetected by ultradeep K_s-band exposures, yielding a $1-\sigma$ upper limit of 23 mJy (Wang et al. 2009[358]) that corresponds to $K_{\rm AB} \geq 28$. Since all galaxies at redshift $z \geq 1.5$ have to be included in the budget, mass functions of high redshift massive

galaxies based on optical or near-IR selected samples should be regarded as lower limits to the high redshift counterparts of local ETGs (see Silva et al. 2005[307] for a more detailed discussion). As a consequence, only upper limits to evolution in mass allowed by the data obtains by assuming that the galaxy number density keeps constant.

In addition, it is apparent from Figure 1 of van Dokkum et al. (2010)[347] that the upper limit to mass evolution slightly depends on mass or correspondingly on the reference number density. van Dokkum et al. (2010)[347] adopt as a reference number density 2×10^{-4} Mpc^{-3} dex^{-1} and find that galaxies with this number density at $z \approx 1.6$ are endowed with $M_{\star} \approx 1.7 \times 10^{11}$ $M_{\odot}$, while at $z \approx 0.1$ the same number density pertains to galaxies with $M_{\star} \approx 2.8 \times 10^{11}$ $M_{\odot}$ (the adopted local number density is that of Cole et al. 2001[73]); the ensuing upper limit to mass evolution is $\leq 70\%$. Applying the same argument to galaxies with number density 2×10^{-5} Mpc^{-3} dex^{-1} yields an upper limit to mass evolution $\leq 40\%$. If the local number density of Bernardi et al. (2010)[25] is adopted, the upper limit to mass evolution is $\leq 50\%$ since $z \approx 1.6$ with practically no dependence on mass, as shown in Figure 5.3.

These upper limits are compatible with evidences that most, if not all, massive ETGs are already in place at redshift $z \approx 1$ (see Drory et al. 2005[98]; Pérez-González et al. 2008[257]; Fontana et al. 2006[116]; Cirasuolo et al. 2010[69]; Kajisawa et al. 2009[167]) and that only a fraction $\leq 30\%$ of their stellar mass can be added at later times. Collins et al. (2009) have estimated the masses of the Brightest Cluster Galaxies (BCGs) in 5 of the most distant X-ray-emitting galaxy clusters at redshifts $z \sim 1.2 - 1.5$, finding that they are perfectly compatible with the local average mass of BCGs. If the two galaxies, which have companions, incorporated them, their mass would increase in one case by about 20% and in the other by 40%.

The results of numerical simulations on DM halos are compatible with such a mass increase. More in detail, Boylan-Kolchin et al. (2008)[43] showed that only merging of satellites with mass ratio $\eta \geq 0.1$ can efficiently increase the mass of their host galaxies. Also the merging rate for massive galaxies inferred from numerical simulations by Stewart et al. (2008)[316] confirms that most of the mass is added by merging of satellites with mass ratio $\eta \geq 0.1$. We stress, however, that these simulations refers to the DM halos and its translation to stellar component of merging halos is not trivial.

To sum up, the data allow, at most, for a mass increase by a factor of ≈ 2 since $z \approx 2$ and by a factor of $\approx 1.5 - 1.7$ since $z \approx 1.5$. We notice also that if the growth occurs

via minor dry mergers, with no evolution of the galaxy number density, practically all massive galaxies gradually increased their mass throughout their entire lifetime, from the formation redshift to $z = 0$ [see, e. g. , the simulations by Naab et al. (2009)[233] and Stewart et al. (2008)[316]]. But then also the galaxy sizes should increase gradually over the full galaxy lifetime, and this can be hardly reconciled with the much larger scatter in size observed for ETG progenitors at $z \geq 1.\ 5$ compared to that at lower redshifts.

5.4.2 Size evolution

The comparison of available data on $z \geq 1$ ETGs with the local size distribution clearly points toward a mean size increase by about a factor of 3 in order to bring the average $M_\star$ vs. R_e relationship of high redshift ETGs to the local average (cf. Figure 5.1), though we caution that larger samples of high redshift ETGs are needed. We stress that the observed small sizes at high-z are indeed expected (cf. Equation [5.5]) if ETG progenitors formed most of their stars in a rapid, dissipative collapse.

As a matter of fact, we expect that high redshift passively evolving ETGs formed at redshift $z_{\rm form} \geq 4$ larger than the formation redshift $z_{\rm form} \approx 1.\ 5 - 2$ of most local ETGs. From the number density of halos with $M_{\rm H} \geq 10^{12}\ M_\odot$ as a function of redshift, we estimate that massive galaxies (with $M_\star \geq 10^{11}\ M_\odot$) formed at redshift $z_{\rm form} \geq 4$ are only 10% of those formed at $z_{\rm form} \approx 2$. Therefore, since $R_e \propto (1 + z_{\rm form})^{-0.75}$ (see Section. 5.1.1), the local counterparts of high-z ETGs, 10% of the total number of ETGs, are expected to exhibit a half-light radius smaller than the average by a factor around 1. 4.

Taking into account this bias, data in Figure 5.1 and in Figure 5.2 show that a significant fraction of local ETG precursors already at $z \geq 1.\ 5$ exhibit the same size as their local counterparts of the same mass. On the other hand, there are also ETG progenitors much more compact than their local counterparts, with sizes smaller by a factor $\leq 1/6$. As a matter of fact, the dispersion in size at high redshift is larger than in the local samples of ETGs. These properties of the size distribution can be accounted for by a model yielding evolution in size by large factors (≥ 5) on timescales shorter than the Hubble time t_H at $z \geq 1.\ 5$. Ejection of large amounts of gas by quasar feedback can reproduce the observed phenomenology. From Equation 5.11 it is apparent that large size expansions are possible, even though gravity of DM halos will constrain them. Also

from Equation 5.13 it is apparent that timescales from a few to several 10^8 yr can be required for the expansion. In this context the scatter of sizes mirrors the spread of formation time and the spread in the expansion phase, as illustrated by Figure 5.1 and Figure 5.2. In particular, in Figure 5.1 lines with an arrow represent the size evolution predicted by G04 model. The lower horizontal lines represent the time (translated to Δz) spent by ETG progenitors in their dusty phase with quite large star formation rate; submm surveys are quite efficient in selecting this phase. Then the (almost vertical) lines represent the epoch of the large size increase due to the gas outflow triggered by the quasar activity; this phase begins with the quasar appearance and lasts $\Delta T_{\rm size}$ (here $\Delta T_{\rm size} \approx 2 \times 10^8$ yr has been assumed). Then a longer phase lasting for about the present Hubble time follows, during which the size can increase by a smaller factor because of mass loss due to galactic winds and/or minor dry mergers.

We note that quasar feedback has not been introduced specifically to solve the size problem, but first by Silk and Rees (1998)[306] to predict the correlation in ETGs between galaxy velocity dispersion and the present-day BH mass. Soon after, Granato et al. (2001, 2004)[137][136] have shown that the gas removal by quasar activity is also needed in order to stop the star formation, preventing formation of exceedingly massive galaxies, too blue and with no enhancement of α-elements (cf. Section 5.4.1). Sterilization of star formation by quasar feedback implies that in a quite short timescale, an enormous mass of gas is evacuated from the central galaxy regions and possibly from the entire halo and subhalos. The gas evacuated from the central regions can be of the same order of the mass in stars, so about $10 - 20\%$ of the total baryons in the galactic halo. Observations of high redshift star forming galaxies do find evidence of large fractions of gas in various states, from molecular to highly ionized; in starforming galaxies at $z \approx 2$ the mass in gas is of the same order of the mass in stars (Cresci et al. 2009[82]; Tacconi et al. 2008, 2010[322][321]). Such winds would then push out gas from the halo at a rate

$$\dot{M}_{\rm out} \approx 1000 \ \frac{v_{\rm gas}}{1000 \ \ {\rm km \ s^{-1}}} \ \left(\frac{R_{\rm H}}{100 \ \ {\rm kpc}} \right)^{-1} \ \frac{M_{\rm gas}}{10^{11} \ \ M_\odot} \ M_\odot \ {\rm yr}^{-1} \ , \qquad (5.17)$$

where the reference values are for a DM halo with $M_{\rm H} \approx 2 \times 10^{12} \ M_\odot$ formed at $z_{\rm form} \approx 3$; $v_{\rm gas}$ is the escape velocity from $r \approx 1$ kpc and the gas mass is close to the stellar mass. As pointed out by Silk & Rees (1998)[306] and by Granato et al. (2001, 2004)[137][136] the

energy released by a luminous quasar in its last $e-$folding time is a factor of 20 larger than the energy associated to these winds. On the observational side, hints of massive outflows from high redshift quasars, consistent with this scenario, have been reported (e. g. Simcoe et al. 2006[309]; Prochaska & Hennawy 2009[268]). Therefore there are strong reasons to believe that large gas outflows occurred in high redshift quasar hosts.

As discussed in Section 5.3.1, the removal of a mass in gas close to the mass in stars destabilizes the mass distribution in the innermost galaxy regions. In the case of strong quasar winds the ejection and dynamical timescale are similar $\tau_{\rm ej} \approx 1-3\ \tau_{\rm dyn}$. Therefore the effect could be intermediate between those described by Equation (5.11) and by Equation (5.12), as found with numerical simulations by Geyer & Burkert (2001)[126] and by Baumgardt & Kroupa (2007)[16]. A basic question is how long it takes for the stellar structure to readjust to a new equilibrium. In simulations of star clusters, i. e. , without DM halo, the new equilibrium is reached in $30-50$ initial crossing times (Geyer & Burkert 2001[126]; Boily & Kroupa 2003[31]; Bastian & Goodwin 2006[15]). In the hypothesis that the same number of crossing times are also requested for massive galaxies, the expected timescale for size evolution would be $\Delta T_{\rm size} \approx 1.\ 5 \times 10^8$ yr. On the other hand, specific numerical simulations with high temporal resolution are needed in order to assess the size evolution timescale, since the presence of the DM halo, dominating the potential well at $r \geq R_e$, could slow down the expansion increasing the time needed to reach the new size and equilibrium. On the observational side, the duty cycle can be inferred only by studying the distribution of large samples of high-z galaxies in the R_e vs. $M_\star$ plane.

Since quasar winds follow the time pattern of quasar shining, the same is expected for the size evolution, except for a delay by $\Delta T_{\rm size}$. As a consequence, the inverse hierarchy or downsizing seen in the quasar evolution is mirrored in the size evolution.

Quasar activity is the main feedback mechanism for more massive ETGs ($M_\star \geq 10^{11}\ M_\odot$), while supernova feedback dominates at $M_\star \leq 2 \times 10^{10}\ M_\odot$ (see Granato et al. 2004[136]; Lapi et al. 2006[190]; Shankar et al. 2006[298]). Correspondingly, larger size evolution is expected for larger mass ETGs, while the evolution is progressively decreasing for lower mass and should be negligible for $M_\star \leq 10^{10}\ M_\odot$; in addition, the scatter in size at high z is much wider for more massive ETGs. Interestingly, Lauer et al. (2007)[193] and Bernardi et al. (2007)[24] found that the relationship between effective radius R_e and luminosity steepens for ETGs brighter than $M_V \approx -21$, corresponding

to a stellar mass $10^{11}\ M_{\odot}$.

If we assume that the change in size of ETGs is due to minor dry mergers, we face a couple of problems. The upper limit to the mass evolution ($M_f/M_i \approx 1.\ 7-2$ since $z \approx 1.\ 5-2$), plus the fact that this happens gradually, implies that *almost all* high redshift massive ETGs must increase their size at most by a factor $\approx 2.\ 2-3$. While this may be consistent with the average size evolution, it does not account for the decreased scatter of the size distribution from high to low redshifts. In particular, since dry minor mergers require a long timescale ≈ 10 Gyr to produce their full effects, they can not not explain why a significant fraction of the high-z ETGs are already on the local mass-size relationship. Moreover, the upper limit on the increase in mass entails an upper limit of factor of 3 for the size increase since $z \approx 2$, while at this redshift there are ETGs with sizes smaller than the local one by factors of $6-10$.

5.4.3 Projected Central Mass evolution

Clearly, the mass within the central regions after the expansion driven by quasar winds in ETGs, when a new virial equilibrium is reached *with the same mass in stars*, has to be lower than that of the initial compact structure, analogously to what happens for stellar clusters (Boily & Kroupa 2003[31]; Baumgardt & Kroupa 2007[16]). To test this implication against the data we compare the projected mass within the half-mass radius $R_e(z \geq 1)$ of each passively evolving galaxies at high redshift with the average projected mass within the *same physical radius* for local ETGs of the same overall stellar mass.

We stress that this test bypasses the problem of the reliability for the estimates of the effective radius in high redshift ETGs, since the mass inside the estimated effective radius is much less uncertain than the value of the radius itself. We checked that following the method by Hopkins et al. (2010), who have illustrated the effect of a limited dynamical range in surface brightness available for high redshift galaxies on the estimate of the intrinsic index n_t and of half-mass radius R_t. These authors shifted some of the Virgo clusters ETGs to $z \approx 2$ and simulated HST observations on these objects. Specifically, for NGC 4552 shifted to high redshift and assuming $\Delta\mu \approx 4.\ 5$, Hopkins et al. (2010) find that the original $n_t = 9.\ 22$ is fitted with $n_f \approx 6$ and $R_f \approx R_t/3$; as a results, the total luminosity L_f obtained by the fitting procedure is lower than the 'true' one L_t by a factor 1. 5. In the case of NGC 4365 the corresponding luminosity ratio amounts to

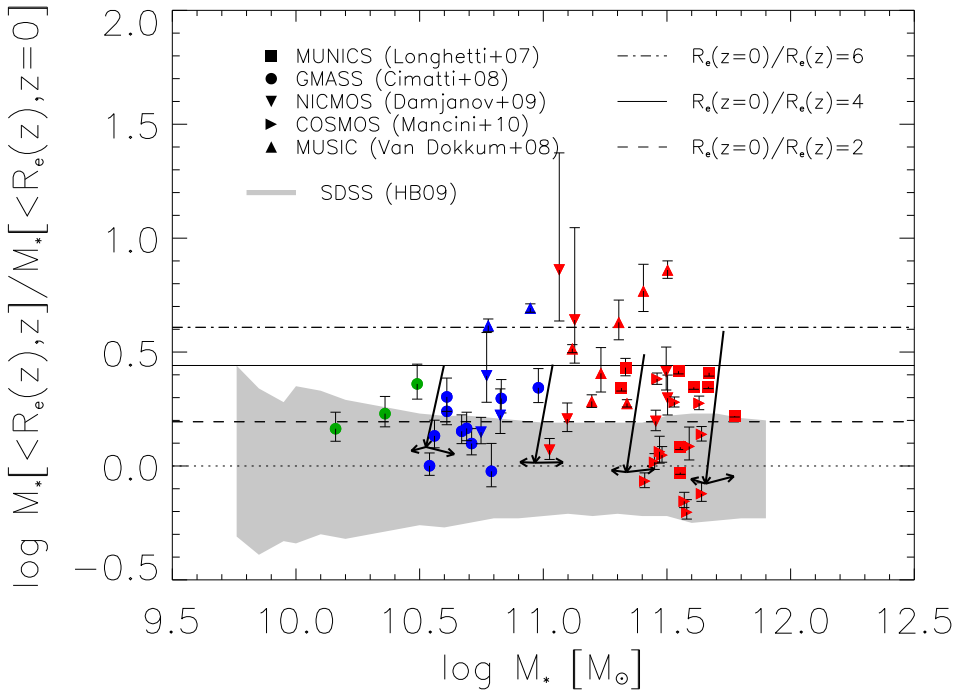

Figure 5.4: Ratio between the projected stellar mass within the estimated half-mass radius R_e for passively evolving ETG progenitors at $z \geq 1$ and the average local value within the same physical radius and for the same overall stellar mass. The data points include observations of individual passively evolving galaxies with spectroscopic redshifts $z \geq 1$ by Longhetti et al. (2007), Cimatti et al. (2008), Damjanov et al. (2009), Mancini et al. (2010), and van Dokkum et al. (2008). The shaded area shows the distribution of local SDSS galaxies (Hyde & Bernardi 2009). The thin lines illustrate the expected stellar mass ratio for different size increase from high$-z$ to the present, on adopting a local Sérsic index $n = 4$ (see § 5.4.3 for more details). As in Figure 2, thick lines with arrows illustrate typical evolutionary tracks of massive galaxies according to G04 model (with $f_\sigma = 1.\,5$ and $z_{\rm form} = 3$).

1. 12. However, the luminosity $L_f(R_f)$ inside R_f estimated through the fit is a good estimate of the true luminosity, with errors within 20% even in the case of large values of n_t. For instance, in the case of NGC 4552 we get $L_f(R_f)/L_t(R_f) \approx 1.\,15$. In conclusion, while the fitting procedure for high redshift galaxies with large intrinsic n index underestimates the half-mass radius by a factor of $3-4$ and the total luminosity by a factor 1. 5, but yields accurate estimates of the luminosity (and of the mass) inside the radius R_f. By the way, the same holds for the stellar mass, after proper translation of the luminosity in mass.

In Figure 5.4 we plot the ratio between the projected mass of high redshift and local ETGs *within the same physical radius*, namely, the half-luminosity radius of high-redshift ETGs. In detail, since for high redshift ETGs $M_\star(< R_e(z),\ z) = M_{\star,\ \rm tot}/2$, the ratio

comes to

$$\frac{M_\star(< R_e(z),\ z=0)}{M_\star(< R_e(z),\ z)} = 2\ \Gamma\left[2\ n,\ b_n\ \left(\frac{R_e(z)}{\langle R_e(z=0)\rangle}\right)^{1/n}\right], \tag{5.18}$$

where Γ is the (normalized) incomplete Gamma function. Thus if the total mass does not change significantly, the quantity $M_\star(< R_e(z),\ z)/M_\star(< R_e(z),\ z=0)$ depends only on the ratio $r = R_e(z)/\langle R_e(z=0)\rangle$ and on the final Sérsic index n.

To plot the data points under the hypothesis of no mass evolution, we compute the ratio r using the observed $R_e(z)$, and exploiting the observed stellar mass $M_\star$ to derive $\langle R_e(z=0)\rangle$ from the local $R_e - M_\star$ relation presented in Figure 2. The horizontal lines has been computed for three values of r; for the sake of definiteness we adopt $n = 4$. The thick lines with arrows illustrate the evolutionary track of massive galaxies according to G04 model with $f_\sigma = 1.\ 5$ and $z_{\rm form} = 3$; these are found to be in encouraging agreement with the distribution of data points.

In the case of local ETGs we can define a ratio $r' \equiv R_e(z=0)/\langle R_e(z=0)\rangle$ and compute the analogous of the mass ratio defined by Equation 5.18. The shaded area, containing 65% of local ETGs, illustrates the uncertainty of data points and of the horizontal lines associated to the assumption of an average half radius $\langle R_e(z=0)\rangle$.

Data points in Figure 4 show that a significant fraction of high redshift passively evolving galaxies exhibit stellar mass inside their inferred half-mass radius larger by a factor $2-6$ than the mass of their local counterparts within the same physical radius.

Keeping mass and structural index $n = 4$ constant, larger mass ratios can be obtained increasing the half luminosity radius by a factor from 2 to 6 (cf. horizontal lines). If we allow the structural index n to vary by one, as suggested by the simulations of Naab et al. (2009)[233], the change is minimal; even structural changes from $n = 4$ to $n = 8$ still would require a size increase by a factor of ≈ 6 in order to explain galaxies with the largest mass ratio.

This result suggests that the mass inside this physical radius has on the average decreased and disfavors mechanisms that increase the size by only adding stars in the outer regions of the ETGs. We notice that our argument involves a significant fraction of the total galaxy mass. Contrariwise, the comparison of stellar surface density profiles within $R_e/50$ as performed by Hopkins et al. (2009a) refers only to a tiny fraction of the mass. It is interesting to note that Naab et al. (2009)[233] find in their simulations that the dynamical friction is able to decrease the total mass inside ≤ 1 kpc.

On the same line, massive ETGs with their large sizes, steeper correlation between effective radii and mass and large Sérsic index (Lauer et al. 2007[193]; Kormendy et al. 2009[179]) clearly stand as representative cases of galaxies which experienced robust puffing up by quasar feedback. Moreover, the correlation of the central BH mass with Sérsic index n (Graham et al. 2003[134]; Graham & Driver 2007[133]) for massive ETGs is consistent with the hypothesis that the strong feedback from the most massive BHs has led to a substantial increase of n.

5.4.4 Velocity dispersion evolution

Applying the virial theorem to the galaxies before and after their growth in size, we have that the final line of sight central stellar velocity dispersion $\sigma_{0,\,\mathrm{f}}$ is related to the initial one $\sigma_{0,\,\mathrm{i}}$ by:

$$\sigma^2_{0,\,f} = \sigma^2_{0,\,i}\ \frac{S_D(n_i)}{S_D(n_f)}\ \frac{M_f}{M_i}\ \frac{R_{e,\,i}}{R_{e,\,f}} = \frac{f_\sigma^2\ V^2_{\mathrm{H}}(z_{\mathrm{form}})}{3\ S_K(n_i)}\ \frac{S_D(n_i)}{S_D(n_f)}\ \frac{M_f}{M_i}\ \frac{R_{e,\,i}}{R_{e,\,f}}\ ; \tag{5.19}$$

here the indices i and f label quantities in the initial and final configuration, and $S_D(n)$ is the structure factor defined by Prugniel & Simien (1997)[269], n being the Sérsic index. In the last expression we have used Equation (5.4) and the relation $\sigma^2_\star = 3\ S_K(n_i)\ \sigma^2_{0,\,i}$. In the case of an homologous growth of the galaxy size, the velocity dispersion scales as $(M/r)^{1/2}$, so that it remains constant if both the mass and the size increase by the same factor and decreases as $r^{-1/2}$ if the growth occurs at constant mass. However, the size growth is not necessarily homologous. All the mechanisms so far proposed predict an increase of the Sérsic index with increasing size. This effect together with a possible increase in mass within the limits imposed by the mass function evolution, tend to soften the decrease of the velocity dispersion. A further attenuation of the evolution is expected because of dynamical friction with the DM component.

The above equation shows that the size evolution of ETGs is paralleled by velocity dispersion evolution and that the present-day velocity dispersion keeps track of the potential well of the host halo when the galaxy forms. This is expected, since in a galaxy halo the gas is channeled toward the central regions during the fast accretion phase under the effect of the DM potential well. The duration of the star formation process depends on halo mass, feedbacks and redshift at which the fast accretion phase occurs. The velocity dispersion of the collapsed galaxy is not affected by the minor fraction of DM

added subsequently to the external regions of a halo during the slow accretion phase (see Lapi & Cavaliere 2009[188]).

Observations of the kinematics of passively evolving ETGs at $z \geq 1$ are quite difficult. Nonetheless for two galaxies reliable estimates of the velocity dispersion have been obtained (Cappellari et al. 2009[58]; van Dokkum et al. 2009[345]). For other objects only average estimates have been inferred from stacked spectra (Cenarro & Trujillo 2009[59]; Cappellari et al. 2009[58]). In all cases the main conclusion is that stellar masses derived from spectrophotometry are in good agreement with virial masses or with masses derived from dynamical models, if one adopts an IMF flattening below 1 $M_\odot$, such as those proposed by Kroupa (2001)[184] or by Chabrier (2003)[60]. This finding is also confirmed at intermediate redshifts $0.4 \leq z \leq 0.9$ by van der Wel et al. (2008)[343].

One of the two high redshift ETGs with a good determination of the velocity dispersion, GMASS 2470 (Cappellari et al. 2009[58]), falls in the σ vs. R_e plane quite close to the area covered by local ETGs. On the other hand, the best fit value of the stellar velocity dispersion, $\sigma_0 = 510^{+165}_{-95}$, for the galaxy 1255-0 at $z \approx 2.2$ (van Dokkum et al. 2009[345]) exceeds the measured values for even the most massive local galaxies (Bernardi et al. 2008[23]). Although we cannot do statistics with a single case, its existence lends support to the possibility of a significant evolution of the galaxy velocity dispersion.

Cappellari et al. (2009[58]; see also Bernardi 2009[22]), based on stacked spectra of 13 galaxies at $1.4 \leq z \leq 2.0$ (cf. their Table 1), find a mild evolution of the velocity dispersion, that decrease from about 202 km s^{-1} at $z \approx 1.6$ down to about 160 km s^{-1} at $z \approx 0$ for $M_\star \approx 7 \times 10^{10}$ $M_\odot$, and find an increase of the source size by a factor around 3.5. This evolution can be understood if the Sérsic's index n increases from an initial value n_i to $n_f = n_i + 2$ and the mass increases by 30%; in that case the velocity dispersion decreases by a factor 1.35, or less if dynamical friction with DM has a role. Note that if the DM is dynamically irrelevant in the inner regions of galaxies, and mergers accrete matter in the outer regions, the mass within R_e does not change and the same velocity dispersion evolution applies also to the minor merger scenario.

A quite interesting upper limit to the velocity dispersion, $\sigma_\star \leq 326$ km s^{-1}, for a massive $M_\star \approx 3 - 4 \times 10^{11}$ $M_\odot$ at redshift $z \approx 1.82$ has been found by Onodera et al. (2010)[244]. The same authors also find that the size of this galaxy is as expected for a local galaxy with the same mass. The velocity dispersion and the size yield a virial

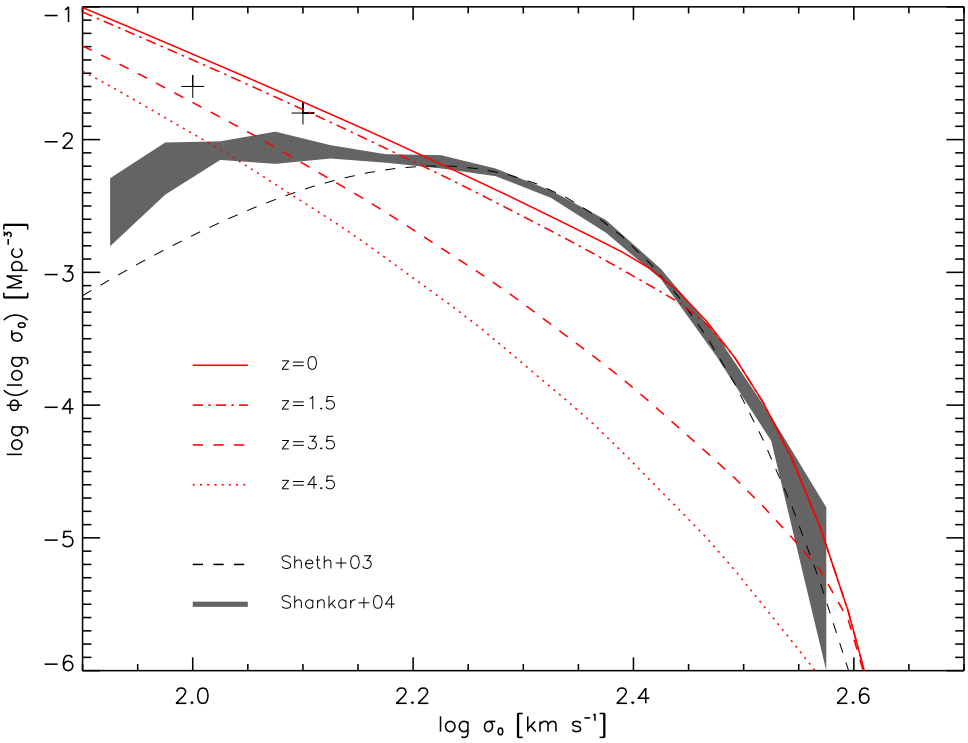

Figure 5.5: Velocity distribution function. Our results at different redshifts are compared with the observational estimates of the local velocity distribution function by Sheth et al. (2003)[303] and Shankar et al. (2004)[299].

mass upper limit $M_H \leq 7 \times 10^{11}\ M_\odot$, quite close to the stellar mass. This galaxy has the same structural properties of a local ETG. Recalling that a significant fraction of $z \geq 1.5$ galaxies already exhibit a size close to the size of their local counterparts, this galaxy appears as a well studied case of an already evolved galaxy, suggesting that the timescale for the size evolution is shorter than the Hubble time at those redshifts $\Delta T_{\rm size} < t_H(z)$.

Velocity dispersion has so far been determined only for a few individual high-z spheroidal galaxies. The galaxy GMASS 2470 at $z \approx 1.4$ (Cappellari et al. 2009[58]) and galaxy #250425 at $z = 1.82$ (Onodera et al. 2010[244]) are already close to the local value for their mass, while $1255 - 0$ at $z \approx 2.2$ has a best fit velocity dispersion significantly higher than the most massive local galaxies. Thus in the two first cases evolution should have occurred before the cosmic time corresponding to the observed redshift, whereas significant evolution in size and velocity dispersion has to occur for the higher redshift galaxy. The studies of velocity dispersions by Cenarro & Trujillo (2009)[59] and Cappellari et al. (2009)[58], based on stacked spectra, suggest that velocity dispersion evolution is on the average needed.

An interesting hint on size and velocity dispersion average evolution can be derived by

studying the velocity dispersion distribution (VDF) of local ETGs (Sheth et al. 2003[303]), following the approach by Cirasuolo et al. (2005). From Equation. (5.19) and (5.11), taking $n_i = 3$ and $n_f = 5$, we find, for the typical values of the parameters discusses above ($f_\sigma = 1.5$, $r = 4$), the relation $\sigma_{0,f} = 0.6\ V_{\rm H}$; this associates to each forming halo the final velocity dispersion of the most massive hosted galaxy. By combining it with the formation rate of halos (see Appendix A) for redshifts $z \geq 1$ we get the distribution function of the stellar velocity dispersions (VDF). From Figure 5.5 it is apparent that the predicted VDF is in good agreement with the observational estimate by Sheth et al. (2003). We stress that the observed VDF highly constrains the global history of DM galaxy halos and of their stellar content, and therefore is an important benchmark for models of ETG formation (see also Loeb & Peebles 2003[197]).

A change of the slope of the relationship between luminosity and velocity dispersion at low luminosity has been claimed by several authors (Shankar et al. 2006[298]; Lauer et al. 2007[193]). In particular, Lauer et al. (2007)[193] show that the change in slope occurs at about the same luminosity $M_V \approx -21$, where the slope of the size vs. luminosity relation also changes (see § 6.2). Once more this feature occurs at the transition from supernova-dominated to quasar-dominated feedback regime.

An additional relevant aspect is related to the $M_\bullet$ vs. σ_0 and $M_\bullet$ vs. $M_\star$ correlations. G04 model predicts that the mass in stars formed before the quasar shining is strictly related to the mass of the central BH, since the growth of the reservoir, which eventually furnishes the mass to the BH, is strictly proportional to the starforming activity . Marconi & Hunt (2003)[214] and Häring & Rix (2004)[145] pointed out that the $M_\bullet$ vs. $M_\star$ relation for ETGs and bulges exhibits a scatter comparable with that in the $M_\bullet$ vs. σ_0 relation.

In this context it is interesting to mention that, according to Lauer et al. (2007)[193], the extrapolation of the σ_0 vs. $M_\bullet$ relationship holding at low mass to higher mass galaxies would predict BH masses smaller than those inferred from the stellar mass. This is expected if the velocity dispersion decreased more significantly for higher mass galaxies, hosting more massive BHs and subject to stronger quasar feedback.

5.5 Summary

In this Chapter, we review the recent results on the observed size evolution of ETGs.We try to answer the two following questions: 1) How did the small size of massive ETGs form at high redshift? 2) How did the compact, massive ETGs evolve to 'catch up' the local relation?

We show that the observed compact size (kpc or even sub-kpc) of high redshift ETGs is expected by theoretical predictions based on the largely accepted assumption that most of the stars have been formed during dissipative collapse of cold gas. The other possibility for the formation of compact size is according to the wet merger of gas-rich discs suggested by simulations.

We also discuss the several mechanisms which can contribute to the observed size evolution ETGs.Among them, the rapid gas expulsion and the dry minor merger may be the most important. The available observational data strongly suggests that most of the size evolution occurs at $z \geq 1$, while at $z < 1$ sizes increase by no more than 40%. Moreover, a large fraction of high-z passively evolving galaxies have projected stellar mass within their effective radii a factor of 2 larger than those of local ETGs with the same stellar mass, within the same physical radius. It is also shown that the size distribution of high redshift ETG progenitors is broader than the corresponding distribution for local ETGs. While a significant fraction of massive high redshift ETGs already exhibit sizes as large as those of their local counterparts with the same mass, for a bunch of ETGs the size has to increase by a factor of 4-6 to match the local half mass radius. All the above results are easily accounted for if most of the size evolution is due to a puffing up driven by the rapid expulsion of large amounts of mass. The contribution of dry minor merger to the size evolution can be up to a factor of 2 which is constrained by the mass function evolution.

Chapter 6

CONCLUSION

Although the widely held view is that the formation and evolution of the visible part of ETGs is driven by merger in the framework of the hierarchical evolution of the dark matter galaxy halos, this scenario has difficulties to reconcile several observational evidences. Instead, the monolithic collapse scenario considering both the halo formation and QSOs/SNae feedback can explain the recent observed results on the massive ETGs formation and evolution at high redshift.

In this thesis, we review a physical model for the massive ETGs formation and evolution at high redshift, by Granato et al. (2001, 2004), further elaborated by Lapi et al. (2006). In this model, an evolutionary sequence for massive ETGs at high redshift has been proposed:1) a very short UV bright phase with dust-free star formation, 2) following by submillimeter bright phase with intense dust-enshrouded star formation, which is quenched by QSOs feedback, and 3) following by a optically luminous QSOs phase, 4) and finally passively evolving towards the local ETGs, allowing limited stellar increase contributed by (dry) minor merger. We show the success of this model to match simultaneously various observations following the proposed evolutionary sequence.

Adopting a power-law relation between UV attenuation, SFR, and metallicity (Equation 2.1), G04 model predicts the UV attenuation should be increasing with galactic age and with increasing galaxy mass. With this additional ingredient the model accounts also for the observed LFs of LBGs at different redshifts. The larger attenuation for more massive objects implies that the UV LF evolves between $z \approx 6$ and $z \approx 3$ much less than

the halo mass function. This is due to the fact that the higher dust attenuation mitigates the fast increase with decreasing redshift of the number density of massive halos. We also expect the space density of LBGs will decrease drastic towards to $z \approx 10$ because of extreme sparsity of massive halo at $z \approx 10$.

We construct a sample of 298 spectroscopically confirmed z_{850}-band-selected galaxies at redshift $z \sim 2$ from the GOODS-MUSIC sample, with a well sampled SED from the rest-frame UV to NIR. We also combine a local sample to build the local $L_8 - L_{IR}$ relation. With this relation, we can estimate the IR luminosity from the Spitzer MIPS $24\mu m$ observation if assuming it still holds at redshift 2. The observed $IRX - \beta$ diagram of our $z \sim 2$ sample shows a large spread around the average Meurer relation. The locus of z_{850}-band selected galaxies on the $IRX - \beta$ diagram show a tendency dependent on their bolometric luminosities. We interpreted this fact as a real difference between an extinction law and an attenuation law, the latter being the result of the combination of many effects, such as an age dependent extinction, different geometries between dust and stars and possible differences between grain compositions and sizes. This may indicate the variable extinction law should be needed. Based on this idea, we outline a new method of of the spectral population synthesis technique in which we add the far infrared luminosity to the global SED and use of a generalized Calzetti law with variable R_V . With this new method we could determine in a unprecedent robust way the physical parameters , especially the attenuation , of $z \sim 2$ galaxies. We find there is a general trend of increasing attenuation with SFR, or, equivalently, the unobscured absolute UV magnitude, but the correlation is not tight. R_V shows a large scatter at all values of the SFR indicating a variety of concomitant effects that may bear on the combined attenuation law. This was already suggested by our $IRX - \beta$ diagram but the run of the scatter with the star formation rate is more indicative that these processes appear at any scale. The relation between the attenuation and the SFR become tighter toward larger wavelengths. This is consistent with the fact that, in general at shorter wavelengths images show more knotty structures that overall combine to give a different attenuation curve. Especially high values of R_V were generally required to fit the SEDs of ULIRGs. In this case the attenuation curve is very flat and the attenuation remains relatively significant even in the NIR. Indeed from the analysis of local ULIRGs, it was expected that a fraction of the star formation could be significantly attenuated even at these long wavelengths. This effect is important to explain the observed mass-to-light

ratio at NIR bands which can vary by a factor of 100. Some observed mass-to-light ratio at H and K bands at $z \sim 2$ galaxies are comparable to the local values, which has been claimed by Shapley et al. (2005). We argue this is due to relatively significant attenuation even at these bands.

Short UV bright phase is expected due to the rapid increasing of SFR and rapid metal enrichment in massive halos. UV photons will be absorbed by newly produced dust and reradiated in FIR band. The galaxy will transfer from UV bright phase to FIR/submm bright phase. The feature of negative K-correction of SMGs makes it possible to study them up to high redshift ($z \sim 10$), especially with the new generation FIR/submm satellite Herschel. We have exploited the H-ATLAS SDP survey data to investigate the evolution of the 100 and 250 μm LFs of bright star-forming galaxies ($SFR \geq 10^2 M_{\odot} yr^{-1}$) at $z > 1$. Redshifts have been estimated using the SED of SMM J2135-0102 as the template. The rms uncertainties on redshift estimates have been assessed comparing our redshift estimates with spectroscopic redshift measurements for 39 H-ATLAS galaxies at $z > 0.5$ as well as by means of simulations. Both methods yield rms values of $\Delta z/(1+z) \approx 0.2$ or smaller. The uncertainties due to the spread of redshift estimates are added in quadrature to Poisson errors to compute the global uncertainties on the LFs. Our LF estimates are in close agreement (in the common redshift and luminosity range, after applying the same $K - corrections$) with those at 250 μm by Eales et al. (2010b)[104], as well with those at 90 μm by Gruppioni et al. (2010)[139]. We find a significant luminosity evolution at least up to $z \approx 2.5$, while a weaker evolution at higher z is indicated. We show that the evolution of the LF reflects that of the halo formation rate if the star-formation rate obeys a simple relationship with halo mass and redshift and the lifetime of the main star-formation phase is $\Delta t_{sf} \sim 7 \times 10^8$yr, consistent with the constraint coming from the α-enhancement observed in the most massive ETGs. G04 model is able to reproduce not only the 100 μm and 250μm LFs at different redshifts $z > 1$ but also the counts at wavelengths ranging from 250 μm to ≈ 1 mm. We also show , under the guide of the model, an simple , but effective, method has been developed to select the high redshift, strongly-lensed SMGs, which has been proven to be at work (Negrello et al. 2010[239], González-Nuevo et al. in prep.)

In the meanwhile, G04 model reproduces the B-band LFs of QSOs at different redshifts(Lapi et al. 2006[190]). QSOs feedback is an important ingredient in G04 model which is needed in order to stop the star formation, preventing formation of exceedingly

massive galaxies, too blue and with no enhancement of α-elements. Sterilization of star formation by quasar feedback implies that in a quite short timescale, an enormous mass of gas is evacuated from the central galaxy regions and possibly from the entire halo and subhalos. The gas evacuated from the central regions can be of the same order of the mass in stars, so about 10 - 20% of the total baryons in the galactic halo. The rapid gas removal from the galaxy by QSOs feedback can puff up the size of the galaxy. This effect combined with other mechanisms, especially dry minor merger, can be used to explain the observed size evolution of massive ETGs.

Now we recall the first problem asked in the Introduction:Why was there no significant star formation before the onset of collapse? We can't give a positive answer by the model itself. However, the recent result from the 'classic' merger model indicates that the merger model overestimates the number of dwarf galaxies $M_\star <\sim 10^{10} M_\odot$ at $z > 0.8$ even by one order of magnitude(Guo et al. 2011[140]). This indicates that some mechanism must be needed to prevent star formation in low massive halos at high redshift.

For the second question, 'why did all star formation cease immediately after collapse?, the answer is the co-evolution of spheroidal and supermassive black holes, from which the feedback can cease the ongoing star formation.

We can get the indication from Chapter 2 to answer the question : ' why the brightest UV selected galaxies at high redshift are relatively rare, when compared to the present number density of massive ETGs?' The rare number of the brightest UV selected galaxies is the result of the rapid dust production in massive galaxies, which transfer the UV bright phase into the submillimeter bright phase in a short time.

For the last question, we may have some insight from the recent work by Cook et al.(2009)[75] who propose a two-phase galaxy formation model. They take into account an effect pointed out in the past few years by a number of studies mostly based on intensive N-body simulations, namely that typical halo growth occurs in two phases: an early, fast collapse phase featuring several major merger events, followed by a late, quiescent accretion on to the halo outskirts. They propose that the two modes of halo growth drive two distinct modes for the evolution of baryonic matter, favoring the development of the spheroidal and disc components of galaxies, respectively.

ACKNOWLEDGEMENTS

First of all, I would like to thank my three supervisors: Prof. Luigi Danese, Prof. Alessandro Bressan, and Dr. Andrea Lapi. Gigi has always been very nice with me, and taught me how to catch the physical essence of a physical problem. Sandro was very patient in explaining me the basics of stellar population synthesis. Andrea helped me to learn the basics of our galaxy formation and evolution model. I also would like to acknowledge Prof. Gianfranco De Zotti for his critical reading of my manuscripts, and the very interesting scientific discussions we made. I also thank Joaquin Gonzalez-Nuevo for explaining me some details of his simulations, and providing me valuable material, concerning the selection method of strongly lensed submm galaxies. I thank all other staff members of the SISSA astrophysics sector for their help during my research activities; these include Annalisa Celotti, Carlo Baccigalupi, Samuel Leach, Stefano Liberati, John Miller, Francesca Perrotta, Paolo Salucci and Riccardo Valdarnini. I am indebted to the student secretariats Riccardo Iancer and Federica Tuniz who helped me to solve various problems, especially concerning the documents for my permit of stay in Italy. I thanks Maria Sole who helped me to apply for my family reunion, and Lorena Bencina who gave me a lot of help for managing research activities out of SISSA. I also acknowledge the library head Andrea Wehrenfennig who was so kind for me as I had the 150 hours job in the library for three years. I thank the staff of the SISSA housing office who helped me to find my first accommodation in Trieste. I thank my Chinese supervisor Prof. Fuzhen Cheng who introduced me to the field of astrophysics. I also thank

Prof. Tinggui Wang, Prof. Junxian Wang, Prof. Yefei Yuan, Prof. Xu Kong, Dr. Huiyuan Wang, Dr. Hongyan Zhou and Dr. Xiaobo Dong in CfA of USTC, for their valuable collaborations. I thank Prof. Shude Mao in NAOC, Prof Cheng Li in SHAO and Prof. Houjun Mo in UMass who offered me a job chance. I thank my colleagues and friends in SISSA: Goffredo Chirco, Laura Bonavera, Claudia Cremaschini, Zhenyi Cai, Junqing Xia, Pratika Dayal, Carmelo Evoli, Yabebal Tadesse Fantaye, Ambra Nanni, Luca Naso, Emilio Tejeda Rodrigue, Jorge Moreno and Vincenzo Vitagliano, and in particular Stefano Finazzi who provided me the Latex template for writing this Thesis. Finally, special thanks to my family who has always supported me.

Appendix A

OVERVIEW OF G04 MODEL

In the recent years we have developed a model of galaxy formation with focus on the evolution of baryons within protogalactic spheroids. Baryons have been followed through simple physical recipes emphasizing the effects of the collapse and cooling and of the energy fed back to the intragalactic gas by supernova (SN) explosions and by accretion onto the nuclear supermassive black holes (BHs; see Granato et al. 2001, 2004[137][136]; Lapi et al. 2006, 2008[190][189]; Mao et al. 2007[211]; Fan et al. 2008[109]). The main motivation was to enlighten the relevant physical processes shaping galaxy formation, to keep calculations easily reproducible and to suggest which processes should be implemented in the much more complex and much less reproducible numerical simulations.

The model transparently shows how physical processes acting on the baryons speeds up the formation of more massive galaxies. As a result, although the DM assembly follows a bottom-up hierarchy, galaxies and their active nuclei evolve in a way that appears opposite to the hierarchy in DM, following a pattern that we named Antihierarchical Baryon Collapse (ABC). We notice that it fully corresponds from the observational point of view to the so called downsizing.

Here we present a full summary of its main features, and provide useful analytic approximations for quantities of relevance in this thesis.

A.1 DM SECTOR

As for the treatment of the DM in galaxies, the model follows the standard hierarchical clustering framework, and takes into account the outcomes of recent intensive high-resolution $N-$body simulations of halo formation in a cosmological context (see Zhao et al. 2003[364]; Diemand et al. 2007[95]; Hoffman et al. 2007[150]; Ascasibar & Gottloeber 2008)[9]. In these studies, two distinct phases in the growth of DM halos have been recognized: an early fast collapse, and a later slow accretion phase. During the early collapse, a substantial mass is gathered through major mergers, which effectively reconfigure the gravitational potential wells and cause the collisionless DM particles to undergo dynamical relaxation and isotropization (Lapi & Cavaliere 2009[188]). During the later phase, moderate amounts of mass, around $20-50\%$, are slowly accreted mainly onto the halo outskirts, little affecting the inner structure and potential, but quiescently rescaling upward the overall halo size. From the baryon point of view, the early phase — our main interest here — supports the dissipationless collapse of baryons to originate a spheroidal structure dominated by random motions (see also Cook et al. 2009[75]).

Halos harboring a massive elliptical galaxy once created, even at high redshift, are rarely destroyed, while at low redshifts they are possibly incorporated within galaxy groups and clusters. Thus at $z \geq 1$, the halo formation rate can be reasonably well approximated by the positive term in the derivative of the halo mass function with respect to cosmic time (e. g. , Haehnelt & Rees 1993[142]; Sasaki 1994[289]). The halo mass function derived from numerical simulations (e. g. , Jenkins et al. 2001[163]) is well fit by the Sheth & Tormen (1999, 2002)[304][305] formula, that improves over the original Press & Schechter (1974)[266] expression (well known to under-predict by a large factor the massive halo abundance at high redshift). Adopting the Sheth & Tormen (1999)[304] mass function $N_{\rm ST}(M_{\rm H},\ t)$, the formation rate of DM halos is given by

$$\frac{{\rm d}^2\ N_{\rm ST}}{{\rm d}M_{\rm H}\ {\rm d}t} = \left[\frac{a\ \delta_c(t)}{\sigma^2(M_{\rm H})} + \frac{2\ p}{\delta_c(t)}\ \frac{\sigma^{2\ p}(M_{\rm H})}{\sigma^{2\ p}(M_{\rm H}) + a^p\ \delta_c^{2\ p}(t)}\right]\ \left|\frac{{\rm d}\delta_c}{{\rm d}t}\right|\ N_{\rm ST}(M_{\rm H},\ t)\ ; \qquad (A.1)$$

here $a = 0.707$ and $p = 0.3$ are constants obtained by comparison with N-body simulations, $\sigma(M_{\rm H})$ is the mass variance of the primordial perturbation field computed from the Bardeen et al. (1986)[13] power spectrum with correction for baryons (Sugiyama 1995[317]) and normalized to $\sigma_8 \approx 0.8$ on a scale of 8 h^{-1} Mpc, and $\delta_c(t)$ is the critical

threshold for collapse extrapolated from the linear perturbation theory.

As for the density distribution of DM halos we adopt as a reference the profile proposed by Navarro et al. (1997)[238]:

$$\rho(r) = \frac{\rho(r_s)}{cx(1+cx)^2} \tag{A.2}$$

where $x = r/R_{\rm H}$, r_s is the scale radius and c is the concentration parameter, $c = R_{\rm H}/r_s$, with typical values around 4 at halo formation (e. g. , Zhao et al. 2003[364]). Bullock et al. (2001)[50] found that c is the weak function of the mass as $c \propto M^{-0.13}$ while at fixed mass $c \propto (1+z)^{-1}$.

The halo circular velocity $V_{\rm H} = (G\ M_{\rm H}/R_{\rm H})^{1/2}$ characterizes the DM potential well; the associated velocity dispersion is $\sigma_{\rm DM} = f(c)^{1/2}\ V_{\rm H}$, where $f(c) \approx 2/3 + (c/21.\ 5)^{0.7}$ is a weak function of the concentration parameter of order 1 (see Mo et al. 1998).

A.2 Baryonic sector

A.2.1 Gas cooling and Star formation

During the fast collapse phase, a rapid sequence of major mergers build up a DM halo of mass $M_{\rm H}$. At that time a mass $M_{\rm inf} = f_b\ M_{\rm H}$ of baryonic matter, in cosmic proportion $f_b \approx 0.2$ with the DM, is shock heated to the virial temperature by falling into the forming DM gravitational potential well.

We consider that gas in proto-galaxies is divided between a hot phase at virial temperature and cold gas phase at low enough temperature to allow star formation; we also consider additional galaxy components: the stars, a reservoir of low angular momentum gas and the growing central Black hole.

This hot gas cools and flows toward the central region at a rate

$$\dot{M}_{\rm cond} = \frac{M_{\rm inf}}{t_{\rm cond}} \tag{A.3}$$

over the *condensation* timescale

$$t_{\rm cond} = \max[t_{\rm cool}(R_{\rm H}),\ t_{\rm dyn}(R_{\rm H})] \tag{A.4}$$

Namely, the condensing time is the maximum between the dynamical timescale

$$t_{\rm dyn} = \sqrt{\frac{3\pi}{32 G \rho_{DM}}} \tag{A.5}$$

and the cooling time at the halo virial radius $R_{\rm H}$:

$$t_{\rm cool} = \frac{3kT}{2\mu C f_b \rho_{DM} \Lambda(T)} \tag{A.6}$$

where $\Lambda(T)$ is the cooling function and $C =< n_e^2(r) > / < n_e(r) >^2$ is the clumping factor, assumed to be constant.

The clumping factor in the gas $\mathcal{C} \geq$ a few, as suggested by numerical simulations (e. g. , Gnedin & Ostriker 1997[130]; Iliev et al. 2006[159]), implies $t_{\rm cool}(R_{\rm H}) \leq t_{\rm dyn}(R_{\rm H})$ on relevant galaxy scales at $z \geq 1$. We exploit the cooling and the dynamical time at the virial radius of a halo with a NFW or similar distribution, since most of the mass is located in outer low density regions. The dynamic time at virial radius R_H depends on the redshift $\propto (1+z)^{-3/2}$ and on the concentration parameter c. When compared to the cooling time, it turns out that usually the dynamic time is longer, except at the very initial steps of the star formation, when the cold gas has still a primordial composition. At this epoch the clumping factor is important in order to keep the condensation time t_{cond} short enough. However soon later than a few 10^7 yrs the metallicity increases to a level that makes the cooling time shorter than the dynamical time even in the case of almost uniform gas.

We recall that the star formation in galaxy halos is a quite inefficient process , since only a minor fraction $10-20\%$ of the available baryons are cycled through stars in more massive halos and the fraction is rapidly decreasing with decreasing halo mass. As a result, the present-day cosmic mass density in stars is only a few percent of the mass density in baryons (e. g. , Shankar et al. 2006[298]). Thus the formation of the most massive galaxy in a halo is a process that involves only a fraction smaller than $20-30\%$ of its original baryons and DM. It is natural to assume that the material is rapidly put together by a few major mergers in the central regions of the halo. In these mergers the angular momentum decays on a dynamical friction timescale $t_{\rm DF} \approx 0.2\ (\xi/\ln\xi)\ t_{\rm dyn}$, where $\xi \equiv M_{\rm H}/M_{\rm c}$ holds in terms of typical cloud mass $M_{\rm c}$ involved in major mergers (e. g. Mo & Mao 2004); these are very frequent at high redshift and in the central regions of halos during the fast collapse phase of DM evolution, implying $\xi \sim$

a few and hence a short $t_{\rm DF}$. Thus the effects of angular momentum can be neglected.

The model also assumes that quasar (QSO) activity removes not only cold gas from the galaxy, but also hot gas from the halo through winds at a rate $\dot{M}_{\rm inf}^{QSO}$, to be quantitatively discussed next; the equation for the diffuse hot gas is then

$$\dot{M}_{\rm inf} = -\dot{M}_{\rm cond} - \dot{M}_{\rm inf}^{QSO} \ . \tag{A.7}$$

The cold gas piled up by the cooling of hot gas, is partially consumed by star formation ($\dot{M}_\star$), and partially removed to a warm/hot phase endowed with long cooling time by the energy feedback from SNae ($\dot{M}_{\rm cold}^{SN}$) and QSO activity ($\dot{M}_{\rm cold}^{QSO}$):

$$\dot{M}_{\rm cold} = \dot{M}_{\rm cond} - [1-\mathcal{R}(t)]\dot{M}_\star - \dot{M}_{\rm cold}^{SN} - \dot{M}_{\rm cold}^{QSO} \ , \tag{A.8}$$

where $\mathcal{R}(t)$ is the fraction of gas restituted to the cold component by the evolved stars

$$\mathcal{R}(t) = \frac{1}{\dot{M}_\star(t)} \int_{m_{\star,\ t}}^{m_\star^{sup}} dm_\star (m_\star - m_{rem}) \phi(m_\star) \dot{M}_\star(t-\tau_{m_\star}) \tag{A.9}$$

where $\tau_{m_\star}$ is the lifetime of stars with mass $m_\star$, $m_{\star,\ t}$ is the mass with lifetime t and m_{rem} is the remaining mass locked in the white dwarf and black holes. The value of $\mathcal{R}(t)$ depends on time (particularly soon after the onset of star formation) and on the assumed initial mass function (IMF). We adopt for reference a pseudo-Chabrier IMF of shape $\phi(m_\star) = m_\star^{-x}$ with $x = 1.\ 4$ for $0.1 \leq m_\star \leq 1\ M_\odot$ and $x = 2.\ 35$ for $m_\star > 1\ M_\odot$. The often used approximation of instantaneous recycling implies $\mathcal{R} \approx 0.54$ (for a Salpeter IMF one has $\mathcal{R} \approx 0.3$). The mass of cold baryons that is going to be accreted onto the central supermassive BH is small enough to be neglected in the above equation.

Stars are formed at a rate

$$\dot{M}_\star = \int \frac{{\rm d}M_{\rm cold}}{\max[t_{\rm cool},\ t_{\rm dyn}]} \approx \frac{M_{\rm cold}}{t_\star} \ , \tag{A.10}$$

where now $t_{\rm cool}$ and $t_{\rm dyn}$ refer to a mass shell ${\rm d}M_{\rm cold}$, and $t_\star$ is the star formation timescale averaged over the mass distribution.

A.2.2 Black hole growth

Now we consider the equations ruling the matter accretion onto the central black hole. The matter flows onto the BH in two stops. At first cool gas loses angular momen-

tum through radiation drag (or other mechanism possibly related to merger even with a small fraction of gas) and it flows into a reservoir around the BH (the hypothetical primordial torus) at a rate $\dot{M}_{inflow}$. Then from the reservoir the gas is accreted toward the BH through the accretion radius $r_a = GM_\bullet/\sigma^2$, where σ is the characteristic velocity dispersion of gas and stars in the central galaxy regions. The typical timescale of the accretion is the viscous drag timescale $\tau_{visc} \sim r^2/\nu$, where for the viscosity we assume $\nu \approx Re_{crit}^{-1} V(r_a) r_a$, where $V(r_a)$ is the rotational velocity at r_a and Re is the critical Reynolds number. By assuming $V(r_a) = \sigma$, the viscous timescale reads(Burkert & Silk 2001)

$$\tau_{visc} = \frac{GM_\bullet Re_{crit}}{\sigma^3} \tag{A.11}$$

If we admit that radiation pressure is able to restrict the accretion at λ times the Eddington limit, the maximum allowed accretion rate is M_{bullet}/τ_{ef}, where $\tau_{ef} = 4 \times 10^8 [\eta/(1-\eta)]/\lambda$ yr and η is the mass to energy conversion efficiency. Thus the accretion rate turns out to be

$$\dot{M}_{acc} = \frac{\dot{M}_\bullet}{1-\eta} = min[\frac{M_{res}}{\tau_{visc}}, \ \frac{M_\bullet}{\tau_{ef}}] \tag{A.12}$$

The mass of the reservoir is changing at a rate

$$\dot{M}_{res} = \dot{M}_{inflow} - \dot{M}_\bullet \tag{A.13}$$

This equation shows that a massive reservoir can form around the growing BH when $\dot{M}_{inflow} \gg \dot{M}_\bullet$ holds for long time enough. For reasonable values of $Re \simeq 100 - 1000$, τ_{visc} is always much shorter than Eddington timescale $\tau_{ef} = 4 \times 10^8 [\eta/(1-\eta)]/\lambda$ yr and η, even for large BH mass. Therefore if the supply to the reservoir is large enough, the BH accretion is limited by its own radiation pressure for long time. In particular we leave the possibility of having only slightly super-Eddington accretion restricting $\lambda \leq 4$. During this period the BH can accrete close to the Eddington limit

$$\dot{M}_\bullet = \lambda_{\rm Edd} \ \frac{1-\eta}{\eta} \ \frac{M_\bullet}{t_{\rm Edd}} \tag{A.14}$$

and grows almost exponentially from a seed of $10^2 \ M_\odot$; the $e-$folding time involves the Eddington timescale $t_{\rm Edd} \approx 4 \times 10^8$ yr, the radiative efficiency $\eta \approx 0.1$, and the actual Eddington ratio $\lambda_{\rm Edd} \sim 0.3 - 3$.

In any case at the end of accretion the BH mass will match the mass passed through

the reservoir $M_\bullet \simeq \int \dot{M}_{inflow} dt$.

Radiation drag is a physical mechanism that can remove large amount of angular momentum from gas in the central region of protogalaxies and, as a consequence, it can afford mass to the reservoir(Umemura 2001[338]). In this case we can imagine that during major episodes of star formation in the inner regions of galaxies there are a huge number of thick clouds where stars form;photons traveling from cloud to cloud are able to strip gas which loses angular momentum. The angular momentum loss rate per unit mass has been estimated by Umemura (2001[338]) and Kawakatu & Umemura (2002)[170] to be

$$\frac{dlnJ}{dt} \simeq -\frac{L_\star}{M_{cold}c^2}(1 - e^{-\tau_{RD}}) \tag{A.15}$$

where $L_\star$ is the luminosity associated with the star formation and the τ_{RD} is the total optical depth of photons traveling from cloud to cloud.

The total optical depth is related to the physical conditions of inner regions of primeval galaxies. Dust forms quite soon (on a timescale of a few $\sim 10^7$ yr) in large halos which subsequently are going to host QSOs. The star formation are expected to occur in molecular clouds of high optical depth $\tau_{1\mu m} \sim 30$ at $\lambda = 1\mu m$. Thus in these halos the far IR photons ($\tau_{FIR} \sim 10^{-2}\tau_{1\mu m}$) can escape from molecular clouds and be absorbed by other clouds, yielding a total optical depth $\tau_{RD} \approx \tau_{FIR} N_{int}$ (Kawakatu & Umemura 2002[170]). The mean number of clouds intersected by a FIR photon $N_{int} \approx \frac{N_{cl}}{V_{cl}} \pi r_{cl} r_b$, where r_b is the typical bulge radius of the spheroidal component in a galaxy and N_{cl}, V_{cl} and r_{cl} are the total number of molecular clouds within this radius, the typical volume of these molecular clouds and their typical radius respectively. For a typical large galaxy $r_b \sim 10$ kpc and the mass in cold gas can reach $M_{cold} \sim 10^{12} M_\odot$. Assuming for a typical molecular cloud $M_{cl} \sim 10^5 M_\odot$ and $r_c \sim 10$ pc, we estimate $N_{int} \approx 10$ and as a consequence $\tau_{RD} \approx 3$. In general the optical depth due to dust depends on dust mass and on the clumpy dust distribution. We set

$$\tau_{\rm RD}(t) = \tau^0_{\rm RD} \ \frac{Z(t)}{Z_\odot} \ \frac{M_{\rm cold}(t)}{10^{12} \ M_\odot} \ \left(\frac{M_{\rm H}}{10^{13} \ M_\odot}\right)^{-2/3} \tag{A.16}$$

where the dust mass is assumed to be proportional to the mass in metals, the typical radius of the dust and gas distribution is taken to be proportional to the virial radius scaled down by a large factor; the constant $\tau^0_{\rm RD}$ is meant to include the effects of clumps in dust distribution. The above discussion suggests that $\tau^0_{\rm RD} \sim 1$. It is worth noticing that

the optical depth decreases with decreasing mass because metal abundance and mass of cold gas decreases.

The luminosity of stars can be estimated on the basis of simple arguments. In the first phases of galaxy formation it depends on young stars, i. e. mainly on star formation rate $\dot{M}_\star$ and on the IMF $\phi(m)$. The luminosity in stars is

$$L_\star(t) = \int_{m_{inf}}^{m_{sup}} \phi(m) dm \int_0^\tau \dot{M}_\star(t-t') l_m(t-t') dt' \tag{A.17}$$

where τ is the minimum between t and the time $\tau_{MS}(m)$ spent in the main sequence by star of mass m and $l_m(t)$ is the luminosity. Assuming that the $l_m(t)$ is constant during in the main sequence and the $\dot{m}_\star(t)$ varies slowly, the luminosity amounts to

$$L_\star(t) \approx 3.\,5 \times 10^{43} \left(\frac{\dot{M}_\star(t)}{M_\odot yr^{-1}} \right) ergs^{-1} \tag{A.18}$$

for a Chabrier IMF. A Salpeter IMF would imply $L_\star(t) \approx 2 \times 10^{43} \left(\frac{\dot{M}_\star(t)}{M_\odot yr^{-1}} \right) ergs^{-1}$ (see e. g. Kennicutt 1998[171], Panuzzo et al. 2003[250]). The luminosity from stars can also be written as

$$L_\star(t) \sim \epsilon_{nuc} c^2 f_H \psi(t) \approx 4 \times 10^{43} (\frac{\epsilon_{nuc}}{0.007}) (\frac{f_H}{0.1}) \left(\frac{\dot{M}_\star(t)}{M_\odot yr^{-1}} \right) ergs^{-1} \tag{A.19}$$

where f_H is the fraction of stellar mass of H converted into He during the main sequence in stars in the relevant range of mass. Under the assumption that the reservoir is fed at a rate $\dot{M}_{inflow} \sim M_{cold} \frac{dlnJ}{dt}$, the mass of the reservoir increases at a rate

$$\dot{M}_{\rm inflow} \approx \frac{L_\star}{c^2} \left(1 - e^{-\tau_{\rm RD}}\right) \approx \alpha_{\rm RD} \times 10^{-3} \ \dot{M}_\star \ \left(1 - e^{-\tau_{\rm RD}}\right) \ ; \tag{A.20}$$

the constant of proportionality $\alpha_{\rm RD} \sim 1-3$ can be fixed to produce a good match to the correlation between the spheroid and the supermassive BH masses observed in the local Universe.

Eventually all the mass passed through the reservoir is accumulated in the BH, i. e.

$$M_\bullet \simeq M_\bullet^0 + \int \dot{M}_{inflow} dt \simeq M_\bullet^0 + \alpha_{\rm RD} \times 10^{-3} \ M_\star(t) \ (1 - e^{-\tau_{\rm RD}}) \tag{A.21}$$

where $M_\star(t)$ is the overall mass of the stars formed during the epoch when the reservoir has been fed through radiation drag and $M_\bullet^0$ is the BH seed mass. With $\alpha_{\rm RD} \sim 1-3$, this

equation naturally predicts the $M_\bullet - M_\star$ relation (Magorrian et al. 1998[204] ;see Ferrarese & Ford 2005[113] for a review). However the most reliable mass estimates are quite difficult, because they are based on very high angular resolution spectroscopy in order to determine the dynamics within the very central galaxy regions. As a consequence high mass BHs are more easily weighed than less massive ones. As a result we may expect that the true variance in the $M_\bullet - M_\star$ relation is higher than the observed. We stress in particular that Equation A.21 shows that the relation depends also on τ_{RD}, which decreases significantly for low mass galaxies. This implies that the $M_\bullet - M_\star$ relation should exhibit two regimes: (1)when $\tau_{RD} > 1$ $M_\bullet \propto M_\star$;(2) while for lower mass galaxies $M_\bullet \propto M_\star \times \tau_{RD}$. Since τ_{RD} significantly declines with star and halo mass, e. g. $\tau_{RD} \propto M_H^{2/3}$ (Shankar et al. 2006), the relationship between BH mass and halo mass (or stellar mass) significantly steepens at small halo mass (or stellar mass).

A.2.3 Feedback from SNae

The effects of SNae on ISM in a galaxy are very important(e. g. McKee & Ostriker 1977[223], Efstathiou 2000[105]). The distinction between type 1 and type 2 SNae is relevant in studying their respective effects. Core collapse type 2 SNae are associated to massive stars with typical lifetime $\tau_s \leq$ a few 10^7 years, a timescale which is negligible when studying galaxy evolution even at large redshift; as a consequence we can assume that their explosion rate is directly proportional to the current star formation rate. Instead type 1 SNae are associated to binary systems. Recently, Kobayashi & Nomoto(2009)[176] reviewed the model of single degenerate star, wherein the system is composed by a white dwarf(WD) and a main sequence (MS) or a red giant star (RG) losing mass. Since the mass loss depends on the metal abundance, the expected SNIa rate is strongly suppressed when the metallicity is $Z \leq 0.1 Z_\odot$. Kobayashi and Nomoto(2000)[176] showed that the WD+MS systems produce a peak of SNae at $t \sim 10^9$ yr for low chemical abundance $Z \leq 0.1 Z_\odot$ while for solar abundance the peak moves to $t \sim 10^8$ yr. The WD+RG binaries exhibit the same behavior only with timescale a factor of 2 larger. However the rates of SNIa are quite penalized by the peculiar conditions required for their occurrence. Thus they transfer to the galactic gas an amount of energy that is comparable or greater than that associated to type 2 SNae only when the star formation rate has significantly declined. In this sense we shall see that they are relevant in removing the gas restituted

from stars at late times. Thus we neglect in the analytical description of the model the energy input of SNIa in the first 10^9 yr of the galaxy life. For late times we will present the results of numerical studies and an analytical approximation.

The type 2 SNae feedback can be parameterized as

$$\dot{M}_{\rm cold}^{SN} = \beta_{SN}\ \dot{M}_\star\ , \tag{A.22}$$

where the efficiency of gas removal

$$\beta_{SN} = \frac{N_{SN}\ \epsilon_{SN}\ E_{SN}}{E_{\rm bind}} \approx 0.6 \left(\frac{N_{SN}}{8\times10^{-3}/M_\odot}\right)\left(\frac{\epsilon_{SN}}{0.05}\right)\left(\frac{E_{SN}}{10^{51}{\rm erg}}\right)\left(\frac{M_{\rm H}}{10^{12}M_\odot}\right)^{-2/3}\left(\frac{1+z}{4}\right)^{-1} \tag{A.23}$$

depends on the number of SNae per unit solar mass of condensed stars N_{SN} (of order $1.\,4\times10^{-2}$ for the Chabrier IMF and 8×10^{-3} for Salpeter IMF), on the energy per SN explosion $E_{SN}\approx10^{51}$ ergs, on its coupling to the surrounding medium $\epsilon_{SN}\approx5\%$, and on the specific binding energy of the gas within the DM halo, $E_{\rm bind}$. Following Zhao et al. (2003)[364] and Mo & Mao (2004)[228], the latter quantity has been estimated for $z\geq1$ as

$$E_{\rm bind} = V_{\rm H}^2\ f(c)\ (1+f_{\rm b,\ i})/2 \approx 3.\,2\times10^{14}\ (M_{\rm H}/10^{12}\ M_\odot)^{2/3}\ [(1+z)/4]\ {\rm cm}^2\ {\rm s}^{-2} \tag{A.24}$$

A.2.4 QSOs FEEDBACK

The BH accretion can transfer energy and momentum to the interstellar medium(ISM) of the host galaxy and even to the gas far away from the central regions of the hosting halo through radiation and gas outflows. Quasar outflows can be divided into two main sectors:relativeistic radio jets and much less collimated outflows with $v\sim0.03-0.2c$(so-called broad absorption line(BAL) QSOs). Relativistic jets are able to transport large amount of energy very far away from the host galaxy, up to a few Mpc. On the other hand the BAL QSOs outflows are much less collimated and they soon impinge into the gas closer to the central BH. Though both mechanisms are relevant to carry away kinetic energy extracted by accretion, the BAL QSOs outflows are more generic. At the brightest luminosities, a large fraction ($\sim\ 20-40\%$) of optically selected quasars show BALs(Hewett & Foltz 2003[148];Dai et al. 2008[88]). And it is likely that all bright quasars exhibit BALs, although they may not be visible due to geometric effects(Reichard et al. 2003[273]; Elvis

2000[107];Gallagher et al. 2006[120]; Priddey et al. 2007[267], Fan et al. 2009[110]).

Following Murray et al. (1995)[231], an approximate solution for the wind velocity is

$$v \approx v_\infty \left(1 - \frac{r_f}{r}\right)^{2.\ 35} \tag{A.25}$$

with

$$v_\infty = \left(\gamma \frac{GM_\star}{r_f}\right)^{1/2} \tag{A.26}$$

where $r_f \sim 10^{16}$cm is the radius at which the wind is launched and the γ is a factor related to the force multiplier (the reference values $\gamma \sim 3$, see Laor & Brandt 2002[187]). The asymptotic speed is reached at $r_\infty \geq 40 r_f$. The outflow rate at radius r is $\dot{M}_\omega(r) \approx 4\pi f_c \rho(r) v(r)$, where f_c is the covering factor of the outflow. Assuming that most of the mass is placed at around r_∞, the global outflow can be written as

$$\dot{M}_\omega \approx 4\pi f_c m_H N_H r_\infty v_\infty \approx 3 N_{23} \left(\frac{f_c}{0.1}\right) \left(\frac{M_\bullet}{10^8 M_\odot}\right)^{1/2} M_\odot yr^{-1} \tag{A.27}$$

The associated total kinetic luminosity reads

$$L_K = \frac{1}{2}\dot{M}_\omega v_\infty^2 \approx 4 \times 10^{44} N_{23} \left(\frac{f_c}{0.1}\right) \left(\frac{M_\bullet}{10^8 M_\odot}\right)^{3/2} erg\ s^{-1} \tag{A.28}$$

In general the kinetic luminosity is a fraction of the accretion luminosity. The accretion luminosity $L_{acc} = \frac{\eta}{1-\eta}\dot{M}_\bullet c^2$ depends on the capability of the radiation drag to funnel gas into the reservoir. There are two possible cases:1)the reservoir is able to keep a radiation limited regime or 2) the accretion regime is sub-Eddington. In the second case, the feedback from SNae dominates and the quasar feedback is negligible. In the other case the BH mass is increasing exponentially on τ_{ef} timescale and therefore the accretion luminosity can be written as $L_{acc} \simeq 1.\ 4 \times 10^{46} \lambda \left(\frac{M_\bullet}{10^8 M_\odot}\right) ergs^{-1}$. As a result, the kinetic luminosity is only $\leq 20\%$ of the accretion luminosity even in the case of extremely massive BHs.

$$\frac{L_K}{L_{acc}} = \frac{2.\ 8 \times 10^{-2}}{\lambda} N_{23} \left(\frac{f_c}{0.1}\right) \left(\frac{M_\bullet}{10^8 M_\odot}\right)^{1/2} \tag{A.29}$$

For large accretion rates occurring in large protogalaxies, the quasar feedback will be expressed through kinetic luminosity as reported in Equation A.29, while it turns out to be negligible respect to the SNae feedback in less massive primeval galaxies.

The next key point is how to evaluate the effects of injected kinetic energy on the envi-

ronmental gas. Numerical simulations (e. g. Begelman 2004[18]) have been exploited in order to assess the basic aspects of the phenomenon. Two main mechanisms can influence the gas in the halos. First the gas can be shock heated to such a temperature that it can become unbound. Alternatively, ram pressure can act on the gas clouds and remove them from the halos. In a simplified approach we assume that a fraction f_h of the kinetic energy transfers to the halo gas, bringing it to a hot phase that its cooling time becomes longer than the Hubble time. Nath & Roychowdhury(2002)[237] have estimated that the mechanical work done by cocoons in the case of radio jets can amount to a fraction $f_h \sim 0.5$ of the total luminosity in the outflow. We assume that similar efficiencies hold also for BAL outflows. Then the QSOs deliver the kinetic energy to the gas at a rate

$$L_{QSO} = f_h \times L_K \approx 2 \times 10^{44} \ \epsilon_{QSO} \left(\frac{M_\bullet}{10^8 \ M_\odot} \right)^{3/2} \ \mathrm{erg \ s^{-1}} \ . \tag{A.30}$$

Here $\epsilon_{QSO} = (f_h/0.5) \ (f_c/0.1) \ N_{23}$ is the strength of QSO feedback, expected to be close to unity; f_c is the covering factor of such winds and N_{23} is the hydrogen column density toward the BH in units of 10^{23} cm^{-2} (cf. Equations [29], [30] and [31] in Granato et al. 2004[136]). With $\epsilon_{\rm QSO} \approx 1.3$ the bright end of the galaxy luminosity function is reproduced (Lapi et al. 2006[190]).

We assume that the energy is shared between the infalling and cold gas component on the basis of their respective mass fraction over the baryon mass. Since $M_{inf} \gg M_{cold}$ this assumption implies that most of the energy is given to the diffuse gas in the halo. The rate of gas removal of each component is estimated as the ratio between the rate of energy released to the component and the specific binding energy

$$\dot{M}^{QSO}_{cold, \ inf} = \frac{L_{QSO}}{E_{bind}} \frac{M_{cold, \ inf}}{f_b M_H} \tag{A.31}$$

As a consequence, the QSO feedback grows exponentially during the early phases of galaxy evolution, following the exponential growth of the supermassive BH mass. It is is negligible in the first 0.5 Gyr in all halos, but abruptly becomes dominant in DM halos more massive than $10^{12} \ M_\odot$. Eventually, in these systems most of the gas becomes unbound from the potential well of the galaxy halo, so that star formation and BH activity itself come to an end on a timescale which is shorter for more massive galaxies.

Indeed, the positive feedback on BH growth caused by star formation, in cooperation with the immediate and negative feedback of SN, and the abrupt and dramatic effect of

QSO feedback, are able to reverse the formation sequence of the baryonic component of galaxies compared to that of DM halos: the star formation and the buildup of central BHs are completed more rapidly in the more massive halos, thus accounting for the phenomenon now commonly referred to as *downsizing*.

A.2.5 Chemical evolution

The evolution of chemical abundance of the cold gas in presence of gas inflow and outflow is

$$\frac{d}{dt}[M_{cold}Z_{cold}] = \dot{M}_{cond}Z_{inf} - (1-\xi(t))\dot{M}_{\star}Z_{cold} - (\dot{M}^{SN}_{cold} + \dot{M}^{QSO}_{cold})Z_{cold} + \xi_Z(t)\dot{M}_{\star} \quad \text{(A.32)}$$

where the function $\xi(t)$ describes the contribution to the metallicity by non processed gas restored by stars at the end of their life:

$$\xi(t) = \int_{m_{\star,\ t}}^{m_{\star}^{sup}} dm_{\star}(m_{\star} - m_{rem})\phi(m_{\star})\frac{Z_{cold}(t-\tau_{m_{\star}})\dot{M}_{\star}(t-\tau_{m_{\star}})}{Z_{cold}(t)\dot{M}_{\star}(t)} \quad \text{(A.33)}$$

The function $\xi_Z(t)$ gives the total amount of newly formed metals ejected from stars

$$\xi_Z(t) = \int_{m_{\star,\ t}}^{m_{\star}^{sup}} dm_{\star}m_{\star}q_Z(m_{\star})\phi(m_{\star})\frac{\dot{M}_{\star}(t-\tau_{m_{\star}})}{\dot{M}_{\star}(t)} \quad \text{(A.34)}$$

where $q_Z(m_{\star})$ is the fraction of the stellar mass $m_{\star}$ ejected as freshly produced metals. Notice that in this treatment we neglect the dependence that the metal yield my depend on the initial chemical composition of the stars. Combining the Equations A.3, A.8 and A.10, Equation A.32 can be written as

$$\dot{Z}_{cold} = \frac{Z_{inf} - Z_{cold}}{t_{cond}}\frac{M_{inf}(t)}{M_{cold}(t)} + \frac{R_Z(t)}{t_{\star}} + \frac{Z_{cold}(\xi(t) - R(t))}{t_{\star}} \quad \text{(A.35)}$$

where Z_{inf} is the initial metallicity of infalling gas.

The main effect of the QSOs feedback is to remove the gas and to stop star formation in a few e-folding time, freezing also the chemical composition. This is the key point to produce the observed α-enhancement in massive ETGs. On the other hand, SNae feedback plays its role through the parameter γ which is relevant to fix the ration of the cold to the infalling gas.

$R_Z(t)$ is almost independent of the halo mass and virialization epoch and it is well

described for $t > 3\ Myr$ by

$$R_Z(t) \approx A_Z + B_Z ln(\frac{t}{t_Z}) \quad t \leq t_{sat} \tag{A.36}$$

$$R_Z(t) \approx A_Z + B_Z ln(\frac{t_{sat}}{t_Z}) \quad t > t_{sat} \tag{A.37}$$

where $t_Z \approx 10$ Myr and $t_{sat} \approx 30$ Myr; $A_Z \approx 0.043(0.021)$ and $B_Z \approx 0.030(0.015)$ for Romano IMF (Romano et al. 2005[283]) and Salpeter IMF(Salpter 1955[284]), respectively.

A.2.6 Analytic approximations

The model yields as outputs the time evolutions of stars and gas (including metals) components of the galaxies and of the associated active galactic nuclei. When the star formation, gas abundance and the chemical evolution history of a galaxy within a DM halo of given mass have been computed, the dust abundance can be inferred (e. g. , Mao et al. 2007[211]). Then the spectral energy distribution as a function of time from extreme-UV to radio frequencies can be obtained through spectrophotometric codes, such as GRASIL, which includes a treatment of dust reprocessing (Silva et al. 1998 [308]; Schurer et al. 2009[294]). Coupling these results with the DM halo formation rate, we can obtain the statistics of galaxies and supermassive BHs/QSOs as a function of cosmic time, in different observational bands.

By analyzing the results of the numerical solution for the full set of equations given above, it is apparent that in massive galaxies the term of QSO feedback is important only during the final stage of BH growth, around $2-3$ $e-$folding times (approximately 10^8 yr) before the peak of QSO luminosity, when the energy discharged by the QSO is so powerful to unbind most of the residual gas, quenching both star formation and further accretion onto the supermassive BH. On the other hand, in less massive galaxies the central BH mass and the associated accretion is not able to stop star formation, which lasts for several Gyrs. The duration of the star formation $\Delta t_{\rm burst}$ can be approximated by a simple analytical form

$$\Delta t_{\rm burst} \approx 6 \times 10^8 \ \left(\frac{1+z}{4}\right)^{-1.\ 5} \ \mathcal{F}\left(\frac{M_{\rm H}}{10^{12}\ M_\odot}\right) \ \ {\rm yr}\ , \tag{A.38}$$

where $\mathcal{F}(x) = 1$ for $x \geq 1$ and $\mathcal{F}(x) = x^{-1}$ for $x \leq 1$. A good approximation for the star

formation history in massive galaxies is obtained by neglecting the QSO feedback effect in Equation A.7 and A.8 and by abruptly stopping star formation and accretion onto the central BH after $\Delta t_{\rm burst}$ since halo formation.

Then Equation A.7 and A.8 can be easily solved, with the outcome that the infalling mass declines exponentially as

$$M_{\rm inf}(t) = M^0_{inf}\ {\rm e}^{-t/t_{\rm cond}}\ , \tag{A.39}$$

The cold gas mass evolves according to

$$M_{\rm cold}(t) = \frac{f_b M_{\rm H}}{s\gamma - 1}\ \left[{\rm e}^{-t/t_{\rm cond}} - {\rm e}^{-s\ \gamma\ t/t_{\rm cond}}\right]\ ; \tag{A.40}$$

here we have introduces the shorthand $\gamma \equiv 1 - \mathcal{R} + \beta_{\rm SN}$. The quantity $s \equiv t_{\rm cond}/t_\star$ is the ratio between the timescale for the large-scale infall estimated at the virial radius and the star formation timescale in the central region; it corresponds to $s \approx 5$, both for an isothermal or NFW density profile with standard value of the concentration parameter $c \approx 4$ at halo formation. We notice that the dependence on the fraction of gas restituted by the stars is quite weak and that the value obtained by the hypothesis of instantaneous recycling can be used.

The corresponding stellar mass reads:

$$M_\star(t) = \frac{s\ f_b M_{\rm H}}{s\gamma - 1}\ \left[1 - {\rm e}^{-t/t_{\rm cond}} - \frac{1}{s\gamma}\ \left(1 - {\rm e}^{-s\ \gamma\ t/t_{\rm cond}}\right)\right]\ ; \tag{A.41}$$

the mass of all stars formed during the main episode of star formation is then $M^{\rm f}_\star \approx M_\star(\Delta t_{\rm burst})$.

In Equation. A.38, and A.40 the condensation timescale is well approximated by

$$t_{\rm cond} \approx 9 \times 10^8\ \left(\frac{1+z}{4}\right)^{-1.\ 5}\ \left(\frac{M_{\rm H}}{10^{12}\ M_\odot}\right)^{0.2}\ {\rm yr}\ . \tag{A.42}$$

The scaling with redshift and mass mainly reflects the behavior of the dynamical/cooling time, while a mild dependence on $M_{\rm H}$ is also related to the impact of the energy feedback from the QSO on the infalling gas, which is stronger for more massive halos hosting more massive BH.

A good approximation for $f_{\rm gas}$, i. e. the ratio between the stellar and gaseous mass immediately before the gas is swept away by the QSO feedback, can be obtained using

Equation. A.40 and A.41. The gas mass includes both the cold gas and the gas restituted by the stars. The latter is estimated as $\mathcal{R}\ M_\star$ with $\mathcal{R} = 0.3$, which corresponds to the gas returned by the stars about 0.1 Gyr after a burst of star formation with a Chabrier's IMF(Chabrier 2003[60]). We find that the results are well approximated by $f_{\rm gas} \approx (M_\star/10^{11}\ M_\odot)^{0.2}$.

For $M_{\rm H} \geq 3 \times 10^{11}\ M_\odot$, corresponding to $M_\star \geq 10^{10}\ M_\odot$, the dependence on halo mass and formation redshift of ratio m between the halo mass and the surviving stellar mass (i. e. the present day stellar mass fraction) can be approximated as $m \approx 25\ (M_{\rm H}/10^{12}\ M_\odot)^{0.1}\ [(1+z_{\rm form})/4]^{-0.25}$. At lower masses m increases rapidly with decreasing $M_\star$ (see Shankar et al. 2006[298]).

Finally, considering that all the mass flowed into the reservoir is eventually accreted by the BH and neglecting the mass of the seed BH ($M_\bullet^0 \approx 10^2\ M_\odot$), one can write the relic BH mass as function of the overall mass in stars formed during the star forming phase $\Delta t_{\rm burst}$ as

$$M_\bullet^{\rm f} \approx \alpha_{\rm RD} \times 10^{-3}\ M_\star^{\rm f}\ (1 - {\rm e}^{-\langle\tau_{\rm RD}\rangle})\ . \tag{A.43}$$

The time average of the optical depth $\langle\tau_{\rm RD}\rangle$ can be approximated as

$$\langle\tau_{\rm RD}\rangle \approx \tau_{\rm RD}^0\ \left(\frac{M_{\rm H}}{10^{13}\ M_\odot}\right)^{2/3}\ \left(\frac{1+z}{4}\right), \tag{A.44}$$

implying $1 - {\rm e}^{-\langle\tau_{\rm RD}\rangle} \approx 1$ for massive galaxies and $1 - {\rm e}^{-\langle\tau_{\rm RD}\rangle} \approx \langle\tau_{\rm RD}\rangle \propto M_{\rm H}^{2/3}$ for less massive galaxies. As expected, most of the mass flows from the reservoir to the central BH in the final couple of $e-$folding times. At early times the ratio of the BH to the stellar mass is predicted to be much lower than the final value .

Appendix B

SIMPLE STELLAR POPULATION AND MODEL PROCEDURE

To compute the SSP models we have adopted the Bressan et al. (1998)[46] isochrones. Here we have used the new empirical stellar spectral library, MILES (Sánchez-Blázquez et al., 2007[286]), which covers well the parameter space of metallicity, effective temperature and gravity and thus ensure good optical broad band starting colours. To cope with its spectral range limitations we have extended the stellar spectra of MILES by means of matched NEXTGEN (Allard et al. 2000[3]) models both in the FAR-UV and in the NIR/MIR spectral region. For temperatures above 10000K we do not have NEXTGEN models and we have used the library by Munari et al (2005)[230] with the extension of the Lejeune et al.(2001)[195] models below 2500Åand above 10000 Å.

In this way we have obtained three core libraries with average [M/H]=-0.5, 0.0 and +0.3. The stellar spectra extend from 10Åto 160μm and the spectral resolution is of about 2ÅFWHM, from 2500Åto 10000 Å. To take into account the effects of mass loss in hot supergiant stars we have considered two further extensions. For O stars we have considered the spectral models by Schaerer & de Koter (1997)[291] while, for Wolf Rayet stars we have included the spectral models by Schmutz, Leitherer & Gruenwald (1992)[293]. The latter library provides only the continuum distribution of Wolf Rayet stars while there are more recent stellar libraries that provide also spectral features (e.g. Smith et al. 2002[311]). However Schmutz et al. library is suitable for our purposes because we

are considering only broad band magnitudes here and, more important, because its parametrization as a function of core temperature, T^*, and transformed radius, R_t, allows a fair interpolation between stellar evolution quantities (L & T_{eff}) and spectral models of thick winds. To this purpose, for each WR star along the isochrone we compute the mass loss rate and, following the indications provided in the above paper, we compute the corresponding terminal velocity and the transformed radius, which we use together with T_{eff} to interpolate in the spectral library.

For the young populations we have also considered the nebular spectrum, which is calculated by means of CLOUDY (Ferland 1996[112]) assuming case B recombination. To compute the nebular emission at different ages we have considered the corresponding spectra of the SSPs using the following parameters: mass of the ionizing cluster $10^5 M_\odot$, electron number density n=100 cm^{-3}, inner radius 15 pc, and the metallicity rescaled to that of the SSP. The nebular emission has been then suitably rescaled to the original mass of the SSP. The main effect we noticed on broad band fluxes is the contribution of nebular continuum in very young stellar populations. Changing the nebular parameters would not affect our conclusions significantly.

For intermediate age stellar populations we have also considered the effects of dusty envelopes around asymptotic giant branch stars, as described in Bressan et al. (1998)[46], but after revisiting the mass loss rate formulation and the expected dust composition, as described in Marigo et al (2008)[216]. In particular we have included carbon star spectra (Nowotny et al. 2005[242]) and graphite dust composition when, along the isochrone, the star appears as a Carbon star. We have finally checked that the ischrones reproduce well the observed integrated (V-K) colours of LMC star clusters (Persson et al. 1983[260], Kyeong et al. 2003[185] and Pessev et al. 2006[261]), especially at intermediate ages.

Despite the different SSP we adopt here, our modeling procedure is similar to that of Shapley et al.(2001, 2005)[300][301]. We used the SSP with solar metallicity and a Salpeter IMF extending from 0.15 to 120 $M_\odot$.Just as shown by Shapley et al.(2005)[301], solar metallicity is a good approximation.The different choices of the IMF, such as Kroupa IMF and Chabrier IMF, and the stellar mass range of IMF will change the formed stellar mass by a factor(1 2). Dust extinction is taken into account with a Calzetti et al.(2000)[54] starburst attenuation law which is widely adopted for the high redshift star-forming galaxies.We need notice that the extinction law may depend on the bolometric luminosity. If necessary, we can take the extinction law as a fitting parameter (See Chapter 2). We

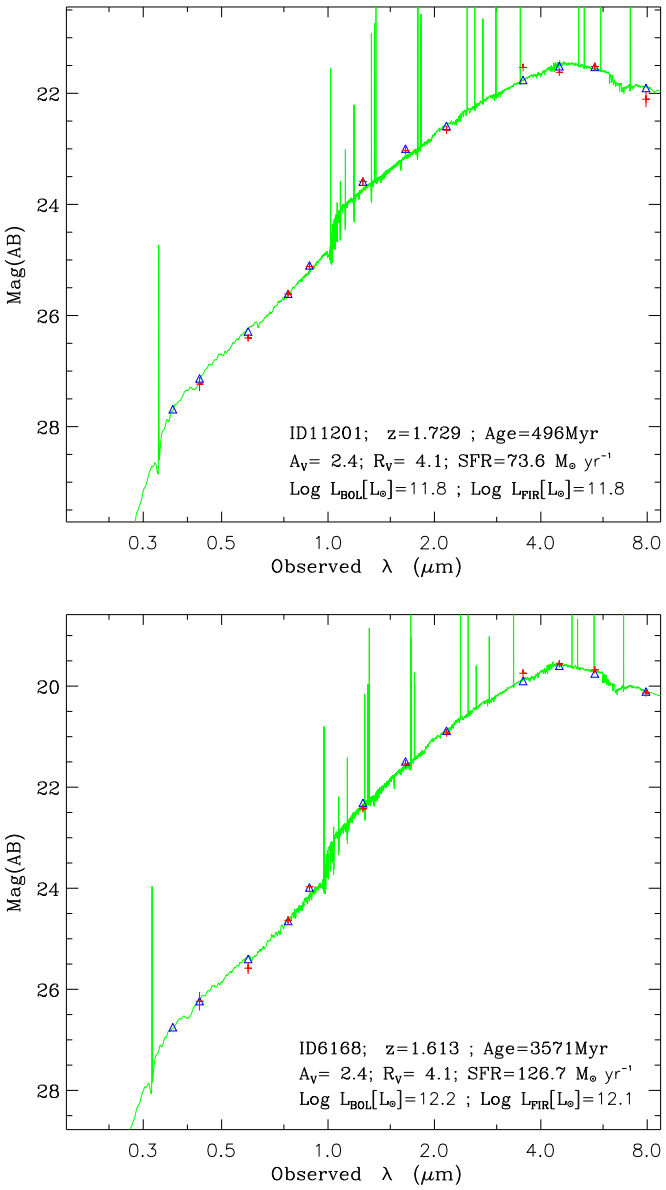

Figure B.1: SED fitting technique. We plot the observed fluxes (crosses) and corresponding model fluxes after convolution with the filter transmission (triangles). The solid curve is the best fit model. We write the star formation rate of the best fit model, sampled at discrete SSP ages and the corresponding visual attenuation A_V on the right bottom . Both the SFR and the attenuation are kept constant with the age of the stellar populations Error bars on fluxes are also plotted bat are in general smaller than the symbol size.

assumed that the extinction value E(B-V) is constant during the whole star formation histories. In order to compare the galaxies properties at different redshift, we only considered the simplest model, the continuous star formation (CSF) models.In order to construct the CSF model spectrum with a given galaxy age t, we integrated all SSP spectra with age same as or smaller than t.Each SSP is weighed by its duration.The duration of the i-th SSP equals to half of the difference between the age of (i+1)th SSP and (i-1)th SSP

except for the first and last one.The first duration equals to half of the difference between the age of the second SSP and the first SSP. And the last one equals to the galaxy age t minus the age of the last SSP.For the purpose of constraining the stellar properties of each galaxies, we use four fitting parameters:the extinction value E(B-V), the galaxy age t_g, the constant star formation rate SFR and the formed stellar mass $M_\star$.The extinction value E(B-V) ranged between 0.0 and 1.0.And the galaxy age ranged between 1 Myr and the age of the universe at the redshift of the galaxy being modeled.For a set of given E(B-V) and t, we can compute the intrinsic model galaxy spectrum.Then we reddened it by dust adopting the Calzetti law and further attenuated it by intergalactic medium of neutral hydrogen (Madau 1995)[202].Then the redshifted model SED (M_i) were computed corresponding the observed SED (O_i).Then a merit function MF was defined:

$$\mathrm{MF} = \sum_{i=1}^{n} \left(\frac{M_i - O_i}{E_i} \right)^2 \tag{B.1}$$

where E_i is the corresponding errors. To evaluate the best-fit model, we minimized the merit function MF adopting the Adaptive Simulated Annealing algorithm (ASA, Ingber 2001[160]).

Appendix C

PHOTOMETRIC REDSHIFT OF HIGH REDSHIFT SMGS

C.1 SEDs of high redshift SMGs

The dust re-radiation in starburst galaxies is expected to come from at least three astrophysical settings (e.g. Silva et al. 1998[306]): molecular clouds, diffuse low-density clouds (cirrus), and circum-nuclear regions, heated by Active Galactic Nuclei (AGNs). The AGN dust emission peaks in the mid-IR (Granato & Danese 1994[135]; Andreani et al. 2010[5]; Lutz et al. 2010[201]) and can be safely ignored in the SPIRE wavelength range. Molecular clouds are the preferential sites of star formation implying that they are endowed with intense radiation fields and relatively warm dust temperatures. The cirrus component is exposed to the less intense general radiation field due to older stellar populations that have come out from their native molecular clouds and is therefore characterized by lower dust temperatures.

For the high redshift SMGs, with SFR $\geq 100 M_{\odot}\ yr^{-1}$, only the 'warm' starburst component is relevant. It is important to take into account, however, that also its SED is much broader than a single temperature grey-body. Over the $50-500\mu m$ range (in the rest-frame) such a SED can be approximated, to better than $10-20\%$, by a sum of two

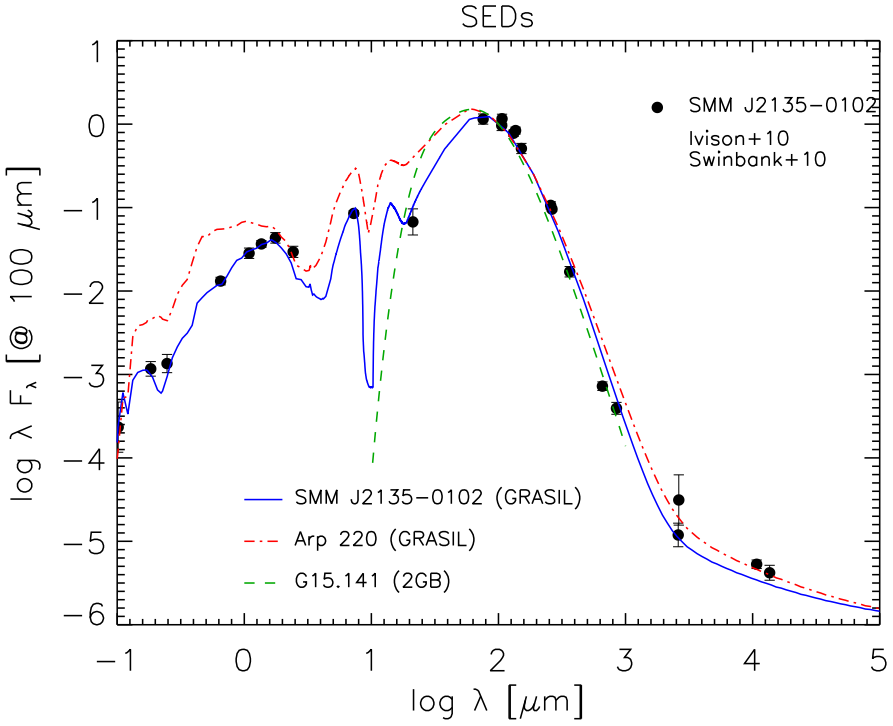

Figure C.1: The SED of SMM J2135-0102 as modeled by GRASIL (blue solid line); data are from Ivison et al. (2010)[162] and Swinbank et al. (2010)[319]. The SED of Arp220 (red dot-dashed line) as modeled by GRASIL, and that of G15.141 modeled as a double-temperature grey-body (green dashed line) are also shown for comparison. All SEDs are in the rest-frame and are normalized at 100 μm.

grey-bodies, each described by

$$S_\nu \propto \frac{\nu^{3+\beta}}{e^{h\nu/kT_d} - 1} \; ; \tag{C.1}$$

with dust temperatures $T_d \approx 30K$ and $60K$, and the dust emissivity indices $\beta = 1.7$ and 2, respectively.A fit to the observed SEDs of standard template starburst galaxies with quite different SFRs (M82, Arp220), and of the $z \approx 2.3$ strongly lensed galaxy SMM J2135-0102, confirms the validity of this approximation and shows that the relative normalization of the two grey bodies varies by factors of several. Mid/far-IR data on starburst galaxies emphasize the warmer component, while sub-mm data emphasize the colder one; if a single temperature dust is used, data in different wavelength ranges may yield substantially different temperatures. If the source redshift is in the range $1 \leq z \leq 3.5$, PACS and SPIRE wavelengths extend across the dust emission peak (which is typically at a rest-frame wavelength $\lambda \approx 90 - 100 \mu m$). This may allow reasonably accurate redshift estimates using only Herschel data (Negrello et al. 2010[239]).

Arp220 and SMM J2135-0102 are of particular interest because their SEDs are well

determined and have SFRs quite typical of the galaxies considered here. We have modeled their spectral energy distributions from extreme-UV to radio frequencies through the spectrophotometric code GRASIL, which includes a sophisticated treatment of dust reprocessing (Silva et al. 1998[308]; Schurer et al. 2009[294]). The results are illustrated in Figure C.1; it must be stressed that the dominant contribution for wavelengths $\lambda \geq 30\mu m$ is provided by molecular clouds.In Figure C.1 we also sketch the far-IR SED of G15.141 (H-ATLAS J142413.9+022304), a strongly lensed sub-mm galaxy at $z \approx 4.24$ with estimated SFR of several hundreds $M_{\odot}\ yr^{-1}$ (Cox et al. 2011[80]), modeled as the sum of two grey-bodies with $T_1 = 32K$, $T_2 = 60K$, $\beta = 2$, and a ratio of 0.02 between the coefficients of the warm and of the cold components. We choose the SEDs of these 3 galaxies (Arp220, SMM J2135-01012, and G15.141) as our candidate templates for our photometric redshift estimates.

C.2 Redshift estimates

We focus on the redshift estimates of high redshift ($z > 1$) SMGs. It's difficult to measure the spectroscopic/photometric redshifts according to optical/Near-IR bands, because of heavy dust obscuration in these galaxies.The only way to obtain the solid spectroscopic redshift is to measure the molecular rotation and atomic fine-structure transition line emissions.Among them, the CO-line is most commonly used.However, these kinds of observations are very time-expensive and cannot be done for a large sample.

In case of absence of reliable spectroscopic redshift, we want to know if it is possible to get the acceptable photometric redshift only based on the Herschel observations of FIR/submm bands. We discuss in the previous section that the FIR/submm SED of the high redshift SMGs can be reproduced by two gray-body spectra, one 'warm' component which is dominate and one 'cold' component. If choosing the proper template, it's very likely to obtain the reasonably accurate redshift estimates.In previous section, we choose three SEDs as our templates: Arp220, SMM J2135-01012, and G15.141. Using these three template SEDs, We estimated the photometric redshifts of 39 H-ATLAS galaxies at $z > 0.5$ for which spectroscopic redshifts are available. The results are presented in Figure C.2 . The average SED of low-z H-ATLAS SDP galaxies, determined by Smith et al. (2011b), was also used, for comparison. There is no indication that photometric

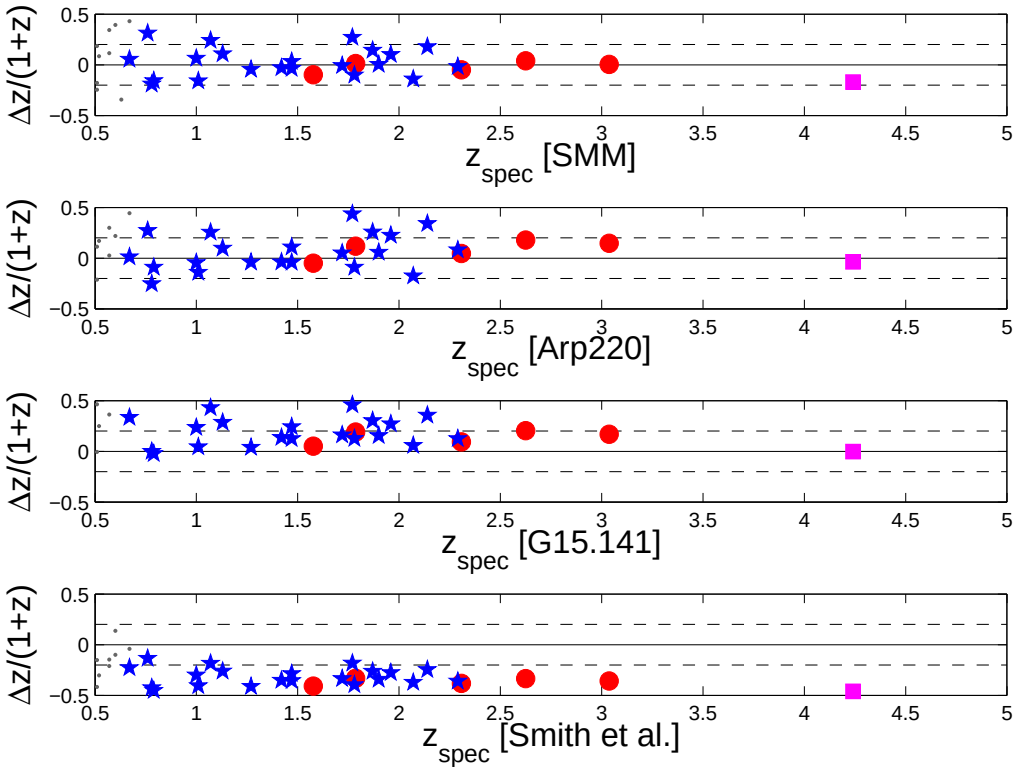

Figure C.2: Photometric redshift estimates based on the SEDs of (from top to bottom) SMM J2135-0102, Arp220, G15.141, and the average low-z SED from Smith et al. (2011) compared in terms of the quantity $\Delta z/(1+z) = (z_{phot} - z_{spec})/(1+z_{spec})$ with spectroscopic measurements for the strongly lensed galaxies of Negrello et al. (2010; red filled circles) and Cox et al. (2011; purple filled square), and for the H-ATLAS SDP galaxies with $z > 0.5$ of Bonfield et al. (2011; blue asterisks) and Smith et al. (2010; black dots). The dashed lines correspond to a 20% difference.

redshifts are systematically overestimated when we use the SED of SMM J2135-0102 as a template. The median value of $\Delta z/(1+z) = (z_{phot} - z_{spec})/(1+z_{spec})$ is 0.01 with a dispersion of 0.21. The situation is only slightly worse in the case of Arp220: the median value of $\Delta z/(1+z)$ is 0.06 with a dispersion of 0.27. The median offset between photometric and spectroscopic redshifts increases to 0.18, with a dispersion of 0.28, if we use the cooler SED of G15.141. In the redshift range ($z \geq 1$) we are most interested in there are 24 objects. The median values of $\Delta z/(1+z)$ are -0.002 (dispersion 0.12) for SMM J2135-0102, 0.07 (dispersion 0.16) for Arp220, 0.16 (dispersion 0.13) for G15.141. Note that the 'warm' starburst dominated FIR/submm SED is only representative for the high redshift SMGs, but not for the low z galaxies.

We estimate the redshifts of objects in the samples defined in Chapter 3. The redshift estimate is the result of a minimum χ^2-fit of each of the three templates to the SPIRE and PACS data. Figure C.3 shows that, after correcting for the offsets highlighted by Figure C.2, the derived redshift distributions are only moderately affected by the choice

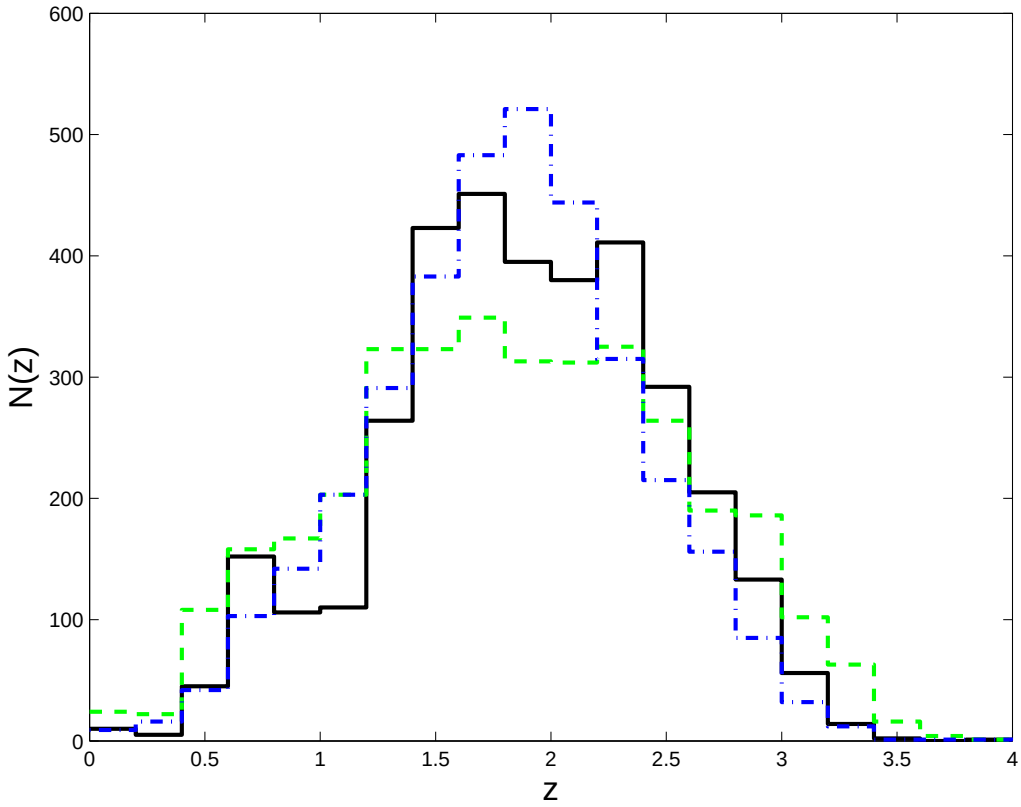

Figure C.3: Comparison of the redshift distributions of sources in our reference sample ($S_{250\mu m} > 35mJy$, $S_{350\mu m} > 3\sigma$, and no $R > 0.8$ optical identifications; 3469 sources, i.e. $\approx 50\%$ of the 6876 H-ATLAS SDP galaxies) estimated using the SEDs of Arp 220 (green dashed line), G15.141 (blue dot-dashed line), and of SMM J2135-0102 (black solid line).

of the template SED; they have broad maxima in the range $1.5 \leq z \leq 2.5$ and a tail extending up to $z > 3.5$, consistent with earlier estimates for BLAST (Ivison et al. 2010b[161]) and Herschel (Amblard et al. 2010[4]; Eales et al. 2010[103]) samples.

BIBLIOGRAPHY

[1] K. L. Adelberger and C. C. Steidel. Multiwavelength Observations of Dusty Star Formation at Low and High Redshift. *ApJ* **544**, 218 (2000). arXiv:astro-ph/0001126.

[2] D. M. Alexander, F. E. Bauer, S. C. Chapman, I. Smail, A. W. Blain, W. N. Brandt, and R. J. Ivison. The X-Ray Spectral Properties of SCUBA Galaxies. *ApJ* **632**, 736 (2005). arXiv:astro-ph/0506608.

[3] F. Allard, P. H. Hauschildt, and A. Schweitzer. Spherically Symmetric Model Atmospheres for Low-Mass Pre-Main-Sequence Stars with Effective Temperatures between 2000 and 6800 K. *ApJ* **539**, 366 (2000). arXiv:astro-ph/0008464.

[4] A. Amblard, A. Cooray, P. Serra, P. Temi, E. Barton, M. Negrello, R. Auld, M. Baes, I. K. Baldry, S. Bamford, A. Blain, J. Bock, D. Bonfield, D. Burgarella, S. Buttiglione, E. Cameron, A. Cava, D. Clements, S. Croom, A. Dariush, G. de Zotti, S. Driver, J. Dunlop, L. Dunne, S. Dye, S. Eales, D. Frayer, J. Fritz, J. P. Gardner, J. Gonzalez-Nuevo, D. Herranz, D. Hill, A. Hopkins, D. H. Hughes, E. Ibar, R. J. Ivison, M. Jarvis, D. H. Jones, L. Kelvin, G. Lagache, L. Leeuw, J. Liske, M. Lopez-Caniego, J. Loveday, S. Maddox, M. Michałowski, P. Norberg, H. Parkinson, J. A. Peacock, C. Pearson, E. Pascale, M. Pohlen, C. Popescu, M. Prescott, A. Robotham, E. Rigby, G. Rodighiero, S. Samui, A. Sansom, D. Scott, S. Serjeant, R. Sharp, B. Sibthorpe, D. J. B. Smith, M. A. Thompson, R. Tuffs, I. Valtchanov, E. van Kampen, P. van der Werf, A. Verma, J. Vieira, and C. Vlahakis. Herschel-ATLAS: Dust temperature and redshift distribution of SPIRE and PACS detected sources using submillimetre colours. *A&A* **518**, L9+ (2010). 1005.2412.

[5] P. Andreani, M. Magliocchetti, and G. de Zotti. MAMBO observations at 240GHz of optically obscured Spitzer sources: source clumps and radio activity at high redshift. *MNRAS* **401**, 15 (2010). 0909.3461.

[6] F. Annibali, A. Bressan, R. Rampazzo, W. W. Zeilinger, and L. Danese. Nearby early-type galaxies with ionized gas. III. Analysis of line-strength indices with new stellar population models. *A&A* **463**, 455 (2007). arXiv:astro-ph/0609175.

[7] N. Arimoto and Y. Yoshii. Chemical and photometric properties of a galactic wind model for elliptical galaxies. *A&A* **173**, 23 (1987).

[8] M. Arrigoni, S. C. Trager, R. S. Somerville, and B. K. Gibson. Galactic chemical evolution in hierarchical formation models - I. Early-type galaxies in the local Universe. *MNRAS* **402**, 173 (2010). 0905.4189.

[9] Y. Ascasibar and S. Gottlöber. The dynamical structure of dark matter haloes. *MNRAS* **386**, 2022 (2008). 0802.4348.

[10] J. E. Austermann, I. Aretxaga, D. H. Hughes, Y. Kang, S. Kim, J. D. Lowenthal, T. A. Perera, D. B. Sanders, K. S. Scott, N. Scoville, G. W. Wilson, and M. S. Yun. AzTEC Millimetre Survey of the COSMOS field - II. Source count overdensity and correlations with large-scale structure. *MNRAS* **393**, 1573 (2009). 0812.0814.

[11] J. E. Austermann, J. S. Dunlop, T. A. Perera, K. S. Scott, G. W. Wilson, I. Aretxaga, D. H. Hughes, O. Almaini, E. L. Chapin, S. C. Chapman, M. Cirasuolo, D. L. Clements, K. E. K. Coppin, L. Dunne, S. Dye, S. A. Eales, E. Egami, D. Farrah, D. Ferrusca, S. Flynn, D. Haig, M. Halpern, E. Ibar, R. J. Ivison, E. van Kampen, Y. Kang, S. Kim, C. Lacey, J. D. Lowenthal, P. D. Mauskopf, R. J. McLure, A. M. J. Mortier, M. Negrello, S. Oliver, J. A. Peacock, A. Pope, S. Rawlings, G. Rieke, I. Roseboom, M. Rowan-Robinson, D. Scott, S. Serjeant, I. Smail, A. M. Swinbank, J. A. Stevens, M. Velazquez, J. Wagg, and M. S. Yun. AzTEC half square degree survey of the SHADES fields - I. Maps, catalogues and source counts. *MNRAS* **401**, 160 (2010). 0907.1093.

[12] S. Bajtlik, R. C. Duncan, and J. P. Ostriker. Quasar ionization of Lyman-alpha clouds - The proximity effect, a probe of the ultraviolet background at high redshift. *ApJ* **327**, 570 (1988).

[13] J. M. Bardeen, J. R. Bond, N. Kaiser, and A. S. Szalay. The statistics of peaks of Gaussian random fields. *ApJ* **304**, 15 (1986).

[14] A. J. Barger, L. L. Cowie, R. F. Mushotzky, Y. Yang, W.-H. Wang, A. T. Steffen, and P. Capak. The Cosmic Evolution of Hard X-Ray-selected Active Galactic Nuclei. *AJ* **129**, 578 (2005). arXiv:astro-ph/0410527.

[15] N. Bastian and S. P. Goodwin. Evidence for the strong effect of gas removal on the internal dynamics of young stellar clusters. *MNRAS* **369**, L9 (2006). arXiv:astro-ph/0602465.

[16] H. Baumgardt and P. Kroupa. A comprehensive set of simulations studying the influence of gas expulsion on star cluster evolution. *MNRAS* **380**, 1589 (2007). 0707.1944.

[17] N. Bavouzet, H. Dole, E. Le Floc'h, K. I. Caputi, G. Lagache, and C. S. Kochanek. Estimating the total infrared luminosity of galaxies up to $z \sim 2$ from mid- and far-infrared observations. *A&A* **479**, 83 (2008). 0712.0965.

[18] M. C. Begelman. AGN Feedback Mechanisms. *Coevolution of Black Holes and Galaxies* pp. 374–+ (2004). arXiv:astro-ph/0303040.

[19] E. F. Bell, D. H. McIntosh, N. Katz, and M. D. Weinberg. The Optical and Near-Infrared Properties of Galaxies. I. Luminosity and Stellar Mass Functions. *ApJS* **149**, 289 (2003). arXiv:astro-ph/0302543.

[20] A. J. Benson. Galaxy formation theory. *Phys. Rep.* **495**, 33 (2010). 1006.5394.

[21] A. J. Benson, R. G. Bower, C. S. Frenk, C. G. Lacey, C. M. Baugh, and S. Cole. What Shapes the Luminosity Function of Galaxies? *ApJ* **599**, 38 (2003). arXiv:astro-ph/0302450.

[22] M. Bernardi. Evolution in the structural properties of early-type brightest cluster galaxies at small lookback time and dependence on the environment. *MNRAS* **395**, 1491 (2009). 0901.1318.

[23] M. Bernardi, J. B. Hyde, A. Fritz, R. K. Sheth, K. Gebhardt, and R. C. Nichol. A search for the most massive galaxies - II. Structure, environment and formation. *MNRAS* **391**, 1191 (2008). 0809.2602.

[24] M. Bernardi, J. B. Hyde, R. K. Sheth, C. J. Miller, and R. C. Nichol. The Luminosities, Sizes, and Velocity Dispersions of Brightest Cluster Galaxies: Implications for Formation History. *AJ* **133**, 1741 (2007). arXiv:astro-ph/0607117.

[25] M. Bernardi, F. Shankar, J. B. Hyde, S. Mei, F. Marulli, and R. K. Sheth. Galaxy luminosities, stellar masses, sizes, velocity dispersions as a function of morphological type. *MNRAS* **404**, 2087 (2010). 0910.1093.

[26] R. Bezanson, P. G. van Dokkum, T. Tal, D. Marchesini, M. Kriek, M. Franx, and P. Coppi. The Relation Between Compact, Quiescent High-redshift Galaxies and Massive Nearby Elliptical Galaxies: Evidence for Hierarchical, Inside-Out Growth. *ApJ* **697**, 1290 (2009). 0903.2044.

[27] P. Biermann and S. L. Shapiro. Puffing up flat galaxies by rapid stripping and the formation of S0 galaxies. *ApJL* **230**, L33 (1979).

[28] J. Binney and G. Tabor. Evolving Cooling Flows. *MNRAS* **276**, 663 (1995).

[29] A. W. Blain. Galaxy-galaxy gravitational lensing in the millimetre/submillimetre waveband. *MNRAS* **283**, 1340 (1996).

[30] A. W. Blain. Gravitational lensing by clusters of galaxies in the millimetre/submillimetre waveband. *MNRAS* **290**, 553 (1997).

[31] C. M. Boily and P. Kroupa. The impact of mass loss on star cluster formation - II. Numerical N-body integration and further applications. *MNRAS* **338**, 673 (2003). arXiv:astro-ph/0211026.

[32] A. Borriello, P. Salucci, and L. Danese. The fundamental plane of ellipticals - I. The dark matter connection. *MNRAS* **341**, 1109 (2003). arXiv:astro-ph/0208268.

[33] N. Bouché, G. Cresci, R. Davies, F. Eisenhauer, N. M. Förster Schreiber, R. Genzel, S. Gillessen, M. Lehnert, D. Lutz, N. Nesvadba, K. L. Shapiro, A. Sternberg, L. J. Tacconi, A. Verma, A. Cimatti, E. Daddi, A. Renzini, D. K. Erb, A. Shapley, and C. C. Steidel. Dynamical Properties of z ˜ 2 Star-forming Galaxies and a Universal Star Formation Relation. *ApJ* **671**, 303 (2007). 0706.2656.

[34] P. Bouchet, J. Lequeux, E. Maurice, L. Prevot, and M. L. Prevot-Burnichon. The visible and infrared extinction law and the gas-to-dust ratio in the Small Magellanic Cloud. *A&A* **149**, 330 (1985).

[35] F. Bournaud, C. J. Jog, and F. Combes. Galaxy mergers with various mass ratios: Properties of remnants. *A&A* **437**, 69 (2005). arXiv:astro-ph/0503189.

[36] R. J. Bouwens and G. D. Illingworth. Rapid evolution of the most luminous galaxies during the first 900million years. *Nature* **443**, 189 (2006). arXiv:astro-ph/0607087.

[37] R. J. Bouwens, G. D. Illingworth, I. Labbe, P. A. Oesch, M. Trenti, C. M. Carollo, P. G. van Dokkum, M. Franx, M. Stiavelli, V. González, D. Magee, and L. Bradley. A candidate redshift z˜10 galaxy and rapid changes in that population at an age of 500Myr. *Nature* **469**, 504 (2011). 0912.4263.

[38] R. J. Bouwens, G. D. Illingworth, P. A. Oesch, M. Stiavelli, P. van Dokkum, M. Trenti, D. Magee, I. Labbé, M. Franx, C. M. Carollo, and V. Gonzalez. Discovery of z ˜ 8 Galaxies in the Hubble Ultra Deep Field from Ultra-Deep WFC3/IR Observations. *ApJL* **709**, L133 (2010). 0909.1803.

[39] R. G. Bower, A. J. Benson, R. Malbon, J. C. Helly, C. S. Frenk, C. M. Baugh, S. Cole, and C. G. Lacey. Breaking the hierarchy of galaxy formation. *MNRAS* **370**, 645 (2006). arXiv:astro-ph/0511338.

[40] R. G. Bower, J. R. Lucey, and R. S. Ellis. Precision Photometry of Early Type Galaxies in the Coma and Virgo Clusters - a Test of the Universality of the Colour / Magnitude Relation - Part Two - Analysis. *MNRAS* **254**, 601 (1992).

[41] M. Boylan-Kolchin, C.-P. Ma, and E. Quataert. Dissipationless mergers of elliptical galaxies and the evolution of the fundamental plane. *MNRAS* **362**, 184 (2005). arXiv:astro-ph/0502495.

[42] M. Boylan-Kolchin, C.-P. Ma, and E. Quataert. Red mergers and the assembly of massive elliptical galaxies: the fundamental plane and its projections. *MNRAS* **369**, 1081 (2006). arXiv:astro-ph/0601400.

[43] M. Boylan-Kolchin, C.-P. Ma, and E. Quataert. Dynamical friction and galaxy merging time-scales. *MNRAS* **383**, 93 (2008). 0707.2960.

[44] G. B. Brammer, P. G. van Dokkum, and P. Coppi. EAZY: A Fast, Public Photometric Redshift Code. *ApJ* **686**, 1503 (2008). 0807.1533.

[45] A. Bressan, C. Chiosi, and F. Fagotto. Spectrophotometric evolution of elliptical galaxies. 1: Ultraviolet excess and color-magnitude-redshift relations. *ApJS* **94**, 63 (1994).

[46] A. Bressan, G. L. Granato, and L. Silva. Modelling intermediate age and old stellar populations in the Infrared. *A&A* **332**, 135 (1998). arXiv:astro-ph/9709084.

[47] A. Bressan, L. Silva, and G. L. Granato. Far infrared and radio emission in dusty starburst galaxies. *A&A* **392**, 377 (2002). arXiv:astro-ph/0206029.

[48] V. Buat, A. Boselli, G. Gavazzi, and C. Bonfanti. Star formation and dust extinction in nearby star-forming and starburst galaxies. *A&A* **383**, 801 (2002).

[49] F. Buitrago, I. Trujillo, C. J. Conselice, R. J. Bouwens, M. Dickinson, and H. Yan. Size Evolution of the Most Massive Galaxies at $1.7 < z < 3$ from GOODS NICMOS Survey Imaging. *ApJL* **687**, L61 (2008). 0807.4141.

[50] J. S. Bullock, T. S. Kolatt, Y. Sigad, R. S. Somerville, A. V. Kravtsov, A. A. Klypin, J. R. Primack, and A. Dekel. Profiles of dark haloes: evolution, scatter and environment. *MNRAS* **321**, 559 (2001). arXiv:astro-ph/9908159.

[51] A. J. Bunker, E. R. Stanway, R. S. Ellis, and R. G. McMahon. The star formation rate of the Universe at z˜ 6 from the Hubble Ultra-Deep Field. *MNRAS* **355**, 374 (2004). arXiv:astro-ph/0403223.

[52] D. Burstein, R. Bender, S. Faber, and R. Nolthenius. Global Relationships Among the Physical Properties of Stellar Systems. *AJ* **114**, 1365 (1997). arXiv:astro-ph/9707037.

[53] D. Calzetti. The Dust Opacity of Star-forming Galaxies. *PASP* **113**, 1449 (2001). arXiv:astro-ph/0109035.

[54] D. Calzetti, L. Armus, R. C. Bohlin, A. L. Kinney, J. Koornneef, and T. Storchi-Bergmann. The Dust Content and Opacity of Actively Star-forming Galaxies. *ApJ* **533**, 682 (2000). arXiv:astro-ph/9911459.

[55] D. Calzetti, R. C. Kennicutt, C. W. Engelbracht, C. Leitherer, B. T. Draine, L. Kewley, J. Moustakas, M. Sosey, D. A. Dale, K. D. Gordon, G. X. Helou, D. J. Hollenbach, L. Armus, G. Bendo, C. Bot, B. Buckalew, T. Jarrett, A. Li, M. Meyer, E. J. Murphy, M. Prescott, M. W. Regan, G. H. Rieke, H. Roussel, K. Sheth, J. D. T. Smith, M. D. Thornley, and F. Walter. The Calibration of Mid-Infrared Star Formation Rate Indicators. *ApJ* **666**, 870 (2007). 0705.3377.

[56] N. Caon, M. Capaccioli, and M. D'Onofrio. On the Shape of the Light Profiles of Early Type Galaxies. *MNRAS* **265**, 1013 (1993). arXiv:astro-ph/9309013.

[57] M. Cappellari, R. Bacon, M. Bureau, M. C. Damen, R. L. Davies, P. T. de Zeeuw, E. Emsellem, J. Falcón-Barroso, D. Krajnović, H. Kuntschner, R. M. McDermid, R. F. Peletier, M. Sarzi, R. C. E. van den Bosch, and G. van de Ven. The SAURON project - IV. The mass-to-light ratio, the virial mass estimator and the Fundamental Plane of elliptical and lenticular galaxies. *MNRAS* **366**, 1126 (2006). arXiv:astro-ph/0505042.

[58] M. Cappellari, S. di Serego Alighieri, A. Cimatti, E. Daddi, A. Renzini, J. D. Kurk, P. Cassata, M. Dickinson, A. Franceschini, M. Mignoli, L. Pozzetti, G. Rodighiero, P. Rosati, and G. Zamorani. Dynamical Masses of Early-Type Galaxies at z ˜ 2: Are they Truly Superdense? *ApJL* **704**, L34 (2009). 0906.3648.

[59] A. J. Cenarro and I. Trujillo. Mild Velocity Dispersion Evolution of Spheroid-Like Massive Galaxies Since z ˜ 2. *ApJL* **696**, L43 (2009). 0902.4893.

[60] G. Chabrier. Galactic Stellar and Substellar Initial Mass Function. *PASP* **115**, 763 (2003). arXiv:astro-ph/0304382.

[61] S. C. Chapman, A. W. Blain, R. J. Ivison, and I. R. Smail. A median redshift of 2.4 for galaxies bright at submillimetre wavelengths. *Nature* **422**, 695 (2003). arXiv:astro-ph/0304235.

[62] S. C. Chapman, A. W. Blain, I. Smail, and R. J. Ivison. A Redshift Survey of the Submillimeter Galaxy Population. *ApJ* **622**, 772 (2005). arXiv:astro-ph/0412573.

[63] S. C. Chapman, R. J. Ivison, I. G. Roseboom, R. Auld, J. Bock, D. Brisbin, D. Burgarella, P. Chanial, D. L. Clements, A. Cooray, S. Eales, A. Franceschini, E. Giovannoli, J. Glenn, M. Griffin, A. M. J. Mortier, S. J. Oliver, A. Omont, M. J. Page, A. Papageorgiou, C. P. Pearson, I. Pérez-Fournon, M. Pohlen, J. I. Rawlings, G. Raymond, G. Rodighiero, M. Rowan-Robinson, D. Scott, N. Seymour, A. J. Smith, M. Symeonidis, K. E. Tugwell, M. Vaccari, J. D. Vieira, L. Vigroux, L. Wang, and G. Wright. Herschel-SPIRE, far-infrared properties of millimetre-bright and -faint radio galaxies. *MNRAS* **409**, L13 (2010). 1009.3001.

[64] S. Charlot and S. M. Fall. A Simple Model for the Absorption of Starlight by Dust in Galaxies. *ApJ* **539**, 718 (2000). arXiv:astro-ph/0003128.

[65] R. Chary and D. Elbaz. Interpreting the Cosmic Infrared Background: Constraints on the Evolution of the Dust-enshrouded Star Formation Rate. *ApJ* **556**, 562 (2001). arXiv:astro-ph/0103067.

[66] C. Chiosi and G. Carraro. Formation and evolution of elliptical galaxies. *MNRAS* **335**, 335 (2002).

[67] A. Cimatti, P. Cassata, L. Pozzetti, J. Kurk, M. Mignoli, A. Renzini, E. Daddi, M. Bolzonella, M. Brusa, G. Rodighiero, M. Dickinson, A. Franceschini, G. Zamorani, S. Berta, P. Rosati, and C. Halliday. GMASS ultradeep spectroscopy of galaxies at z ˜ 2. II. Superdense passive galaxies: how did they form and evolve? *A&A* **482**, 21 (2008). 0801.1184.

[68] L. Ciotti, B. Lanzoni, and M. Volonteri. The Importance of Dry and Wet Merging on the Formation and Evolution of Elliptical Galaxies. *ApJ* **658**, 65 (2007). arXiv:astro-ph/0611328.

[69] M. Cirasuolo, R. J. McLure, J. S. Dunlop, O. Almaini, S. Foucaud, and C. Simpson. A new measurement of the evolving near-infrared galaxy luminosity function out to z ˜= 4: a continuing challenge to theoretical models of galaxy formation. *MNRAS* **401**, 1166 (2010). 0804.3471.

[70] M. Cirasuolo, F. Shankar, G. L. Granato, G. De Zotti, and L. Danese. Dynamical and Photometric Imprints of Feedback Processes on the Formation and Evolution of E/S0 Galaxies. *ApJ* **629**, 816 (2005). arXiv:astro-ph/0504600.

[71] M. S. Clemens, A. Bressan, B. Nikolic, and R. Rampazzo. The history of star formation and mass assembly in early-type galaxies. *MNRAS* **392**, L35 (2009). 0809.1189.

[72] D. L. Clements, E. Rigby, S. Maddox, L. Dunne, A. Mortier, C. Pearson, A. Amblard, R. Auld, M. Baes, D. Bonfield, D. Burgarella, S. Buttiglione, A. Cava, A. Cooray, A. Dariush, G. de Zotti, S. Dye, S. Eales,

D. Frayer, J. Fritz, J. P. Gardner, J. Gonzalez-Nuevo, D. Herranz, E. Ibar, R. Ivison, M. J. Jarvis, G. Lagache, L. Leeuw, M. Lopez-Caniego, M. Negrello, E. Pascale, M. Pohlen, G. Rodighiero, S. Samui, S. Serjeant, B. Sibthorpe, D. Scott, D. J. B. Smith, P. Temi, M. Thompson, I. Valtchanov, P. van der Werf, and A. Verma. Herschel-ATLAS: Extragalactic number counts from 250 to 500 microns. *A&A* **518**, L8+ (2010). 1005.2409.

[73] S. Cole, P. Norberg, C. M. Baugh, C. S. Frenk, J. Bland-Hawthorn, T. Bridges, R. Cannon, M. Colless, C. Collins, W. Couch, N. Cross, G. Dalton, R. De Propris, S. P. Driver, G. Efstathiou, R. S. Ellis, K. Glazebrook, C. Jackson, O. Lahav, I. Lewis, S. Lumsden, S. Maddox, D. Madgwick, J. A. Peacock, B. A. Peterson, W. Sutherland, and K. Taylor. The 2dF galaxy redshift survey: near-infrared galaxy luminosity functions. *MNRAS* **326**, 255 (2001). arXiv:astro-ph/0012429.

[74] J. J. Condon, Z.-P. Huang, Q. F. Yin, and T. X. Thuan. Compact starbursts in ultraluminous infrared galaxies. *ApJ* **378**, 65 (1991).

[75] M. Cook, A. Lapi, and G. L. Granato. Two-phase galaxy formation. *MNRAS* **397**, 534 (2009). 0903.2390.

[76] A. Cooray, A. Amblard, L. Wang, V. Arumugam, R. Auld, H. Aussel, T. Babbedge, A. Blain, J. Bock, A. Boselli, V. Buat, D. Burgarella, N. Castro-Rodriguez, A. Cava, P. Chanial, D. L. Clements, A. Conley, L. Conversi, C. D. Dowell, E. Dwek, S. Eales, D. Elbaz, D. Farrah, M. Fox, A. Franceschini, W. Gear, J. Glenn, M. Griffin, M. Halpern, E. Hatziminaoglou, E. Ibar, K. Isaak, R. J. Ivison, A. A. Khostovan, G. Lagache, L. Levenson, N. Lu, S. Madden, B. Maffei, G. Mainetti, L. Marchetti, G. Marsden, K. Mitchell-Wynne, A. M. J. Mortier, H. T. Nguyen, B. O'Halloran, S. J. Oliver, A. Omont, M. J. Page, P. Panuzzo, A. Papageorgiou, C. P. Pearson, I. Perez Fournon, M. Pohlen, J. I. Rawlings, G. Raymond, D. Rigopoulou, D. Rizzo, I. G. Roseboom, M. Rowan-Robinson, B. Schulz, D. Scott, P. Serra, N. Seymour, D. L. Shupe, A. J. Smith, J. A. Stevens, M. Symeonidis, M. Trichas, K. E. Tugwell, M. Vaccari, I. Valtchanov, J. D. Vieira, L. Vigroux, R. Ward, G. Wright, C. K. Xu, and M. Zemcov. HerMES: Halo occupation number and bias properties of dusty galaxies from angular clustering measurements. *A&A* **518**, L22+ (2010). 1005.3303.

[77] K. Coppin, E. L. Chapin, A. M. J. Mortier, S. E. Scott, C. Borys, J. S. Dunlop, M. Halpern, D. H. Hughes, A. Pope, D. Scott, S. Serjeant, J. Wagg, D. M. Alexander, O. Almaini, I. Aretxaga, T. Babbedge, P. N. Best, A. Blain, S. Chapman, D. L. Clements, M. Crawford, L. Dunne, S. A. Eales, A. C. Edge, D. Farrah, E. Gaztañaga, W. K. Gear, G. L. Granato, T. R. Greve, M. Fox, R. J. Ivison, M. J. Jarvis, T. Jenness, C. Lacey, K. Lepage, R. G. Mann, G. Marsden, A. Martinez-Sansigre, S. Oliver, M. J. Page, J. A. Peacock, C. P. Pearson, W. J. Percival, R. S. Priddey, S. Rawlings, M. Rowan-Robinson, R. S. Savage, M. Seigar, K. Sekiguchi, L. Silva, C. Simpson, I. Smail, J. A. Stevens, T. Takagi, M. Vaccari, E. van Kampen, and C. J. Willott. The SCUBA Half-Degree Extragalactic Survey - II. Submillimetre maps, catalogue and number counts. *MNRAS* **372**, 1621 (2006). arXiv:astro-ph/0609039.

[78] K. E. K. Coppin, A. M. Swinbank, R. Neri, P. Cox, D. M. Alexander, I. Smail, M. J. Page, J. A. Stevens, K. K. Knudsen, R. J. Ivison, A. Beelen, F. Bertoldi, and A. Omont. Testing the evolutionary link between submillimetre galaxies and quasars: CO observations of QSOs at z ˜ 2. *MNRAS* **389**, 45 (2008). 0806.0618.

[79] M. Covington, A. Dekel, T. J. Cox, P. Jonsson, and J. R. Primack. Predicting the properties of the remnants of dissipative galaxy mergers. *MNRAS* **384**, 94 (2008). 0710.4584.

[80] P. Cox, M. Krips, R. Neri, A. Omont, R. Gusten, K. M. Menten, F. Wyrowski, A. Weiss, A. Beelen, M. A. Gurwell, H. Dannerbauer, R. J. Ivison, M. Negrello, I. Aretxaga, D. H. Hughes, R. Auld, M. Baes,

R. Blundell, S. Buttiglione, A. Cava, A. Cooray, A. Dariush, L. Dunne, S. Dye, S. A. Eales, D. Frayer, J. Fritz, R. Gavazzi, R. Hopwood, E. Ibar, M. Jarvis, S. Maddox, M. Michalowski, E. Pascale, M. Pohlen, E. Rigby, D. J. B. Smith, A. M. Swinbank, P. Temi, I. Valtchanov, P. van der Werf, and G. de Zotti. Gas and dust in a submillimeter galaxy at z = 4.24 from the Herschel ATLAS. *ArXiv e-prints* (2011). 1107.2924.

[81] T. J. Cox, P. Jonsson, J. R. Primack, and R. S. Somerville. Feedback in simulations of disc-galaxy major mergers. *MNRAS* **373**, 1013 (2006). arXiv:astro-ph/0503201.

[82] G. Cresci, E. K. S. Hicks, R. Genzel, N. M. F. Schreiber, R. Davies, N. Bouché, P. Buschkamp, S. Genel, K. Shapiro, L. Tacconi, J. Sommer-Larsen, A. Burkert, F. Eisenhauer, O. Gerhard, D. Lutz, T. Naab, A. Sternberg, A. Cimatti, E. Daddi, D. K. Erb, J. Kurk, S. L. Lilly, A. Renzini, A. Shapley, C. C. Steidel, and K. Caputi. The SINS Survey: Modeling the Dynamics of z ˜ 2 Galaxies and the High-z Tully-Fisher Relation. *ApJ* **697**, 115 (2009). 0902.4701.

[83] S. M. Croom, B. J. Boyle, T. Shanks, R. J. Smith, L. Miller, P. J. Outram, N. S. Loaring, F. Hoyle, and J. da Ângela. The 2dF QSO Redshift Survey - XIV. Structure and evolution from the two-point correlation function. *MNRAS* **356**, 415 (2005). arXiv:astro-ph/0409314.

[84] S. M. Croom, R. J. Smith, B. J. Boyle, T. Shanks, L. Miller, P. J. Outram, and N. S. Loaring. The 2dF QSO Redshift Survey - XII. The spectroscopic catalogue and luminosity function. *MNRAS* **349**, 1397 (2004). arXiv:astro-ph/0403040.

[85] D. J. Croton, V. Springel, S. D. M. White, G. De Lucia, C. S. Frenk, L. Gao, A. Jenkins, G. Kauffmann, J. F. Navarro, and N. Yoshida. The many lives of active galactic nuclei: cooling flows, black holes and the luminosities and colours of galaxies. *MNRAS* **365**, 11 (2006). arXiv:astro-ph/0508046.

[86] E. Daddi, H. Dannerbauer, M. Krips, F. Walter, M. Dickinson, D. Elbaz, and G. E. Morrison. A CO Emission Line from the Optical and Near-IR Undetected Submillimeter Galaxy GN10. *ApJL* **695**, L176 (2009). 0903.3046.

[87] E. Daddi, M. Dickinson, G. Morrison, R. Chary, A. Cimatti, D. Elbaz, D. Frayer, A. Renzini, A. Pope, D. M. Alexander, F. E. Bauer, M. Giavalisco, M. Huynh, J. Kurk, and M. Mignoli. Multiwavelength Study of Massive Galaxies at z˜2. I. Star Formation and Galaxy Growth. *ApJ* **670**, 156 (2007). 0705.2831.

[88] X. Dai, F. Shankar, and G. R. Sivakoff. 2MASS Reveals a Large Intrinsic Fraction of BALQSOs. *ApJ* **672**, 108 (2008). 0704.2882.

[89] D. A. Dale, A. Gil de Paz, K. D. Gordon, H. M. Hanson, L. Armus, G. J. Bendo, L. Bianchi, M. Block, S. Boissier, A. Boselli, B. A. Buckalew, V. Buat, D. Burgarella, D. Calzetti, J. M. Cannon, C. W. Engelbracht, G. Helou, D. J. Hollenbach, T. H. Jarrett, R. C. Kennicutt, C. Leitherer, A. Li, B. F. Madore, D. C. Martin, M. J. Meyer, E. J. Murphy, M. W. Regan, H. Roussel, J. D. T. Smith, M. L. Sosey, D. A. Thilker, and F. Walter. An Ultraviolet-to-Radio Broadband Spectral Atlas of Nearby Galaxies. *ApJ* **655**, 863 (2007). arXiv:astro-ph/0610688.

[90] I. Damjanov, P. J. McCarthy, R. G. Abraham, K. Glazebrook, H. Yan, E. Mentuch, D. Le Borgne, S. Savaglio, D. Crampton, R. Murowinski, S. Juneau, R. G. Carlberg, I. Jørgensen, K. Roth, H.-W. Chen, and R. O. Marzke. Red Nuggets at z ˜ 1.5: Compact Passive Galaxies and the Formation of the Kormendy Relation. *ApJ* **695**, 101 (2009). 0807.1744.

[91] G. de Zotti, R. Ricci, D. Mesa, L. Silva, P. Mazzotta, L. Toffolatti, and J. González-Nuevo. Predictions for high-frequency radio surveys of extragalactic sources. *A&A* **431**, 893 (2005). arXiv:astro-ph/0410709.

[92] A. Dekel, R. Sari, and D. Ceverino. Formation of Massive Galaxies at High Redshift: Cold Streams, Clumpy Disks, and Compact Spheroids. *ApJ* **703**, 785 (2009). 0901.2458.

[93] M. Dickinson, M. Giavalisco, and GOODS Team. The Great Observatories Origins Deep Survey. In *The Mass of Galaxies at Low and High Redshift*, edited by R. Bender & A. Renzini, pp. 324–+ (2003). arXiv:astro-ph/0204213.

[94] M. Dickinson, D. Stern, M. Giavalisco, H. C. Ferguson, Z. Tsvetanov, R. Chornock, S. Cristiani, S. Dawson, A. Dey, A. V. Filippenko, L. A. Moustakas, M. Nonino, C. Papovich, S. Ravindranath, A. Riess, P. Rosati, H. Spinrad, and E. Vanzella. Color-selected Galaxies at z ˜ 6 in the Great Observatories Origins Deep Survey. *ApJL* **600**, L99 (2004). arXiv:astro-ph/0309070.

[95] J. Diemand, M. Kuhlen, and P. Madau. Formation and Evolution of Galaxy Dark Matter Halos and Their Substructure. *ApJ* **667**, 859 (2007). arXiv:astro-ph/0703337.

[96] S. Djorgovski and M. Davis. Fundamental properties of elliptical galaxies. *ApJ* **313**, 59 (1987).

[97] B. T. Draine. Interstellar Dust Grains. *ARA&A* **41**, 241 (2003). arXiv:astro-ph/0304489.

[98] N. Drory, M. Salvato, A. Gabasch, R. Bender, U. Hopp, G. Feulner, and M. Pannella. The Stellar Mass Function of Galaxies to z˜5 in the FORS Deep and GOODS-South Fields. *ApJL* **619**, L131 (2005). arXiv:astro-ph/0412167.

[99] L. Dunne, R. J. Ivison, S. Maddox, M. Cirasuolo, A. M. Mortier, S. Foucaud, E. Ibar, O. Almaini, C. Simpson, and R. McLure. The star formation history of K-selected galaxies. *MNRAS* **394**, 3 (2009). 0808.3139.

[100] E. Dwek, R. G. Arendt, D. J. Fixsen, T. J. Sodroski, N. Odegard, J. L. Weiland, W. T. Reach, M. G. Hauser, T. Kelsall, S. H. Moseley, R. F. Silverberg, R. A. Shafer, J. Ballester, D. Bazell, and R. Isaacman. Detection and Characterization of Cold Interstellar Dust and Polycyclic Aromatic Hydrocarbon Emission, from COBE Observations. *ApJ* **475**, 565 (1997). arXiv:astro-ph/9610198.

[101] S. Dye, S. A. Eales, I. Aretxaga, S. Serjeant, J. S. Dunlop, T. S. R. Babbedge, S. C. Chapman, M. Cirasuolo, D. L. Clements, K. E. K. Coppin, L. Dunne, E. Egami, D. Farrah, R. J. Ivison, E. van Kampen, A. Pope, R. Priddey, G. H. Rieke, A. M. Schael, D. Scott, C. Simpson, T. Takagi, T. Takata, and M. Vaccari. The SCUBA HAlf Degree Extragalactic Survey (SHADES) - VII. Optical/IR photometry and stellar masses of submillimetre galaxies. *MNRAS* **386**, 1107 (2008). 0802.0497.

[102] S. Eales, E. L. Chapin, M. J. Devlin, S. Dye, M. Halpern, D. H. Hughes, G. Marsden, P. Mauskopf, L. Moncelsi, C. B. Netterfield, E. Pascale, G. Patanchon, G. Raymond, M. Rex, D. Scott, C. Semisch, B. Siana, M. D. P. Truch, and M. P. Viero. BLAST: The Redshift Survey. *ApJ* **707**, 1779 (2009). 0907.4156.

[103] S. Eales, L. Dunne, D. Clements, A. Cooray, G. de Zotti, S. Dye, R. Ivison, M. Jarvis, G. Lagache, S. Maddox, M. Negrello, S. Serjeant, M. A. Thompson, E. van Kampen, A. Amblard, P. Andreani, M. Baes, A. Beelen, G. J. Bendo, D. Benford, F. Bertoldi, J. Bock, D. Bonfield, A. Boselli, C. Bridge, V. Buat, D. Burgarella, R. Carlberg, A. Cava, P. Chanial, S. Charlot, N. Christopher, P. Coles, L. Cortese, A. Dariush, E. da Cunha, G. Dalton, L. Danese, H. Dannerbauer, S. Driver, J. Dunlop, L. Fan, D. Farrah, D. Frayer, C. Frenk, J. Geach, J. Gardner, H. Gomez, J. González-Nuevo, E. González-Solares, M. Griffin, M. Hardcastle, E. Hatziminaoglou, D. Herranz, D. Hughes, E. Ibar, W.-S. Jeong, C. Lacey, A. Lapi, A. Lawrence, M. Lee, L. Leeuw, J. Liske, M. López-Caniego, T. Müller, K. Nandra, P. Panuzzo, A. Papageorgiou, G. Patanchon, J. Peacock, C. Pearson, S. Phillipps, M. Pohlen, C. Popescu, S. Rawlings,

E. Rigby, M. Rigopoulou, A. Robotham, G. Rodighiero, A. Sansom, B. Schulz, D. Scott, D. J. B. Smith, B. Sibthorpe, I. Smail, J. Stevens, W. Sutherland, T. Takeuchi, J. Tedds, P. Temi, R. Tuffs, M. Trichas, M. Vaccari, I. Valtchanov, P. van der Werf, A. Verma, J. Vieria, C. Vlahakis, and G. J. White. The Herschel ATLAS. *PASP* **122**, 499 (2010). 0910.4279.

[104] S. A. Eales, G. Raymond, I. G. Roseboom, B. Altieri, A. Amblard, V. Arumugam, R. Auld, H. Aussel, T. Babbedge, A. Blain, J. Bock, A. Boselli, D. Brisbin, V. Buat, D. Burgarella, N. Castro-Rodríguez, A. Cava, P. Chanial, D. L. Clements, A. Conley, L. Conversi, A. Cooray, C. D. Dowell, E. Dwek, S. Dye, D. Elbaz, D. Farrah, M. Fox, A. Franceschini, W. Gear, J. Glenn, E. A. González Solares, M. Griffin, M. Harwit, E. Hatziminaoglou, J. Huang, E. Ibar, K. Isaak, R. J. Ivison, G. Lagache, L. Levenson, C. J. Lonsdale, N. Lu, S. Madden, B. Maffei, G. Mainetti, L. Marchetti, G. E. Morrison, A. M. J. Mortier, H. T. Nguyen, B. O'Halloran, S. J. Oliver, A. Omont, F. N. Owen, M. J. Page, M. Pannella, P. Panuzzo, A. Papageorgiou, C. P. Pearson, I. Pérez-Fournon, M. Pohlen, J. I. Rawlings, D. Rigopoulou, D. Rizzo, M. Rowan-Robinson, M. Sánchez Portal, B. Schulz, D. Scott, N. Seymour, D. L. Shupe, A. J. Smith, J. A. Stevens, V. Strazzullo, M. Symeonidis, M. Trichas, K. E. Tugwell, M. Vaccari, I. Valtchanov, L. Vigroux, L. Wang, R. Ward, G. Wright, C. K. Xu, and M. Zemcov. First results from HerMES on the evolution of the submillimetre luminosity function. *A&A* **518**, L23+ (2010). 1005.2189.

[105] G. Efstathiou. A model of supernova feedback in galaxy formation. *MNRAS* **317**, 697 (2000). arXiv:astro-ph/0002245.

[106] O. J. Eggen, D. Lynden-Bell, and A. R. Sandage. Evidence from the motions of old stars that the Galaxy collapsed. *ApJ* **136**, 748 (1962).

[107] M. Elvis. A Structure for Quasars. *ApJ* **545**, 63 (2000). arXiv:astro-ph/0008064.

[108] L. Fan, A. Lapi, A. Bressan, M. Bernardi, G. De Zotti, and L. Danese. Cosmic Evolution of Size and Velocity Dispersion for Early-type Galaxies. *ApJ* **718**, 1460 (2010). 1006.2303.

[109] L. Fan, A. Lapi, G. De Zotti, and L. Danese. The Dramatic Size Evolution of Elliptical Galaxies and the Quasar Feedback. *ApJL* **689**, L101 (2008). 0809.4574.

[110] L. L. Fan, H. Y. Wang, T. Wang, J. Wang, X. Dong, K. Zhang, and F. Cheng. The Correlation Between X-ray and UV Properties of BAL QSOs. *ApJ* **690**, 1006 (2009). 0809.2464.

[111] H. C. Ferguson, M. Dickinson, M. Giavalisco, C. Kretchmer, S. Ravindranath, R. Idzi, E. Taylor, C. J. Conselice, S. M. Fall, J. P. Gardner, M. Livio, P. Madau, L. A. Moustakas, C. M. Papovich, R. S. Somerville, H. Spinrad, and D. Stern. The Size Evolution of High-Redshift Galaxies. *ApJL* **600**, L107 (2004). arXiv:astro-ph/0309058.

[112] G. J. Ferland. *Hazy, A Brief Introduction to Cloudy 90* (University of Kentucky Internal Report, 1996).

[113] L. Ferrarese and H. Ford. Supermassive Black Holes in Galactic Nuclei: Past, Present and Future Research. *Space Sci. Rev.* **116**, 523 (2005). arXiv:astro-ph/0411247.

[114] L. Ferrarese and D. Merritt. A Fundamental Relation between Supermassive Black Holes and Their Host Galaxies. *ApJL* **539**, L9 (2000). arXiv:astro-ph/0006053.

[115] I. Ferreras, T. Lisker, A. Pasquali, S. Khochfar, and S. Kaviraj. On the formation of massive galaxies: a simultaneous study of number density, size and intrinsic colour evolution in GOODS. *MNRAS* **396**, 1573 (2009). 0901.4555.

[116] A. Fontana, S. Salimbeni, A. Grazian, E. Giallongo, L. Pentericci, M. Nonino, F. Fontanot, N. Menci, P. Monaco, S. Cristiani, E. Vanzella, C. de Santis, and S. Gallozzi. The Galaxy mass function up to z =4 in the GOODS-MUSIC sample: into the epoch of formation of massive galaxies. *A&A* **459**, 745 (2006). arXiv:astro-ph/0609068.

[117] N. M. Förster Schreiber, R. Genzel, N. Bouché, G. Cresci, R. Davies, P. Buschkamp, K. Shapiro, L. J. Tacconi, E. K. S. Hicks, S. Genel, A. E. Shapley, D. K. Erb, C. C. Steidel, D. Lutz, F. Eisenhauer, S. Gillessen, A. Sternberg, A. Renzini, A. Cimatti, E. Daddi, J. Kurk, S. Lilly, X. Kong, M. D. Lehnert, N. Nesvadba, A. Verma, H. McCracken, N. Arimoto, M. Mignoli, and M. Onodera. The SINS Survey: SINFONI Integral Field Spectroscopy of z ˜ 2 Star-forming Galaxies. *ApJ* **706**, 1364 (2009). 0903.1872.

[118] D. T. Frayer, A. I. Harris, A. J. Baker, R. J. Ivison, I. Smail, M. Negrello, R. Maddalena, I. Aretxaga, M. Baes, M. Birkinshaw, D. G. Bonfield, D. Burgarella, S. Buttiglione, A. Cava, D. L. Clements, A. Cooray, H. Dannerbauer, A. Dariush, G. De Zotti, J. S. Dunlop, L. Dunne, S. Dye, S. Eales, J. Fritz, J. Gonzalez-Nuevo, D. Herranz, R. Hopwood, D. H. Hughes, E. Ibar, M. J. Jarvis, G. Lagache, L. L. Leeuw, M. Lopez-Caniego, S. Maddox, M. J. Michałowski, A. Omont, M. Pohlen, E. Rigby, G. Rodighiero, D. Scott, S. Serjeant, D. J. B. Smith, A. M. Swinbank, P. Temi, M. A. Thompson, I. Valtchanov, P. P. van der Werf, and A. Verma. Green Bank Telescope Zpectrometer CO(1-0) Observations of the Strongly Lensed Submillimeter Galaxies from the Herschel ATLAS. *ApJL* **726**, L22+ (2011). 1009.2194.

[119] M. Fukugita, O. Nakamura, S. Okamura, N. Yasuda, J. C. Barentine, J. Brinkmann, J. E. Gunn, M. Harvanek, T. Ichikawa, R. H. Lupton, D. P. Schneider, M. A. Strauss, and D. G. York. A Catalog of Morphologically Classified Galaxies from the Sloan Digital Sky Survey: North Equatorial Region. *AJ* **134**, 579 (2007). 0704.1743.

[120] S. C. Gallagher, W. N. Brandt, G. Chartas, R. Priddey, G. P. Garmire, and R. M. Sambruna. An Exploratory Chandra Survey of a Well-defined Sample of 35 Large Bright Quasar Survey Broad Absorption Line Quasars. *ApJ* **644**, 709 (2006). arXiv:astro-ph/0602550.

[121] A. Gallazzi, S. Charlot, J. Brinchmann, and S. D. M. White. Ages and metallicities of early-type galaxies in the Sloan Digital Sky Survey: new insight into the physical origin of the colour-magnitude and the $Mg_2-\sigma_V$ relations. *MNRAS* **370**, 1106 (2006). arXiv:astro-ph/0605300.

[122] K. Gebhardt, R. Bender, G. Bower, A. Dressler, S. M. Faber, A. V. Filippenko, R. Green, C. Grillmair, L. C. Ho, J. Kormendy, T. R. Lauer, J. Magorrian, J. Pinkney, D. Richstone, and S. Tremaine. A Relationship between Nuclear Black Hole Mass and Galaxy Velocity Dispersion. *ApJL* **539**, L13 (2000). arXiv:astro-ph/0006289.

[123] R. Genzel, L. J. Tacconi, F. Eisenhauer, N. M. Förster Schreiber, A. Cimatti, E. Daddi, N. Bouché, R. Davies, M. D. Lehnert, D. Lutz, N. Nesvadba, A. Verma, R. Abuter, K. Shapiro, A. Sternberg, A. Renzini, X. Kong, N. Arimoto, and M. Mignoli. The rapid formation of a large rotating disk galaxy three billion years after the Big Bang. *Nature* **442**, 786 (2006). arXiv:astro-ph/0608344.

[124] O. Gerhard, A. Kronawitter, R. P. Saglia, and R. Bender. Dynamical Family Properties and Dark Halo Scaling Relations of Giant Elliptical Galaxies. *AJ* **121**, 1936 (2001). arXiv:astro-ph/0012381.

[125] O. E. Gerhard and J. Binney. Triaxial galaxies containing massive black holes or central density cusps. *MNRAS* **216**, 467 (1985).

[126] M. P. Geyer and A. Burkert. The effect of gas loss on the formation of bound stellar clusters. *MNRAS* **323**, 988 (2001). arXiv:astro-ph/0007413.

[127] M. Giavalisco, M. Dickinson, H. C. Ferguson, S. Ravindranath, C. Kretchmer, L. A. Moustakas, P. Madau, S. M. Fall, J. P. Gardner, M. Livio, C. Papovich, A. Renzini, H. Spinrad, D. Stern, and A. Riess. The Rest-Frame Ultraviolet Luminosity Density of Star-forming Galaxies at Redshifts $z > 3.5$. *ApJL* **600**, L103 (2004). arXiv:astro-ph/0309065.

[128] B. K. Gibson and F. Matteucci. Infall models of elliptical galaxies: further evidence for a top-heavy initial mass function. *MNRAS* **291**, L8 (1997). arXiv:astro-ph/9707314.

[129] J. Glenn, A. Conley, M. Béthermin, B. Altieri, A. Amblard, V. Arumugam, H. Aussel, T. Babbedge, A. Blain, J. Bock, A. Boselli, V. Buat, N. Castro-Rodríguez, A. Cava, P. Chanial, D. L. Clements, L. Conversi, A. Cooray, C. D. Dowell, E. Dwek, S. Eales, D. Elbaz, T. P. Ellsworth-Bowers, M. Fox, A. Franceschini, W. Gear, M. Griffin, M. Halpern, E. Hatziminaoglou, E. Ibar, K. Isaak, R. J. Ivison, G. Lagache, G. Laurent, L. Levenson, N. Lu, S. Madden, B. Maffei, G. Mainetti, L. Marchetti, G. Marsden, H. T. Nguyen, B. O'Halloran, S. J. Oliver, A. Omont, M. J. Page, P. Panuzzo, A. Papageorgiou, C. P. Pearson, I. Pérez-Fournon, M. Pohlen, D. Rigopoulou, D. Rizzo, I. G. Roseboom, M. Rowan-Robinson, M. S. Portal, B. Schulz, D. Scott, N. Seymour, D. L. Shupe, A. J. Smith, J. A. Stevens, M. Symeonidis, M. Trichas, K. E. Tugwell, M. Vaccari, I. Valtchanov, J. D. Vieira, L. Vigroux, L. Wang, R. Ward, G. Wright, C. K. Xu, and M. Zemcov. HerMES: deep galaxy number counts from a P(D) fluctuation analysis of SPIRE Science Demonstration Phase observations. *MNRAS* **409**, 109 (2010). 1009.5675.

[130] N. Y. Gnedin and J. P. Ostriker. Reionization of the Universe and the Early Production of Metals. *ApJ* **486**, 581 (1997). arXiv:astro-ph/9612127.

[131] J. D. Goldader, G. Meurer, T. M. Heckman, M. Seibert, D. B. Sanders, D. Calzetti, and C. C. Steidel. Far-Infrared Galaxies in the Far-Ultraviolet. *ApJ* **568**, 651 (2002). arXiv:astro-ph/0112352.

[132] S. P. Goodwin and N. Bastian. Gas expulsion and the destruction of massive young clusters. *MNRAS* **373**, 752 (2006). arXiv:astro-ph/0609477.

[133] A. W. Graham and S. P. Driver. A Log-Quadratic Relation for Predicting Supermassive Black Hole Masses from the Host Bulge Sérsic Index. *ApJ* **655**, 77 (2007). arXiv:astro-ph/0607378.

[134] A. W. Graham, P. Erwin, I. Trujillo, and A. Asensio Ramos. A New Empirical Model for the Structural Analysis of Early-Type Galaxies, and A Critical Review of the Nuker Model. *AJ* **125**, 2951 (2003). arXiv:astro-ph/0306023.

[135] G. L. Granato and L. Danese. Thick Tori around Active Galactic Nuclei - a Comparison of Model Predictions with Observations of the Infrared Continuum and Silicate Features. *MNRAS* **268**, 235 (1994).

[136] G. L. Granato, G. De Zotti, L. Silva, A. Bressan, and L. Danese. A Physical Model for the Coevolution of QSOs and Their Spheroidal Hosts. *ApJ* **600**, 580 (2004). arXiv:astro-ph/0307202.

[137] G. L. Granato, L. Silva, P. Monaco, P. Panuzzo, P. Salucci, G. De Zotti, and L. Danese. Joint formation of QSOs and spheroids: QSOs as clocks of star formation in spheroids. *MNRAS* **324**, 757 (2001). arXiv:astro-ph/9911304.

[138] A. Grazian, A. Fontana, C. de Santis, M. Nonino, S. Salimbeni, E. Giallongo, S. Cristiani, S. Gallozzi, and E. Vanzella. The GOODS-MUSIC sample: a multicolour catalog of near-IR selected galaxies in the GOODS-South field. *A&A* **449**, 951 (2006). arXiv:astro-ph/0603094.

[139] C. Gruppioni, F. Pozzi, P. Andreani, G. Rodighiero, A. Cimatti, B. Altieri, H. Aussel, S. Berta, A. Bongiovanni, D. Brisbin, A. Cava, J. Cepa, E. Daddi, H. Dominguez-Sanchez, D. Elbaz, N. Förster Schreiber, R. Genzel, E. Le Floc'h, D. Lutz, G. Magdis, M. Magliocchetti, B. Magnelli, R. Maiolino, R. Nordon, A. M. Peréz-García, A. Poglitsch, P. Popesso, L. Riguccini, A. Saintonge, M. Sanchez-Portal, P. Santini, L. Shao, E. Sturm, L. Tacconi, and I. Valtchanov. PEP: First Herschel probe of dusty galaxy evolution up to z ˜ 3. *A&A* **518**, L27+ (2010). 1005.1473.

[140] Q. Guo, S. White, M. Boylan-Kolchin, G. De Lucia, G. Kauffmann, G. Lemson, C. Li, V. Springel, and S. Weinmann. From dwarf spheroidals to cD galaxies: simulating the galaxy population in a ΛCDM cosmology. *MNRAS* **413**, 101 (2011). 1006.0106.

[141] Q. Guo and S. D. M. White. High-redshift galaxy populations and their descendants. *MNRAS* **396**, 39 (2009). 0809.4259.

[142] M. G. Haehnelt and M. J. Rees. The formation of nuclei in newly formed galaxies and the evolution of the quasar population. *MNRAS* **263**, 168 (1993).

[143] Z. Haiman and R. Cen. A Constraint on the Gravitational Lensing Magnification and Age of the Redshift z=6.28 Quasar SDSS 1030+0524. *ApJ* **578**, 702 (2002). arXiv:astro-ph/0205143.

[144] Z. Haiman and L. Hui. Constraining the Lifetime of Quasars from Their Spatial Clustering. *ApJ* **547**, 27 (2001). arXiv:astro-ph/0002190.

[145] N. Häring and H.-W. Rix. On the Black Hole Mass-Bulge Mass Relation. *ApJL* **604**, L89 (2004). arXiv:astro-ph/0402376.

[146] T. M. Heckman, C. Robert, C. Leitherer, D. R. Garnett, and F. van der Rydt. The Ultraviolet Spectroscopic Properties of Local Starbursts: Implications at High Redshift. *ApJ* **503**, 646 (1998). arXiv:astro-ph/9803185.

[147] L. Hernquist, D. N. Spergel, and J. S. Heyl. Structure of Merger Remnants. III. Phase-Space Constraints. *ApJ* **416**, 415 (1993).

[148] P. C. Hewett and C. B. Foltz. The Frequency and Radio Properties of Broad Absorption Line Quasars. *AJ* **125**, 1784 (2003). arXiv:astro-ph/0301191.

[149] J. G. Hills. The effect of mass loss on the dynamical evolution of a stellar system - Analytic approximations. *ApJ* **235**, 986 (1980).

[150] Y. Hoffman, E. Romano-Díaz, I. Shlosman, and C. Heller. Evolution of the Phase-Space Density in Dark Matter Halos. *ApJ* **671**, 1108 (2007). 0706.0006.

[151] P. F. Hopkins, K. Bundy, L. Hernquist, S. Wuyts, and T. J. Cox. Discriminating between the physical processes that drive spheroid size evolution. *MNRAS* **401**, 1099 (2010). 0909.2039.

[152] P. F. Hopkins, K. Bundy, N. Murray, E. Quataert, T. R. Lauer, and C.-P. Ma. Compact high-redshift galaxies are the cores of the most massive present-day spheroids. *MNRAS* **398**, 898 (2009). 0903.2479.

[153] P. F. Hopkins, T. J. Cox, D. Kereš, and L. Hernquist. A Cosmological Framework for the Co-evolution of Quasars, Supermassive Black Holes, and Elliptical Galaxies. II. Formation of Red Ellipticals. *ApJS* **175**, 390 (2008). 0706.1246.

[154] P. F. Hopkins, L. Hernquist, T. J. Cox, T. Di Matteo, P. Martini, B. Robertson, and V. Springel. Black Holes in Galaxy Mergers: Evolution of Quasars. *ApJ* **630**, 705 (2005). arXiv:astro-ph/0504190.

[155] P. F. Hopkins, L. Hernquist, T. J. Cox, S. N. Dutta, and B. Rothberg. Dissipation and Extra Light in Galactic Nuclei. I. Gas-Rich Merger Remnants. *ApJ* **679**, 156 (2008). 0802.0508.

[156] P. F. Hopkins, L. Hernquist, T. J. Cox, D. Keres, and S. Wuyts. Dissipation and Extra Light in Galactic Nuclei. IV. Evolution in the Scaling Relations of Spheroids. *ApJ* **691**, 1424 (2009). 0807.2868.

[157] P. F. Hopkins, L. Hernquist, P. Martini, T. J. Cox, B. Robertson, T. Di Matteo, and V. Springel. A Physical Model for the Origin of Quasar Lifetimes. *ApJL* **625**, L71 (2005). arXiv:astro-ph/0502241.

[158] J. B. Hyde and M. Bernardi. The luminosity and stellar mass Fundamental Plane of early-type galaxies. *MNRAS* **396**, 1171 (2009). 0810.4924.

[159] I. T. Iliev, G. Mellema, U.-L. Pen, H. Merz, P. R. Shapiro, and M. A. Alvarez. Simulating cosmic reionization at large scales - I. The geometry of reionization. *MNRAS* **369**, 1625 (2006). arXiv:astro-ph/0512187.

[160] L. Ingber, C. Chen, R. P. Mondescu, D. Muzzall, and M. Renedo. Probability tree algorithm for general diffusion processes. *Phys. Rev. E* **64**, 056702 (2001). arXiv:physics/0103013.

[161] R. J. Ivison, D. M. Alexander, A. D. Biggs, W. N. Brandt, E. L. Chapin, K. E. K. Coppin, M. J. Devlin, M. Dickinson, J. Dunlop, S. Dye, S. A. Eales, D. T. Frayer, M. Halpern, D. H. Hughes, E. Ibar, A. Kovács, G. Marsden, L. Moncelsi, C. B. Netterfield, E. Pascale, G. Patanchon, D. A. Rafferty, M. Rex, E. Schinnerer, D. Scott, C. Semisch, I. Smail, A. M. Swinbank, M. D. P. Truch, G. S. Tucker, M. P. Viero, F. Walter, A. Weiß, D. V. Wiebe, and Y. Q. Xue. BLAST: the far-infrared/radio correlation in distant galaxies. *MNRAS* **402**, 245 (2010). 0910.1091.

[162] R. J. Ivison, A. M. Swinbank, B. Swinyard, I. Smail, C. P. Pearson, D. Rigopoulou, E. Polehampton, J.-P. Baluteau, M. J. Barlow, A. W. Blain, J. Bock, D. L. Clements, K. Coppin, A. Cooray, A. Danielson, E. Dwek, A. C. Edge, A. Franceschini, T. Fulton, J. Glenn, M. Griffin, K. Isaak, S. Leeks, T. Lim, D. Naylor, S. J. Oliver, M. J. Page, I. Pérez Fournon, M. Rowan-Robinson, G. Savini, D. Scott, L. Spencer, I. Valtchanov, L. Vigroux, and G. S. Wright. Herschel and SCUBA-2 imaging and spectroscopy of a bright, lensed submillimetre galaxy at z = 2.3. *A&A* **518**, L35+ (2010). 1005.1071.

[163] A. Jenkins, C. S. Frenk, S. D. M. White, J. M. Colberg, S. Cole, A. E. Evrard, H. M. P. Couchman, and N. Yoshida. The mass function of dark matter haloes. *MNRAS* **321**, 372 (2001). arXiv:astro-ph/0005260.

[164] P. Jonsson, T. J. Cox, J. R. Primack, and R. S. Somerville. Simulations of Dust in Interacting Galaxies. I. Dust Attenuation. *ApJ* **637**, 255 (2006). arXiv:astro-ph/0503135.

[165] I. Jorgensen, M. Franx, and P. Kjaergaard. Sources of scatter in the fundamental plane and the Dn-sigma relation. *ApJ* **411**, 34 (1993).

[166] M. R. Joung, R. Cen, and G. L. Bryan. Galaxy Size Problem at z = 3: Simulated Galaxies are too Small. *ApJL* **692**, L1 (2009). 0805.3150.

[167] M. Kajisawa, T. Ichikawa, I. Tanaka, M. Konishi, T. Yamada, M. Akiyama, R. Suzuki, C. Tokoku, Y. K. Uchimoto, T. Yoshikawa, M. Ouchi, I. Iwata, T. Hamana, and M. Onodera. MOIRCS Deep Survey. IV. Evolution of Galaxy Stellar Mass Function Back to z ˜ 3. *ApJ* **702**, 1393 (2009). 0907.0133.

[168] S. Kaviraj, S. Khochfar, K. Schawinski, S. K. Yi, E. Gawiser, J. Silk, S. N. Virani, C. N. Cardamone, P. G. van Dokkum, and C. M. Urry. The UV colours of high-redshift early-type galaxies: evidence for recent star formation and stellar mass assembly over the last 8 billion years. *MNRAS* **388**, 67 (2008). 0709.0806.

[169] S. Kaviraj, S. Peirani, S. Khochfar, J. Silk, and S. Kay. The role of minor mergers in the recent star formation history of early-type galaxies. *MNRAS* **394**, 1713 (2009). 0711.1493.

[170] N. Kawakatu and M. Umemura. Radiation drag driven mass accretion in a clumpy interstellar medium: implications for the supermassive black hole-to-bulge relation. *MNRAS* **329**, 572 (2002). arXiv:astro-ph/0111436.

[171] R. C. Kennicutt, Jr. Star Formation in Galaxies Along the Hubble Sequence. *ARA&A* **36**, 189 (1998). arXiv:astro-ph/9807187.

[172] S. Khochfar and A. Burkert. On the origin of isophotal shapes in elliptical galaxies. *MNRAS* **359**, 1379 (2005). arXiv:astro-ph/0409705.

[173] S. Khochfar and J. Silk. The specific star formation rate of high redshift galaxies: the case for two modes of star formation. *MNRAS* **410**, L42 (2011). 1007.1463.

[174] M. Kleinheinrich, P. Schneider, H. . Rix, T. Erben, C. Wolf, M. Schirmer, K. Meisenheimer, A. Borch, S. Dye, Z. Kovacs, and L. Wisotzki. Weak lensing measurements of dark matter halos of galaxies from COMBO-17. *ArXiv Astrophysics e-prints* (2004). arXiv:astro-ph/0412615.

[175] K. K. Knudsen, P. P. van der Werf, and J.-P. Kneib. Probing the submillimetre number counts at $f_{850\mu m} <$ 2mJy. *MNRAS* **384**, 1611 (2008). 0712.1904.

[176] C. Kobayashi and K. Nomoto. The Role of Type Ia Supernovae in Chemical Evolution. I. Lifetime of Type Ia Supernovae and Metallicity Effect. *ApJ* **707**, 1466 (2009). 0801.0215.

[177] C. S. Kochanek and M. White. Global Probes of the Impact of Baryons on Dark Matter Halos. *ApJ* **559**, 531 (2001). arXiv:astro-ph/0102334.

[178] T. Kodama, N. Arimoto, A. J. Barger, and A. Arag'on-Salamanca. Evolution of the colour-magnitude relation of early-type galaxies in distant clusters. *A&A* **334**, 99 (1998). arXiv:astro-ph/9802245.

[179] J. Kormendy, D. B. Fisher, M. E. Cornell, and R. Bender. Structure and Formation of Elliptical and Spheroidal Galaxies. *ApJS* **182**, 216 (2009). 0810.1681.

[180] J. Kormendy and K. Gebhardt. Supermassive black holes in galactic nuclei. In *20th Texas Symposium on relativistic astrophysics*, edited by J. C. Wheeler & H. Martel, *American Institute of Physics Conference Series*, volume 586, pp. 363–381 (2001). arXiv:astro-ph/0105230.

[181] J. Kormendy and D. Richstone. Inward Bound—The Search For Supermassive Black Holes In Galactic Nuclei. *ARA&A* **33**, 581 (1995).

[182] M. Kriek, P. G. van Dokkum, I. Labbé, M. Franx, G. D. Illingworth, D. Marchesini, and R. F. Quadri. An Ultra-Deep Near-Infrared Spectrum of a Compact Quiescent Galaxy at z = 2.2. *ApJ* **700**, 221 (2009). 0905.1692.

[183] A. Kronawitter, R. P. Saglia, O. Gerhard, and R. Bender. Orbital structure and mass distribution in elliptical galaxies. *A&AS* **144**, 53 (2000).

[184] P. Kroupa. On the variation of the initial mass function. *MNRAS* **322**, 231 (2001). arXiv:astro-ph/0009005.

[185] J.-M. Kyeong, M.-J. Tseng, and Y.-I. Byun. Near-infrared color evolution of LMC clusters. *A&A* **409**, 479 (2003).

[186] C. G. Lacey, C. M. Baugh, C. S. Frenk, A. J. Benson, A. Orsi, L. Silva, G. L. Granato, and A. Bressan. Predictions for Herschel from Λ-cold dark matter: unveiling the cosmic star formation history. *MNRAS* **405**, 2 (2010). 0909.1567.

[187] A. Laor and W. N. Brandt. The Luminosity Dependence of Ultraviolet Absorption in Active Galactic Nuclei. *ApJ* **569**, 641 (2002).

[188] A. Lapi and A. Cavaliere. Structure and History of Dark Matter Halos Probed with Gravitational Lensing. *ApJL* **695**, L125 (2009). 0903.1589.

[189] A. Lapi, N. Kawakatu, Z. Bosnjak, A. Celotti, A. Bressan, G. L. Granato, and L. Danese. Long gamma-ray bursts and their host galaxies at high redshift. *MNRAS* **386**, 608 (2008). 0802.0787.

[190] A. Lapi, F. Shankar, J. Mao, G. L. Granato, L. Silva, G. De Zotti, and L. Danese. Quasar Luminosity Functions from Joint Evolution of Black Holes and Host Galaxies. *ApJ* **650**, 42 (2006). arXiv:astro-ph/0603819.

[191] R. B. Larson. A simple probabilistic theory of fragmentation. *MNRAS* **161**, 133 (1973).

[192] R. B. Larson. Models for the formation of elliptical galaxies. *MNRAS* **173**, 671 (1975).

[193] T. R. Lauer, K. Gebhardt, S. M. Faber, D. Richstone, S. Tremaine, J. Kormendy, M. C. Aller, R. Bender, A. Dressler, A. V. Filippenko, R. Green, and L. C. Ho. The Centers of Early-Type Galaxies with Hubble Space Telescope. VI. Bimodal Central Surface Brightness Profiles. *ApJ* **664**, 226 (2007). arXiv:astro-ph/0609762.

[194] D. R. Law, C. C. Steidel, D. K. Erb, J. E. Larkin, M. Pettini, A. E. Shapley, and S. A. Wright. The Kiloparsec-scale Kinematics of High-redshift Star-forming Galaxies. *ApJ* **697**, 2057 (2009). 0901.2930.

[195] T. Lejeune and D. Schaerer. Database of Geneva stellar evolution tracks and isochrones for $(UBV)_J(RI)_C$ JHKLL'M, HST-WFPC2, Geneva and Washington photometric systems. *A&A* **366**, 538 (2001). arXiv:astro-ph/0011497.

[196] C. J. Lintott, I. Ferreras, and O. Lahav. Massive Elliptical Galaxies: From Cores to Halos. *ApJ* **648**, 826 (2006). arXiv:astro-ph/0512175.

[197] A. Loeb and P. J. E. Peebles. Cosmological Origin of the Stellar Velocity Dispersions in Massive Early-Type Galaxies. *ApJ* **589**, 29 (2003). arXiv:astro-ph/0211465.

[198] M. Longhetti, P. Saracco, P. Severgnini, R. Della Ceca, F. Mannucci, R. Bender, N. Drory, G. Feulner, and U. Hopp. The Kormendy relation of massive elliptical galaxies at z ˜ 1.5: evidence for size evolution. *MNRAS* **374**, 614 (2007). arXiv:astro-ph/0610241.

[199] J. D. Lowenthal, D. C. Koo, R. Guzman, J. Gallego, A. C. Phillips, S. M. Faber, N. P. Vogt, G. D. Illingworth, and C. Gronwall. Keck Spectroscopy of Redshift Z approximately 3 Galaxies in the Hubble Deep Field. *ApJ* **481**, 673 (1997). arXiv:astro-ph/9612239.

[200] R. E. Lupu, Z-Spec Team, and A. Consortium. Z-Spec Measurements of CO Redshifts for Lensed Submillimeter Galaxies Discovered in the H-ATLAS Survey. In *American Astronomical Society Meeting Abstracts #217*, *Bulletin of the American Astronomical Society*, volume 43, pp. 245.14–+ (2011).

[201] D. Lutz, V. Mainieri, D. Rafferty, L. Shao, G. Hasinger, A. Weiß, F. Walter, I. Smail, D. M. Alexander, W. N. Brandt, S. Chapman, K. Coppin, N. M. Förster Schreiber, E. Gawiser, R. Genzel, T. R. Greve, R. J. Ivison, A. M. Koekemoer, P. Kurczynski, K. M. Menten, R. Nordon, P. Popesso, E. Schinnerer, J. D.

Silverman, J. Wardlow, and Y. Q. Xue. The LABOCA Survey of the Extended Chandra Deep Field South: Two Modes of Star Formation in Active Galactic Nucleus Hosts? *ApJ* **712**, 1287 (2010). 1002.0071.

[202] P. Madau. Radiative transfer in a clumpy universe: The colors of high-redshift galaxies. *ApJ* **441**, 18 (1995).

[203] S. J. Maddox, L. Dunne, E. Rigby, S. Eales, A. Cooray, D. Scott, J. A. Peacock, M. Negrello, D. J. B. Smith, D. Benford, A. Amblard, R. Auld, M. Baes, D. Bonfield, D. Burgarella, S. Buttiglione, A. Cava, D. Clements, A. Dariush, G. de Zotti, S. Dye, D. Frayer, J. Fritz, J. Gonzalez-Nuevo, D. Herranz, E. Ibar, R. Ivison, M. J. Jarvis, G. Lagache, L. Leeuw, M. Lopez-Caniego, E. Pascale, M. Pohlen, G. Rodighiero, S. Samui, S. Serjeant, P. Temi, M. Thompson, and A. Verma. Herschel-ATLAS: The angular correlation function of submillimetre galaxies at high and low redshift. *A&A* **518**, L11+ (2010). 1005.2406.

[204] J. Magorrian, S. Tremaine, D. Richstone, R. Bender, G. Bower, A. Dressler, S. M. Faber, K. Gebhardt, R. Green, C. Grillmair, J. Kormendy, and T. Lauer. The Demography of Massive Dark Objects in Galaxy Centers. *AJ* **115**, 2285 (1998). arXiv:astro-ph/9708072.

[205] A. Mahmood, J. E. G. Devriendt, and J. Silk. A simple model for the evolution of supermassive black holes and the quasar population. *MNRAS* **359**, 1363 (2005). arXiv:astro-ph/0401003.

[206] C. Maier, S. J. Lilly, G. Zamorani, M. Scodeggio, F. Lamareille, T. Contini, M. T. Sargent, C. Scarlata, P. Oesch, C. M. Carollo, O. Le Fèvre, A. Renzini, J.-P. Kneib, V. Mainieri, S. Bardelli, M. Bolzonella, A. Bongiorno, K. Caputi, G. Coppa, O. Cucciati, S. de la Torre, L. de Ravel, P. Franzetti, B. Garilli, A. Iovino, P. Kampczyk, C. Knobel, K. Kovač, J.-F. Le Borgne, V. Le Brun, M. Mignoli, R. Pello, Y. Peng, E. Perez Montero, E. Ricciardelli, J. D. Silverman, M. Tanaka, L. Tasca, L. Tresse, D. Vergani, E. Zucca, U. Abbas, D. Bottini, A. Cappi, P. Cassata, A. Cimatti, M. Fumana, L. Guzzo, C. Halliday, A. M. Koekemoer, A. Leauthaud, D. Maccagni, C. Marinoni, H. J. McCracken, P. Memeo, B. Meneux, C. Porciani, L. Pozzetti, and R. Scaramella. The Dependence of Star Formation Activity on Stellar Mass Surface Density and Sersic Index in zCOSMOS Galaxies at $0.5 < z < 0.9$ Compared with SDSS Galaxies at $0.04 < z < 0.08$. *ApJ* **694**, 1099 (2009). 0901.0550.

[207] A. H. Maller, N. Katz, D. Kereš, R. Davé, and D. H. Weinberg. Galaxy Merger Statistics and Inferred Bulge-to-Disk Ratios in Cosmological SPH Simulations. *ApJ* **647**, 763 (2006). arXiv:astro-ph/0509474.

[208] C. Mancini, E. Daddi, A. Renzini, F. Salmi, H. J. McCracken, A. Cimatti, M. Onodera, M. Salvato, A. M. Koekemoer, H. Aussel, E. Le Floc'h, C. Willott, and P. Capak. High-redshift elliptical galaxies: are they (all) really compact? *MNRAS* **401**, 933 (2010). 0909.3088.

[209] C. L. Mancone, A. H. Gonzalez, M. Brodwin, S. A. Stanford, P. R. M. Eisenhardt, D. Stern, and C. Jones. The Formation of Massive Cluster Galaxies. *ApJ* **720**, 284 (2010). 1007.1454.

[210] R. Mandelbaum, U. Seljak, G. Kauffmann, C. M. Hirata, and J. Brinkmann. Galaxy halo masses and satellite fractions from galaxy-galaxy lensing in the Sloan Digital Sky Survey: stellar mass, luminosity, morphology and environment dependencies. *MNRAS* **368**, 715 (2006). arXiv:astro-ph/0511164.

[211] J. Mao, A. Lapi, G. L. Granato, G. de Zotti, and L. Danese. The Role of the Dust in Primeval Galaxies: A Simple Physical Model for Lyman Break Galaxies and Lyα Emitters. *ApJ* **667**, 655 (2007). arXiv:astro-ph/0611799.

[212] C. Maraston, J. Pforr, A. Renzini, E. Daddi, M. Dickinson, A. Cimatti, and C. Tonini. Star formation rates and masses of z ˜ 2 galaxies from multicolour photometry. *MNRAS* **407**, 830 (2010). 1004.4546.

[213] D. Marchesini, P. G. van Dokkum, N. M. Förster Schreiber, M. Franx, I. Labbé, and S. Wuyts. The Evolution of the Stellar Mass Function of Galaxies from z = 4.0 and the First Comprehensive Analysis of its Uncertainties: Evidence for Mass-Dependent Evolution. *ApJ* **701**, 1765 (2009). 0811.1773.

[214] A. Marconi and L. K. Hunt. The Relation between Black Hole Mass, Bulge Mass, and Near-Infrared Luminosity. *ApJL* **589**, L21 (2003). arXiv:astro-ph/0304274.

[215] A. Marconi, G. Risaliti, R. Gilli, L. K. Hunt, R. Maiolino, and M. Salvati. Local supermassive black holes, relics of active galactic nuclei and the X-ray background. *MNRAS* **351**, 169 (2004). arXiv:astro-ph/0311619.

[216] P. Marigo, L. Girardi, A. Bressan, M. A. T. Groenewegen, L. Silva, and G. L. Granato. Evolution of asymptotic giant branch stars. II. Optical to far-infrared isochrones with improved TP-AGB models. *A&A* **482**, 883 (2008). 0711.4922.

[217] P. Martini and D. H. Weinberg. Quasar Clustering and the Lifetime of Quasars. *ApJ* **547**, 12 (2001). arXiv:astro-ph/0002384.

[218] J. S. Mathis. Interstellar dust and extinction. *ARA&A* **28**, 37 (1990).

[219] F. Matteucci. Abundance ratios in ellipticals and galaxy formation. *A&A* **288**, 57 (1994).

[220] Y. D. Mayya, A. Bressan, M. Rodríguez, J. R. Valdes, and M. Chavez. Star Formation History and Extinction in the Central Kiloparsec of M82-like Starbursts. *ApJ* **600**, 188 (2004). arXiv:astro-ph/0309339.

[221] R. M. McDermid, R. Bacon, H. Kuntschner, E. Emsellem, K. L. Shapiro, M. Bureau, M. Cappellari, R. L. Davies, J. Falcón-Barroso, D. Krajnović, R. F. Peletier, M. Sarzi, and T. de Zeeuw. Stellar kinematics and populations of early-type galaxies with the SAURON and OASIS integral-field spectrographs. *New Astronomy Reviews* **49**, 521 (2006). arXiv:astro-ph/0508631.

[222] D. H. McIntosh, E. F. Bell, H.-W. Rix, C. Wolf, C. Heymans, C. Y. Peng, R. S. Somerville, M. Barden, S. V. W. Beckwith, A. Borch, J. A. R. Caldwell, B. Häußler, K. Jahnke, S. Jogee, K. Meisenheimer, S. F. Sánchez, and L. Wisotzki. The Evolution of Early-Type Red Galaxies with the GEMS Survey: Luminosity-Size and Stellar Mass-Size Relations Since z=1. *ApJ* **632**, 191 (2005). arXiv:astro-ph/0411772.

[223] C. F. McKee and J. P. Ostriker. A theory of the interstellar medium - Three components regulated by supernova explosions in an inhomogeneous substrate. *ApJ* **218**, 148 (1977).

[224] R. J. McLure and J. S. Dunlop. On the black hole-bulge mass relation in active and inactive galaxies. *MNRAS* **331**, 795 (2002). arXiv:astro-ph/0108417.

[225] R. J. McLure and J. S. Dunlop. The cosmological evolution of quasar black hole masses. *MNRAS* **352**, 1390 (2004). arXiv:astro-ph/0310267.

[226] D. Merritt and T. Fridman. Triaxial Galaxies with Cusps. *ApJ* **460**, 136 (1996). arXiv:astro-ph/9511021.

[227] G. R. Meurer, T. M. Heckman, and D. Calzetti. Dust Absorption and the Ultraviolet Luminosity Density at Z˜3 as Calibrated by Local Starburst Galaxies. *ApJ* **521**, 64 (1999). arXiv:astro-ph/9903054.

[228] H. J. Mo and S. Mao. Galaxy formation in pre-processed dark haloes. *MNRAS* **353**, 829 (2004). arXiv:astro-ph/0311459.

[229] B. P. Moster, R. S. Somerville, C. Maulbetsch, F. C. van den Bosch, A. V. Macciò, T. Naab, and L. Oser. Constraints on the Relationship between Stellar Mass and Halo Mass at Low and High Redshift. *ApJ* **710**, 903 (2010). 0903.4682.

[230] U. Munari, R. Sordo, F. Castelli, and T. Zwitter. An extensive library of 2500 10 500 Å synthetic spectra. *A&A* **442**, 1127 (2005). arXiv:astro-ph/0502047.

[231] N. Murray, J. Chiang, S. A. Grossman, and G. M. Voit. Accretion Disk Winds from Active Galactic Nuclei. *ApJ* **451**, 498 (1995).

[232] N. Murray, E. Quataert, and T. A. Thompson. On the Maximum Luminosity of Galaxies and Their Central Black Holes: Feedback from Momentum-driven Winds. *ApJ* **618**, 569 (2005). arXiv:astro-ph/0406070.

[233] T. Naab, P. H. Johansson, and J. P. Ostriker. Minor Mergers and the Size Evolution of Elliptical Galaxies. *ApJL* **699**, L178 (2009). 0903.1636.

[234] T. Naab, P. H. Johansson, J. P. Ostriker, and G. Efstathiou. Formation of Early-Type Galaxies from Cosmological Initial Conditions. *ApJ* **658**, 710 (2007). arXiv:astro-ph/0512235.

[235] T. Naab, S. Khochfar, and A. Burkert. Properties of Early-Type, Dry Galaxy Mergers and the Origin of Massive Elliptical Galaxies. *ApJL* **636**, L81 (2006). arXiv:astro-ph/0509667.

[236] P. B. Nair, S. van den Bergh, and R. G. Abraham. The Environmental Dependence of the Luminosity-Size Relation for Galaxies. *ApJ* **715**, 606 (2010). 1004.1107.

[237] B. B. Nath and S. Roychowdhury. Heating of the intracluster medium by quasar outflows. *MNRAS* **333**, 145 (2002). arXiv:astro-ph/0202201.

[238] J. F. Navarro, C. S. Frenk, and S. D. M. White. A Universal Density Profile from Hierarchical Clustering. *ApJ* **490**, 493 (1997). arXiv:astro-ph/9611107.

[239] M. Negrello, R. Hopwood, G. De Zotti, A. Cooray, A. Verma, J. Bock, D. T. Frayer, M. A. Gurwell, A. Omont, R. Neri, H. Dannerbauer, L. L. Leeuw, E. Barton, J. Cooke, S. Kim, E. da Cunha, G. Rodighiero, P. Cox, D. G. Bonfield, M. J. Jarvis, S. Serjeant, R. J. Ivison, S. Dye, I. Aretxaga, D. H. Hughes, E. Ibar, F. Bertoldi, I. Valtchanov, S. Eales, L. Dunne, S. P. Driver, R. Auld, S. Buttiglione, A. Cava, C. A. Grady, D. L. Clements, A. Dariush, J. Fritz, D. Hill, J. B. Hornbeck, L. Kelvin, G. Lagache, M. Lopez-Caniego, J. Gonzalez-Nuevo, S. Maddox, E. Pascale, M. Pohlen, E. E. Rigby, A. Robotham, C. Simpson, D. J. B. Smith, P. Temi, M. A. Thompson, B. E. Woodgate, D. G. York, J. E. Aguirre, A. Beelen, A. Blain, A. J. Baker, M. Birkinshaw, R. Blundell, C. M. Bradford, D. Burgarella, L. Danese, J. S. Dunlop, S. Fleuren, J. Glenn, A. I. Harris, J. Kamenetzky, R. E. Lupu, R. J. Maddalena, B. F. Madore, P. R. Maloney, H. Matsuhara, M. J. Michaowski, E. J. Murphy, B. J. Naylor, H. Nguyen, C. Popescu, S. Rawlings, D. Rigopoulou, D. Scott, K. S. Scott, M. Seibert, I. Smail, R. J. Tuffs, J. D. Vieira, P. P. van der Werf, and J. Zmuidzinas. The Detection of a Population of Submillimeter-Bright, Strongly Lensed Galaxies. *Science* **330**, 800 (2010). 1011.1255.

[240] M. Negrello, F. Perrotta, J. González-Nuevo, L. Silva, G. de Zotti, G. L. Granato, C. Baccigalupi, and L. Danese. Astrophysical and cosmological information from large-scale submillimetre surveys of extragalactic sources. *MNRAS* **377**, 1557 (2007). arXiv:astro-ph/0703210.

[241] C. Nipoti, P. Londrillo, and L. Ciotti. Galaxy merging, the fundamental plane of elliptical galaxies and the $M_{BH} - \sigma_0$ relation. *MNRAS* **342**, 501 (2003). arXiv:astro-ph/0302423.

[242] W. Nowotny, B. Aringer, S. Höfner, R. Gautschy-Loidl, and W. Windsteig. Atmospheric dynamics in carbon-rich Miras. I. Model atmospheres and synthetic line profiles. *A&A* **437**, 273 (2005). arXiv:astro-ph/0503652.

[243] P. A. Oesch, R. J. Bouwens, G. D. Illingworth, I. Labbe, M. Trenti, V. Gonzalez, C. M. Carollo, M. Franx, P. G. van Dokkum, and D. Magee. Expanded Search for z˜10 Galaxies from HUDF09, ERS, and CANDELS Data: Evidence for Accelerated Evolution at z > 8? *ArXiv e-prints* (2011). 1105.2297.

[244] M. Onodera, E. Daddi, R. Gobat, M. Cappellari, N. Arimoto, A. Renzini, Y. Yamada, H. J. McCracken, C. Mancini, P. Capak, M. Carollo, A. Cimatti, M. Giavalisco, O. Ilbert, X. Kong, S. Lilly, K. Motohara, K. Ohta, D. B. Sanders, N. Scoville, N. Tamura, and Y. Taniguchi. A z = 1.82 Analog of Local Ultra-massive Elliptical Galaxies. *ApJL* **715**, L6 (2010). 1004.2120.

[245] E. O'Sullivan and T. J. Ponman. XMM-Newton and Chandra observations of three X-ray-faint early-type galaxies. *MNRAS* **349**, 535 (2004). arXiv:astro-ph/0312266.

[246] M. Ouchi, K. Shimasaku, S. Okamura, H. Furusawa, N. Kashikawa, K. Ota, M. Doi, M. Hamabe, M. Kimura, Y. Komiyama, M. Miyazaki, S. Miyazaki, F. Nakata, M. Sekiguchi, M. Yagi, and N. Yasuda. Subaru Deep Survey. V. A Census of Lyman Break Galaxies at z˜=4 and 5 in the Subaru Deep Fields: Photometric Properties. *ApJ* **611**, 660 (2004). arXiv:astro-ph/0309655.

[247] G. Paciga, D. Scott, and E. L. Chapin. Strong lensing of submillimetre galaxies: a tracer of foreground structure? *MNRAS* **395**, 1153 (2009). 0801.0274.

[248] M. J. Page and F. J. Carrera. An improved method of constructing binned luminosity functions. *MNRAS* **311**, 433 (2000). arXiv:astro-ph/9909434.

[249] M. Pannella, C. L. Carilli, E. Daddi, H. J. McCracken, F. N. Owen, A. Renzini, V. Strazzullo, F. Civano, A. M. Koekemoer, E. Schinnerer, N. Scoville, V. Smolčić, Y. Taniguchi, H. Aussel, J. P. Kneib, O. Ilbert, Y. Mellier, M. Salvato, D. Thompson, and C. J. Willott. Star Formation and Dust Obscuration at z $\sim$ 2: Galaxies at the Dawn of Downsizing. *ApJL* **698**, L116 (2009). 0905.1674.

[250] P. Panuzzo, A. Bressan, G. L. Granato, L. Silva, and L. Danese. Dust and nebular emission. I. Models for normal galaxies. *A&A* **409**, 99 (2003). arXiv:astro-ph/0307096.

[251] C. Papovich, L. A. Moustakas, M. Dickinson, E. Le Floc'h, G. H. Rieke, E. Daddi, D. M. Alexander, F. Bauer, W. N. Brandt, T. Dahlen, E. Egami, P. Eisenhardt, D. Elbaz, H. C. Ferguson, M. Giavalisco, R. A. Lucas, B. Mobasher, P. G. Pérez-González, A. Stutz, M. J. Rieke, and H. Yan. Spitzer Observations of Massive, Red Galaxies at High Redshift. *ApJ* **640**, 92 (2006). arXiv:astro-ph/0511289.

[252] R. B. Partridge and P. J. E. Peebles. Are Young Galaxies Visible? *ApJ* **147**, 868 (1967).

[253] P. J. E. Peebles and A. Nusser. Nearby galaxies as pointers to a better theory of cosmic evolution. *Nature* **465**, 565 (2010). 1001.1484.

[254] C. Y. Peng, C. D. Impey, H.-W. Rix, C. S. Kochanek, C. R. Keeton, E. E. Falco, J. Lehár, and B. A. McLeod. Probing the Coevolution of Supermassive Black Holes and Galaxies Using Gravitationally Lensed Quasar Hosts. *ApJ* **649**, 616 (2006). arXiv:astro-ph/0603248.

[255] L. Pentericci, A. Grazian, A. Fontana, S. Salimbeni, P. Santini, C. de Santis, S. Gallozzi, and E. Giallongo. Physical properties of z ˜ 4 LBGs: differences between galaxies with and without Lyα emission. *A&A* **471**, 433 (2007). arXiv:astro-ph/0703013.

[256] T. A. Perera, E. L. Chapin, J. E. Austermann, K. S. Scott, G. W. Wilson, M. Halpern, A. Pope, D. Scott, M. S. Yun, J. D. Lowenthal, G. Morrison, I. Aretxaga, J. J. Bock, K. Coppin, M. Crowe, L. Frey, D. H. Hughes, Y. Kang, S. Kim, and P. D. Mauskopf. An AzTEC 1.1mm survey of the GOODS-N field - I. Maps, catalogue and source statistics. *MNRAS* **391**, 1227 (2008). 0806.3791.

[257] P. G. Pérez-González, G. H. Rieke, V. Villar, G. Barro, M. Blaylock, E. Egami, J. Gallego, A. Gil de Paz, S. Pascual, J. Zamorano, and J. L. Donley. The Stellar Mass Assembly of Galaxies from z = 0 to z = 4: Analysis of a Sample Selected in the Rest-Frame Near-Infrared with Spitzer. *ApJ* **675**, 234 (2008). 0709.1354.

[258] F. Perrotta, C. Baccigalupi, M. Bartelmann, G. De Zotti, and G. L. Granato. Gravitational lensing of extended high-redshift sources by dark matter haloes. *MNRAS* **329**, 445 (2002).

[259] F. Perrotta, M. Magliocchetti, C. Baccigalupi, M. Bartelmann, G. De Zotti, G. L. Granato, L. Silva, and L. Danese. Predictions for statistical properties of forming spheroidal galaxies. *MNRAS* **338**, 623 (2003).

[260] S. E. Persson, M. Aaronson, J. G. Cohen, J. A. Frogel, and K. Matthews. Photometric studies of composite stellar systems. V - Infrared photometry of star clusters in the Magellanic clouds. *ApJ* **266**, 105 (1983).

[261] P. M. Pessev, P. Goudfrooij, T. H. Puzia, and R. Chandar. A Database of 2MASS Near-Infrared Colors of Magellanic Cloud Star Clusters. *AJ* **132**, 781 (2006). arXiv:astro-ph/0607617.

[262] B. M. Poggianti, A. Bressan, and A. Franceschini. Star Formation and Selective Dust Extinction in Luminous Starburst Galaxies. *ApJ* **550**, 195 (2001). arXiv:astro-ph/0011160.

[263] P. Popesso, M. Dickinson, M. Nonino, E. Vanzella, E. Daddi, R. A. E. Fosbury, H. Kuntschner, V. Mainieri, S. Cristiani, C. Cesarsky, M. Giavalisco, A. Renzini, and GOODS Team. The great observatories origins deep survey. VLT/VIMOS spectroscopy in the GOODS-south field. *A&A* **494**, 443 (2009). 0802.2930.

[264] C. Porciani, M. Magliocchetti, and P. Norberg. Cosmic evolution of quasar clustering: implications for the host haloes. *MNRAS* **355**, 1010 (2004). arXiv:astro-ph/0406036.

[265] L. Pozzetti, M. Bolzonella, F. Lamareille, G. Zamorani, P. Franzetti, O. Le Fèvre, A. Iovino, S. Temporin, O. Ilbert, S. Arnouts, S. Charlot, J. Brinchmann, E. Zucca, L. Tresse, M. Scodeggio, L. Guzzo, D. Bottini, B. Garilli, V. Le Brun, D. Maccagni, J. P. Picat, R. Scaramella, G. Vettolani, A. Zanichelli, C. Adami, S. Bardelli, A. Cappi, P. Ciliegi, T. Contini, S. Foucaud, I. Gavignaud, H. J. McCracken, B. Marano, C. Marinoni, A. Mazure, B. Meneux, R. Merighi, S. Paltani, R. Pellò, A. Pollo, M. Radovich, M. Bondi, A. Bongiorno, O. Cucciati, S. de la Torre, L. Gregorini, Y. Mellier, P. Merluzzi, D. Vergani, and C. J. Walcher. The VIMOS VLT Deep Survey. The assembly history of the stellar mass in galaxies: from the young to the old universe. *A&A* **474**, 443 (2007). 0704.1600.

[266] W. H. Press and P. Schechter. Formation of Galaxies and Clusters of Galaxies by Self-Similar Gravitational Condensation. *ApJ* **187**, 425 (1974).

[267] R. S. Priddey, S. C. Gallagher, K. G. Isaak, R. G. Sharp, R. G. McMahon, and H. M. Butner. A sensitive submillimetre survey of broad absorption-line quasars. *MNRAS* **374**, 867 (2007). arXiv:astro-ph/0610472.

[268] J. X. Prochaska and J. F. Hennawi. Quasars Probing Quasars. III. New Clues to Feedback, Quenching, and the Physics of Massive Galaxy Formation. *ApJ* **690**, 1558 (2009). 0806.0862.

[269] P. Prugniel and F. Simien. The fundamental plane of early-type galaxies: non-homology of the spatial structure. *A&A* **321**, 111 (1997).

[270] N. A. Reddy, D. K. Erb, M. Pettini, C. C. Steidel, and A. E. Shapley. Dust Obscuration and Metallicity at High Redshift: New Inferences from UV, Hα, and 8 μm Observations of z ˜ 2 Star-forming Galaxies. *ApJ* **712**, 1070 (2010). 1002.0837.

[271] N. A. Reddy and C. C. Steidel. A Steep Faint-End Slope of the UV Luminosity Function at z ˜ 2-3: Implications for the Global Stellar Mass Density and Star Formation in Low-Mass Halos. *ApJ* **692**, 778 (2009). 0810.2788.

[272] N. A. Reddy, C. C. Steidel, D. Fadda, L. Yan, M. Pettini, A. E. Shapley, D. K. Erb, and K. L. Adelberger. Star Formation and Extinction in Redshift z˜2 Galaxies: Inferences from Spitzer MIPS Observations. *ApJ* **644**, 792 (2006). arXiv:astro-ph/0602596.

[273] T. A. Reichard, G. T. Richards, D. P. Schneider, P. B. Hall, A. Tolea, J. H. Krolik, Z. Tsvetanov, D. E. Vanden Berk, D. G. York, G. R. Knapp, J. E. Gunn, and J. Brinkmann. A Catalog of Broad Absorption Line Quasars from the Sloan Digital Sky Survey Early Data Release. *AJ* **125**, 1711 (2003). arXiv:astro-ph/0301019.

[274] A. Renzini. Stellar Population Diagnostics of Elliptical Galaxy Formation. *ARA&A* **44**, 141 (2006). arXiv:astro-ph/0603479.

[275] G. T. Richards, M. Lacy, L. J. Storrie-Lombardi, P. B. Hall, S. C. Gallagher, D. C. Hines, X. Fan, C. Papovich, D. E. Vanden Berk, G. B. Trammell, D. P. Schneider, M. Vestergaard, D. G. York, S. Jester, S. F. Anderson, T. Budavári, and A. S. Szalay. Spectral Energy Distributions and Multiwavelength Selection of Type 1 Quasars. *ApJS* **166**, 470 (2006). arXiv:astro-ph/0601558.

[276] D. Richstone, E. A. Ajhar, R. Bender, G. Bower, A. Dressler, S. M. Faber, A. V. Filippenko, K. Gebhardt, R. Green, L. C. Ho, J. Kormendy, T. R. Lauer, J. Magorrian, and S. Tremaine. Supermassive black holes and the evolution of galaxies. *Nature* **395**, A14+ (1998). arXiv:astro-ph/9810378.

[277] D. O. Richstone and M. D. Potter. Galactic mass loss - A mild evolutionary correction to the angular size test. *ApJ* **254**, 451 (1982).

[278] G. H. Rieke, A. Alonso-Herrero, B. J. Weiner, P. G. Pérez-González, M. Blaylock, J. L. Donley, and D. Marcillac. Determining Star Formation Rates for Infrared Galaxies. *ApJ* **692**, 556 (2009). 0810.4150.

[279] E. E. Rigby, S. J. Maddox, L. Dunne, M. Negrello, D. J. B. Smith, J. González-Nuevo, D. Herranz, M. López-Caniego, R. Auld, S. Buttiglione, M. Baes, A. Cava, A. Cooray, D. L. Clements, A. Dariush, G. de Zotti, S. Dye, S. Eales, D. Frayer, J. Fritz, R. Hopwood, E. Ibar, R. J. Ivison, M. Jarvis, P. Panuzzo, E. Pascale, M. Pohlen, G. Rodighiero, S. Serjeant, P. Temi, and M. A. Thompson. Herschel-ATLAS: first data release of the Science Demonstration Phase source catalogues. *MNRAS* **415**, 2336 (2011). 1010.5787.

[280] B. Robertson, T. J. Cox, L. Hernquist, M. Franx, P. F. Hopkins, P. Martini, and V. Springel. The Fundamental Scaling Relations of Elliptical Galaxies. *ApJ* **641**, 21 (2006). arXiv:astro-ph/0511053.

[281] G. Rodighiero, A. Cimatti, C. Gruppioni, P. Popesso, P. Andreani, B. Altieri, H. Aussel, S. Berta, A. Bongiovanni, D. Brisbin, A. Cava, J. Cepa, E. Daddi, H. Dominguez-Sanchez, D. Elbaz, A. Fontana, N. Förster Schreiber, A. Franceschini, R. Genzel, A. Grazian, D. Lutz, G. Magdis, M. Magliocchetti, B. Magnelli, R. Maiolino, C. Mancini, R. Nordon, A. M. Perez Garcia, A. Poglitsch, P. Santini, M. Sanchez-Portal, F. Pozzi, L. Riguccini, A. Saintonge, L. Shao, E. Sturm, L. Tacconi, I. Valtchanov, M. Wetzstein, and E. Wieprecht. The first Herschel view of the mass-SFR link in high-z galaxies. *A&A* **518**, L25+ (2010). 1005.1089.

[282] B. Rogers, I. Ferreras, R. Peletier, and J. Silk. Exploring the star formation history of elliptical galaxies: beyond simple stellar populations with a new line strength estimator. *MNRAS* **402**, 447 (2010). 0812.2029.

[283] D. Romano, C. Chiappini, F. Matteucci, and M. Tosi. Quantifying the uncertainties of chemical evolution studies. I. Stellar lifetimes and initial mass function. *A&A* **430**, 491 (2005).

[284] E. E. Salpeter. The Luminosity Function and Stellar Evolution. *ApJ* **121**, 161 (1955).

[285] P. Sánchez-Blázquez, D. A. Forbes, J. Strader, J. Brodie, and R. Proctor. Spatially resolved spectroscopy of early-type galaxies over a range in mass. *MNRAS* **377**, 759 (2007). arXiv:astro-ph/0702572.

[286] P. Sánchez-Blázquez, R. F. Peletier, J. Jiménez-Vicente, N. Cardiel, A. J. Cenarro, J. Falcón-Barroso, J. Gorgas, S. Selam, and A. Vazdekis. Medium-resolution Isaac Newton Telescope library of empirical spectra. *MNRAS* **371**, 703 (2006). arXiv:astro-ph/0607009.

[287] D. B. Sanders, B. T. Soifer, J. H. Elias, B. F. Madore, K. Matthews, G. Neugebauer, and N. Z. Scoville. Ultraluminous infrared galaxies and the origin of quasars. *ApJ* **325**, 74 (1988).

[288] P. Santini, A. Fontana, A. Grazian, S. Salimbeni, F. Fiore, F. Fontanot, K. Boutsia, M. Castelllano, S. Cristiani, C. de Santis, S. Gallozzi, E. Giallongo, M. Nonino, N. Menci, D. Paris, L. Pentericci, and E. Vanzella. GOODS-MUSIC catalog updated version (Santini+, 2009). *VizieR Online Data Catalog* **350**, 40751 (2009).

[289] S. Sasaki. Formation rate of bound objects in the hierarchical clustering model. *PASJ* **46**, 427 (1994).

[290] M. Sawicki and D. Thompson. Keck Deep Fields. I. Observations, Reductions, and the Selection of Faint Star-forming Galaxies at Redshifts z ˜ 4, 3, and 2. *ApJ* **635**, 100 (2005). arXiv:astro-ph/0507424.

[291] D. Schaerer and A. de Koter. Combined stellar structure and atmosphere models for massive stars. III. Spectral evolution and revised ionizing fluxes of O3-B0 stars. *A&A* **322**, 598 (1997). arXiv:astro-ph/9611068.

[292] M. Schmidt. Space Distribution and Luminosity Functions of Quasi-Stellar Radio Sources. *ApJ* **151**, 393 (1968).

[293] W. Schmutz, C. Leitherer, and R. Gruenwald. Theoretical continuum energy distributions for Wolf-Rayet stars. *PASP* **104**, 1164 (1992).

[294] A. Schurer, F. Calura, L. Silva, A. Pipino, G. L. Granato, F. Matteucci, and R. Maiolino. Modelling the effects of dust evolution on the SEDs of galaxies of different morphological type. *MNRAS* **394**, 2001 (2009). 0901.1207.

[295] K. S. Scott, M. S. Yun, G. W. Wilson, J. E. Austermann, E. Aguilar, I. Aretxaga, H. Ezawa, D. Ferrusca, B. Hatsukade, D. H. Hughes, D. Iono, M. Giavalisco, R. Kawabe, K. Kohno, P. D. Mauskopf, T. Oshima, T. A. Perera, J. Rand, Y. Tamura, T. Tosaki, M. Velazquez, C. C. Williams, and M. Zeballos. Deep 1.1mm-wavelength imaging of the GOODS-S field by AzTEC/ASTE - I. Source catalogue and number counts. *MNRAS* **405**, 2260 (2010). 1003.1768.

[296] N. Scoville, H. Aussel, M. Brusa, P. Capak, C. M. Carollo, M. Elvis, M. Giavalisco, L. Guzzo, G. Hasinger, C. Impey, J.-P. Kneib, O. LeFevre, S. J. Lilly, B. Mobasher, A. Renzini, R. M. Rich, D. B. Sanders, E. Schinnerer, D. Schminovich, P. Shopbell, Y. Taniguchi, and N. D. Tyson. The Cosmic Evolution Survey (COSMOS): Overview. *ApJS* **172**, 1 (2007). arXiv:astro-ph/0612305.

[297] S. Serjeant and D. Harrison. The local submillimetre luminosity functions and predictions from Spitzer to Herschel. *MNRAS* **356**, 192 (2005). arXiv:astro-ph/0409498.

[298] F. Shankar, A. Lapi, P. Salucci, G. De Zotti, and L. Danese. New Relationships between Galaxy Properties and Host Halo Mass, and the Role of Feedbacks in Galaxy Formation. *ApJ* **643**, 14 (2006). arXiv:astro-ph/0601577.

[299] F. Shankar, P. Salucci, G. L. Granato, G. De Zotti, and L. Danese. Supermassive black hole demography: the match between the local and accreted mass functions. *MNRAS* **354**, 1020 (2004). arXiv:astro-ph/0405585.

[300] A. E. Shapley, C. C. Steidel, K. L. Adelberger, M. Dickinson, M. Giavalisco, and M. Pettini. The Rest-Frame Optical Properties of z˜=3 Galaxies. *ApJ* **562**, 95 (2001). arXiv:astro-ph/0107324.

[301] A. E. Shapley, C. C. Steidel, D. K. Erb, N. A. Reddy, K. L. Adelberger, M. Pettini, P. Barmby, and J. Huang. Ultraviolet to Mid-Infrared Observations of Star-forming Galaxies at z˜2: Stellar Masses and Stellar Populations. *ApJ* **626**, 698 (2005). arXiv:astro-ph/0503485.

[302] S. Shen, H. J. Mo, S. D. M. White, M. R. Blanton, G. Kauffmann, W. Voges, J. Brinkmann, and I. Csabai. The size distribution of galaxies in the Sloan Digital Sky Survey. *MNRAS* **343**, 978 (2003). arXiv:astro-ph/0301527.

[303] R. K. Sheth, M. Bernardi, P. L. Schechter, S. Burles, D. J. Eisenstein, D. P. Finkbeiner, J. Frieman, R. H. Lupton, D. J. Schlegel, M. Subbarao, K. Shimasaku, N. A. Bahcall, J. Brinkmann, and Ž. Ivezić. The Velocity Dispersion Function of Early-Type Galaxies. *ApJ* **594**, 225 (2003). arXiv:astro-ph/0303092.

[304] R. K. Sheth and G. Tormen. Large-scale bias and the peak background split. *MNRAS* **308**, 119 (1999). arXiv:astro-ph/9901122.

[305] R. K. Sheth and G. Tormen. An excursion set model of hierarchical clustering: ellipsoidal collapse and the moving barrier. *MNRAS* **329**, 61 (2002). arXiv:astro-ph/0105113.

[306] J. Silk and M. J. Rees. Quasars and galaxy formation. *A&A* **331**, L1 (1998). arXiv:astro-ph/9801013.

[307] L. Silva, G. De Zotti, G. L. Granato, R. Maiolino, and L. Danese. Observational tests of the evolution of spheroidal galaxies. *MNRAS* **357**, 1295 (2005). arXiv:astro-ph/0412340.

[308] L. Silva, G. L. Granato, A. Bressan, and L. Danese. Modeling the Effects of Dust on Galactic Spectral Energy Distributions from the Ultraviolet to the Millimeter Band. *ApJ* **509**, 103 (1998).

[309] R. A. Simcoe, W. L. W. Sargent, M. Rauch, and G. Becker. Observations of Chemically Enriched QSO Absorbers near z˜2.3 Galaxies: Galaxy Formation Feedback Signatures in the Intergalactic Medium. *ApJ* **637**, 648 (2006). arXiv:astro-ph/0508116.

[310] D. J. B. Smith, L. Dunne, S. J. Maddox, S. Eales, D. G. Bonfield, M. J. Jarvis, W. Sutherland, S. Fleuren, E. E. Rigby, M. A. Thompson, I. K. Baldry, S. Bamford, S. Buttiglione, A. Cava, D. Clements, A. Cooray, S. Croom, A. Dariush, G. de Zotti, S. P. Driver, J. S. Dunlop, J. Fritz, D. T. Hill, A. Hopkins, R. Hopwood, E. Ibar, R. J. Ivison, D. H. Jones, L. Kelvin, L. Leeuw, J. Liske, J. Loveday, B. F. Madore, P. Norberg, P. Panuzzo, E. Pascale, M. Pohlen, C. C. Popescu, M. Prescott, A. Robotham, G. Rodighiero, D. Scott, M. Seibert, R. Sharp, P. Temi, R. J. Tuffs, P. van der Werf, and E. van Kampen. Herschel-ATLAS: counterparts from the UV–NIR in the science demonstration phase catalogue. *ArXiv e-prints* (2010). 1007.5260.

[311] L. J. Smith, R. P. F. Norris, and P. A. Crowther. Realistic ionizing fluxes for young stellar populations from 0.05 to 2 $Z_{\odot}$. *MNRAS* **337**, 1309 (2002). arXiv:astro-ph/0207554.

[312] C. C. Steidel, K. L. Adelberger, M. Giavalisco, M. Dickinson, and M. Pettini. Lyman-Break Galaxies at z $>$ ˜4 and the Evolution of the Ultraviolet Luminosity Density at High Redshift. *ApJ* **519**, 1 (1999). arXiv:astro-ph/9811399.

[313] C. C. Steidel, K. L. Adelberger, A. E. Shapley, M. Pettini, M. Dickinson, and M. Giavalisco. Lyman Break Galaxies at Redshift z ˜ 3: Survey Description and Full Data Set. *ApJ* **592**, 728 (2003). arXiv:astro-ph/0305378.

[314] C. C. Steidel, M. Giavalisco, M. Pettini, M. Dickinson, and K. L. Adelberger. Spectroscopic Confirmation of a Population of Normal Star-forming Galaxies at Redshifts $Z > 3$. *ApJL* **462**, L17+ (1996). arXiv:astro-ph/9602024.

[315] C. C. Steidel and D. Hamilton. Deep imaging of high redshift QSO fields below the Lyman limit. II - Number counts and colors of field galaxies. *AJ* **105**, 2017 (1993).

[316] K. R. Stewart, J. S. Bullock, R. H. Wechsler, A. H. Maller, and A. R. Zentner. Merger Histories of Galaxy Halos and Implications for Disk Survival. *ApJ* **683**, 597 (2008). 0711.5027.

[317] N. Sugiyama. Cosmic Background Anisotropies in Cold Dark Matter Cosmology. *ApJS* **100**, 281 (1995). arXiv:astro-ph/9412025.

[318] M. Sullivan, B. Mobasher, B. Chan, L. Cram, R. Ellis, M. Treyer, and A. Hopkins. A Comparison of Independent Star Formation Diagnostics for an Ultraviolet-selected Sample of Nearby Galaxies. *ApJ* **558**, 72 (2001). arXiv:astro-ph/0104425.

[319] A. M. Swinbank, I. Smail, S. Longmore, A. I. Harris, A. J. Baker, C. De Breuck, J. Richard, A. C. Edge, R. J. Ivison, R. Blundell, K. E. K. Coppin, P. Cox, M. Gurwell, L. J. Hainline, M. Krips, A. Lundgren, R. Neri, B. Siana, G. Siringo, D. P. Stark, D. Wilner, and J. D. Younger. Intense star formation within resolved compact regions in a galaxy at z = 2.3. *Nature* **464**, 733 (2010). 1003.3674.

[320] G. Tabor and J. Binney. Elliptical Galaxy Cooling Flows Without Mass Drop-Out. *MNRAS* **263**, 323 (1993).

[321] L. J. Tacconi, R. Genzel, R. Neri, P. Cox, M. C. Cooper, K. Shapiro, A. Bolatto, N. Bouché, F. Bournaud, A. Burkert, F. Combes, J. Comerford, M. Davis, N. M. F. Schreiber, S. Garcia-Burillo, J. Gracia-Carpio, D. Lutz, T. Naab, A. Omont, A. Shapley, A. Sternberg, and B. Weiner. High molecular gas fractions in normal massive star-forming galaxies in the young Universe. *Nature* **463**, 781 (2010). 1002.2149.

[322] L. J. Tacconi, R. Genzel, I. Smail, R. Neri, S. C. Chapman, R. J. Ivison, A. Blain, P. Cox, A. Omont, F. Bertoldi, T. Greve, N. M. Förster Schreiber, S. Genel, D. Lutz, A. M. Swinbank, A. E. Shapley, D. K. Erb, A. Cimatti, E. Daddi, and A. J. Baker. Submillimeter Galaxies at z ˜ 2: Evidence for Major Mergers and Constraints on Lifetimes, IMF, and $CO - H_2$ Conversion Factor. *ApJ* **680**, 246 (2008). 0801.3650.

[323] D. Thomas. Abundance ratios in hierarchical galaxy formation. *MNRAS* **306**, 655 (1999). arXiv:astro-ph/9901226.

[324] D. Thomas and G. Kauffmann. Probing Star Formation Timescales in Elliptical Galaxies. In *Spectrophotometric Dating of Stars and Galaxies*, edited by I. Hubeny, S. Heap, & R. Cornett, *Astronomical Society of the Pacific Conference Series*, volume 192, pp. 261–+ (1999). arXiv:astro-ph/9906216.

[325] D. Thomas, C. Maraston, R. Bender, and C. Mendes de Oliveira. The Epochs of Early-Type Galaxy Formation as a Function of Environment. *ApJ* **621**, 673 (2005). arXiv:astro-ph/0410209.

[326] D. Thomas, C. Maraston, K. Schawinski, M. Sarzi, and J. Silk. Environment and self-regulation in galaxy formation. *MNRAS* **404**, 1775 (2010). 0912.0259.

[327] S. Toft, M. Franx, P. van Dokkum, N. M. Förster Schreiber, I. Labbe, S. Wuyts, and D. Marchesini. The Size-Star Formation Relation of Massive Galaxies at $1.5 < z < 2.5$. *ApJ* **705**, 255 (2009). 0909.0750.

[328] S. Toft, P. van Dokkum, M. Franx, I. Labbe, N. M. Förster Schreiber, S. Wuyts, T. Webb, G. Rudnick, A. Zirm, M. Kriek, P. van der Werf, J. P. Blakeslee, G. Illingworth, H.-W. Rix, C. Papovich, and A. Moorwood. Hubble Space Telescope and Spitzer Imaging of Red and Blue Galaxies at z ˜ 2.5: A Correlation between Size and Star Formation Activity from Compact Quiescent Galaxies to Extended Star-forming Galaxies. *ApJ* **671**, 285 (2007). 0707.4484.

[329] A. Toomre. Theories of spiral structure. *ARA&A* **15**, 437 (1977).

[330] A. Toomre and J. Toomre. Galactic Bridges and Tails. *ApJ* **178**, 623 (1972).

[331] C. Tortora, N. R. Napolitano, A. J. Romanowsky, M. Capaccioli, and G. Covone. Central mass-to-light ratios and dark matter fractions in early-type galaxies. *MNRAS* **396**, 1132 (2009). 0901.3781.

[332] S. Tremaine, K. Gebhardt, R. Bender, G. Bower, A. Dressler, S. M. Faber, A. V. Filippenko, R. Green, C. Grillmair, L. C. Ho, J. Kormendy, T. R. Lauer, J. Magorrian, J. Pinkney, and D. Richstone. The Slope of the Black Hole Mass versus Velocity Dispersion Correlation. *ApJ* **574**, 740 (2002). arXiv:astro-ph/0203468.

[333] I. Trujillo, A. J. Cenarro, A. de Lorenzo-Cáceres, A. Vazdekis, I. G. de la Rosa, and A. Cava. Superdense Massive Galaxies in the Nearby Universe. *ApJL* **692**, L118 (2009). 0901.1032.

[334] I. Trujillo, C. J. Conselice, K. Bundy, M. C. Cooper, P. Eisenhardt, and R. S. Ellis. Strong size evolution of the most massive galaxies since z ˜ 2. *MNRAS* **382**, 109 (2007). 0709.0621.

[335] I. Trujillo, G. Feulner, Y. Goranova, U. Hopp, M. Longhetti, P. Saracco, R. Bender, V. Braito, R. Della Ceca, N. Drory, F. Mannucci, and P. Severgnini. Extremely compact massive galaxies at z ˜ 1.4. *MNRAS* **373**, L36 (2006). arXiv:astro-ph/0608657.

[336] I. Trujillo, G. Rudnick, H.-W. Rix, I. Labbé, M. Franx, E. Daddi, P. G. van Dokkum, N. M. Förster Schreiber, K. Kuijken, A. Moorwood, H. Röttgering, A. van der Wel, P. van der Werf, and L. van Starkenburg. The Luminosity-Size and Mass-Size Relations of Galaxies out to z ˜ 3. *ApJ* **604**, 521 (2004). arXiv:astro-ph/0307015.

[337] Y. Ueda, M. Akiyama, K. Ohta, and T. Miyaji. Cosmological Evolution of the Hard X-Ray Active Galactic Nucleus Luminosity Function and the Origin of the Hard X-Ray Background. *ApJ* **598**, 886 (2003). arXiv:astro-ph/0308140.

[338] M. Umemura. A Radiation-Hydrodynamical Model for Supermassive Black Hole-to-Bulge Mass Relation and Quasar Formation. *ApJL* **560**, L29 (2001). arXiv:astro-ph/0108482.

[339] J. R. Valdés, S. Berta, A. Bressan, A. Franceschini, D. Rigopoulou, and G. Rodighiero. NIR spectroscopy of luminous infrared galaxies and the hydrogen recombination photon deficit. *A&A* **434**, 149 (2005). arXiv:astro-ph/0412706.

[340] A. Vale and J. P. Ostriker. Linking halo mass to galaxy luminosity. *MNRAS* **353**, 189 (2004). arXiv:astro-ph/0402500.

[341] T. Valentinuzzi, J. Fritz, B. M. Poggianti, A. Cava, D. Bettoni, G. Fasano, M. D'Onofrio, W. J. Couch, A. Dressler, M. Moles, A. Moretti, A. Omizzolo, P. Kjærgaard, E. Vanzella, and J. Varela. Superdense Massive Galaxies in Wings Local Clusters. *ApJ* **712**, 226 (2010). 0907.2392.

[342] A. van der Wel, E. F. Bell, F. C. van den Bosch, A. Gallazzi, and H.-W. Rix. On the Size and Comoving Mass Density Evolution of Early-Type Galaxies. *ApJ* **698**, 1232 (2009). 0903.4857.

[343] A. van der Wel, B. P. Holden, A. W. Zirm, M. Franx, A. Rettura, G. D. Illingworth, and H. C. Ford. Recent Structural Evolution of Early-Type Galaxies: Size Growth from z = 1 to z = 0. *ApJ* **688**, 48 (2008). 0808.0077.

[344] P. G. van Dokkum, M. Franx, M. Kriek, B. Holden, G. D. Illingworth, D. Magee, R. Bouwens, D. Marchesini, R. Quadri, G. Rudnick, E. N. Taylor, and S. Toft. Confirmation of the Remarkable Compactness of Massive Quiescent Galaxies at z ˜ 2.3: Early-Type Galaxies Did not Form in a Simple Monolithic Collapse. *ApJL* **677**, L5 (2008). 0802.4094.

[345] P. G. van Dokkum, M. Kriek, and M. Franx. A high stellar velocity dispersion for a compact massive galaxy at redshift z = 2.186. *Nature* **460**, 717 (2009). 0906.2778.

[346] P. G. van Dokkum and S. A. Stanford. The Fundamental Plane at z=1.27: First Calibration of the Mass Scale of Red Galaxies. *ApJ* **585**, 78 (2003). arXiv:astro-ph/0210643.

[347] P. G. van Dokkum, K. E. Whitaker, G. Brammer, M. Franx, M. Kriek, I. Labbé, D. Marchesini, R. Quadri, R. Bezanson, G. D. Illingworth, A. Muzzin, G. Rudnick, T. Tal, and D. Wake. The Growth of Massive Galaxies Since z = 2. *ApJ* **709**, 1018 (2010). 0912.0514.

[348] E. Vanzella, S. Cristiani, M. Dickinson, M. Giavalisco, H. Kuntschner, J. Haase, M. Nonino, P. Rosati, C. Cesarsky, H. C. Ferguson, R. A. E. Fosbury, A. Grazian, L. A. Moustakas, A. Rettura, P. Popesso, A. Renzini, D. Stern, and GOODS Team. The great observatories origins deep survey. VLT/FORS2 spectroscopy in the GOODS-South field: Part III. *A&A* **478**, 83 (2008). 0711.0850.

[349] E. Vanzella, S. Cristiani, M. Dickinson, H. Kuntschner, L. A. Moustakas, M. Nonino, P. Rosati, D. Stern, C. Cesarsky, S. Ettori, H. C. Ferguson, R. A. E. Fosbury, M. Giavalisco, J. Haase, A. Renzini, A. Rettura, P. Serra, and The Goods Team. The Great Observatories Origins Deep Survey. VLT/FORS2 spectroscopy in the GOODS-South Field. *A&A* **434**, 53 (2005). arXiv:astro-ph/0406591.

[350] E. Vanzella, S. Cristiani, M. Dickinson, H. Kuntschner, M. Nonino, A. Rettura, P. Rosati, J. Vernet, C. Cesarsky, H. C. Ferguson, R. A. E. Fosbury, M. Giavalisco, A. Grazian, J. Haase, L. A. Moustakas, P. Popesso, A. Renzini, D. Stern, and GOODS Team. The great observatories origins deep survey. VLT/FORS2 spectroscopy in the GOODS-South Field: Part II. *A&A* **454**, 423 (2006). arXiv:astro-ph/0601367.

[351] O. Vega, M. S. Clemens, A. Bressan, G. L. Granato, L. Silva, and P. Panuzzo. Modelling the spectral energy distribution of ULIRGs. II. The energetic environment and the dense interstellar medium. *A&A* **484**, 631 (2008). 0712.1202.

[352] O. Vega, L. Silva, P. Panuzzo, A. Bressan, G. L. Granato, and M. Chavez. The evolution of actively star-forming galaxies in the mid-infrared. *MNRAS* **364**, 1286 (2005). arXiv:astro-ph/0510080.

[353] M. Vestergaard. Early Growth and Efficient Accretion of Massive Black Holes at High Redshift. *ApJ* **601**, 676 (2004). arXiv:astro-ph/0309521.

[354] J. D. Vieira, T. M. Crawford, E. R. Switzer, P. A. R. Ade, K. A. Aird, M. L. N. Ashby, B. A. Benson, L. E. Bleem, M. Brodwin, J. E. Carlstrom, C. L. Chang, H.-M. Cho, A. T. Crites, T. de Haan, M. A. Dobbs, W. Everett, E. M. George, M. Gladders, N. R. Hall, N. W. Halverson, F. W. High, G. P. Holder, W. L. Holzapfel, J. D. Hrubes, M. Joy, R. Keisler, L. Knox, A. T. Lee, E. M. Leitch, M. Lueker, D. P. Marrone,

V. McIntyre, J. J. McMahon, J. Mehl, S. S. Meyer, J. J. Mohr, T. E. Montroy, S. Padin, T. Plagge, C. Pryke, C. L. Reichardt, J. E. Ruhl, K. K. Schaffer, L. Shaw, E. Shirokoff, H. G. Spieler, B. Stalder, Z. Staniszewski, A. A. Stark, K. Vanderlinde, W. Walsh, R. Williamson, Y. Yang, O. Zahn, and A. Zenteno. Extragalactic Millimeter-wave Sources in South Pole Telescope Survey Data: Source Counts, Catalog, and Statistics for an 87 Square-degree Field. *ApJ* **719**, 763 (2010). 0912.2338.

[355] C. Vignali, W. N. Brandt, and D. P. Schneider. X-Ray Emission from Radio-Quiet Quasars in the Sloan Digital Sky Survey Early Data Release: The α_{ox} Dependence upon Ultraviolet Luminosity. *AJ* **125**, 433 (2003). arXiv:astro-ph/0211125.

[356] U. P. Vijh, A. N. Witt, and K. D. Gordon. The Dust in Lyman Break Galaxies. *ApJ* **587**, 533 (2003). arXiv:astro-ph/0301121.

[357] B. Wang and T. M. Heckman. Internal Absorption and the Luminosity of Disk Galaxies. *ApJ* **457**, 645 (1996).

[358] W.-H. Wang, A. J. Barger, and L. L. Cowie. Ultradeep Near-Infrared Observations of Goods 850-5. *ApJ* **690**, 319 (2009). 0805.3503.

[359] S. D. M. White and C. S. Frenk. Galaxy formation through hierarchical clustering. *ApJ* **379**, 52 (1991).

[360] S. D. M. White and M. J. Rees. Core condensation in heavy halos - A two-stage theory for galaxy formation and clustering. *MNRAS* **183**, 341 (1978).

[361] R. J. Williams, R. F. Quadri, M. Franx, P. van Dokkum, and I. Labbé. Detection of Quiescent Galaxies in a Bicolor Sequence from Z = 0-2. *ApJ* **691**, 1879 (2009). 0806.0625.

[362] K. Yabe, K. Ohta, I. Iwata, M. Sawicki, N. Tamura, M. Akiyama, and K. Aoki. The Stellar Populations of Lyman Break Galaxies at z ˜ 5. *ApJ* **693**, 507 (2009). 0811.2041.

[363] M. Zemcov, A. Blain, M. Halpern, and L. Levenson. Contribution of Lensed SCUBA Galaxies to the Cosmic Infrared Background. *ApJ* **721**, 424 (2010). 1006.1360.

[364] D. H. Zhao, H. J. Mo, Y. P. Jing, and G. Börner. The growth and structure of dark matter haloes. *MNRAS* **339**, 12 (2003). arXiv:astro-ph/0204108.

[365] A. W. Zirm, A. van der Wel, M. Franx, I. Labbé, I. Trujillo, P. van Dokkum, S. Toft, E. Daddi, G. Rudnick, H.-W. Rix, H. J. A. Röttgering, and P. van der Werf. NICMOS Imaging of DRGs in the HDF-S: A Relation between Star Formation and Size at z ˜ 2.5. *ApJ* **656**, 66 (2007). arXiv:astro-ph/0611245.